D3.1 Initial dimensioning of the system according to general use typologies

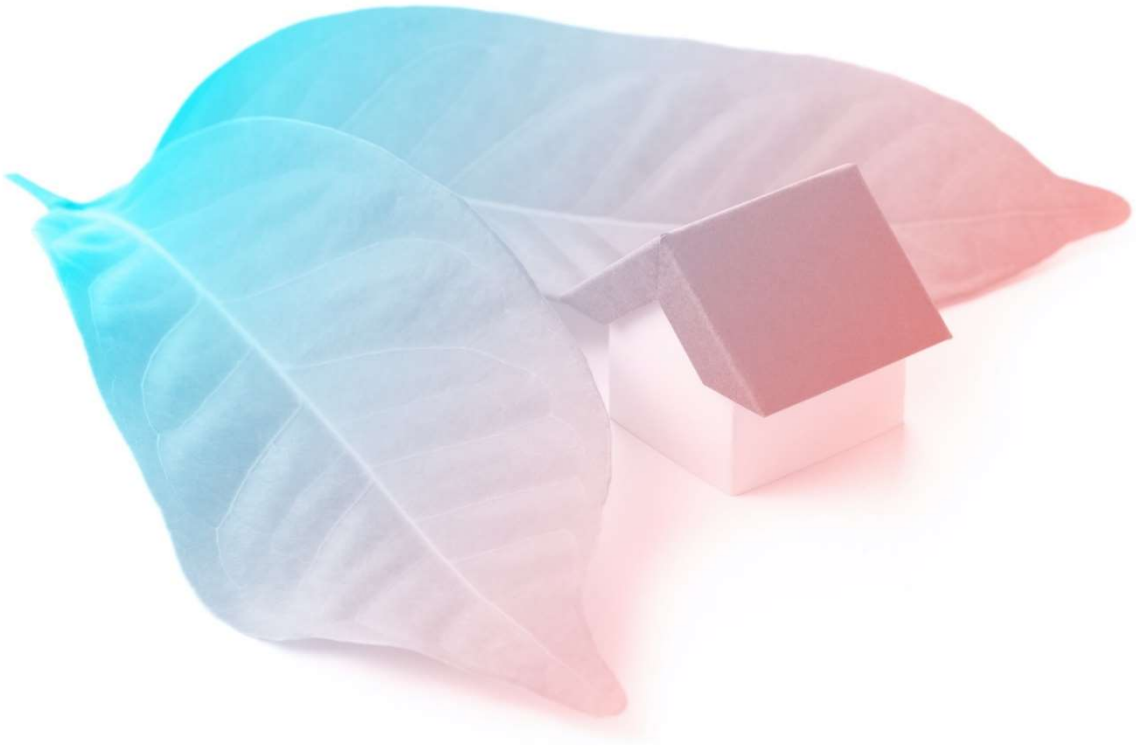

Authors: Georgios Zisopoulos (CERTH), Konstantinos Atsonios (CERTH), Athanasios Nesiadis (CERTH), Nikolaos Nikolopoulos (CERTH), Georgios Martinopoulos, (CERTH), Alexandros Tsimpoukis (CERTH), Isabel Guedea (EndeF), Adriana Coca-Ortegon (EndeF), Alberto Belda González (CARTIF), Ismael Lozano Gabarre (CARTIF) Carlos Ochoa (IERC)

This project has received funding from the European Union´s Horizon 2020 research and innovation programme under the grant agreement No 869821

Initial dimensioning of the system according to general use typologies

Summary

This deliverable presents initial thermal and electrical calculations of the MiniStor system in order to specify the design and operation of its basic components, predicting the electrical and thermal capacity to meet energy demands of different energy usage profiles in all demonstration sites using the proposed material technologies.

The electrical energy model was developed by CARTIF and EndeF in TRNSYS. It analysed, on a monthly basis, electricity production and output from the photovoltaic-thermal panel and the energy flows between this element and the hybrid solar inverter, use of batteries, interactions with the electrical grid and electrical demand coverage. This helped in the design of the Electrical Storage System and the potential savings from using price-based electricity operation of the batteries. A more detailed analysis of the electrical system is expected in task T3.5.

The thermal part of the system was dimensioned using an integrated model developed by CERTH in Aspen Plus Dynamics/ MATLAB-Simulink. It combines the described sub-model of the photovoltaic-thermal panels, with models for the thermochemical reactor, ammonia cycle, heat pump and phase-change materials. The model used weather data from Meteonorm, including outdoor temperature and solar irradiance. It also used the heating and cooling load profiles of the demos as input. The integrated model is able to present the performance of each component and the contribution of the MiniStor system to cover the heating and cooling demands of each demo. The operational principles of each component as well as the modelling methodology are presented in detail.

Deliverable Number	Work Package
D3. 1	WP. 3
Lead Beneficiary	**Deliverable Author(s)**
Centre of Research and Technology Hellas (CERTH)	Georgios Zisopoulos (CERTH), Konstantinos Atsonios (CERTH) Athanasios Nesiadis (CERTH), Nikolaos Nikolopoulos (CERTH), Georgios Martinopoulos (CERTH), Alexandros Tsimpoukis (CERTH), Isabel Guedea (EndeF), Adriana Coca-Ortegon (EndeF), Alberto Belda González (CARTIF), Ismael Lozano Gabarre (CARTIF) Carlos Ochoa (IERC)
Beneficiaries	**Deliverable Reviewer(s)**
Psyctotherm R2M Solution	Pantelis Bakalis Marco Rocchetti
Planned Delivery Date	**Actual Delivery Date**
31/07/2020	Third Revision 01/11/2023

Type of deliverable	R	Report	X
Dissemination Level	CO	Confidential, only for members of the consortium (including the Commission)	
	PU	Public	X

Index

List of Tables

List of Images

1. Introduction

Buildings are responsible for around 40% of EU final energy demand and for 36% of its greenhouse gas emissions [1, 2]. One strategy to drastically change this impact is by reducing the burning of fossil fuels in the building sector by increasing the use of Renewable Energy Sources (RES), as well as by increasing the role of seasonal and daily heat storage. Solar-based solutions can be used for heating and cooling applications, which can mitigate the main energy loads in a building and change its environmental impact.

However, the use of appropriate heat storage technologies for the maximization of RES penetration is essential due to the stochastic nature of solar energy production systems. The implementation of heat storage would allow for the exploitation and management of any excess energy which would otherwise be lost [3].

There are various solutions for Thermal Energy Storage (TES) which can find application at domestic level: Thermal energy can be stored as a change in the internal energy of a material mainly in the form of sensible or latent heat.
In the first case, i.e. in Sensible Heat Storage (SHS), thermal energy is stored by heating or cooling a liquid or solid such as water, sand, molten salts, or rocks, with water being the cheapest option. In Latent Heat Storage (LHS), heat is mainly stored in the phase-change process of a material (e.g. passing from solid to liquid or vice versa) and is directly connected to the latent heat of the substance [4]. There are also other options in which thermochemical energy or a combination of these forms is stored [5] as presented in Figure 1.

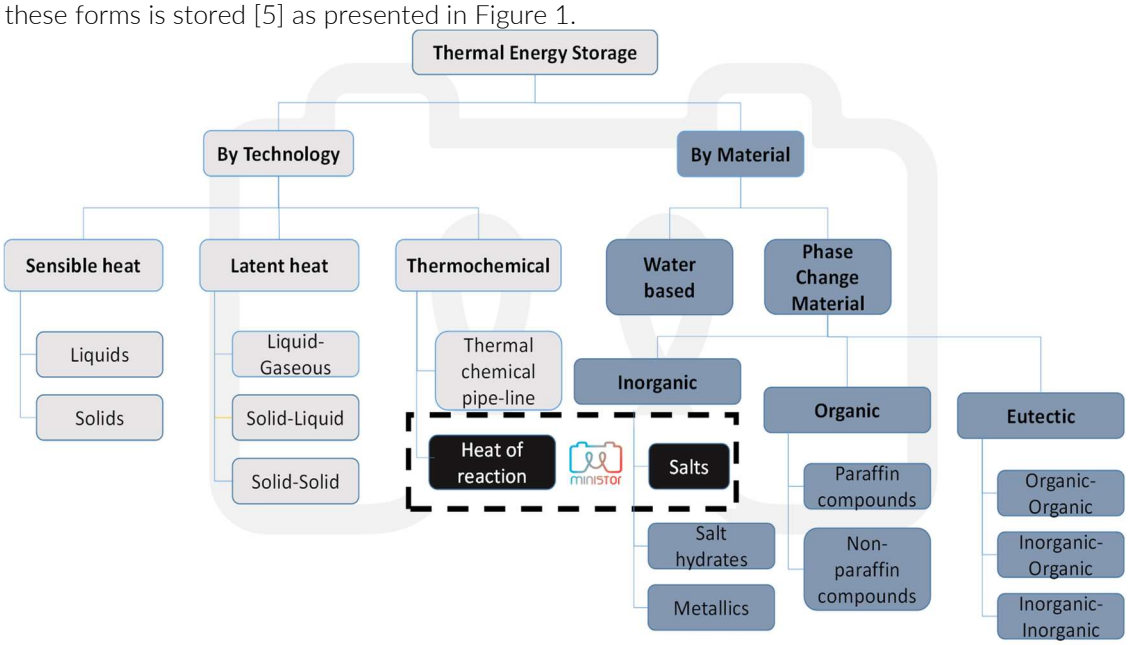

Figure 1: Classification of thermal energy storage systems [5, 6].

Although sensible heat storage is the most common method of thermal energy storage, latent heat storage systems that use Phase Change Materials (PCMs) offer higher energy density compared to water-based storage systems and also have the advantage of the isothermal nature of the storage process, i.e. storing heat compactly in a narrow temperature range [7, 8]. The effect of using PCMs in solar thermal storage systems has been investigated extensively both in experimental and numerical studies [9-15]. The temperature range for these materials can be extremely large. "Low temperature" thermal storage systems (LT-TES), defined for temperatures below 250 °C [16], have been sufficiently developed and are currently used on a commercial level. Companies such as Sunamp Ltd have commercialized applications of high and low temperature PCM-based TES systems in the domestic or industrial scale. The MiniStor project will focus on low temperature systems.

Recently, there has been considerable interest in thermochemical material (TCM) reactor systems for heat storage, particularly in technologies based on solid/gas sorption processes [17, 18]. Among

the various reactants types, ammoniates offer an advantage on heat and mass transfer against hydrates because of the higher pressure levels at which ammoniates/NH_3 working pairs operate [19]. Specifically, ammoniated halide salts are the most attractive sorbents as they are cheap and offer a wide range of thermodynamic properties [20]. CNRS-PROMES has gained a solid expertise on halide salts based thermochemical storage systems at pilot scale, mainly focusing on a $BaCl_2$ – NH_3 cycle for cooling/refrigerant purposes [21-23].

Regarding the working pair of $CaCl_2$-NH_3, there are several studies in the literature. Van der Pal and Critoph [24] performed experimental tests and developed a model for a reactor consisting of 1kg of $CaCl_2$ and 1kg of expanded natural graphite (ENG). Oliveira et al. [25] and Wang et al. [26] developed a $CaCl_2$-based system for refrigeration purposes (ice making). Sakamoto and Yamamoto examined the influence of titanium (Ti) as a heat transfer medium on the reactions' performance [27].

The MiniStor system uses a thermochemical heat storage (TCM) technology based on a $CaCl_2$-NH_3 cycle, utilizing sorption and/or chemical reactions to generate both heat and cooling. As a distinguishing feature, it uses proprietary technology based on ammonia reactions to stabilize the TCM materials and provide long-term operation. The TCM technology is combined with other key components to develop an integrated system capable of providing sustainable heating, cooling and electricity storage, while utilizing renewable energy sources and specifically solar energy.

The scope of this deliverable is the initial dimensioning of the thermal and electrical storage sub-systems of MiniStor, in different locations and usages, leading to a group of virtual prototypes for implementation. More particularly, in order to evaluate the system operation and estimate its key characteristics, the thermodynamic model of the system is developed by CERTH and dynamic simulations are performed in the locations of the project demo sites, i.e. Sopron (Hungary), Cork (Ireland), Kimmeria (Greece) and Santiago (Spain), as well as in the case of Thessaloniki (Greece) pre-pilot, for representative days of the heating and cooling period. Additionally, in the framework of Task 3.1 interaction with Task 3.5, simulations of the yearly operation of the MiniStor electrical sub-system are conducted by CARTIF and EndeF for the cases of Sopron and Thessaloniki and incorporated in D3.1.

The current report has been prepared in the framework of WP3 "Overall System Engineering and Prototyping". Its results will be used as guidelines for the prototyping of peripheral equipment in Task 3.2 "Engineering, installation strategies and prototyping for peripheral equipment" and for applying improvements to the PVT panels (used for supplying heat and electricity to the system) in Tasks 3.3 "Engineering, installation strategies and prototyping for thermal storage system integration with conventional PVT configuration" and 3.4 "Engineering, installation strategies and prototyping for thermal storage system integration with novel PVT configuration". Since the thermal and electrical output of the PVTs are linked to each other, a close interaction with Task 3.5 "Engineering, installation strategies and prototyping for electrical storage system" occurs. Additionally, the information of this document can provide useful input to the activities of WP4 "Design optimization and build-up of the TCM and PCM storage units", WP5 "Automated MiniStor Self-Optimization and Control Management Platform" and WP6 "Demonstration and evaluation".

Useful input for conducting this study originates from Task 2.2 "Survey of European climatic situation, definition of general use typologies and challenges for building characterization", Task 7.1 "MiniStor design evaluation and user behaviour validation through mock-ups and user stories", Task 2.1 "Identification of stakeholder requirements, market needs and barriers for implementation" and Task 2.4 "Characterization of an interoperable and adaptable storage solution, easily integrated with PVT and other local". However, upon the time that this report was prepared only the outcome of Tasks 2.2 and 7.1 was finalized. Therefore, in some cases assumptions based on

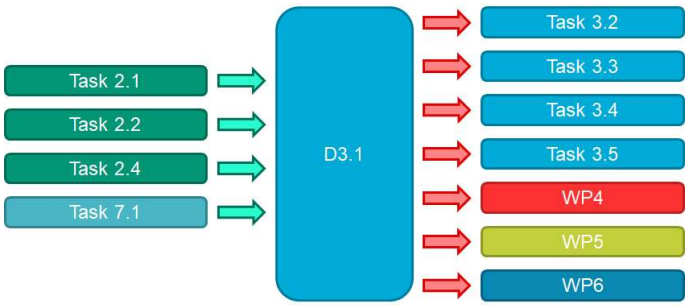

Figure 2: Precedents and dependents of Deliverable 3.1

information provided by the project partners had to be made. Dependences of this task with others in the project is shown in Fig. 2.

2. Description of the MiniStor system

MiniStor is an innovative compact thermal and electrical energy storage system that combines TCM and PCM materials for year-round thermal storage for heating and cooling. It is characterized by a very high energy storage density, over 10.6 times higher than the density of equivalent water-based systems. It also includes an electrical energy storage system and an intelligent energy management system for optimized integration of energy storage in residential buildings. The necessary energy input to MiniStor is provided by various energy systems such as photovoltaic thermal (PVT) panels, solar thermal collectors and Heat Pump (HP), while integration with heat and cold transfer systems for output in HVAC systems is considered

2.1. Main components of the MiniStor system

Section 2.1.1 provides a general overview of the MiniStor system. In Sections 2.1.2 - 2.1.4 the description of the various components of the MiniStor thermal system is carried out. The description of the MiniStor electrical system is included in Section 2.1.5.

2.1.1. Overview of MiniStor system

The main components of the MiniStor system are the following:

- PVT-Solar Collectors and Buffer tank, that provide the necessary heat input to the system
- Thermochemical material reactor TCM, which is the main storage vessel in which energy is stored in the form of chemical energy. It contains ammonia-based salts
- Ammonia cycle - Storage tank, which includes the necessary components of the ammonia refrigeration cycle
- Heat Pump (HP), used for the upgrade of the heat released by the ammonia condensation
- PCM Hot/Cold heat storage modules, which are additional storage vessels of heat and cold
- Battery Energy Storage, used for storing the electrical energy produced by the PVTs
- Heat Pump (HP), located between the PVTs and hot water tank, in the demo site of Santiago

The overall configuration and distribution of the thermal elements is seen in Figure 3.

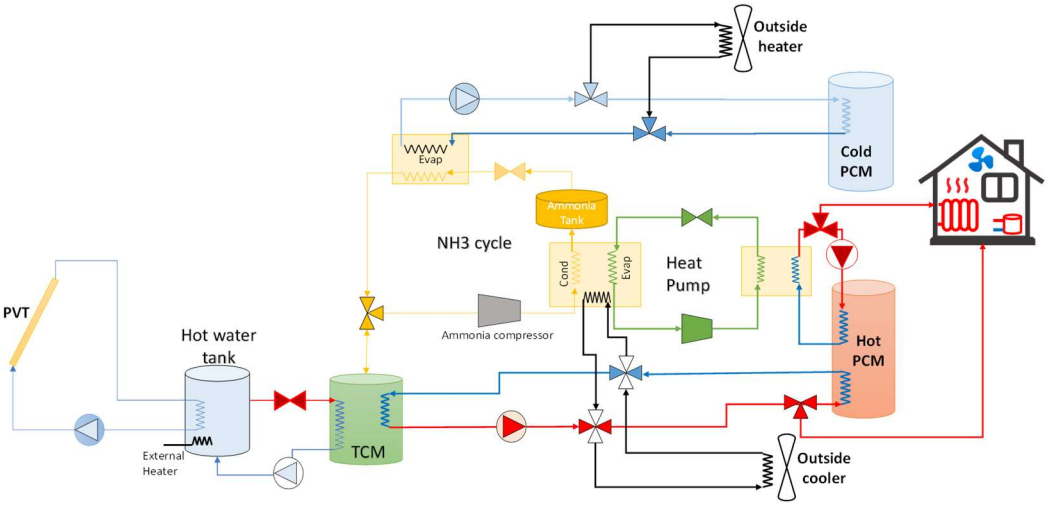

Figure 3: Overview of MiniStor thermal systems components

In the case of the Santiago demo site, an additional heat pump will be installed between the array of PVTs (no solar thermal collectors) and the buffer tank in order to better utilize the electricity generation provided by 20 PVTs. High electrical efficiency PVTs, developed within MiniStor project, will produce the electricity that will drive the extra heat pump's compressor. The aforementioned HP will provide sufficient heat input to the TCM reactor.
The selection of these components is based on the use of solutions that reduce the environmental footprint of existing buildings, for example by utilising solar energy for both electricity and heat and storing it for later use. It is assumed during the calculations that a control system (developed in more detail in WP5) will help manage the complex relationships and signals that need to be sent to the different sub-systems in order to take advantage of grid price signals for electricity, evaluation of human comfort inside the dwelling in order to activate processes in the thermal system or use stored thermal energy, etc. This will result in an increased degree of "smartness" for the buildings where MiniStor is applied, since many of them do not have these energy management systems installed. The estimated energy coverage provided by the system is based on levels where thermal human comfort can be achieved.

These components are combined forming an integrated system that stores heating, cooling and electricity and has the potential to achieve heat energy storage density of over 180 kWh/m^3. The aforementioned key system parts operate jointly as follows:

In the charging phase, the heat coming from the solar field is stored in the thermochemical reactor (TCM) in the form of chemical energy as an endothermic reaction takes place. The ammonia gas stream produced by the reaction is condensed and the heat generated is transferred to the heat pump (HP) for thermal lifting and hot water production. During the discharge phase, the liquid ammonia is evaporated and led to the reactor (TCM) where hot water is produced by the resulting exothermic reaction. In both phases the heat from the produced hot water can be stored in a container with phase change material (Hot PCM) to be utilized through the fan coils system when required by the user.

During the summer season, the operation of the heat pump is not necessary as the thermal needs are limited (charging phase). However, the cooling power produced by the evaporation of ammonia (discharge phase) is utilized for the production of cold water that can be destined for cooling systems. The heat released by the exothermic reaction in this phase can be utilized for other uses such as for the production of domestic hot water (DHW). The cooling power of the produced cold water can be stored in a second container with phase change material (cold PCM) to be utilized through the system of fan coils when required by the user.

2.1.2. Photovoltaic thermal and solar thermal collectors

The MiniStor concept is based on the combination of TCM and PCM materials for achieving high density thermal energy storage. The necessary thermal energy input to the system can be provided by renewable energy systems such as hybrid photovoltaic thermal panels (PVTs), solar thermal collectors (stand-alone or combined with conventional PVs), biomass boilers, HP etc. The basic system design involves the utilization of PVTs as the main system energy source since they present the following advantages:

- Cost-effective utilization of solar energy with overall efficiency exceeding 70% [28]
- Production of both useful heat and electricity at higher rates compared to a combination of conventional PVs and non-hybrid solar thermal collectors of equal sizes and matching combined area [29].

Initially two PVT models produced by EndeF were considered for integration into MiniStor: Ecomesh (Figure 4) and Ecovolt. Both of them consist of high-efficiency monocrystalline silicon cell laminate and an absorber which removes the excess heat through thermally fastened tubes. Water (usually in combination with propylene glycol) is utilized as the heat transfer medium. The main difference between the two models is that Ecomesh incorporates an innovative transparent insulating cover (glazed panel) developed and patented by EndeF (CTA technology) which reduces the heat losses. This feature, combined with a copper absorber results in a stagnation temperature of approximately 150 ^{o}C and energy generation conversion rates up to 70%. On the contrary, the Ecovolt panel lacks

an insulating cover (unglazed panel), utilizes a roll-bond of aluminium as a heat recovery and presents a stagnation temperature of 80ºC. Therefore, it is more suitable for hot climates and combines a more compact design than Ecomesh with increased electricity output.

In the framework of MiniStor project, EndeF further improved the characteristics of the current models by introducing several improvements. For example, changes in the PV laminate and the adhesive placed between the laminate and the absorber. It will also adapt individual components of the panels in order to maximize energy performance and optimize them for integration to the whole system. EndeF's new Prototype 2 PVT will be installed in the Santiago's demo site. The aforementioned PVT has a higher electrical efficiency than that of Ecomesh and Ecovolt. For the purpose of the initial dimensioning of the MiniStor system, the characteristics of the currently available PVT models, depicted in Table 1 are taken into account.

	Ecomesh	Ecovolt	PVT Prototype 2
General features			
Dimensions, L x W x T (m)	1.645 x 0.978 x 0.093 (+ 0.025)	1.640 x 0.992 x 0.400	1.719 x 1.140 x 0.035
Aperture area (m)	1.55	1.55	1.96
Type	Glazed	Unglazed	Unglazed
Thermal specifications			
Absorber	Copper	Aluminum	Aluminum
Fluid content (lt)	1.2	0.88	0.47
Fluid flow rate (kg / m^2h)	30 - 50	30 - 50	30 - 50
Optical efficiency ηo (-)	0.51	0.472	0.405
Heat loss coefficient, α_1 (W/m^2K)	4.93	9.50	8.52
Heat loss coefficient, α_2 (W/m^2K^2)	0.021	0.00	-
Coefficient B_u (s/m)	-	-	0.0175
Coefficient b_2 (Ws/m^3K)	-	-	0.275
Electric specifications (STC conditions)			
Maximum Power (W)	260	300	390
Voltage at maximum power point (V)	31.65	32.50	38.50
Current at maximum power point (A)	8.06	9.25	10.13
Open circuit voltage (V)	38.58	38.80	46.30
Short circuit current (A)	9.06	9.85	10.87

Table 1: Main specifications of the Ecomesh, Ecovolt and Prototype 2 hybrid PVT panels

Figure 4: Installation of Ecomesh PVT panels [30]

In the course of the current investigation, it was revealed that although the PVTs can provide sufficient heat throughout the year for regular residential applications (i.e. DHW production), they cannot deliver the required amount of energy and at the constant high temperatures needed by the TCM reactor during winter. As mentioned in paragraph 2.1.3 a TCM reactor as the examined one, with 17.5 kWh capacity requires an equal amount of heat at a temperature of 56°C for the activation of all the involved reactions. Therefore, in order to increase the energy supply to the MiniStor system and achieve the required temperature, various combinations of PVTs with solar thermal collectors were considered.

The most common type of solar thermal collector is the flat plate collector (FPC). Their structure is quite simple as they consist of a solar energy absorbing plate and tubes, passages or channels attached to the absorber in which the heat transfer medium flows (Figure 5). Transparent covers of the absorber as well as back insulation layers reduce the convective and radiative heat losses [31] Flat plate collectors achieve high energy conversion efficiency as they use both beam and diffuse solar radiation [32] and require no tracking of the sun [31]. Another type of solar thermal collector is the evacuated tube collector (ETC). In this configuration the absorber consists of several long, narrow segments with selective surface coating. Each segment along with the attached tubes are placed within evacuated glass envelopes. The main advantage of this configuration is that the low-pressure conditions inside the glass envelopes result in a considerable reduction of convective heat losses [32]. Inside the tubes, the heat transfer medium undergoes an evaporating – condensing cycle which results in higher efficiencies of ETCs compared to FPCs at temperatures higher than 80°C [31].

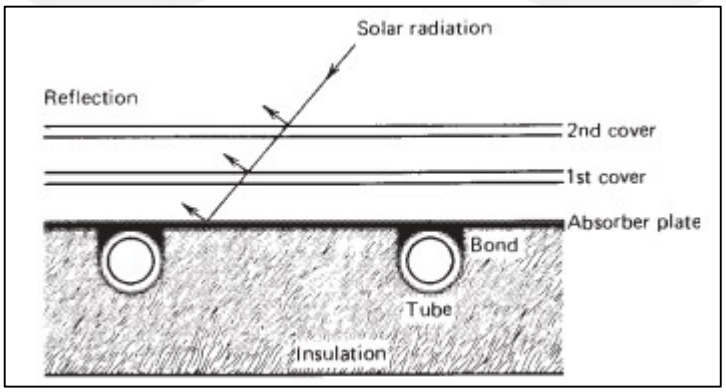

Figure 5: Structure of a flat plate collector [32]

Commercially available FPC and ETC models were also considered in order to contrast the power output values. Their main specifications are depicted in Table 2. However, preliminary simulations presented in paragraph 3.1.2 showed that differences in terms of thermal output between the two designs are very small. Therefore, in the final configuration only combinations of PVTs with FPCs

are included, as the latter have simpler construction, lower maintenance requirements and lower cost than ETCs.

	Considered FPC model		Considered ETC model
Model	FMAX 2.4	FMAX 2.0	
Dimensions L x W x T (m)	1.230 x 1.930 x 0.086	1.010 x 1.980 x 0.086	1.053 x 2.241 x 0.150
Gross area (m^2)	2.37	2	2.36
Absorber area (m^2)	2.23	1.87	1.51
Thermal specifications			
Fluid content (lt)	1.7	1.4	0.87
Fluid flow rate (kg / m^2h) *	20 - 40		20 - 40
Optical efficiency, η_0 (-) **	0.823		0.51
Heat loss coefficient, α_1 (W/m^2K) **	3.36		1.192
Heat loss coefficient, α_2 (W/m^2K^2) **	0.013		0.004
	* values applying to absorber area, ** values applying to gross area		

Table 2: Main specifications of the considered flat plate and evacuated tube collectors

Moreover, in the proposed configuration a water tank is incorporated. Water tanks are considered as the simpler means of storing energy in the form of water sensible heat and are widely used in solar thermal applications. However, the purpose of their inclusion in the MiniStor is not to act as a storage component but as a buffer one. The TCM requirement for heat input at high temperature (above 56°C) makes necessary the incorporation of an automation system that will measure the collectors' water output temperature and control the operation of the water recirculation pump accordingly.

Since the collectors' outlet temperature is affected by many parameters of stochastic nature (solar radiation, outdoor temperature, wind speed etc.), utilizing this quantity as a measurement variable of the control system would result in oscillating control signals and consequently in an intermittent heat supply to the TCM unit. By placing a water tank between the collectors and the TCM, the circuit water quantity and consequently its heat capacity are increased. Furthermore, this additional quantity is located within an insulated vessel and thus is less affected by changes of environmental variables. Therefore, the utilization of the water tank temperature for controlling the hot water supply to the TCM leads to a stable heat provision to the latter.

The tank is an ideal location for placing a back-up heater, i.e. a system that can provide additional heat in cases when the collectors can warm the water up to a certain temperature but not as high as the required one. In this way, a considerable amount of solar energy that would otherwise would not have been taken into account can be utilized and cover a significant portion of the heat supply to the TCM unit. By using a back-up heater, the number of days when MiniStor can store heat energy are increased, leading to higher system cost-effectiveness and reduced investment payback periods.

Water tanks used in solar thermal applications have sizes that range from 50L up to several m^3. The size selected in the current study is the outcome of a parametric investigation presented in Section 5.1. The loop connecting the collectors with the tank can be either closed or open. In the first case, the working mediums of the collectors and the tank are different, they are not in direct contact and exchange heat through a heat exchanger usually placed inside the tank. However, in this project an open loop is considered, i.e. there is no heat exchanger between the collectors and the tank and the heat transfer fluid can flow between them. The same pattern is also taken into account for the

circuit connecting the tank with the TCM reactor, as the exclusion of intermediate heat exchangers enhances the heat transfer efficiency between the various system components.

Finally, several systems can be used as back-up heaters such as electrical heaters, gas heaters and even heat-pumps with low energy consumption. The electrical heaters are reliable, low-cost solutions which can be placed inside or outside and after the buffer tank. Therefore, they are selected as the auxiliary heating system in the cases of Sopron and Thessaloniki. In the case of Cork, a gas heater located after the tank can be used instead, as a gas boiler is the main existing heating device of the building. In Kimmeria, the current hybrid heating system combines an extensive solar thermal park with a biomass boiler, so there is no need for additional back-up options. This is also done with the aim to show the integration of MiniStor into existing home heating systems.

2.1.3. Reactor for thermochemical materials and ammonia cycle

MiniStor's key system component is the Thermochemical Material (TCM) reactor which is a solid-gas sorption process unit for effective and high-density heat energy storage. Thermo-chemical processes can serve for mid – long term energy storage with negligible heat losses [33], for several applications such as solar air conditioning [21], long-term storage of solar energy [34] or cooling and heating [35]. Several of these systems are ammonia-based [36].

The thermochemical sorption process is based on a reversible chemical reaction between a reactive solid ($CaCl_2$) and a liquid/gas phase change refrigerant (NH_3). Thermochemical heat storage material (TCM) is used in the form of salt i.e. $CaCl_2$*$4NH_3$. Coupling ammonia with calcium chloride to form calcium chloride complexes, is attractive for application in heat pumps as these complexes produce a lot of heat per kg adsorbed sorbate but also absorb a considerable higher amount of sorbate per kg of sorbent, compared to absorbents as zeolites[24].

The principle of thermochemical reaction processes is based on the thermal effect of the following reversible reactions:

$$CaCl_2 \cdot 8NH_3 + Heat \leftrightarrow CaCl_2 \cdot 4NH_3 + 4NH_3 \quad (2.1)$$

$$CaCl_2 \cdot 4NH_3 + Heat \leftrightarrow CaCl_2 \cdot 2NH_3 + 2NH_3 \quad (2.2)$$

During charging phase, the thermochemical reactor exploits the heat input and releases a gaseous ammonia stream according to the endothermic decomposition reactions mentioned above. As mentioned in paragraph 2.1.2, in the basic system configuration a combination of PVTs with solar thermal collectors (FPCs) is used to provide the necessary heat. When the solar energy is not enough to allow the reaction to take place, an electrical heater is used for the elevation of the water circuit temperature. In that way it is ensured that the targeted energy density is obtained, thus the 1st reaction is performed for temperatures above 44 °C and the 2nd reaction for temperatures above 56 °C due to the different reaction rates for the operating pressure of 2 bar and at within 44-70°C for the pressure of 3 bar. For obtaining the targeted energy density of 213 kWh/m^3 the advancement rates of the 1st and the 2nd reaction have to be 95% and 46% respectively. However, the introduction of the back-up heater occurs at the expense of the total efficiency of the system which is significantly reduced.

The regeneration takes place within a temperature range of 44-70 °C and under pressure of 2-3 bar (the latter is imposed by the compressor minimum operating pressure ratio). The produced gaseous NH_3 stream is then compressed at 11/16 bar by a semi-hermetic compressor, and afterwards condensed at 11 bar/28 °C or 16 bar/40°C. The ammonia compression is a necessary procedure, as even in cases of PVT heat supply at high temperatures the corresponding equilibrium pressure inside the reactor is steady at 2-3 bar. The compression of gaseous ammonia up to 11/16 bar allows for a reasonable condensing temperature of 28/40 °C to be achieved. After the condensation ammonia is being stored in a tank.

Discharging mode takes place mainly in summer and winter nights. Liquid ammonia is evaporated at temperatures imposed by the ambient conditions, provided that the reactor equilibrium pressure is lower than the evaporation one. When gaseous ammonia enters the reactor, the following exothermic reaction is occurring:

$$CaCl_2 \cdot 4NH_3 + 4NH_3 \leftrightarrow CaCl_2 \cdot 8NH_3 + Heat \quad (2.3)$$

$$CaCl_2 \cdot 2NH_3 + 2NH_3 \leftrightarrow CaCl_2 \cdot 4NH_3 + Heat \quad (2.4)$$

The ammonia evaporation at temperatures around 0-10 °C results in a corresponding evaporation pressure of 4-6 bar. This leads to a released heat from the TCM reactor at a temperature of 57-63°C. The heat produced from the TCM synthesis mode can be stored in the hot PCM or directly used for the covering the heating loads of the building. In the case of summer, where cooling demands exist, liquid ammonia is converted into gaseous form in the evaporator at 0-10 °C and 4-6 bar. In this way, the heat generated in the evaporator is exploited and can be utilized for the cold PCM or directly cover the cooling demands of the building.

The thermochemical reactor is composed of 7 tubed with a length of 1.25 m each and diameter of 114.3 mm, filled in such a way to form 2 sub-reactors.

- 3 tubes connected together: 7 kWh
- 4 tubes connected together: 9.3 kWh
- 6 tubes connected together: 14kWh
- 7 tubes connected together: 16.3 or 17.5 kWh based on the considered 2nd reaction rate of 0.32 or 0.46
- 9 tubes connected together: 21 kWh
- 10 tubes connected together: 23.3 kWh
- 13 tubes connected together: 30.3 kWh

With this configuration, it is possible to modulate the storage capacity to the available solar resource by using independently in the same TCM module 3, 4, 6, 7, 9, 10 or 13 tubes. The following table summarizes the size characteristics of the reactor:

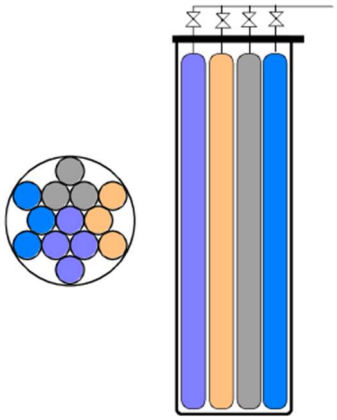

Figure 6: TCM reactor tube configuration

Volume of reactive compound (7 tubes)	82 lt
Mass of salt	35.5kg
Mass of graphite	6.2 kg
Mass of compound	41.7 kg
Total length of tube reactor (7 tubes)	8.82 m with a diameter of 114.3 mm
Cycled ammonia mass	23.7 kg
Total Mass of cycled ammonia	32 kg

Table 3 : Proposed TCM reactor sizing

2.1.4. Heat Pump and Phase Change Material vessels

A Heat Pump (HP) unit is utilised for the energy elevation of the released heat at the ammonia condenser from 28°C up to 63°C. A closed water circuit is employed for the transmission of the condensation heat to the Heat Pump evaporator. The heat pump uses R410A as a refrigerant medium. The heat pump operates according to a standard refrigerant cycle, in which heat from the water circuit (NH_3 Condenser-Heat Pump Evaporator) is transferred to the refrigerant in the evaporator, which is evaporated at 21°C/14 bar and then compressed at 42 bar in the compressor. The compressed, evaporated refrigerant in then condensed to liquid in the condenser, which operates at 64°C/42 bar, delivering heat to the hot PCM or directly used for the heating demands of the house. The heat pump cycle closes as the high-pressure liquid refrigerant is expanded to a lower pressure through the expansion valve. Under these operating conditions the heat pump COP is estimated at 3.61. During summer period, heat release from the Heat Pump condenser can be used for domestic hot water (DHW) heating.

The heating/cooling energy storage system includes also two Phase-Change Material (PCM) tanks that store heat and cool at 58°C (Hot PCM) and 11°C (Cold PCM), respectively. The Hot PCM is connected with both the TCM reactor and the Heat Pump via the independent water circuits for

the heat storage charging and discharging operation mode, respectively. Its main role is to store the excess heat generated either during the decomposition mode (through the Heat Pump condenser) or during the TCM synthesis mode (direct water connection circuit with TCM) providing this energy to the house when it is needed. The Cold PCM is exclusively connected to the evaporator of ammonia through a chilled water circuit. Its main role is to store the excess cooling capacity, which is generated during the discharging operating mode from the evaporator of ammonia at 0-10°C. Consequently, the role of Hot and Cold PCMs is to work supportively to the whole system, but their charging should be carefully scheduled as they must be at least partially charged to cover the peaks of the heating – cooling demands of the building.

2.1.5. Battery Energy Storage System and electrical subcomponents

The PVT electrical system converts, distributes, and stores the electricity produced by the PVT panels. To perform these functions, the system is provided with the following main components: (i) the hybrid solar inverter, (ii) the electrical storage system, based on lithium-ion batteries, (iii) the electrical panel, and the wiring.

In general, the storage of electricity, supplied by the PVT panels, in the lithium-ion batteries is managed by the solar hybrid inverter, depending on the electrical demand of the MiniStor thermal system and the building, and according to the surplus in the electrical production.

The detailed design of the PVT electrical system is part of Task 3.3 and Task 3.5 of the project[1], in the context of which, Deliverables D3.4 (Design and Integration of improved PVT electrical generation system) and D3.8 (Design of the electrical storage system) will be prepared. However, as an interaction of Task 3.5 with Task 3.1, the present Deliverable (D3.1), includes a summary of the principal characteristics of the main system components.

a) Solar Hybrid Inverter

Within the framework of the MiniStor project, the hybrid solar inverter has two main functions: it converts the electricity produced by the PVT panels from DC to AC, and it manages the electricity flows in the system, in order to send the production to the electrical storage system (lithium-ion batteries) or to use it directly in the building and the MiniStor Thermal System.

Since the facilities of the MiniStor project are connected to the external electrical grid, the hybrid solar inverter meets the technical requirements for the grid connection, among which are:

- Limitation and protection against over-voltages
- Impossibility of operating as an electrical island
- Synchronization with the electrical grid, in voltage (+/- 8%), frequency (+/- 0.1Hz) and phase (+/- 10%)
- Limitation of direct current (DC) injection in the AC electrical grid, and harmonic generation rates within the ranges admitted by the electrical grid operator.
- Possibility of charging or discharging the electrical batteries, from the photovoltaic generator, or from the electrical network.
- Possibility of exporting surplus of PV production (AC) to the external electrical grid, with a complementary smart meter[2].

The inverter also manages or regulates the charging-discharging process of the electrical storage system (lithium-ion electrical batteries) within the operating parameters admitted by the electrical batteries technologies. Both batteries and inverter must be compatible for their interconnection.
The inverters selected for the MiniStor project correspond to the hybrid solar inverter models, manufactured by the Austrian company Fronius. The technical characteristics of these inverter models are summarized in Table 4. Fronius is widely consolidated in the current European market and its hybrid solar inverters offer connection compatibility with two of the most advanced global lithium-ion technology battery brands that will be considered for electrical energy storage (BYD and LG Chem).

[1] *Engineering, installation strategies and prototyping for electrical storage system*

[2] *This characteristic should be implemented only in case that local electricity regulations allow the injection of surpluses into the external electrical grid.*

Technical data	Fronius Symo Hybrid	Fronius Symo GEN24 Plus	Fronius Primo GEN24 Plus
Single-phase / three-phase	three-phase 230 / 400 V	three-phase 230 / 400 V	single-phase 230 V
Power classes	3 / 4 / 5 kW	6 / 8 / 10 kW	3 /3.6 / 4 / 4.6 / 5 / 6 kW
MPP-Trackers	1	2	2
Protection class	IP65	IP 66	IP 66
Dimensions (h x w x d)	645 x 631 x 204 mm	594 x 527 x 165 mm	528 x 474 x 164 mm
Weight [kg]	19.9 kg	25 kg	16,6 kg
DC input voltage range [V]	150 V - 1000 V	80 V - 1.000 V	65 V - 600 V
Maxim efficiency [%]	97.7 / 97.9 / 97.9 %	98.2 %	97.6%
European efficiency [%]	95.2 / 95.7 / 96 %	97.7 / 95.8 / 97.9 %	96.8 / 97 / 97.1 / 97.2 / 97.2 / 97.1 %
WLAN / Ethernet LAN	Modbus TCP	Modbus TCP	Modbus TCP
Interface to battery and meter	Modbus RTU (RS485)	Modbus RTU (RS485)	Modbus RTU (RS485)
Availability	Available before 2020 (Current Model)	Available in 2020 (New Model)	Available in 2021 (New Model)

Table 4: Main technical characteristics of the solar hybrid inverters

b) Electrical storage system: lithium-ion Batteries

Surplus of electricity produced by the PVT panels will be stored in the electrical energy storage system (EES), which consists of electrochemical accumulators or electrical batteries, with lithium-ion technology.

Electric storage using electrical batteries, is still concentrated in the industrial market, which represents about 20% of the global market, mainly using lead-acid battery technology [37]. However, lithium-ion technology batteries have gained importance in the last five years, especially in the electric vehicle sector, followed by the grid-connected building sector.

Currently, there are different lithium-ion battery technologies available on the market, such as LFP (Lithium-Iron-Phosphate) and NMC (Nickel-Manganese and Cobalt). They have different benefits in terms of energy density, depth of discharge, safety, cost and useful life. LFP technology is spreading more in the European market, while NMC technology in the North American market. The behaviour in the cycling process (charge-discharge) varies when comparing the different technologies. For example, LFP technology supports a greater depth of discharge, and also offers better performance in terms of safety and useful life. NMC technology, on the other hand, has a higher energy density and lower cost, but supports a lower depth of discharge and has more limitations in terms of safety.

The batteries selected for the MiniStor system use LFP technology, specifically the high-voltage lithium-ion battery model HVS, manufactured by BYD. BYD-brand batteries, in addition to incorporating LFP technology, also offer compatibility with a wider range of inverters from different manufacturers, including Fronius, Goodwe ET, Ingeteam, Kostal and SMA. Regarding the use of batteries, the inverters, that offer greater functionalities to the end-users, correspond to Fronius and Kostal brands. These batteries models have a round-trip efficiency higher than 96%, and they can support a maximum Depth of Discharge (DOD) of 90%. The most relevant technical characteristics of these batteries are summarized in Table 5.

Taking into account the available solar radiation, the size of the hybrid solar field, and the electricity demand profiles of the Demo sites of the MiniStor project, the batteries will have a storage capacity between 5.12 and 7.68 kWh. However, the final sizing of the batteries will be carried out within the framework of Task 3.5 of the MiniStor project.

Model	Nº Modules*	Nominal Storage Capacity [kWh]	Voltage Range [V]	Nominal Voltage [V]	Max Output Current [A]	Dimensions (H/W/D) [mm]	Weight [kg]
BYD - HVS 5.1	2	5.12	160~240	204	25	712x585x298	91
BYD-HVS 7.7	3	7.68	240~360	307	25	945x585x298	129
BYD-HVS 10.2	4	10.24	320~480	409	25	1178x585x298	167
BYD-HVS 12.8	5	12.8	400~600	512	25	1411x585x298	205

Table 5: Main technical characteristics of lithium-ion batteries

**Module HVS: 2.76 kWh, 51.2 V, 38 kg.*

c) Electrical panel and wiring

The main function of the electrical panel of the hybrid solar installation will be to house the DC protections for the electrical DC lines that come from the hybrid solar field to the inverter, as well, the AC protections for the line between the inverter and the AC load side. Likewise, this electrical panel will content the electrical protections for complementary elements of the thermal circuit of the PVT, including the solar circulation pump and the air-dissipator.

Both the DC and AC cables must comply with European and local regulations. For the DC wiring will be used cables with a suitable coating for outdoor installation, assigned voltage 1000 V, type H1Z2Z2-K with 4 mm^2 copper, according to EN50618, or with equivalent local technical characteristics.

2.2. Operational modes of the MiniStor system

2.2.1. Winter mode operation

In winter period, the MiniStor system can provide the house with heat at temperature of 63 ˚C either via the heat pump condenser during the charging mode, or through the TCM reactor during discharging mode.

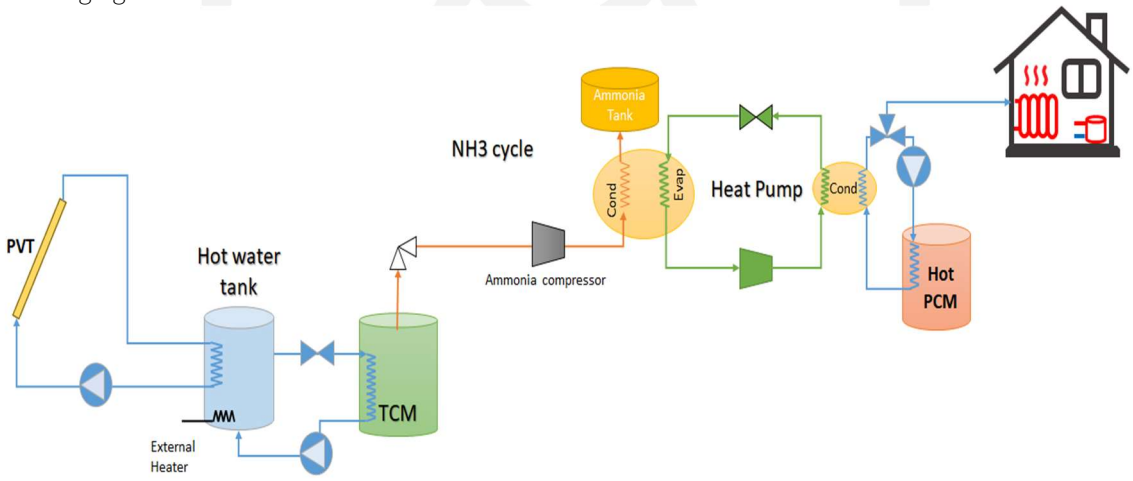

Figure 7: A generic demonstration of the winter operation mode of MiniStor system (decomposition)

During the charging mode, the required heat for the salts' desorption is derived from a hot water that is heated from the PVTs (or other solar thermal collectors supplemented by an electrical resistor (back-up heater) when the solar driven heat is not sufficient. This provided heat to the TCM reactor, results in reactor pressure increase and production of gaseous ammonia according to the endothermic decomposition reaction (Equations 2.1 and 2.2). In the Santiago demo site, a new PVT

prototype will be installed which has improved electrical characteristics. Due to the absence of the backup heater in this demo site, a more energy efficient heat pump (Hitachi Yutaki S80 air-water) will be installed, and its use will be supported by the electrical production of the PVT array.
The gaseous ammonia is then compressed, condensed and stored in a tank. Ammonia compression is a necessary procedure of this configuration, as the corresponding equilibrium pressure inside the reactor is quite low at 2 bar. This in turn results in condensing temperatures lower than 0°C, making the condensation heat rejection practically impossible. The compression of gaseous ammonia up to 11 bar allows for a reasonable condensing temperature of 28°C to be achieved. During winter, the condensation heat is then elevated by the heat pump up to 63°C and can be either stored in the hot PCM vessel or directly used for the coverage of the heating demands of the building.

Discharging mode is expected to occur in summer and winter nights as well as in cloudy winter days. The liquid ammonia stored in the tank, flows into the evaporator and evaporates at a temperature imposed by the ambient conditions, provided that the reactor equilibrium pressure is lower than the evaporation one. Then the gaseous ammonia flows into the reactor where the exothermic synthesis reaction takes place (Equation 2.3 and 2.4).

The ammonia evaporation is taking place at a low temperature such as 0-10^{o}C results in a corresponding evaporation pressure of 4-6 bar respectively. This in turn leads to a heat release from the TCM reactor at a temperature of 57-63^{o}C. Thus, the heat of the exothermic reactor can be stored in the hot PCM or directly used for the coverage of the heating demand of the building.

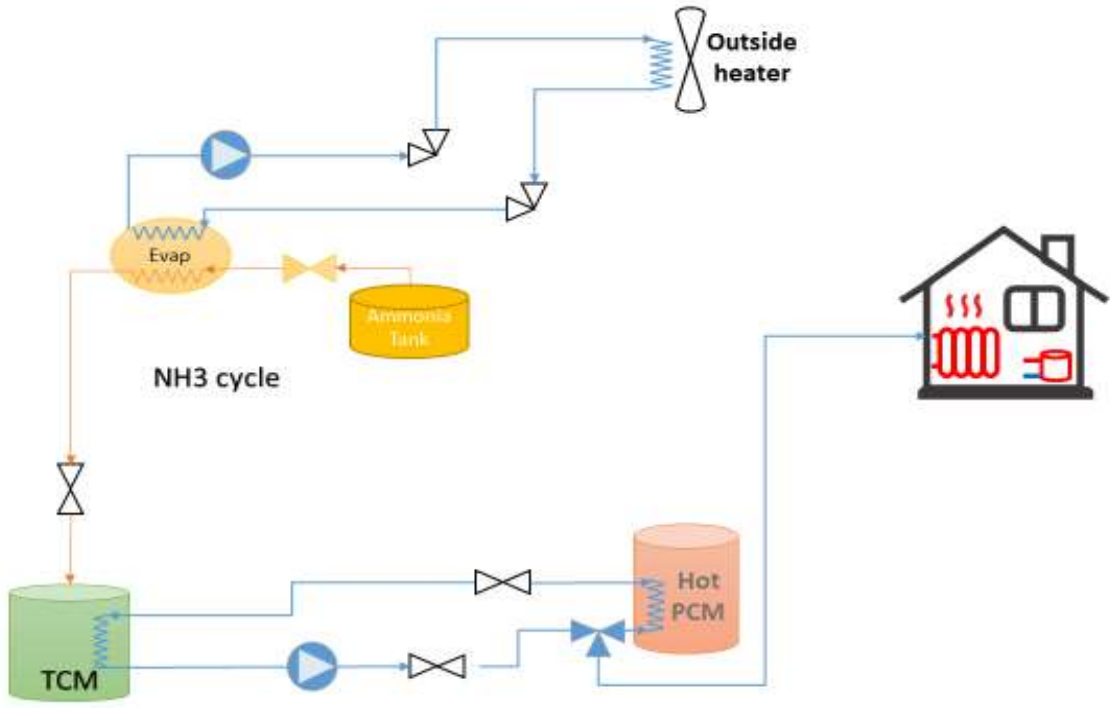

Figure 8: A generic demonstration of the winter operation mode of MiniStor system (composition)

2.2.2. Summer mode operation

During the summer period, the MiniStor system can provide the house with cold only via the utilization of the ammonia evaporation cooling load during the discharging phase. In this case, the cooling capacity from the ammonia evaporation is stored in the cold PCM characterized by a given melting temperature (around 11°C). Additionally, the heat produced from the TCM synthesis reaction can be released to the ambient or used for DHW production.

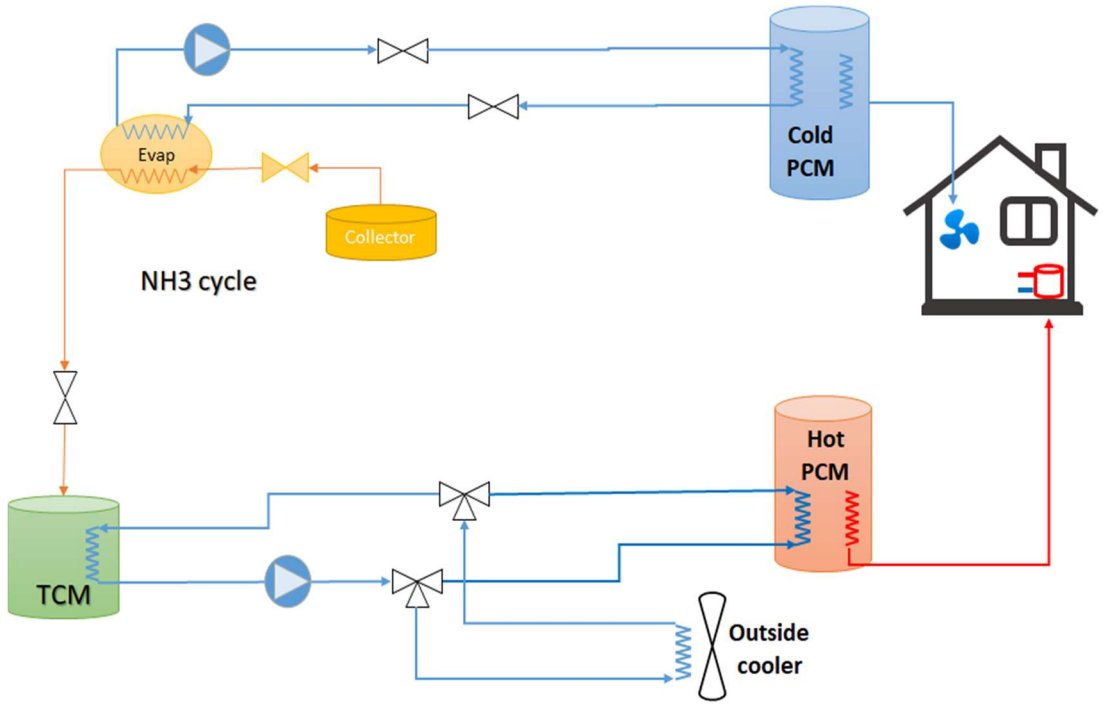

Figure 9: A generic demonstration of the summer operation mode of MiniStor system (synthesis)

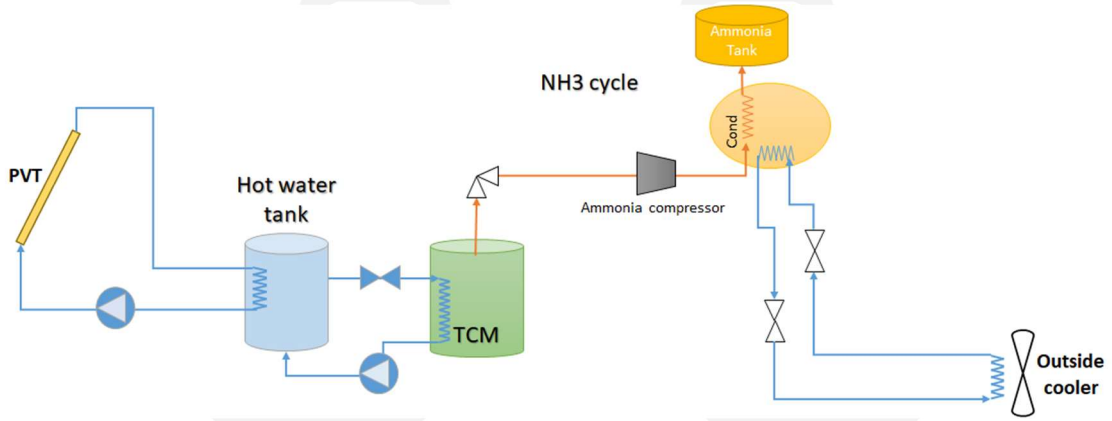

Figure 10: A generic demonstration of the summer operation mode of MiniStor system (decomposition)

3. Integrated Modelling of the MiniStor system

3.1. Photovoltaic thermal and solar thermal collectors' sub-model for thermal output

3.1.1. Methodology for modelling solar collectors for thermal output

During the last decade, many studies have been conducted with the purpose of examining PVT performance using both numerical and experimental means. In the majority of them, the numerical investigation of PVTs operation has been implemented through the use of commercial modelling tools for transient systems. Kalogirou and Tripanagnostopoulos [38] analysed the performance of two experimental hybrid PVT solar systems which were modelled in TRNSYS program by using built-in models. Del Amo et al. [39] designed a new PVT system for covering the DHW requirements of multi-housing buildings. The performance of the developed system was simulated in TRNSYS and the results were validated against monitoring data. The Type 560 TESS component library for TRNSYS was used for modelling the hybrid panels, but first its validity was checked by using test bench data. In another study, Liang et al. [40] used TRNSYS in order to predict the yearly operation of a novel solar heating system based on PVTs. The latter were modelled by using TRNSYS Type 50 component library. The same module was utilized by Buonomano et al. [41] in order to numerically evaluate and compare the performance and economic feasibility of PVTs against conventional PVs in TRNSYS. This tool was also selected by Magalhaes et al. [42] for analysing stagnation in photovoltaic thermal systems and evaluating possible solutions. However, instead of using built-in modules the authors developed a new model. The latter was based on the equations describing the quasi-dynamic test method according to the EN 12975-2:2006 standard. Finally, in a recent study Jonas et al. [43] proposed a novel PVT collector performance model based on the quasi-dynamic method of ISO 9806 combined with a PV performance model for the electrical energy output. The thermal performance model, for which two approaches were explored (two-node with one or two thermal capacities), was implemented in TRNSYS Type 832, whereas the PV performance model in TRNSYS Type 835. The comparison with experimental data revealed the better accuracy of the two node – one thermal capacity approach.

Despite the advantages of commercial modelling tools, the evaluation of novel PVT systems requires the development of in-house numerical codes. Touafek et al. [44] proposed a PVT collector with a novel absorber configuration of tube and sheet galvanized steel. Its performance was numerically investigated with an in-house developed code. Gao et al. [45] proposed a novel PVT collector with both PV/water-heating and PV/air-heating operating modes. The performance of this new model was numerically calculated and validated with experimental results. Furthermore, for the evaluation of hybrid photovoltaic-thermal / solar assisted heat pumps several models have been proposed in the past for modelling the PVT operation [46-49].

In the present study, a simplified version of the model presented in [43] and especially the two-node thermal capacity approach is implemented in the MATLAB / Simulink environment. According to this method the PVT performance can be described by two nodes, one calculating the thermal output of the collector and the other computing the electrical energy generation. For the thermal energy output estimation, an effective specific heat capacity c_{eff} that combines the capacities of the fluid, the absorber and all the other layers of the collector (i.e. insulation, frame etc.) is taken into account. Therefore, the energy balance of the thermal node at each time can be described by the following differential equation:

$$c_{eff}\frac{dT_m}{dt} = q_{rad} - q_{loss} - q_{th} \quad (3.1)$$

, where T_m represents the mean fluid temperature in the thermal node, q_{rad} is the specific energy gain due to radiation, q_{loss} the specific thermal losses due to convection and conduction with the ambient air and q_{th} the specific heat transfer from the collector to the fluid. The latter can be expressed as a function of the mean fluid temperature as below:

$$q_{th} = \frac{\dot{m}\cdot c_{p,f}\cdot 2(T_m - T_{in})}{A_{PVT}} \quad (3.2)$$

In the above equation T_{in} is the inlet fluid temperature in the collector, $\dot{m}$ and $c_{p,f}$ the fluid mass flow rate and specific heat capacity respectively and A_{PVT} the area of the collector. The specific energy gain of the node due to radiation is defined as a function of the collector optical efficiency η_0 as following:

$$q_{rad} = \eta_o \cdot (K_b \cdot G_b + K_d \cdot G_d) \quad (3.3)$$

In the above formula, G_b and G_d are the beam and diffuse radiation on the collector surface respectively, whereas K_b and K_d are the corresponding incident angle modifiers (IAM). The specific thermal losses are defined as below:

$$q_{loss} = \alpha_1 \cdot (T_m - T_\alpha) + \alpha_2 \cdot (T_m - T_\alpha)^2 \quad (3.4)$$

In the previous equation T_α is the outdoor temperature, α_1 is the collector heat loss coefficient and α_2 describes the latter dependence on temperature. These two factors are also mentioned in paragraph 2.1.2 and in combination with the optical efficiency are used for defining the collector efficiency curve [39].

Equation 3 can be further extended by including the long wave radiation exchange and the corresponding losses as well as a correction of the optical efficiency depending on the wind speed. The same applies also to equation 4, where a term describing the dependence of the heat loss coefficient from the wind speed can be added. However, as will be presented further below the utilization of the simplified form of the equations yields accurate results. By introducing equations 3.2, 3.3 and 3.4 into equation 3.1 the latter is transformed as following:

$$c_{eff} \frac{dT_m}{dt} = \eta_o \cdot (K_b \cdot G_b + K_d \cdot G_d) - \alpha_1 \cdot (T_m - T_\alpha) - \alpha_2 \cdot (T_m - T_\alpha)^2 - \frac{\dot{m} \cdot c_{p,f} \cdot 2(T_m - T_{in})}{A_{PVT}} \quad (3.5)$$

Thus, the mean and consequently the outlet fluid temperature can be computed. For calculating the electrical output of the PVT, the estimation of the cell temperature T_{cell} is necessary. This is done by assuming that the thermal and electrical nodes of the collector are connected with an internal heat transfer coefficient U_{PVT}. The cell temperature can be calculated as a function of the mean fluid temperature and the specific heat transfer between the collector and the fluid:

$$T_{cell} = T_m + \frac{q_{th}}{U_{PVT}} \quad (3.6)$$

Although not used in the system electrical modelling, the MATLAB subroutine incorporates the ability to compute the electrical output of a PVT or PV panel. The solar cell is represented by a simplified equivalent circuit of a current source in parallel with a diode and a series resistance R_S. A temperature dependence of the photocurrent I_L and of the diode saturation current I_0 is considered. The main equations of the model are the following [50]:

$$I = I_L - I_0 \cdot \left(e^{q(V+IR_S)/nkT_{cell}} - 1\right) \quad (3.7)$$

$$I_L = \frac{G}{G_{nom}} \cdot I_{SC(T1,nom)} \cdot \left(1 + K_0\left(T_{cell} - T_{cell,1}\right)\right) \quad (3.8)$$

$$I_0 = I_{0(T_{cell,1})} \cdot \left(T_{cell}/T_{cell,1}\right)^{3/n} \cdot e^{-qV_g/nk \cdot (1/T_{cell} - 1/T_{cell,1})} \quad (3.9)$$

In the previous formulas q is the charge of an electron, n is the ideal factor that depends on the panel technology, k is the Boltzmann constant, G is the solar radiation on the cell surface and G_{nom} the same variable under nominal conditions, I_{SC} the short circuit current, K_0 is the temperature coefficient of the short circuit current and V_g the band gap of the cell. It is obvious that the value of short circuit current under nominal radiation and at a specific cell temperature is necessary in order to utilize the presented model. These nominal conditions usually coincide with the Standard Test Conditions (STC) of PV panels. In the end, equation 3.7 enables the determination of both cell current and voltage, the product of which yields the cell electrical power output.

In the case of Flat Plate or Evacuated Tube Collectors (FPCs or ETCs) equations 3.1-3.5 can be utilized without any change in order to estimate the collector energy balance and the resulting mean fluid temperature. This is because of the similar principle that PVTs and FPCs / ETCs share regarding the heat extraction, described in paragraph 2.1.2. However, special attention must be paid to the

correct use of the collector efficiency constants (optical efficiency η_0, heat loss coefficients α_1 & α_2) since they might refer to different area types (aperture area, gross area).

For the initial dimensioning of the system, an open loop between the collectors, the tank and the TCM is considered, i.e. there is no heat exchanger between these components and the heat transfer fluid can flow directly from the collectors to the tank and from the latter to the TCM reactor. In all scenarios and regardless of the tank size, a low degree stratification is taken into account by considering two tank nodes. The hot fluid from the collectors is directed to the warmer top node, whereas it flows back to the collectors from the colder bottom node. The flow to and from the TCM unit presents the opposite pattern, i.e. hot water from the top node reaches the TCM and after the heat exchange returns to the bottom node. A representation of the modelled loop configuration is depicted in the figure below.

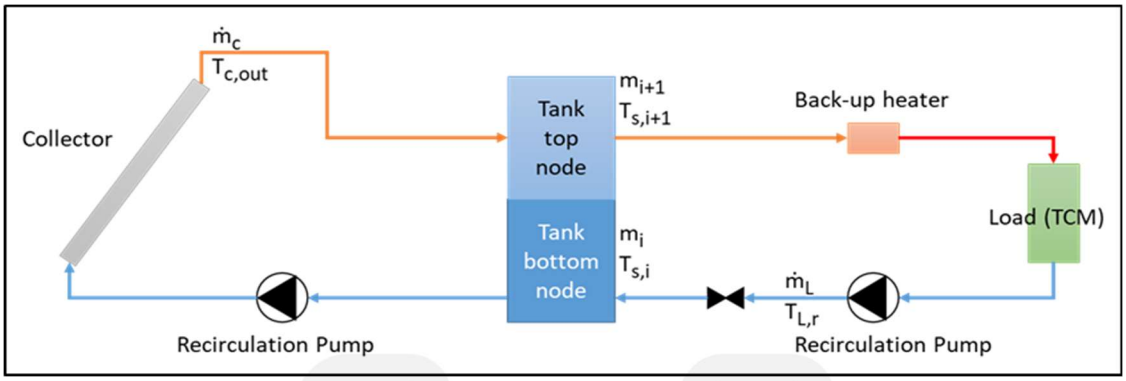

Figure 11: Schematic diagram of the PVT model loop configuration

The temperature $T_{s,i}$ of the fluid in the i^{th} node of the tank at each time step is calculated by the following differential equation [32]:

$$m_i \frac{dT_{s,i}}{dt} = \left(\frac{UA}{C_p}\right)_i \cdot (T_a - T_{s,i}) + f_{c,i} \cdot \dot{m}_c \cdot (T_{c,out} - T_{s,i}) + f_{L,i} \cdot \dot{m}_L (T_{L,r} - T_{s,i}) + f_{m,i} \cdot \dot{m}_{i,i+1} \cdot (T_{s,i} - T_{s,i+1}) \quad (3.10)$$

In the above formula m_i and C_{pi} represent the working medium mass and specific heat capacity in the i^{th} node respectively. The first term of the equation right leg denotes the node heat losses to the environment and the variables U_i and A_i are the node heat loss coefficient and exposed area correspondingly. The second term represents the heat exchange with the fluid exiting the collectors, which has a mass flow rate m_C and a temperature $T_{C,OUT}$. The third term of the right leg calculates the heat exchange with the fluid returning from the load, i.e. the TCM reactor, which presents a mass flow rate m_L and a temperature T_{LR}. The variables $f_{C,i}$ and $f_{L,i}$ are coefficients with values ranging from 0 to 1, that control the heat exchange between the collectors and the node, and between the latter and the TCM vessel respectively. Finally, the last term represents the heat exchange between the two tank nodes due to mass transfer and coefficient $f_{m,i}$ denotes the direction of this mass flow.

Regarding the fluid flow control in the open loop, a strategy common in solar thermal applications is adopted. More specifically, the pump that circulates the working medium between the collectors and the tank is activated when the difference between the collectors' outlet temperature and the temperature of the tank bottom zone is greater than 5°C. As the colder fluid from the tank enters the collectors, its outlet temperature gradually decreases. The recirculation pump stops when the temperature difference drops below 2°C.

3.1.2. Validation

In order to verify the reliability of the results produced by the developed PVT model, yearly simulations are performed for the locations of Sopron and Thessaloniki. Their outcome is compared with the results of calculations performed with TRNSYS commercial software. The examined scenarios concern different arrangements of PVTs that heat the water of a storage tank. An open-loop circuit between the collectors and the buffer tank is considered, whereas the later consists of two nodes. No discharge from the tank is considered, thus the water tank temperature decreases

only due to heat losses to the environment. Weather data of Meteonorm Typical Meteorological Year (TMY) of both locations is used. Table 6 summarizes the main parameters of the examined cases.

Parameter	Scenario 1	Scenario 2
Location	Sopron	Thessaloniki
Number of PVTs	21 (arranged in 3 rows in series of 7 panels each)	3 (connected in series)
PVTs azimuth angle (deg.)	15	75
PVTs tilt angle (deg.)	35	18
Mass flow rate per panel(kg / m^2h)	73.8	73.8
Mass flow rate of open loop (kg / h)	831.6	118.8
Tank capacity (lt)	50	50

Table 6: Main parameters of the scenarios considered for the MATLAB PVT model validation

The computed tank node temperatures from both MATLAB and TRNSYS over one year period are presented in Figure 12 and Figure 13 for Scenario 1 and in Figure 14 and Figure 15 for Scenario 2. The main remarks from their analysis are summarized in Table 7. Apart from the annual results, the model outputs in each month are analysed separately in order to ensure the model credibility regardless of the imposed weather conditions. February and July are depicted as representative months of winter and summer respectively. In general, the annual average temperature differences in both tank nodes are approximately 4-6%, but different patterns are observed in each scenario. More particularly, MATLAB yields lower tank temperatures in Scenario 1 and higher values in Scenario 2. A parameter that has significant effect on the obtained results is the collector effective heat capacity (Equation 3.1). Although its value can be quite accurately estimated taking into account the panel structure, it should further be adjusted in order to consider components such as pipes that are included in TRNSYS model. Thus, its final value – common in both simulations – is the result of a parametric investigation.

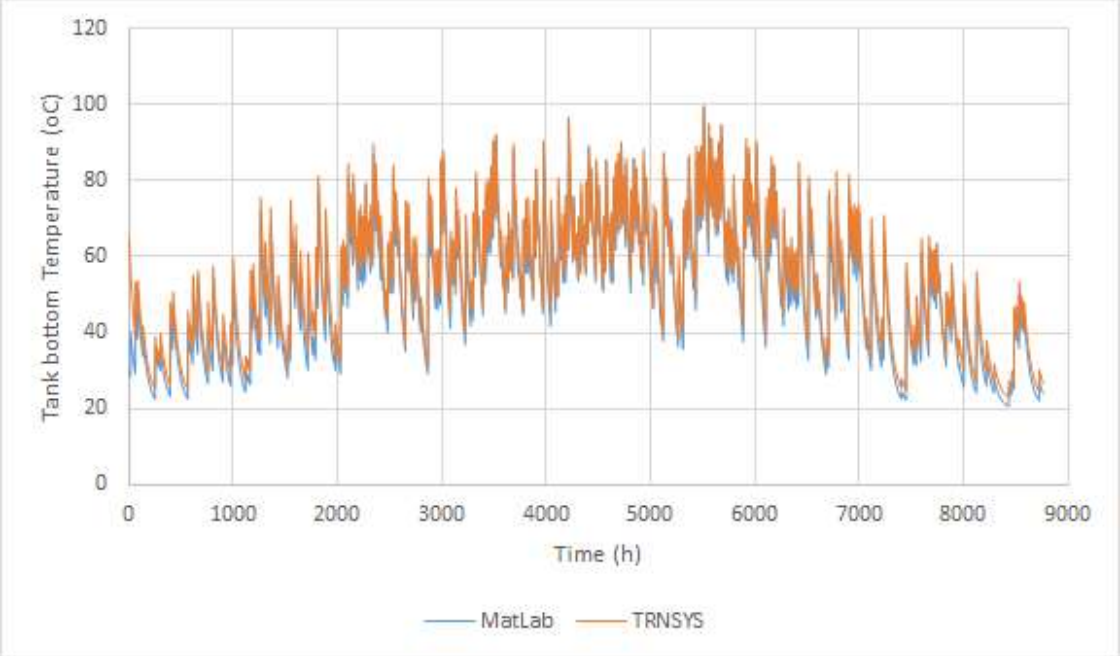

Figure 12: MATLAB and TRNSYS annual results regarding the tank bottom temperature – Scenario 1

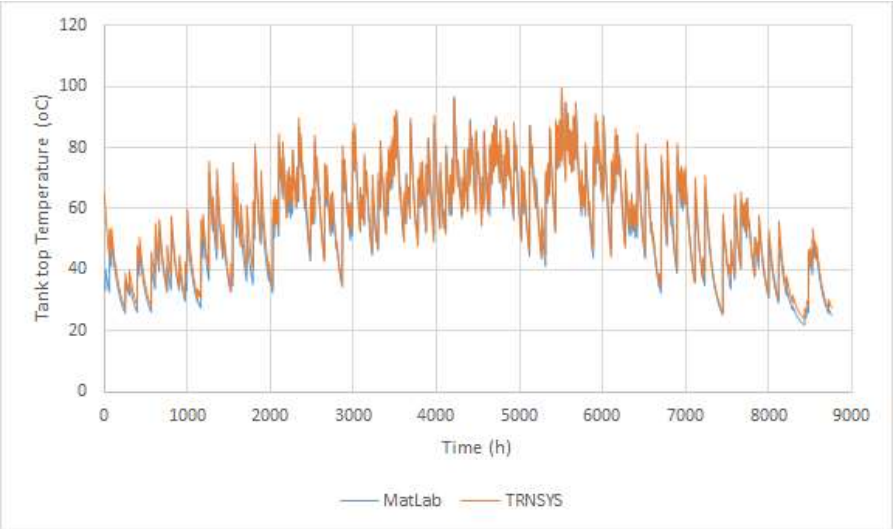

Figure 13: MATLAB and TRNSYS annual results regarding the tank top temperature – Scenario 1

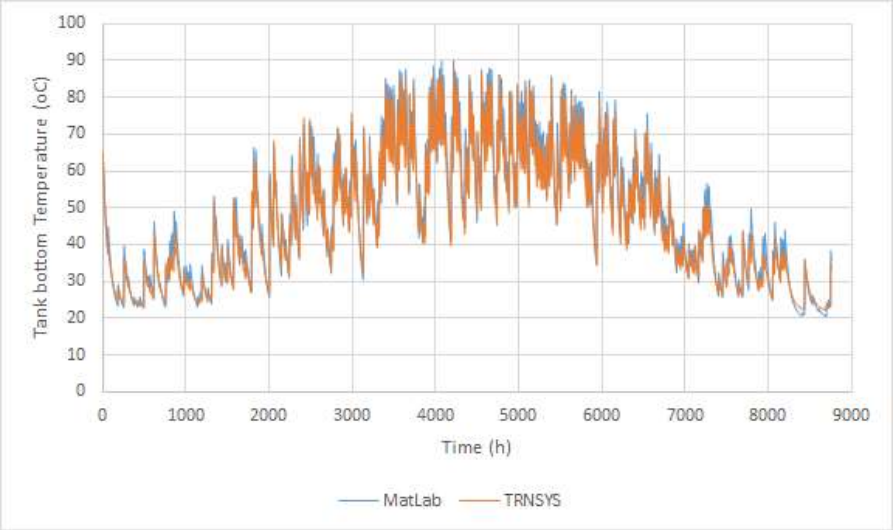

Figure 14: MATLAB and TRNSYS annual results regarding the tank bottom temperature – Scenario 2

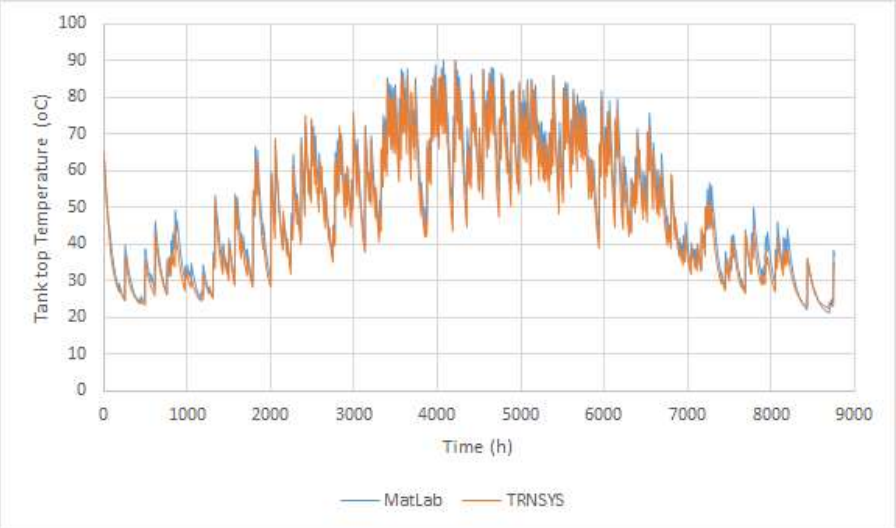

Figure 15: MATLAB and TRNSYS annual results regarding the tank top temperature – Scenario 2

Scenario	Average differences in bottom node temperature	Average differences in top node temperature
Scenario 1 (Sopron)		
Annual	6%	4%
February	10%	7%
July	3%	2%
Scenario 2 (Thessaloniki)		
Annual	5%	6%
February	5%	8%
July	4%	6%

Table 7: Average differences in tank temperature between MATLAB and TRNSYS results

In conclusion, since the mean temperature differences on a monthly basis do not exceed 10%, it can be deduced that the MATLAB model can provide accurate results and therefore can be incorporated in the MiniStor thermodynamic model. A future development could be its more thorough validation against experimental data that will be obtained during the project implementation in each demo site location.

3.1.3. Investigation of PVTs combination with Flat Plate and Evacuated Tube Collectors

The second scenario of the previous study, i.e. the configuration of 3 PVTs connected in series and located in Thessaloniki, is selected so as to estimate the potential effect of FPCs and Evacuated Tube Collectors (ETCs) on the heat delivered to the buffer tank and consequently to the TCM vessel. In this investigation the third PVT is substituted by either a FPC or an ETC. The performance of each configuration is calculated over one-year period with the MATLAB PVT model. Two tank sizes, 50L and 200L are considered, whereas the open loop mass flow rate is equal to 112.7 kg/h. The results of this parametric study are presented in Table 8. Furthermore, indicative results are displayed in Figure 16 and Figure 17.

	Average differences in bottom node temperature	Average differences in top node temperature
FPC Scenario		
Annual, Tank 50L	+17%	+18%
February, Tank 50L	+18%	+19%
Annual, Tank 200L	+18%	+18%
February, Tank 200L	+18%	+19%
ETC Scenario		
Annual, Tank 50L	+21%	+21%
February, Tank 50L	+23%	+23%
Annual, Tank 200L	+20%	+20%
February, Tank 200L	+20%	+20%

Table 8: Average differences of tank temperature between FPC (2PVTs + 1FPC), ETC (2 PVTs + 1 ETC) and reference scenario (3 PVTs)

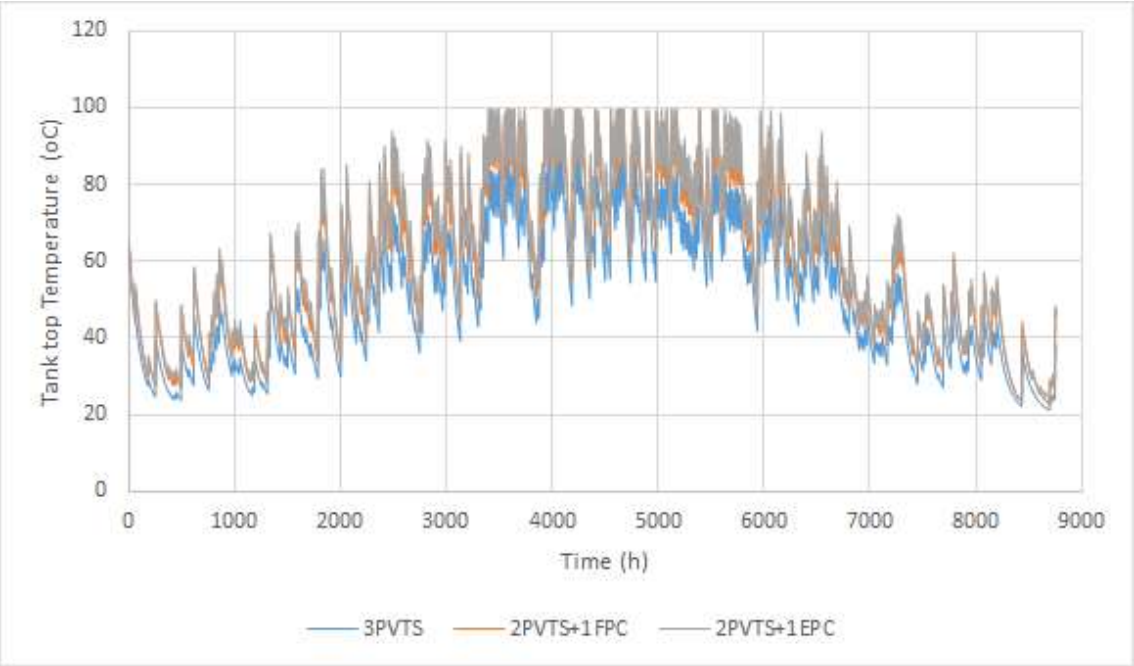

Figure 16: MATLAB annual results regarding the tank top temperature of PVTs and solar thermal collectors' combinations (Tank size 50L)

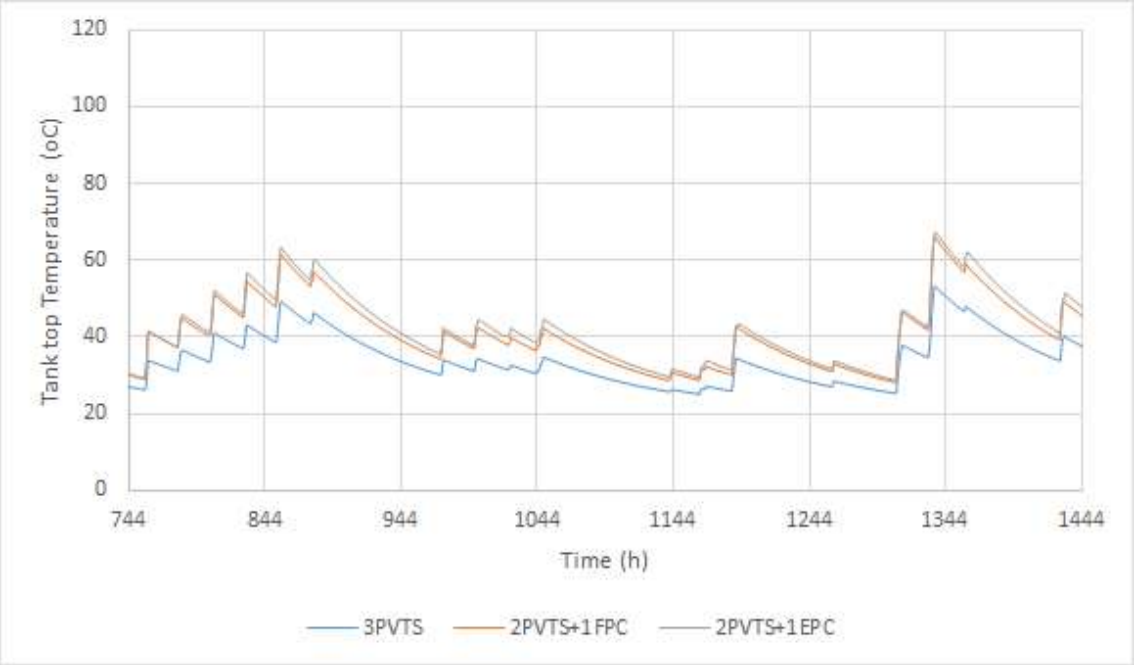

Figure 17: MATLAB results during February regarding the tank top temperature of PVTs and solar thermal collectors' combinations (Tank size 50L)

From the presented results it is evident that the substitution of one row of PVTs with solar thermal collectors leads to a considerable increase of water tank temperatures regardless of the tank size. In particular, the incorporation of a FPC causes a temperature rise by 17-18% annually and by 18-19% in February compared to the only PVTs configuration. Similarly, the introduction of an ETC leads to a temperature increase by 20-21% annually and 20-23% in February. Because of the small differences between the thermal outputs of the examined solar thermal collector designs, in the final system configuration only combinations of PVTs with FPCs are included, as the latter are simpler structures and have lower maintenance requirements and cost than ETCs.

3.1.4. Heat pump Integration between the PVT array and the buffer tank

A simplified Heat Pump model has been developed in MATLAB and integrated afterwards into Simulink. This model represents the commercial Hitachi, Yutaki S80 4 Air-Water HP, which includes an exterior and interior unit and is to be combined with unglazed PVTs with high electricity output for the case of Santiago de Compostela demo site. The nominal capacity and COP of the aforementioned HP is 11 kW and 5 respectively. The HP will be placed between the solar PVT array and the buffer tank.

Regarding the fluctuation of the power consumption, the thermal capacity of the HP condenser and the COP in respect to the ambient temperature and the outlet heated water temperature, four tables with relevant information provided by the HP manufacturer (Hitachi) were used. These datasets concern nominal operating conditions with an output water mass flow of 1260 kg/h. The referred ambient temperature has a range from -20 up to +20 °C with a variable step and the outlet water temperature a range between 20-80 °C with a 5 °C step. In order to incorporate these data into the model and afterwards implement the latter into Simulink, a simplified look up table's method is adopted, which requires a steady step of the variables. To overcome this barrier the tables were first introduced into Matlab where their values were interpolated ending in a very high number of pair values, namely 1000x1000 in relation to the previous one of 13x10 of the tables. The interpolation was realised using the ''griddata'' Matlab function with the linear method. Some indicative comparative figures of the interpolated and the original tables are presented below.

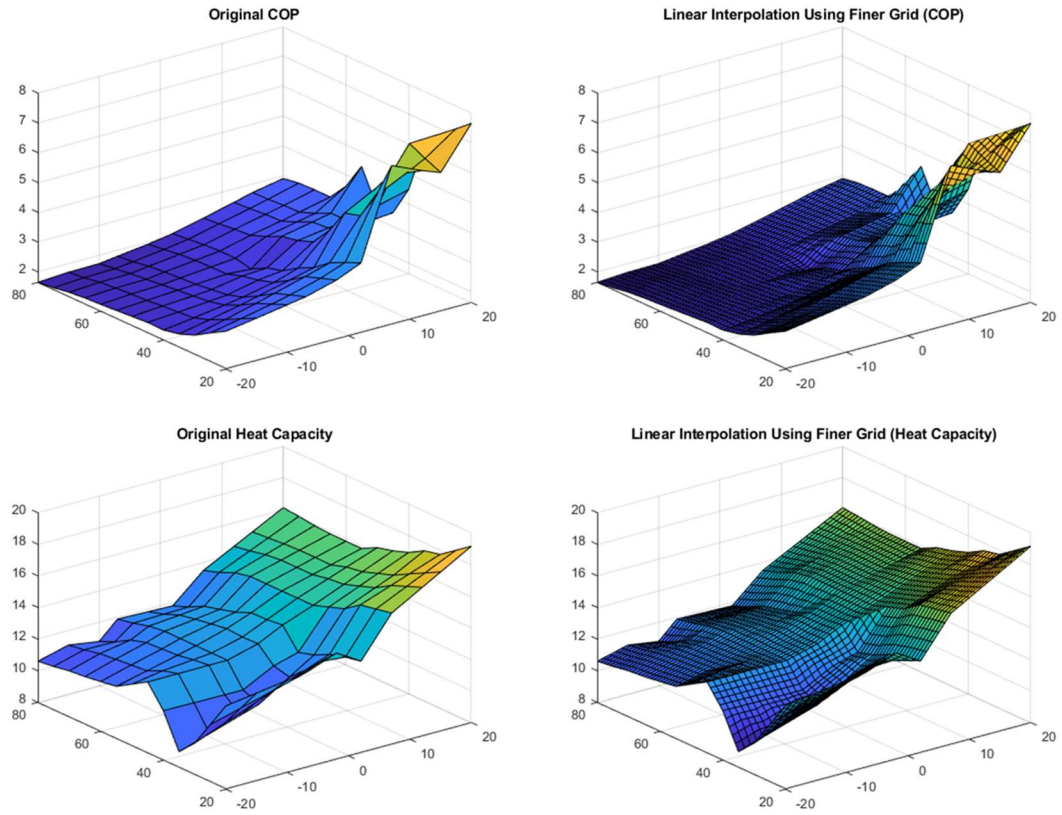

Figure 18: Comparative figures of the Hitachi's HP COP and Heat capacity linear interpolated tables

In order to integrate the aforementioned table into the Simulink model one more table has to be generated, the input temperature table to the HP from the buffer tank. The condenser's heat capacity equation can be expressed as:

$$Q_{HP\ Condenser} = m_{nomW} * Cp_{water}(T_{wat.out} - T_{wat.in}) \quad (3.11)$$

where m_{nomW} is the mass flow of the water (Kg/s), Cp_{water} is the value of the specific heat capacity of the water medium (J kg^{-1} K^{-1}), $T_{wat.out}$ is the temperature of the water at the exit of the condenser and $T_{wat.in}$ is the temperature of water as it exits the buffer tank and enter the HP condenser. Therefore the inlet temperature is associated with the heat capacity of the condenser, so using the rearranged version of the above equation the aforementioned table can be calculated. The equation can be expressed as:

$$T_{wat.in} = T_{wat.out} - \left(\frac{Q_{HP\ Condenser}}{m_{nomW} * Cp_{water}}\right) \quad (3.12)$$

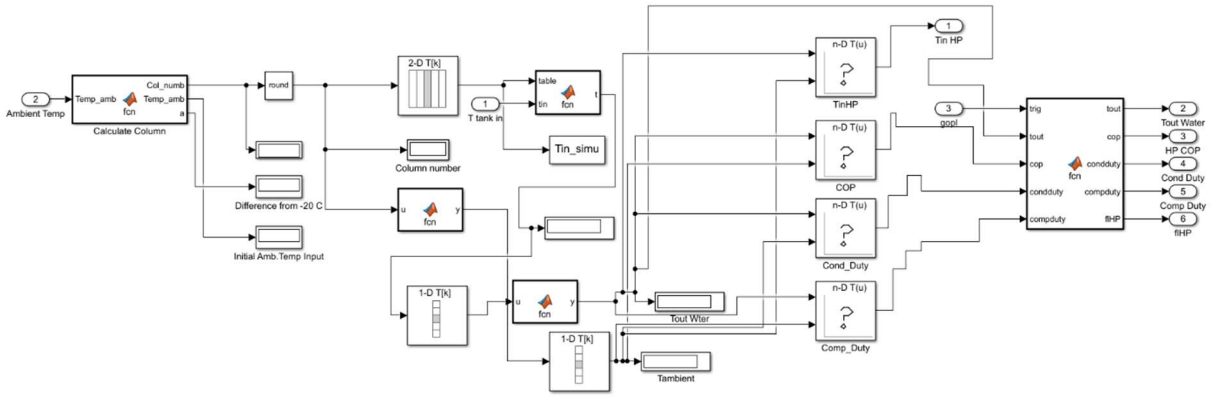

Figure 19: Hitachi HP model in Simulink

The Hitachi HP model is implemented into Simulink as presented in the figure above. The model consists of three main inputs, the exit temperature of the buffer tank, the ambient temperature and the trigger that activates the submodel. The outputs of the HP are four: the outlet water temperature, the condenser heat capacity, the compressor electrical consumption and the COP of the HP. Finally, it must be clarified that for ambient temperatures above 20 °C, the COP, heat capacity and compressor duty remain the same as the 20 °C values, no extrapolation beyond these values has taken place.

3.2. Modelling of the thermochemical materials Reactor

3.2.1. Modelling in Aspen Plus

Within the framework of the MiniStor project, a TCM reactor model has been developed using the commercial software ASPEN PLUS and ASPEN PLUS DYNAMICS. The concept was to accurately calculate the time that the reactions will take place as well as the corresponding heat duty that will be needed (in the decomposition mode) or will be released (in the synthesis mode). Since the compounds databank of Aspen Plus includes all the $CaCl_2$ based salts that appear in the TCM reactor during the decomposition and synthesis phase, they could not be used as they are due to the fact that solid is an invalid phase in Aspen Plus Dynamics. To overcome this barrier, three user-defined hypothetical components that appear only in the MIXED substream (i.e. fluid) were developed based on the main properties of the three salts. Although they are modelled as fluids, the properties of the real salts that were taken into consideration are the following:

- Properties as heat capacity (Cp) and density (ρ) remain constant at any temperature
- The components appear only in liquid phase. This is achieved by setting the vapour pressure of the salts based on the extended Antoine equation equal to zero or $lnp_i^{*,l} = -\infty$
- The enthalpy (ΔH_{form}) and free Gibbs energy of formation (ΔG_{form}) that are necessary for the reactor simulation are calculated based on the ΔH and ΔS of the engaged reactions:

$CaCl_2$*$2NH_3$ + $2NH_3$ → $CaCl_2$*$4NH_3$, Δ H= 42145 kJ/kmol, Δ S= 229.5 kJ/kmolK

$CaCl_2$*$4NH_3$ + $4NH_3$ → $CaCl_2$*$8NH_3$, Δ H= 42433 kJ/kmol, Δ S= 235.4 kJ/kmolK

The physical properties that were inserted in the Aspen Properties sheet are shown in the following table.

Salt		$CaCl_2$*$2NH_3$	$CaCl_2$*$4NH_3$	$CaCl_2$*$8NH_3$
MW	kg/kmol	145.045	179.106	247.228
Cp	J/kg K	1034	1284	1294
ρ	kg/m^3	1606.26	1388.42	1194.34
ΔH_{form}	J/kmol	-9.4982E+08	-1.1255E+09	-1.4782E+09
ΔG_{form}	J/kmol	-1.0832E+09	-1.2623E+09	-1.7588E+09

Table 9: Main properties of the user defined $CaCl_2$ based salts

A continuous stirred tank reactor was decided to be used for the simulation of the thermochemical material reactor. The RCSTR model can account for transient heat transfer between the process gas and the refractory walls. In addition, due to the limitations of Aspen Dynamics to process solids, RCSTR was the only reactor without continuous flow and by refeeding the reactor with its liquid pseudo-salt product, we simulate as close as possible the behaviour of the stationary solid $CaCl_2$ salt. Therefore, the dynamic fidelity of the RCSTR should be better than that of the other types of reactors that exist in the Aspen Plus model palette. The two operational modes of the TCM reactor (Decomposition and Synthesis) were developed each in a separate model.

Equilibrium reactions can be used in the RCSTR model in Aspen Plus, but kinetic reactions are required in Aspen Dynamics. Reaction kinetics formulas were used based on inputs from CNRS work. Aspen plus is very restrictive in the units permitted for overall reaction rates and concentrations. Overall reaction rates must be in kmol s^{-1} m^{-3} if reactor volume is the basis. Reaction rates formulas with the required units for ASPEN PLUS (kmol s^{-1}) were provided by CNRS and can be expressed as:

$$\frac{dX1}{dt} = \frac{Uw_{int} * Aw_{tcm}}{v1 * DH_{r1}} \left(\mathrm{Tw_{tcm}} - \mathrm{T_{eq1(P_{tcm})}} \right) \quad (3.11)$$

$$\frac{dX2}{dt} = \frac{Uw_{int} * Aw_{tcm}}{v2 * DH_{r2}} \left(\mathrm{Tw_{tcm}} - \mathrm{T_{eq2(P_{tcm})}} \right) \quad (3.12)$$

where Uw_{int} is the heat transfer coefficient of internals inside the reactor (equal to 100 W/m^2K), Aw_{tcm} is the surface area of the reactor, $v1$ and $v2$ are the stoichiometric coefficients of the reactions (4 and 2 respectively), DH_{r1} and DH_{r2} are the enthalpy values of the reactions, $\mathrm{Tw_{tcm}}$ is the temperature of the refractory wall and $\mathrm{T_{eq(P_{tcm})}}$ is the measured pressure – temperature relation in comparison with the theoretical correlation based on the Claussius-Clapeyron equation with the DS and DH data for the reactions as shown in Table 9.The Claussius-Clapeyron equation is:

$$P = P_0 e^{-\frac{DH}{RT}} \quad (3.13)$$

Therefore, a temperature associated with the reactor pressure in equilibrium for respectively CaCl2(8-4) NH3 and CaCl2(4-2) NH3 reactions can been calculated using a rearranged version of the above equation:

$$T = \frac{DH}{DS - R1 \frac{P}{P_0}} \quad (3.14)$$

Both equations for the calculation of the reaction rates take into account the TCM reactor temperature and pressure, so the default Aspen kinetic formulas cannot be utilized in this case. Custom User FORTRAN subroutine was the best option not only for using the exact above formulas but also because FORTRAN kinetics subroutines can be exported and used into Aspen Dynamics. The same equations 3.11 and 3.12 were included into both Decomposition and Synthesis models.

The aim of the steady state models developed in Aspen Plus was to create the appropriate conditions for the model so that when it is exported into Aspen Plus Dynamics, we can handle it appropriately. The key goal that has to be achieved in the steady state model is for the temperature

and the pressure inside the reactor to remain at levels at which no reaction will take place. The main difference between the two models is the number of feed streams. Decomposition model has only one feed stream and synthesis model has two feed streams as seen in tables below. TCM reactors were initially dimensioned for 17.5 kWh of thermal energy. The component composition of the liquid feed stream in the TCM synthesis reactor has been taken from the final composition of the decomposition reaction, having obtained the targeted energy density of 213 kWh/m^3.

TCM Decomposition Model	
Temperature (°C)	32
Pressure (bar)	1
Mass flow rate (kg/h)	100
Vapour fraction	0
Components Composition	$CaCl_2$-$8NH_3$

Table 10: TCM decomposition model feed stream inputs (Steady state models)

TCM Synthesis Model		
Temperature (°C)	-	58
Pressure (bar)	6.5	2
Mass flow rate (kg/h)	10	300
Vapour Fraction	1	0
Components Composition	NH_3	1. 7% - $CaCl_2$-$8NH_3$ 2. 55% - $CaCl_2$-$4NH_3$ 38% - $CaCl_2$-$2NH_3$

Table 11: TCM synthesis model feed streams inputs (Steady state model)

Initial inputs and operating condition of the reactor are showed in the following table.

	TCM Decomposition Model	TCM Synthesis Model
Reactor Operating condition		
Temperature (°C)	34	55
Pressure (bar)	1	1.8
Volume (m^3)	0.17	0.17
Dynamic operating inputs		
Vessel type	Vertical – Flat	Vertical – Flat
Heat transfer option	LMTD	LMTD
Medium inlet temperature (°C)	65	55
Temperature approach (K)	5	5
Catalyst		
Catalyst loading (kg)	3.6	3.6
Particle density (kg/m^3)	15	15
Valid Phase (Holdup)	Vapour – Liquid	

Table 12: Initial inputs and operating conditions for TCM reactor for Decomposition& Synthesis (Steady state models)

3.2.2. Aspen Dynamic and Control

The decomposition and synthesis TCM reactors are exported from ASPEN PLUS steady state model into ASPEN PLUS DYNAMICS with the flow driven simulation option. Once exported the initial configuration of the TCM reactors is being carried out. Initial inputs and operating condition of each reactor are summarized in the table below:

	TCM Decomposition Model	TCM Synthesis Model
Initial holdup	69.4 kg - $CaCl_2$*$8NH_3$	3.5 kg - $CaCl_2$*$8NH_3$ 25.8 kg - $CaCl_2$*$4NH_3$ 22.4 kg - $CaCl_2$*$2NH_3$
Area (m^2)	6.37	
Height (m)	8.75	
Diameter (m)	0.1143	
Medium inlet temperature(°C)	32	55
Medium mass flow rate (kg/h)	0	0
Feed Stream (kg/h)	0	1. 10 | NH_3 2. 0 | Salt

Table 13: Initial inputs and operating conditions for TCM reactors (Dynamic state models)

In this updated version of the D3.1, additional initial conditions for the reactors as well as heat transfer coefficients were implemented in the model for the dynamic simulations. The aforementioned settings were introduced in both the decomposition and the synthesis models.

	TCM Decomposition Model	TCM Synthesis Model
Heating option	Dynamic	
Heat medium mass holdup (kg)	40	
Medium heat capacity (kJ/kg/K)	3.92	
Equipment heat transfer settings		
Mass of vessel (kg)	75	
Vessel heat capacity (J/kg/K)	500	
Internals heat transfer settings		
Mass of internals (kg)	41.7	
Heat capacity of internals (J/kg/K)	700	
Heat transfer coefficient of internals ($W/m^2/K$)	100	
Heat transfer coefficient of vessel ($W/m^2/K$)	300	

Table 14: Updated initial inputs and operating conditions for the TCM reactors

3.2.2.1. Decomposition Control strategy

Of particular importance for modelling accurately the TCM reactors operation, is the development of a control strategy by which the main variables of the reactors (Temperature and Pressure) can be successfully controlled while external disturbances such as the medium inlet temperature and mass flow rate are imported. Due to the difference between the two models as regards their operation principle, a separate control structure was developed for each of them. In both models the simple proportional – integral (PI) controller was used.

For the decomposition mode of the TCM reactor the control strategy was straightforward. The model uses one PI controller that keeps the pressure inside the reactor during the decomposition reaction stable by manipulating the mass flow of the gaseous ammonia (expressed in kg/h). In the figure below, it can be observed that the set point for the controller is 2 bar for winter cases and 3 bar for the summer cases because of the limitation imposed by the compressors pressure ratio. The initial mass flow of gaseous ammonia is 0 kg/h and the pressure inside the reactor is constant at 1 bar. Once the heat transfer fluid starts heating up the reactor and the reaction begins, the pressure inside it raises. When the pressure reaches 2-3 bar, the mass flow of the produced ammonia starts. From that point on and until the reaction is completed or the mass flow of the heat transfer fluid stops, the pressure inside of the reactor remains stable at 2-3 bar.

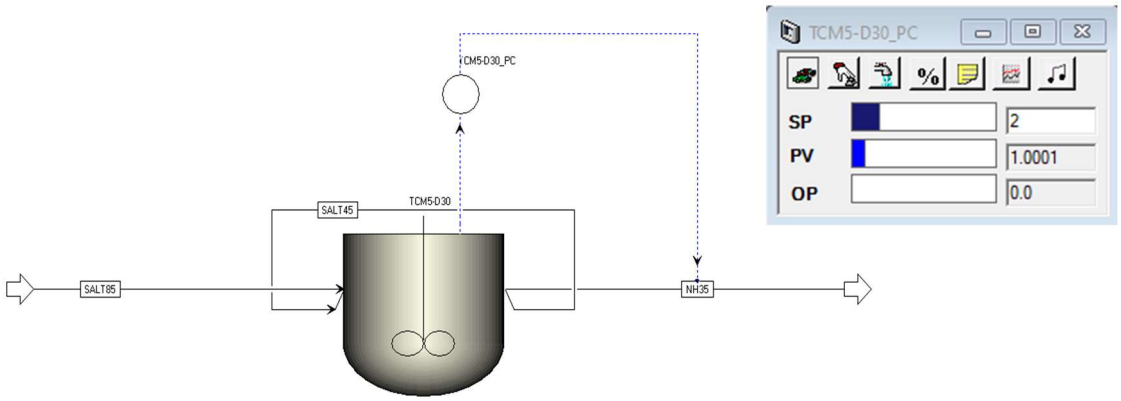

Figure 20: Overview of the TCM reactor for Decomposition with operating pressure PI controller (Dynamic model)

3.2.2.2. Synthesis Control Strategy

For the synthesis mode of the TCM reactor the control strategy offers additional complexity. The model uses two PI controllers as seen in the figure below. The left PI controller keeps the pressure constant inside the reactor during the synthesis reaction by manipulating the mass flow of the artificial outlet gaseous ammonia (kg/h). The difference in the synthesis model, in comparison with the decomposition model, is that the inlet stream of NH_3 has a constant mass flow. This results in an output value of the controller permanently above zero. The actual mass flow of the ammonia being absorbed by the reactor is calculated using a comparator, in which the input mass flow is subtracted from the output mass flow. With this strategy the reactor pressure is kept constant at the set point value. The only condition that must be met is that the incoming stream's mass flow has always to be greater than the output. The PI pressure controller is cascade, which means that it has a remote set point. This feature enables the change of the set point of the reactor pressure through SIMULINK. The right PI controller keeps the temperature inside the reactor constant at the desired set point by manipulating the mass flow of the cooling medium (expressed in kg/h). The initial output of the PI temperature controller is zero because it is desired to keep stable the temperature inside the reactor. In the case shown in the figure below, the set point for the pressure PI is at 2 bar and the temperature is at 63 °C. The set point of 63 °C is constant during the reaction, so that the output heat transfer fluid temperature will be able to charge the Hot PCM. The reaction of the synthesis model starts when the set point of the pressure PI controller is changed.

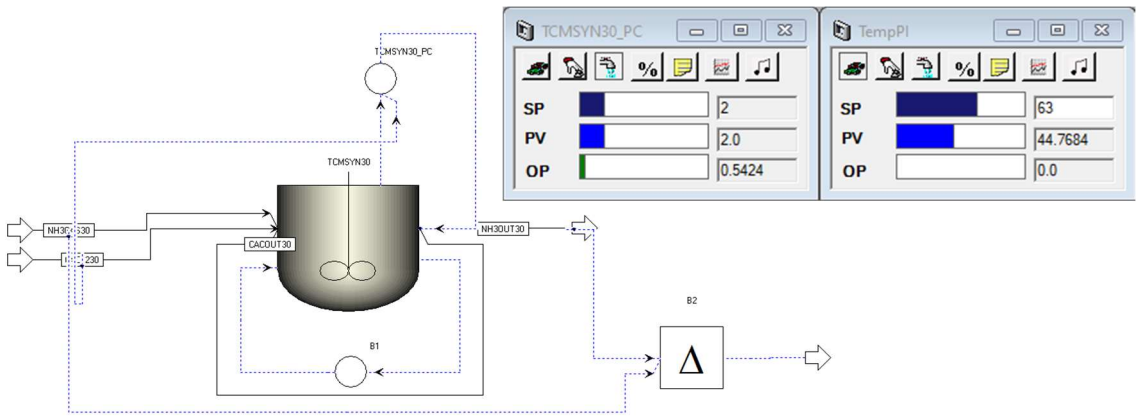

Figure 21: Overview of the TCM reactor for Synthesis with operating pressure and temperature PI controllers (Dynamic model)

3.3. Ammonia cycle and Heat Pump submodels

3.3.1. Modelling in Aspen Plus

The ammonia compression is performed at two stages with intermediate subcooling. The pressure outlet at the first and second stage is 5 and 11 or 16 bar, respectively. The final pressure is determined by the temperature of ammonia condensation, which is fixed at 28°C for the winter months and 40°C for the summer months. The isentropic efficiency is 70% at both stages. The ammonia intercooling is accomplished at 63°C. At the discharging mode, the ammonia liquid that comes from the ammonia tank (not modelled in Aspen) enters a throttle valve that drops its pressure down to the TCM operating pressure and subsequently enters the evaporator. To ensure that complete evaporation is performed, 2°C degrees of superheating is considered.

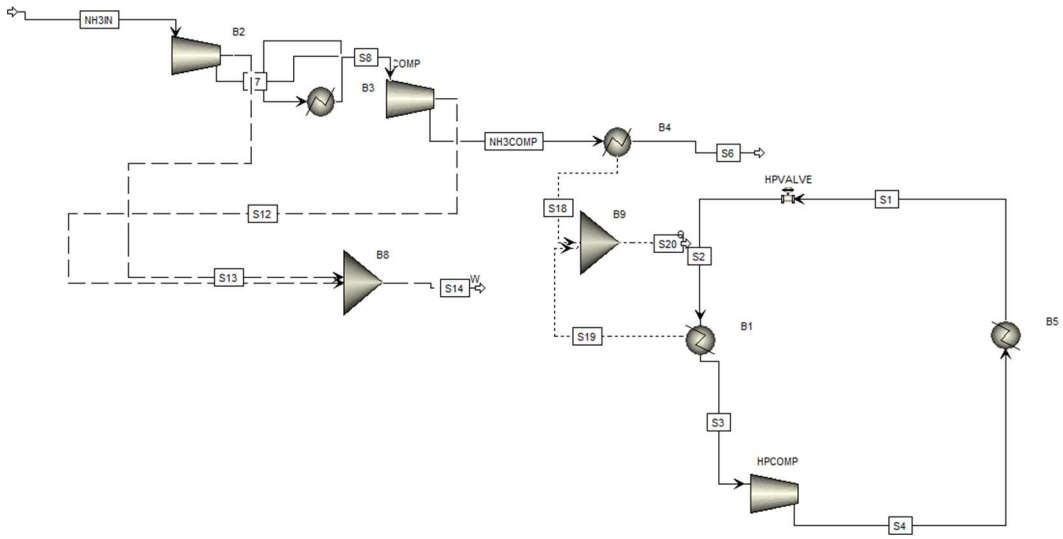

Figure 22. Ammonia cycle & Heat Pump model in Aspen Plus

The main components of the heat pump are the two heat exchangers (evaporator and condenser), the compressor and the throttle valve. The working fluid is set to be R410A, a refrigerant that has widespread application in heat pumps. Its composition is 50% R125 (pentafluoroethane – C_2HF_5) and 50% R32 (difluoromethane – CH_2F_2) on a mass basis. Since the final configuration of the interconnection between ammonia condenser and the pump evaporator has not been defined at the time of preparing this deliverable, a conservative assumption for the heat exchanging was made, considering a temperature difference of ΔT= 7 °C. Based on that, the low-pressure level at the heat pump evaporator, which is determined by the pressure outlet at the throttle valve, is the pressure at which the working fluid evaporates at 21 °C. The high-pressure level, which is controlled by the pressure outlet at the compressor, is determined by that pressure where the refrigerant condenses at a temperature 1°C higher than the hot water circuit, i.e. 64°C. To calculate these two pressure levels, two design specifications based on the former criteria were set up. The compressor isentropic efficiency is set at 70%. The refrigerant flow rate is calculated by a third design specification that guarantees the heat balance between the ammonia condenser and the heat pump evaporator.

For the ammonia cycle model, the selected property method was NRTL-RK (Non Random Two Liquids model [51] combined with Redlich–Kwong equation of state [52]), whereas, the REFPROP [53] was used for the heat pump model. The former is suitable for ammonia-based systems where both phases are considered, while the latter is the most appropriate property method for thermodynamic cycles with refrigerant fluids.

3.3.2. Aspen Dynamic and Control

The ammonia cycle and Heat Pump model for the decomposition reaction is exported from Aspen Plus steady state model into Aspen Plus Dynamics with the flow driven simulation option. Unlike the TCM reactor models, it is not necessary to change any configuration or initial input from the steady state model. The purpose here is to develop a control strategy that keeps constant the key point inputs of both the ammonia cycle and Heat Pump, manipulating variables such as the compressor electrical consumption or the heat exchanger duty.

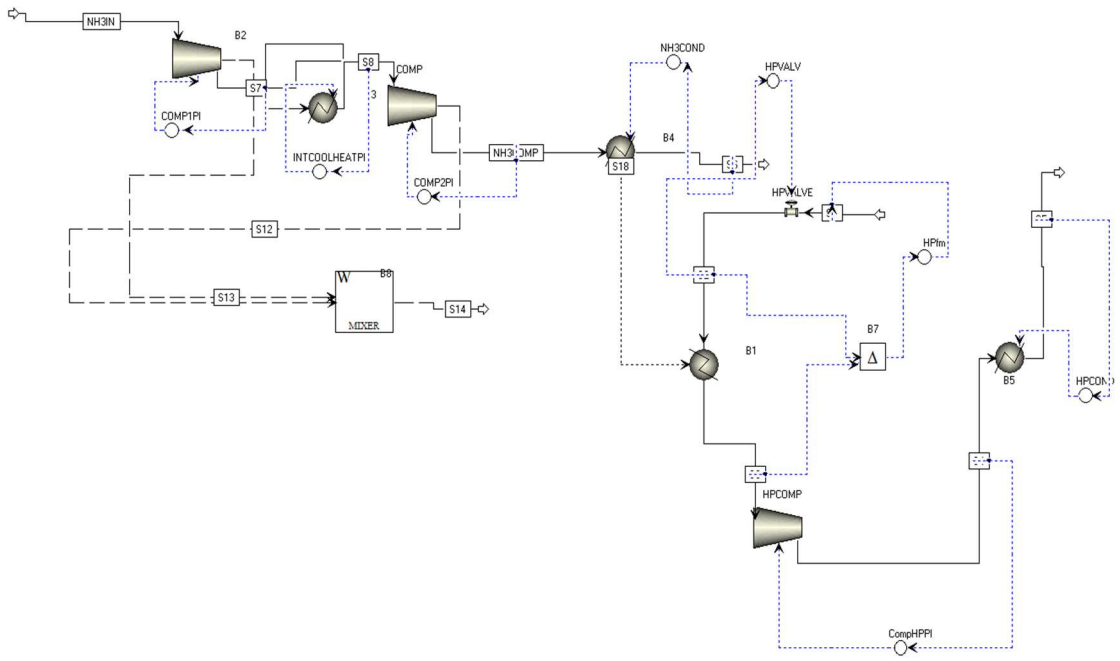

Figure 23: Overview of the ammonia cycle with Heat Pump (Dynamic model)

In addition to the components described in the steady state model, some additional PI controllers involved in the operation of the model are the following:

1. HPCOND: PI control unit for keeping the temperature of the liquid refrigerant fluid at the exit of the heat pump condenser (B5) constant at 64°C by manipulating its heat duty (W).
2. COMPHPPI: PI control unit for keeping the outlet pressure of the refrigerant fluid at the exit of the compressor (HPCOMP) constant at 41.91 bar by manipulating its brake power (W).
3. HPFM: PI control unit for keeping the superheating temperature difference of the refrigerant at the exit of the evaporator (B1) constant at 2°C by manipulating the mass flow of the refrigerant (kg/h).
4. HPVALV: PI control unit for keeping the throttled refrigerants pressure constant at 14 bar by manipulating the opening fraction (%) of the valve (HPVALVE).
5. COMP1PI and COMP2PI: PI control units for keeping the pressure outlet of the gaseous ammonia at the exit of the compressors (B2 and COMP) at 5 bar and 11 bar for the winter case and 16 bar for the summer ones respectively by manipulating their brake power (W).
6. INTCOOLHEATPI: PI control unit for keeping the temperature drop of the gaseous ammonia at the exit of the intercooler heat exchanger constant at 63°C by manipulating its heat duty (W).
7. NH3COND: PI control unit for keeping the temperature of the liquid ammonia at the exit of the condenser constant at 28 for the winter cases and 40°C for the summer cases by manipulating its heat duty (W).

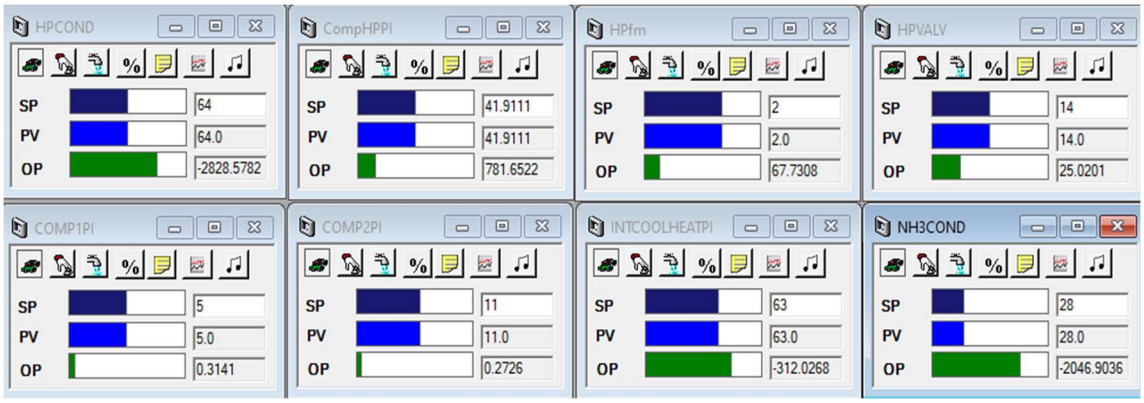

Figure 24: Overview of the PI controller for the ammonia cycle with the Heat Pump.

The only parameter that changes in the system is the supply of gaseous ammonia. Initially, the model is calibrated to an average mass flow of 10 kg/h so that any increase or reduction is within the boundary conditions of the system. Depending on the reaction rates of the decomposition mode, the value of its mass flow can move from 1 kg/h up to 20 kg/h. The PI control parameters (proportional and internal gain) are also calibrated with the proper values so that an abrupt variation does not bring upon any significant change in the process variables of the controllers.

The ammonia cycle for the synthesis reaction is exported from Aspen Plus steady state model into Aspen Plus Dynamics with the flow driven simulation option. As with the Heat Pump cycle, it is not necessary to change any configuration or initial input from the steady state model.

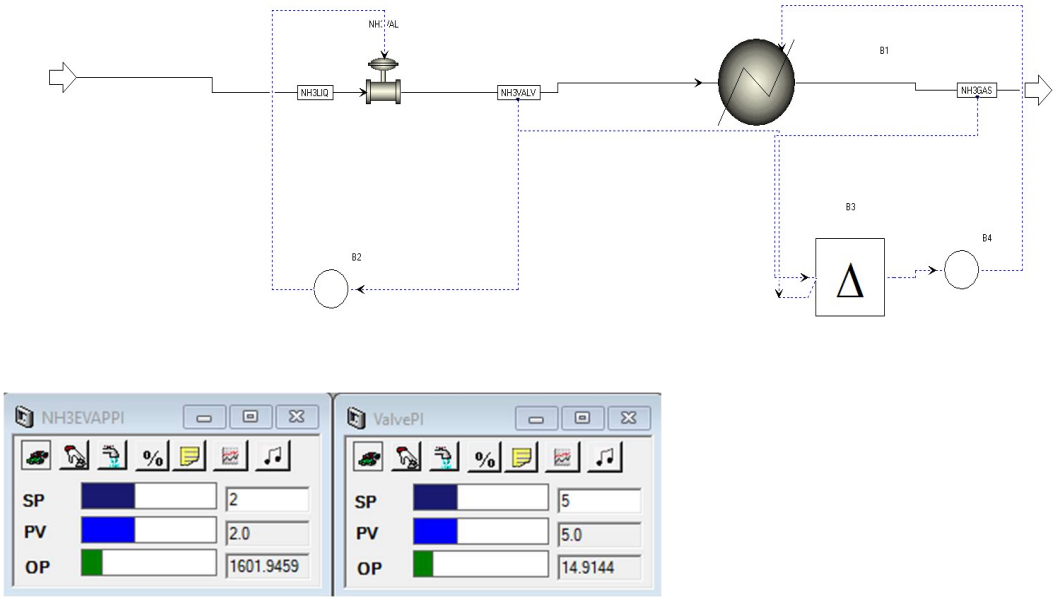

Figure 25: Overview of the ammonia cycle (Synthesis mode) with outlet superheated temperature and outlet pressure PI controllers (Dynamic model)

The controlling strategy in this case is simple. Two PI controllers are being used as seen in the figure above. The right PI controller keeps the pressure constant at the desired set point by manipulating the opening of the valve (%). The left PI controller is keeping the superheating temperature difference of the ammonia at the exit of the evaporator constant at 2°C by manipulating the heat duty of the evaporator (W). Initially the model is calibrated to an average mass flow of 5 kg/h so any abrupt variation is within the boundary condition of the system. Both PI controllers are tuned with the proper values so as the response time of the output variable is reduced to the minimum.

3.4. PCM storage model

A PCM heat storage model has been developed in MATLAB and integrated afterwards into Simulink. The TCM presents an energy storage density of around 213 kWh/m^3, whereas the PCM a density of 107.2 kWh/m^3. Due to the fact that the selected TCM reactor size is 17.5 kWh (resulting in a volume of 0.082 m^3) and the overall systems energy storage density has to be 10.6 higher (KPI) than the respective value for water-based storage systems and for operating heating temperature differences in the range of 15°C (i.e. around 184 kWh/m^3), the PCM volume has to be smaller than 0.036 m^3. Therefore, the heat battery selected for this system has a maximum capacity of 3.5 kWh (and a corresponding volume of 0.025 m^3). The main specifications of the considered PCMs are displayed in Table 15.

Hot PCM storage tank	
Phase Change Material	*Sunamp SU58*
Composition	*Sodium Acetate Trihydrate*
Phase Change Temperature (°C)	*58*
Energy density (over 40-80 °C)	*Up to 133 kWh/m^3*
Cold PCM storage tank	
Phase Change Material	*Sunamp SU11*
Phase Change Temperature (°C)	*8.1*
Energy density (over 10-75 °C)	*Up to 44.7 kWh/m^3*

Table 15: *PCM storage tanks [61]*

In this model, the energy balance equation of the heat battery is defined by the equation:

$$\frac{dE}{dt} = P - Q \tag{3.15}$$

, where E is the stored energy in the heat battery, P is the input power from the system, Q is the heat demand.

Some restrictions for the minimum and maximum value of E (it can't be lower than zero or higher than the maximum capacity Emax as specified by the manufacturer) and maximum value of Q (as specified by the manufacturer) are also introduced.

The state of charge (SOC) of the heat battery is also defined in this model as follows:

$$SOC = \frac{E}{E_{max}} \tag{3.16}$$

where E_{max}: the maximum capacity of the heat battery as specified by the manufacturer.

The model consists of two main inputs, the heat demand (cooling or heating) of the building and the heat produced by the MiniStor thermal system. The outputs of the PCM model are also two: the state of charge of the heat battery and the heat duty (for the case the heat storage discharges). Finally, it must be emphasized that all the thermal outputs of the TCM / Heat Pump system are at least at 63°C so that we can charge the PCM whose melting temperature is 58°C.

3.5. Integration of the thermodynamic submodels and overall simulation strategy

The final integrated thermal system consists of a combination of different programs (MATLAB / Aspen Plus Dynamics) which are integrated through SIMULINK. The purpose is to investigate the behaviours of the system during the charging and the discharging cycles in order to plan an optimum charging and consumption strategy for each case scenario. The modules of the integrated thermal system are:

- PVT-Solar Collectors – Tank (MATLAB)
- Electrical Heater (MATLAB)
- TCM Decomposition/Synthesis modules (Aspen Plus Dynamics)
- Decomposition ammonia cycle – Heat Pump (Aspen Plus Dynamics)

- Ammonia tank (Aspen Plus Dynamics)
- PCM Hot/Cold heat storage modules (MATLAB)
- Hitachi heat pump (MATLAB), only for Santiago's case

The final thermal system takes the following inputs:

- Solar Radiation (W/m^2)
- Ambient Temperature (°C)
- Wind Speed (m/s)
- Thermal demand (Cooling, Heating) of the building (W)

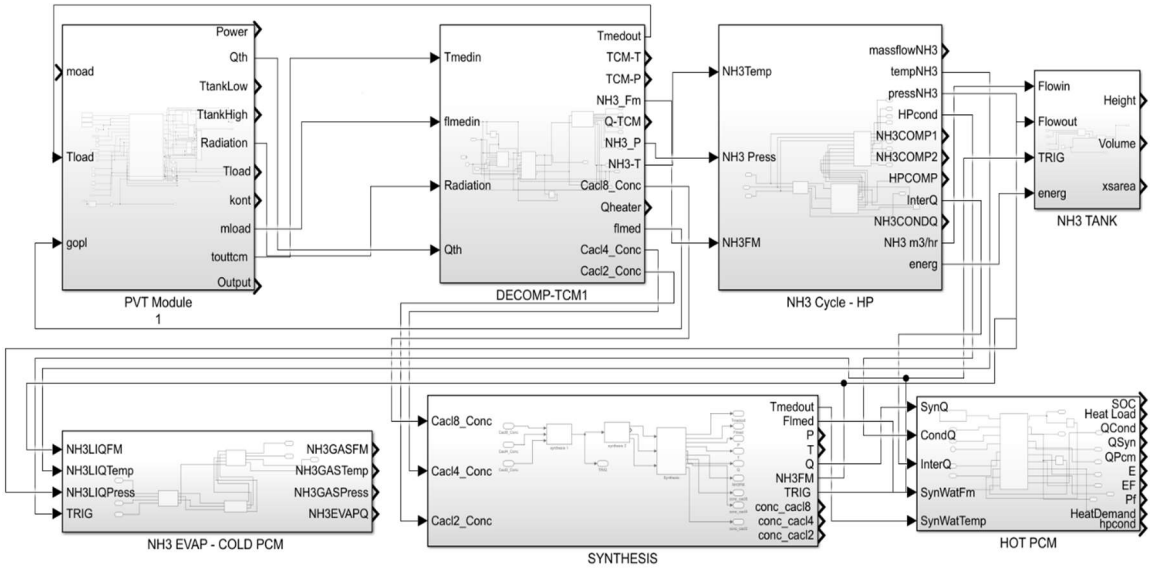

Figure 26: Overview of the integrated thermal system in SIMULINK

Models developed using MATLAB code (PVT-Tank, Electrical Heater, PCM) were introduced in Simulink through a block (MATLAB function) from the Simulink's model palette, with minimal modifications from the original code. Aspen Plus Dynamics models can be loaded into MATLAB and used with the Control System Toolbox to design a process control system. The interface enables an Aspen Plus Dynamics process simulation to be used as a block within a Simulink model.
Finally, the backup electric heater is being added via MATLAB code function. The Electric Heater is defined in this model as follows:

$$Q_{El.Heater} = m_{Load} * Cp_{medfluid}(T_{el.out} - T_{el.in}) \quad (3.17)$$

, where m_{Load} is the massflow of the heat transfer fluid between the TCM reactor and the Tank (Kg/s), $Cp_{medfluid}$ is the value of the specific heat capacity of the medium (J kg^{-1} K^{-1}), $T_{el.out}$ is the temperature of the medium fluid at the exit of the electrical heater and $T_{el.in}$ is the temperature of medium fluid as it enter the electric heater.

Once all the subsystems are added to Simulink the control strategy process begins. In each subsystem which has Aspen Plus Dynamic model inside, two more MATLAB functions are introduced which are responsible for the control strategy of the integrated thermal system. The first is responsible for activating the Aspen Dynamic model. The second is responsible for recording the outputs from the respective model. The two control functions are connected to each other via a trigger. Outputs of the MiniStor's integrated thermal system are exported into MATLAB's workspace as an array.

An additional model, simulating the Hitachi heat pump, is incorporated in Santiago's case. The scope is to simulate the coupling of the array of PVTs, heat pump and buffer tank, which in turn provides heat to the TCM reactor. When there is thermal demand from the demo site and the system is in charging mode, the Hitachi HP will be activated, using electricity either produced concurrently by

the PVTs or being produced at an earlier time and stored in the electrical battery, resulting in temperature elevation of the buffer tank content and consequently in the activation of the decomposition reaction of the TCM. An indicative figure of the SIMULINK model with the Hitachi HP for the Santiago demo site is presented below.

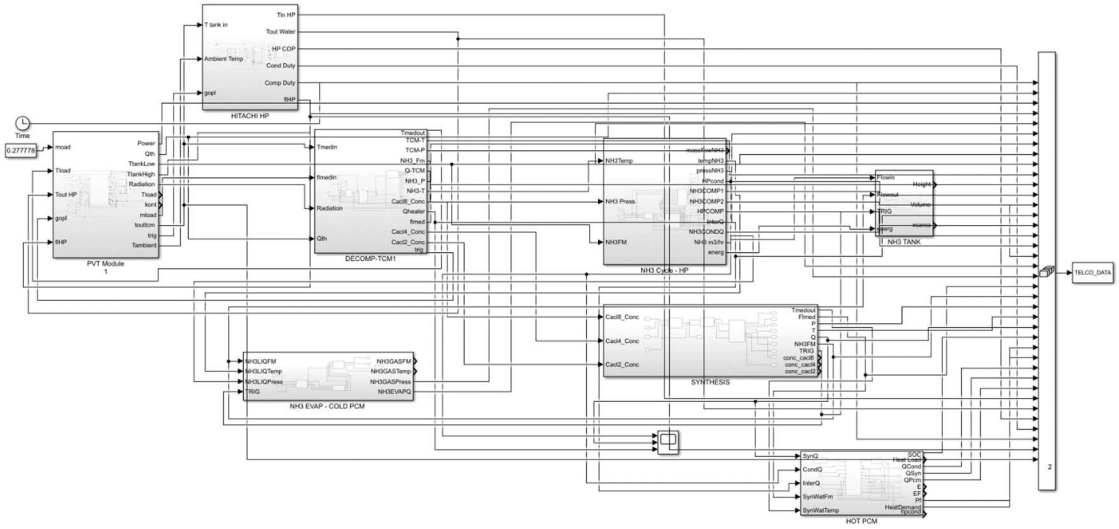

Figure 27: Overview of the integrated thermal system in SIMULINK for the Santiago demo site

3.5.1. Model Execution

As stated before the model has four inputs. Three of them (Radiation, Ambient temperature, Wind speed) are being used in the PVT- Tank sub-model and the fourth one (Thermal demand) is being used in the PCM heat storage model. At the first stages of the simulation, the PVTs together with the Solar Collectors utilize the solar radiation to increase the temperature of the fluid inside the tank. When the latter reaches a certain temperature that has been set, the supply of heat transfer fluid to the TCM reactor is activated. In the case where the solar energy is able to satisfy the energy needed to complete the decomposition reaction, the activation temperature activation of the circuit is 44 °C. Otherwise it is chosen manually when the circuit will be activated, depending on the thermal needs of the house and supplementing the solar heat with the energy output of the backup heater. The maximum power that the electric heater can provide is 2 kW. The supply of heat transfer medium stops when the top tank temperature drops below 44 °C, due to reduced solar radiation, or when the decomposition is completed. In the case of Santiago, the Heat Pump is activated whenever the house has a heating demand or manually. As previously mentioned, the Hitach HP model consists of three main inputs, the exit temperature of the buffer tank, the ambient temperature and the trigger that activates the submodel. While the decomposition reaction is taking place, the Ammonia Cycle - Heat Pump and the Ammonia Tank are activated as well.

When the decomposition mode is completed, the Synthesis mode starts. This mode is flexible in the sense that it can be activated whenever selected depending on the thermal needs of the building. While the synthesis mode is taking place, the Ammonia tank and NH_3 evaporator models are activated. The TCM synthesis sub-model calculates, as previously mentioned, the mass flow of ammonia needed for the reaction and provides the value as input to the respective sub-models. Throughout the simulation the PCM subsystem is responsible for controlling the system during charging and discharging cycles. All the thermal loads produced as well as the weather data for each demo site are imported as inputs to the heat storage model. The control of the heat battery is quite simplified. When the input heat from the system is larger than the thermal demand, the PCM unit charges. In the case that our system does not provide any heat to the building, the PCM heat storage unit discharges. In addition, it operates supportively (discharging) when the MiniStor system cannot fully cover the thermal loads of the house.

3.6. Modelling of the electrical Battery Energy Storage System and electrical subcomponents

The PVT electrical system model presented in this section, is part of Task 3.5[3]. However, as an intermediate action, this deliverable includes a general description of the model developed by CARTIF in collaboration with EndeF.

3.6.1. General description and simulation tool

The dynamic simulation software TRNSYS 18 has been used as a simulation tool [54]. This software enables the different components of energy systems to be analysed in a dynamic and integrated way, in this case, the electrical system, providing results in transient conditions, every hour, or with smaller time steps throughout the year. Although there are other approaches and software tools (such as MATLAB and RC), TRNSYS was selected according to the following main reasons:

- This software is widely recognized within the scientific and research community and is particularly devoted to conducting transient analyses of any dynamic solar thermal and photovoltaic systems
- It provides a wide range of standard and specific models already developed and validated that can be conveniently integrated to meet the MiniStor modelling requirements.
- This tool can also interact with other several simulation tools (co-simulation), and it allows integrate complementary capabilities, such as optimization algorithms, automatic data processing, etc.
- MiniStor partners in charge of conducting the electrical modelling (CARTIF and EndeF), for sizing the electrical storage system, in the framework of Task 3.5, are familiarized with the TRNSYS environment. Besides, CARTIF has a wide experience using this software, in previous R&D projects, which allows development of the model in a solvent and appropriate way.

In general, the PVT electrical system model is focused on the integrated analysis of the different profiles of electricity production and demand in the studied MiniStor demos, with the purpose to quantify both: the excess production of electricity, which can potentially be sent to the electrical storage system (lithium-ion electric batteries), for later use to attend the electrical demand of the thermal system and the building; and the electricity deficit to be taken from the electrical grid. This analysis will allow to properly size the electrical storage system of the project demos, as required in Task 3.5.

The sub-systems included in the model are the following: (i). The solar collection field, through which the electrical production of PVT panels is quantified; (ii) the electrical block or sub-system, which includes the central components of the electrical system (hybrid solar inverter, lithium-ion batteries, and electrical energy balance calculation elements); (iii) the simplified solar thermal circuit, and (4) the different dynamic input data, such as, weather data, electrical load profiles, and energy cost, required to carry out the simulations. Figure 28 shows the general scheme of the model developed in TRNSYS, indicating the sub-systems and types of elements mentioned above.

[3] *Task 3.5: Engineering, installation strategies and prototyping for electrical storage system*

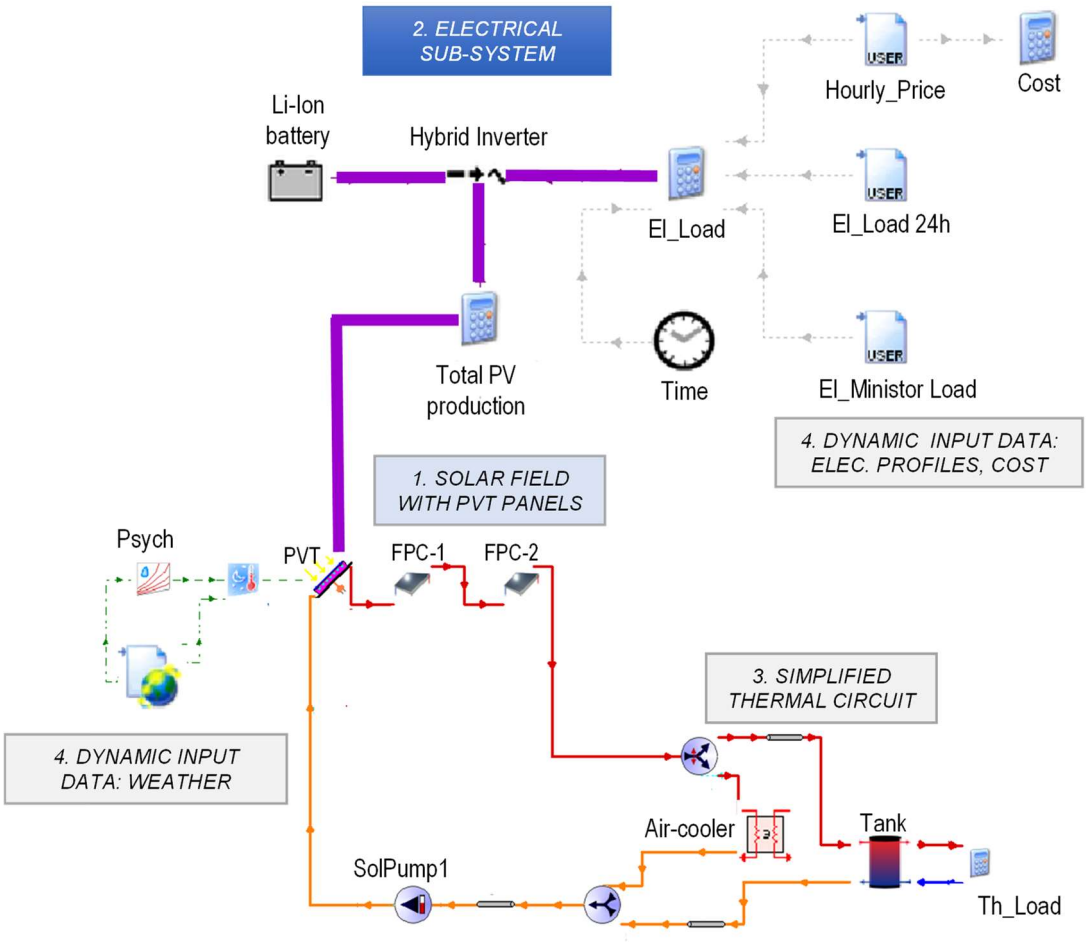

Figure 28: Electrical system model implemented in TRNSYS

3.6.2. Modelling of Electrical component sub-systems

a) Solar field with PVT panels for electrical output

The electricity produced by hybrid solar collectors (PVT) is one of the most important inputs required by the electrical block or subsystem. For quantifying this production, the model includes first the solar collection field, in which hybrid solar panels and flat thermal solar panels are combined, as defined for each demo-site in section 3.1 of this deliverable.

According to section 2.1, the type of hybrid solar panel used in the simulation is a glazed PVT panel, which presents a greater thermal performance than un-glazed PVT panels and meets better the temperature input requirements for the MiniStor system. In the electrical system model, as reference PVT panel was taken into account, i.e. the Ecomesh model manufactured by the EndeF company presented in the section 2.1. The final model of PVT panel will be selected in the context Task 3.3, which includes the dimensioning, prototyping, and production of improved conventional solar hybrid panels.

As hybrid solar panel (PVT) the TRNSYS model Type 560 component library was used, where parameters are adequately adjusted to the constructive characteristics of the PVT glazed panels, with sheet & tubes absorber type. The parameterization of this TRNSYS type was carried out, considering the physical dimensions of the reference PVT glazed, and other complementary parameters were adjusted, considering the thermal parameters and electrical presented in section 2.1.

Similarly, for modelling the flat solar thermal collectors (FPC), Type 1b, included in the TRNSYS standard library, was used. This type, models the thermal collector production, according to the thermal efficiency parameters (optical efficiency, and thermal losses coefficients); besides, it

incorporates complementary data, in regards to the physical collector dimensions, IAM, mass flow rate test, etc. The corresponding data was provided by the collector Manufacturer (Viessmann), and a summary of the main technical characteristics are included in section 2.1 of the present Deliverable.

The solar field was configured according to the design conditions defined for each demo-site, in section 3.1. Specifically, 2 or 3 rows of PVT and FPC collectors were used, with a connection in series between rows. As an example, Table 16 summarizes the base configuration defined for two demo-sites; also, an alternative configuration, included in the electric model, is presented.

Demo	Base configuration	Alternative configuration
Sopron	*Electrical configuration:* 6 glazed PVT panels in serial connection *Hydraulic configuration:* Row 1: 6 solar hybrid panels (PVTs) Row 2: 4 solar flat plate collectors (FPCs) Row 3. 4 solar flat plate collectors (FPCs) Rows in serial connection	*Electrical configuration:* 9 glazed PVT panels in serial connection *Hydraulic configuration:* Row 1: 9 solar hybrid panels (PVTs) Row 2: 6 solar flat plate collectors (FPCs) Rows in serial connection
Thessaloniki	*Electrical configuration:* 10 glazed PVT panels in serial connection *Hydraulic configuration:* Row 1: 5 solar hybrid panels (PVTs) Row 2: 5 solar flat plate collectors (FPCs) Row 3. 5 solar flat plate collectors (FPCs) Rows in serial connection	*Electrical configuration:* 10 glazed PVT panels in serial connection *Hydraulic configuration:* Row 1: 10 solar hybrid panels (PVTs) Row 2: 5 solar flat plate collectors (FPCs) Rows in serial connection

Table 16: Solar field configurations considered in the PVT Electrical model

b) Electrical sub-system

The electrical production obtained from the Solar PVT Field is the main input of the electrical subsystem, which includes components as the electrical storage system, using lithium-ion batteries and the hybrid solar inverter for grid connection, suitable for connection and integration with the batteries. The main technical characteristics of these components were presented in section 2.1.

The hybrid solar inverter performs the conversion of DC / AC electricity, and is also the intelligent component of the system, as it manages the energy flows between the elements of the electrical system (PVT panels, electrical utility grid, electrical batteries and electrical load or demand). The modelling of this element was performed in TRNSYS by using the Type 48b standard library, its characteristics and operation correspond to solar hybrid inverter type, that means it includes two power conditioning functions: on-grid inverter and regulator.

Specifically, this component receives the electricity production data from the hybrid solar collectors (PVTs), the electricity demand or load data, corresponding to the analysed demo, and the information on the state of charge (SOC) of the electrical lithium-ion batteries. This information is used by the component in order to quantify the energy deficit which must be taken from the electrical utility grid and manage/regulate the charging and discharging processes of lithium-ion batteries.

Table 17 shows the parameterization data used for this component.

Parameter	Value
Regulator efficiency	0.99
Inverter efficiency	0.952
High limit on the fractional state of charge (FSOC)	0.99
Low limit of fractional of FSOC	0.10
Charge to discharge limit of FSOC	0.10
Inverter power capacity	3.0 kW
Battery capacity	5.12 kWh
Charging efficiency	0.96

Table 17: Main parameters considered for hybrid solar inverter and electrical batteries system

Lithium-ion batteries, unlike lead-acid batteries, have a stable discharging voltage profile and are less dependent on stored energy. This fact allows modelling the SOC based on the energy balance. For initial dimensioning, the model considers an average round-trip efficiency greater than 96% and a maximum discharge of 90%. TRNSYS modelling was carried out using standard library Type 47. This component is connected to the hybrid solar inverter (Type 48b), which sends to the batteries, during every time step, the corresponding energy information to perform the energy balance and update the SOC of the batteries.

The electrical subsystem also includes complimentary components, "equa", where additional equations are introduced in order to process the energy balances at every time step, and process external dynamic information, such as the electricity load profiles and the electricity cost data.

c) Solar thermal circuit

The electrical production of the PVTs also depends on the average temperature of the fluid that circulates in the thermal absorber, therefore, the model also includes the subsystem corresponding to the thermal solar circuit, which includes: an inertia tank, a solar primary circuit, from the solar field to a buffer tank and a simplified discharge circuit from the buffer tank.

The primary solar circuit (charging circuit) includes the impulsion and return pipes, the circulation pump, and an air-dissipator. This sub-system uses two control elements: a differential control for activating the solar circuit, when the temperature difference between the solar field outlet and the bottom zone of the tank is greater than 5ºC, and a second control element in charge of activating the air-dissipator, in order to control the maximum temperature in the solar primary circuit. The electrical consumption of this air-dissipator is sent as load input data to the electrical sub-system.

The discharging thermal circuit is a simplification of the thermal demand (TCM reactor), which is activated only when the tank temperature is higher than 60°C and stops when the mentioned temperature reaches a minimum value of 55°C. In all cases, a thermal difference of 5 ° C is assumed in the thermal demand. This circuit also includes a control element for the corresponding activation.

Element of solar thermal circuit	Component used in TRNSYS
Pipes	Type 31
Circulation pumps	Type 110
Inertia Tank	Type 534
Air cooler	Type 91
Load	equa
Control units	Type 165
Diverter valves,	Type 11f
Tee piece	Type 11h

Table 18: Summary of main TRNSYS components included in the solar thermal circuit

In order to simulate the elements of the thermal circuit, different characteristics found in the standard TRNSYS library were used, as summarized in Table 18. Thermal behaviour of fluid flow in

pipes was simulated by using Type 31 library. The circulation pump was simulated by using Type110, which allows to vary the mass flow rate of the pump according to a control signal setting. The inertia tank was simulated using the Type 534 library that corresponds to a cylindrical tank with a vertical configuration, divided into isothermal temperature nodes, to consider the tank stratification. The air cooler was modelled by using a heat exchanger with constant effectiveness (Type 91). The model of the simplified discharging circuit used a simple equation incorporated to the "equa" component, for introducing the supply temperature, and calculate the return temperature considering a constant temperature difference of 5 ° C. The controls units were simulated by using the Type 165 library with a proper configuration.

d) Dynamic input data

To perform the simulation, the model uses different dynamic input data: weather data for the corresponding demo site under analysis, daily electrical load profiles for the MiniStor Thermal System and the building, and data regarding electrical cost and tariffs. Section 4.3 summarizes the information related to these input data required by the model.

4. Strategy and Methodology for examining simulation cases

4.1. Weather and thermal load data for the thermodynamic model

4.1.1. Weather data for the thermodynamic model

Taking into account the number of demo sites, the large number of parameters to be examined and the computational cost involved to represent each of them, it was decided to investigate the thermodynamic transient operation of the MiniStor system on specific but representative days of the year. System operation is simulated under both extreme and typical winter and (in most cases) summer weather conditions. Moreover, in order to facilitate the study of MiniStor operational strategies over time periods of variable duration, time segments of three subsequent days are considered in each examined scenario. Thus, a good compromise between computational cost as well as results validity and applicability is achieved.

Consequently, a necessary step before implementing the simulations is the definition of the representative days in each case. Two main parameters were taken into consideration in this procedure: i) outdoor temperature which affects the heat demand of the building in which the MiniStor system will be installed, ii) available solar radiation. The latter has a significant effect on system functionality, as it is the main energy input to MiniStor. In order to quantify the first parameter, the method of the Heating and Cooling Degree Days (HDD, CDD) is implemented. A degree day is defined as the deviation of the ambient temperature from a reference value, known as base temperature [55]. In accordance with D2.2 "Definition of system context and limits for use", the base temperatures used in each case are the following:

Location	Base Temperature for HDD	Base Temperature for CDD
Sopron [56]	15°C	18.3°C
Thessaloniki [57]	15°C	24°C
Kimmeria [57]	15°C	24°C
Cork [58]	18°C	18°C
Santiago [58]	17°C	22°C

Table 19: Used base temperatures for HDD and CDD calculation

The hourly method is utilized for the HDD/CDD calculation as the available weather data enabled the implementation of such level of detail. According to the selected method, the following equations are utilized for computing the daily values of the aforementioned variables [55]:

$$HDD_{daily} = \frac{\sum_{i=1}^{24}(T_b - T_i)^+}{24} \quad (4.1)$$

$$CDD_{daily} = \frac{\sum_{i=1}^{24}(T_i - T_b)^+}{24} \quad (4.2)$$

In the above formulae T_b and T_i are the base temperature and the outdoor temperature at the i^{th} hour of the day respectively, whereas the symbol "+" denotes that only positive differences of the corresponding variables are considered. The "Typical Meteorological Year" (TMY) of each location is utilized to obtain the outdoor temperature as well as the solar radiation and wind speed values in hourly or even 15min basis. In the latter case, the four values occurring within each hour are averaged in order to compute an hourly temperature. In the cases of Sopron, Thessaloniki, Santiago and Cork the TMY files are obtained from the Meteonorm database incorporated into the TRNSYS software. A 15min resolution is available for the first two sites. The Meteonorm database is generally considered to be highly accurate, since it utilizes data derived from meteorological stations. In the case of Kimmeria, data from the nearest available meteorological station does not include solar radiation measurements. As an alternative, a TMY file from the Photovoltaic Geographical Information System (PVGIS)[4], a web-based application developed by the Joint Research Centre (JRC) of the European Commission, is used. The time resolution in this case is one hour and the main data source of PVGIS is mainly high-resolution geostationary meteorological satellite information with corrective algorithms. The tilt angle of the collectors, as derived from the roof slope and other architectural characteristics of each building, is used to estimate global radiation on the tilted collector surface. Tilt angle values along with the collectors' orientation are shown in Table 6.

The time periods that are examined are the outcome of the following procedure:

- For each day of the TMY, the daily HDD and CDD values as well as the daily total solar radiative energy on a tilted surface are computed.
- The days when the maximum HDD and CDD values, the maximum and minimum solar energy values on tilted surface occur are identified.
- For each day the variables LSE and LSA are calculated according to equations 6 and 7. The first one denotes the proximity of the three parameters values that are under investigation from the daily extreme values identified in step 2. Similarly, LSA is indicative of the difference of the daily HDD, CDD and solar energy on tilted surface values from the average ones defined in step 3.
- The daily LSE and LSA values are summed over periods of three subsequent days.
- The three-day period with the lowest LSE and LSA value, is selected as the time segments with weather conditions very close to the extreme and the average ones accordingly.

The LSE and LSA for the j^{th} day of the TMY are defined as following:

$$LSE_j = \frac{(DD_{max} - DD_j)^2}{DD_{max}^2} + \frac{(G_{t,max} - G_{t,j})^2}{G_{t,max}^2} \quad (4.1)$$

$$LSA_j = \frac{(DD_{ave} - DD_j)^2}{DD_{ave}^2} + \frac{(G_{t,ave} - G_{t,j})^2}{G_{t,ave}^2} \quad (4.4)$$

Location	Extreme winter period	Average heating period	Heating period duration	Extreme summer period	Average cooling period	Cooling period duration
Sopron	12-14 Jan	03-05 Mar	Nov-Mar	18-20 Aug	-	-
Thessaloniki	13-15 Dec	11-13 Mar	Nov-Mar	18-20 Aug	11-13 Jun	May-Sep
Kimmeria	09-11 Dec	09-11 Mar	Nov-Mar	14-16 Aug	02-04 Jul	Jun-Sep
Cork	14-16 Jan	17-19 Jan	Nov-Mar	-	-	-
Santiago	22-24 Dec	24-26 Nov 1-3 Oct	Nov-Mar Sep-Nov & Mar-May	- -	- -	- -

Table 20: Three-day periods selected to be examined in each demo site location

[4] *PVGIS: https://ec.europa.eu/jrc/en/pvgis*

In the above formulas DD_{max} is the maximum daily HDD (or CDD) value spotted over the year, DD_{ave} is the average HDD (or CDD) daily value of the heating (or cooling) period and DD_j represents the HDD (or CDD) value of the j^{th} day. The definitions of $G_{t,max}$, $G_{t,ave}$ and $G_{t,j}$ correspond with the previous ones and concern the solar energy on tilted surface. The defined three-day periods using the above procedure are summarized in Table 20.

It must be stated that for Sopron, only an extreme summer period was identified and investigated. This is attributed to the planned use of MiniStor by the demo site managers, who will use it for cooling only when the outdoor temperature exceeds 28°C. According to the TMY for the location, this precondition is met only on eight days of the year. In the case of Cork, no extreme or average summer periods were defined, as according to the analysis made in D2.2 the current cooling needs of the demo site are negligible. On the contrary, since significant HDD values are observed from October until May, an additional average heating period of the spring and autumn months was examined.

The following figures present the hourly temperature and solar radiation on tilted surface values for the identified cases, which are used as input to the thermodynamic model. In the case of Kimmeria, only temperature is used as a model input. This is due to the existing hybrid heat generation system on that site, consisting of a solar thermal park with area 1889 m^2 and a 1.15 MW_{th} biomass boiler combined with 4 hot water storage tanks of 10m^3 capacity each. Such a system is considered to be able to deliver the necessary heat to the TCM reactor and at the required temperature regardless of solar radiation levels. In all the following graphs, local time is considered but does not take into account summer time correction.

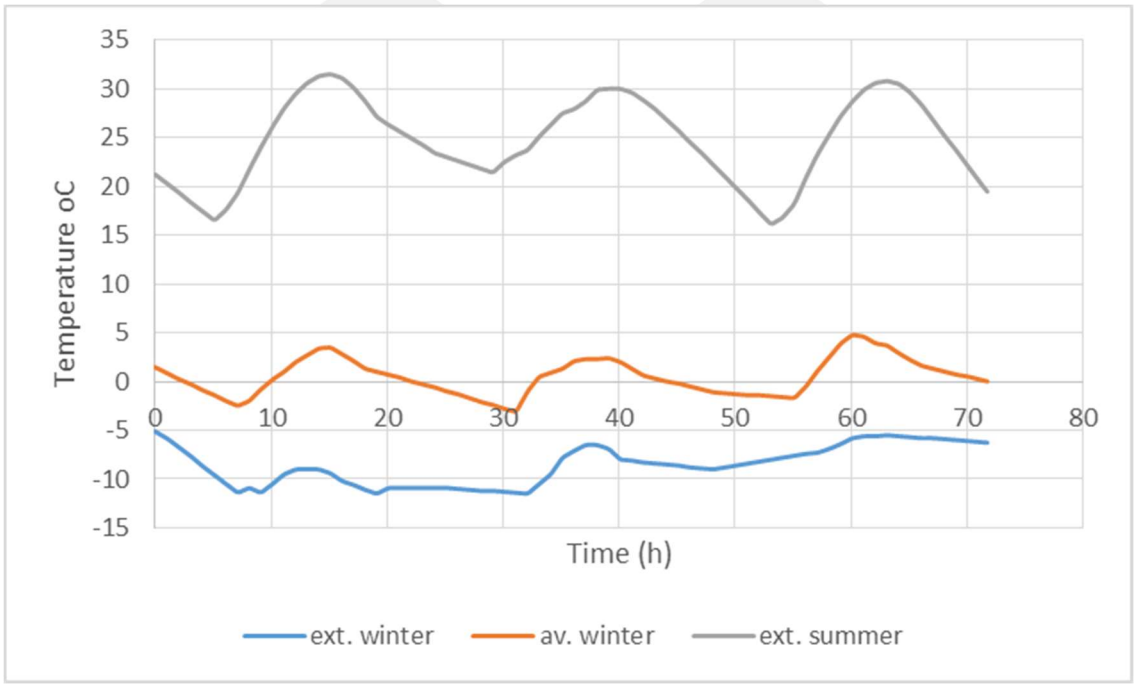

Figure 29: Hourly temperature variation of the extreme winter, average winter and extreme summer scenarios in Sopron

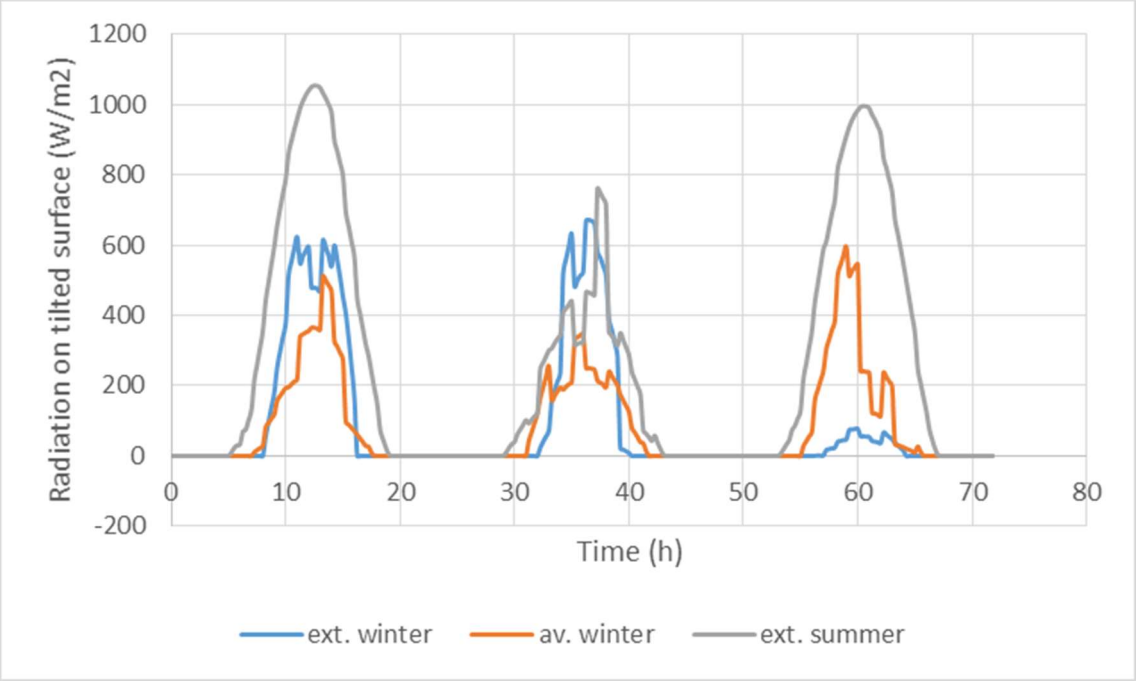

Figure 30: Hourly solar radiation on tilted surface variation of the extreme winter, average winter and extreme summer scenarios in Sopron

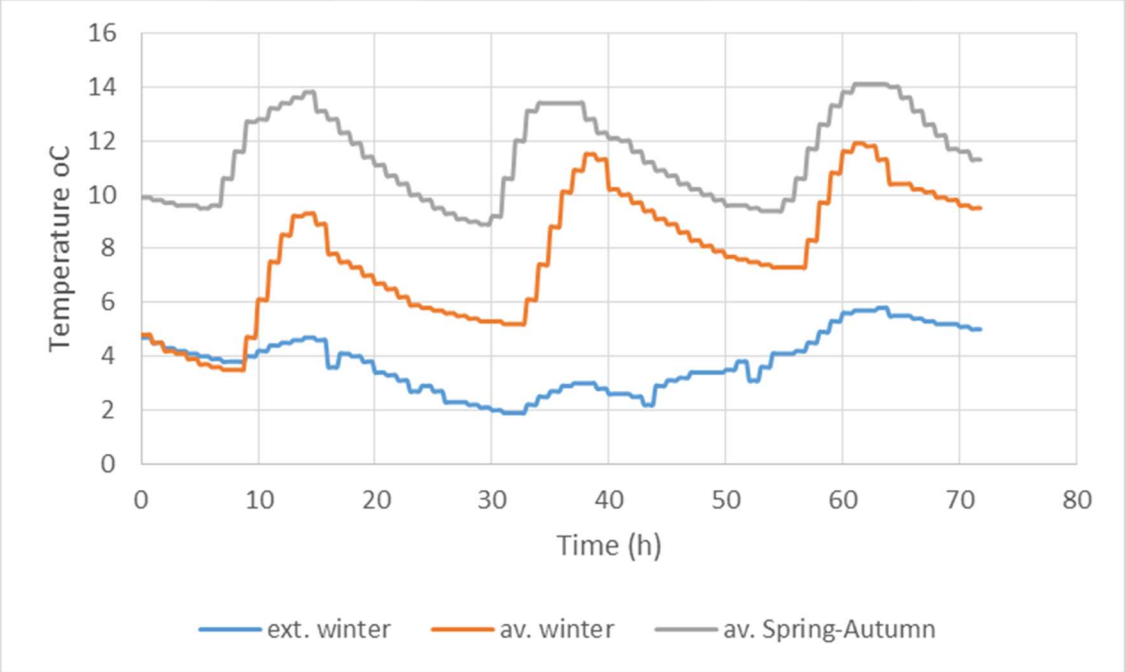

Figure 31: Hourly temperature variation of the extreme winter, average winter and average spring-autumn scenarios in Cork

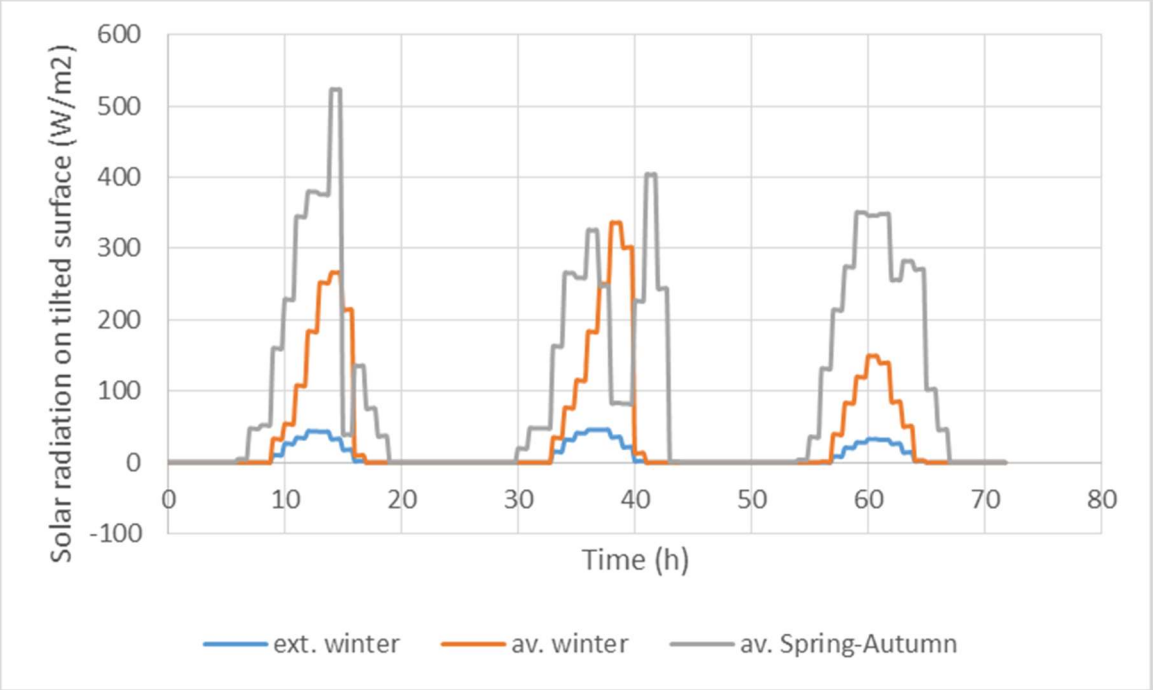

Figure 32: Hourly solar radiation on tilted surface variation of the extreme winter, average winter and average spring-autumn scenarios in Cork

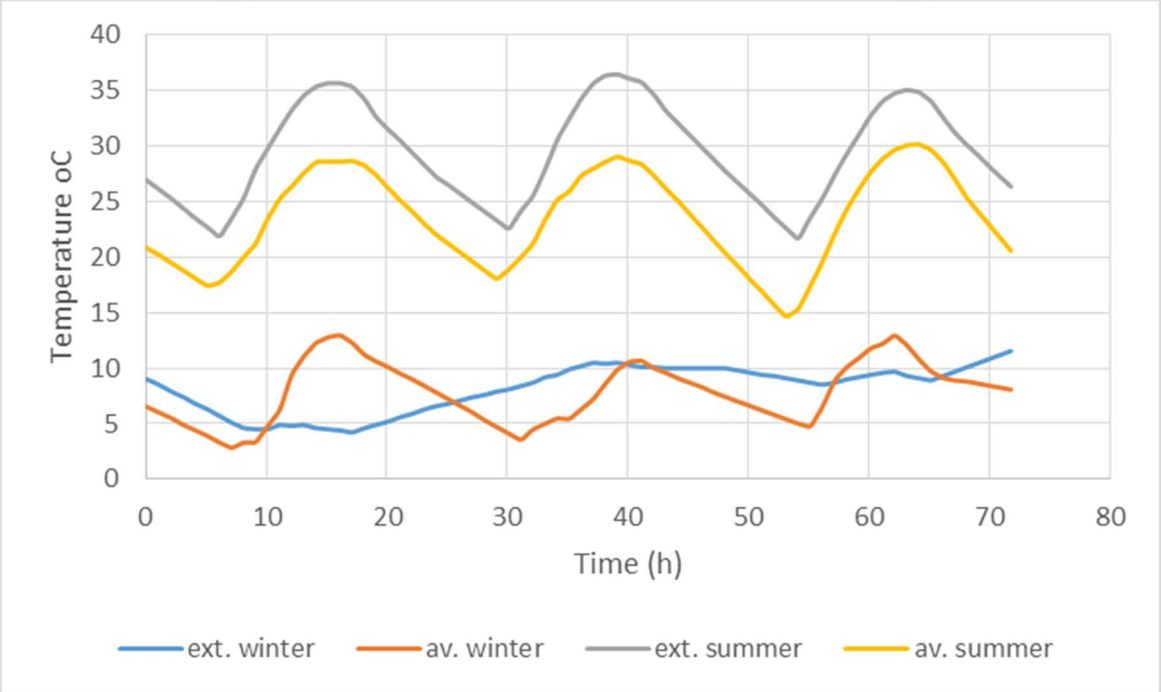

Figure 33: Hourly temperature variation of the extreme and average winter, extreme and average summer scenarios in Thessaloniki

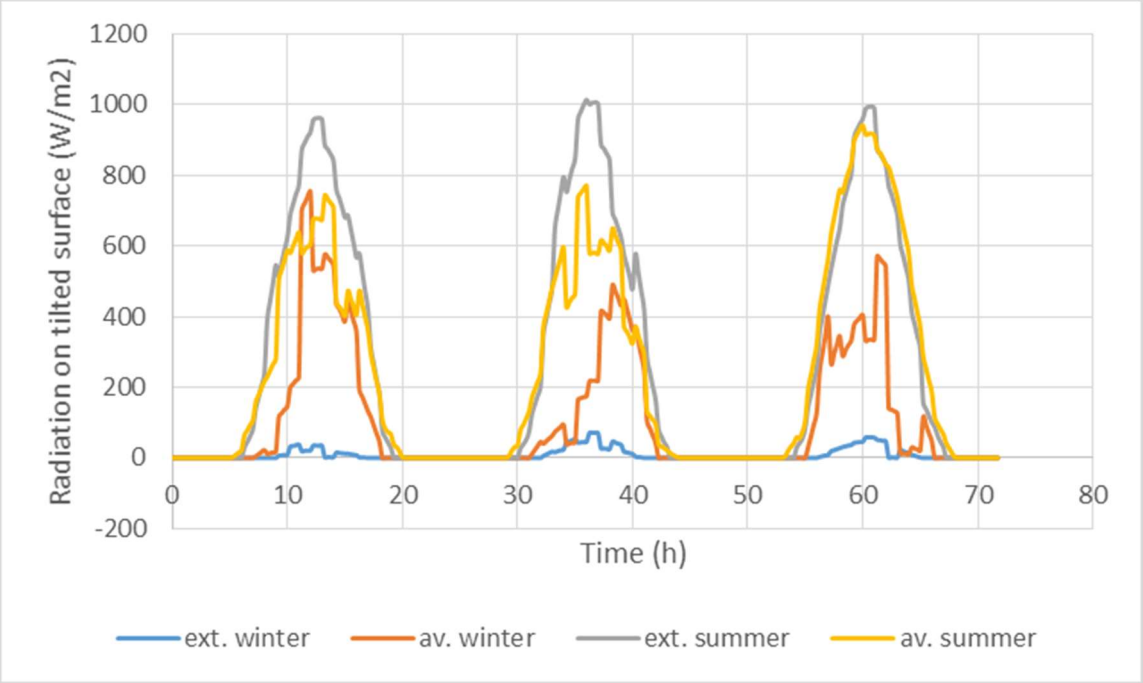

Figure 34: Hourly radiation on tilted surface variation of the extreme and average winter, extreme and average summer scenarios in Thessaloniki

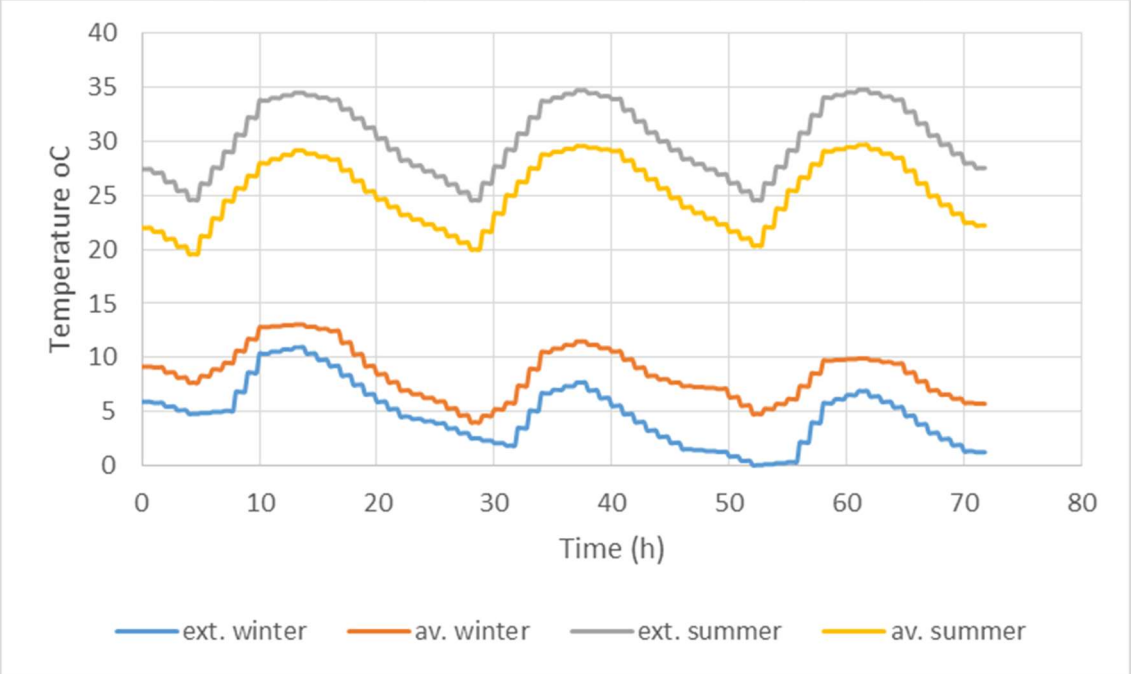

Figure 35: Hourly temperature variation of the extreme and average winter, extreme and average summer scenarios in Kimmeria

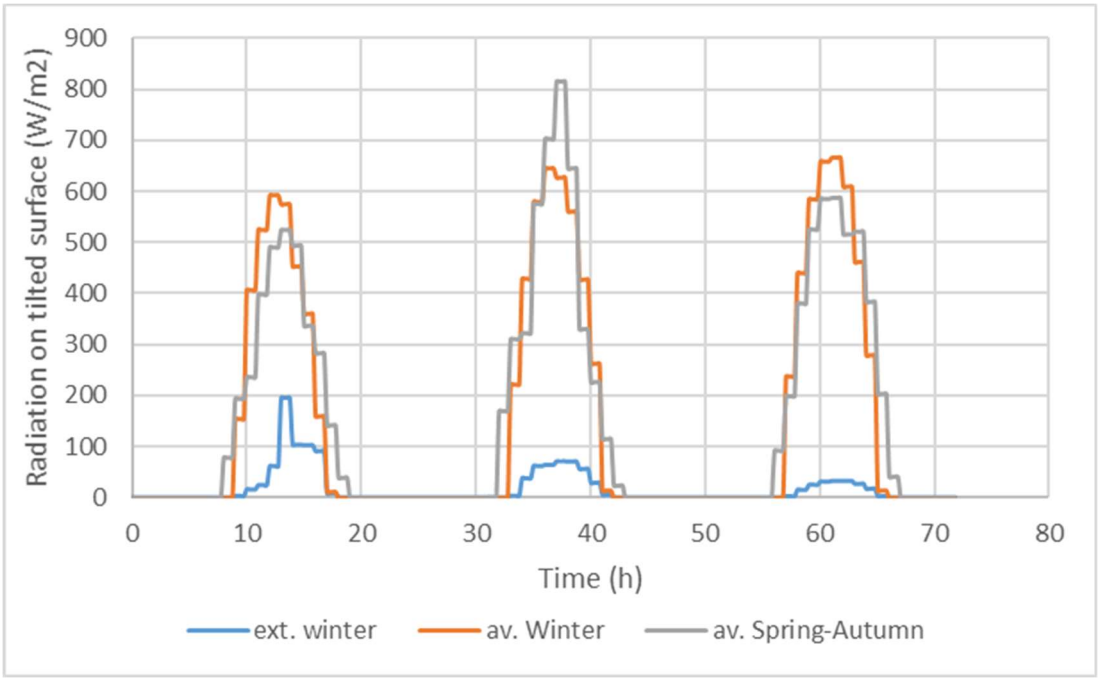

Figure 36: Hourly radiation on tilted surface variation of the extreme winter, average winter and average spring-autumn scenarios in Santiago

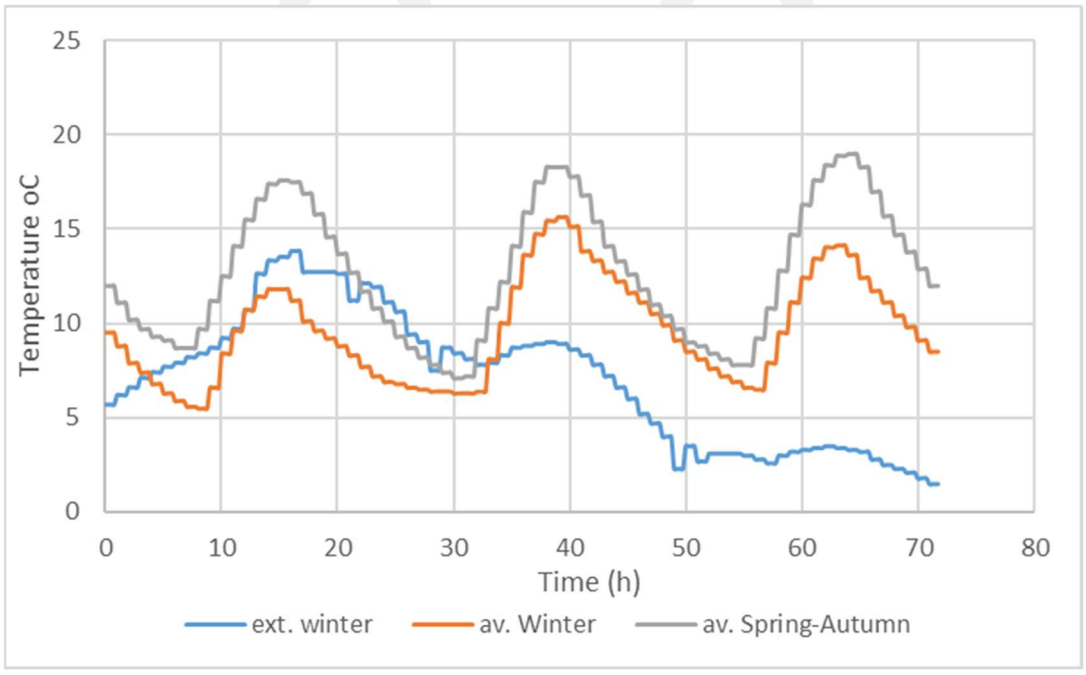

Figure 37: Hourly temperature variation of the extreme winter, average winter and average spring-autumn scenarios in Santiago

4.1.2. Heating and cooling demand in the examined scenarios

Apart from the weather data, another important parameter for conducting accurate simulations is the determination of the heating and cooling needs that MiniStor will have to cover. The heat energy demand of a building is mainly determined by four factors:

- Outdoor weather conditions
- Desired indoor conditions, according to levels that will guarantee comfort and wellbeing levels of the occupants

- Characteristics of the building structure such as floor area, area of the exposed walls, area of windows and doors, the heat transfer coefficient U of the building structural elements etc.
- Air ventilation which may be caused by natural effects or also be assisted by special mechanical equipment

The procedure of estimating the heating needs of a building is described by several standards. The latest relevant European standard is EN 12831:2017 [59]. For calculating the cooling needs of a closed space, the most widely used method is ASHRAE CLTD / CLF along with its revision CLTD / CFL / SCL [60]. According to the latter, the cooling load is shaped not only by the four mentioned factors that determine the heat demand but also by the following parameters that are related with the release of sensible and latent heat:

- Human occupation of the space and the type of the performed activity
- Operation of lighting and other electrical appliances

Table 21 summarizes some characteristics of the demo site dwellings where the MiniStor system will be installed. In particular, for the case of Sopron, MiniStor will provide heating and cooling to a newly constructed building consisting of two floors and a cellar. It is a highly insulated construction as the U values of the various opaque enclosures are lower than 0.2 W/m^{2}K according to data provided by the demo site manager. In Cork, MiniStor will operate in a semi-detached two floor house. Its level of insulation is adequate. According to its BER Assessment the heat transfer coefficients of the opaque elements are below 0.7 W/m^{2}K. In the case of Thessaloniki ("Smart House" testbed building), the system will be verified in a large room with a gross area of approximately 49m^2. This option is preferred as the Smart House building consists of two floors and presents a total area of about 320m^2. Finally, in the case of Kimmeria, the system will cover the heating and cooling needs of 5 rooms in one building of the campus' dormitories. Their gross area is 15m^2 each and have poor thermal insulation. According to information given by the demo site owner, the U value of the opaque enclosures is around 1 W/m^2.

Location	Construction year	Gross area (m^2)	U value of opaque elements (W/m^{2}K)
Sopron	2019	176.6	< 0.2
Thessaloniki	2017	48.9	< 0.35
Kimmeria	1997	75.6	0.85 – 1.05
Cork	1980	89.6	< 0.7
Santiago	1991	14686.9	3.8

Table 21: Characteristics of the demo site spaces where MiniStor will be installed

The following sources were used for the compilation of Table 21: Architectural plans and BER Assessment (Cork), data provided by the building manager (Sopron), Building Energy Assessment (Thessaloniki), information provided by the DUTH personnel (Kimmeria). Regarding Santiago, information was provided by USC personnel (see also D2.4 for more information).

Finally, in order to estimate the required energy output of MiniStor, its operation pattern has to be defined. In the cases of Sopron and Cork a 24-h operating pattern is considered, during which the system will have to cover the needs of all building spaces. In the case of Thessaloniki, where currently the Smart House is occupied only during conventional office working hours, the MiniStor operation pattern coincides with the room occupation. The electrical energy consumption of the building is analysed in order to estimate the latter. In Kimmeria demo site, two different options could be adopted: in the first one the MiniStor operating schedule would coincide with that of the campus central heating system. In the second option the system operating hours would coincide with the presence of students in the rooms. In the current study the second scenario is considered so as to highlight the advantages that MiniStor can offer. The room occupation pattern is approximated by using data provided by the DUTH personnel. In the Santiago Demo, specific periods of time representative of extreme and typical conditions during the heating season (since the system will be used only for providing heating to the selected dwelling) were selected. Based on data from the local building manager and the apartment occupants, a suitable heating operation

schedule was set. This involves 9.5 hours of operation during the coldest period of the year (i.e. in the midst of winter) and a 7-hour operation on days with mildly cold weather (i.e. in autumn and at the end of winter). In spring, a 5-hour operation is foreseen, which is very similar to that of the mildly cold weather with the exception of the function at noon.

Figure 38 presents the MiniStor operation pattern in Sopron,Cork,Thessaloniki and Kimmeria, while Figure 39 in Santiago .

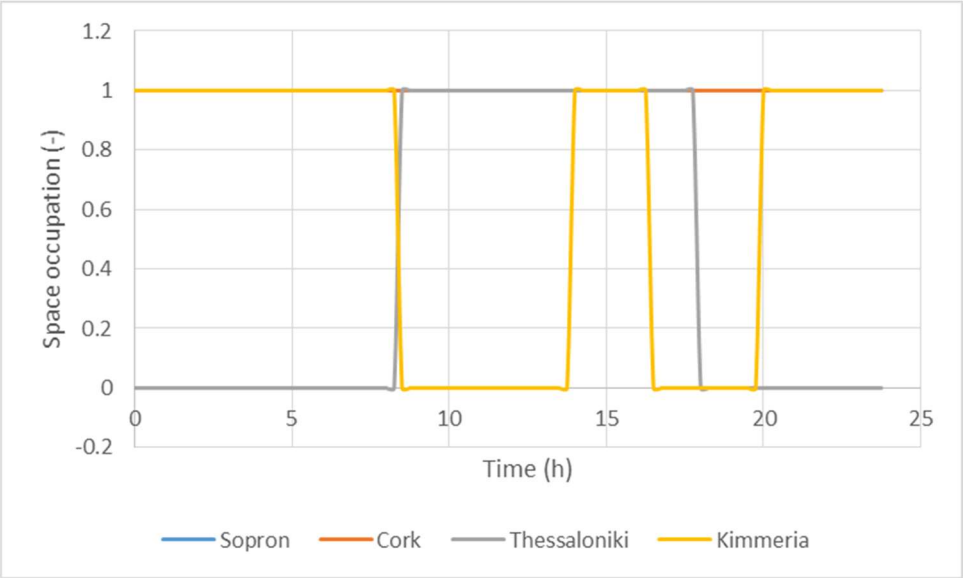

Figure 38: Occupation pattern in Sopron, Cork, Thessaloniki and Kimmeria demo sites

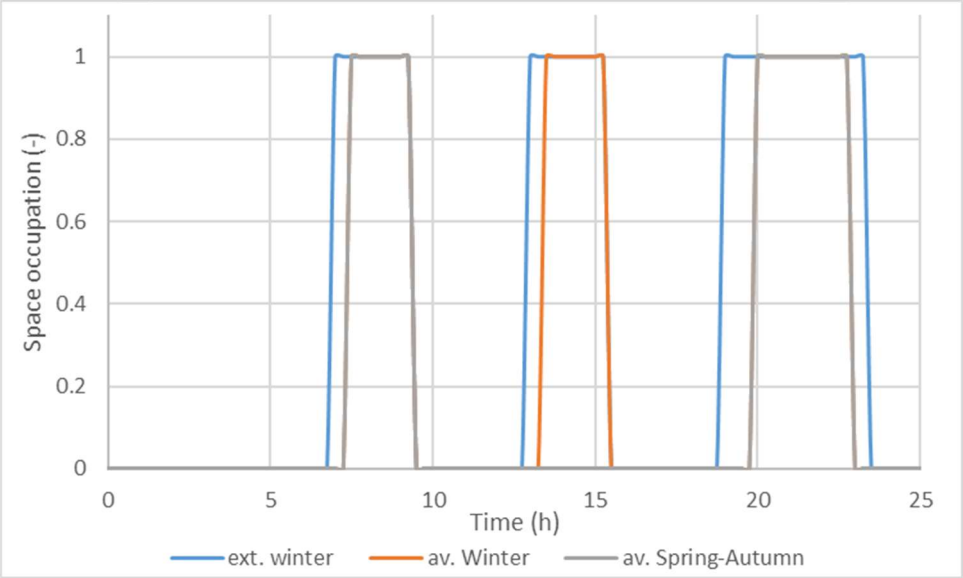

Figure 39: Occupation pattern in Santiago demo site for the different scenarios

Taking into account all the above presented information, the heating and cooling loads that the MiniStor has to cover are estimated for each scenario and presented in Figure 40 to Figure 42. The following steps are followed in this procedure:

- In the case of Sopron, the building thermal demand for various outdoor temperatures are available from calculations conducted by the demo side manager using a specialized numerical tool. These data are used to formulate a relationship between thermal load and outdoor temperature that is used to estimate the demand in all examined scenarios. For estimating the cooling demand, the building 3D model along with heat loss coefficient

values (both given by the demo site manager) are utilized and the ASHRAE CLTD / CFL / SCL method is implemented. In these calculations, the established occupation pattern along with a typical daily profile of electrical energy consumption defined in the framework of Tasks 3.1 and 3.5 are utilized in order to estimate effect of human occupation, lighting and electricity appliances operation.

- For the Cork demo site, the heating load is computed by applying the methodology described in EN 12381 standard. The BER assessment along with architectural plans are utilized in order to gather all the necessary information.
- In the case of Thessaloniki, the heating and cooling needs are estimated according to EN 12381 and ASHRAE CLTD / CFL / SCL method accordingly. The Building Energy Assessment is utilized for data gathering. For the cooling load estimation, the above presented occupation pattern is used for considering the human presence effect. Typical office equipment is considered to be in operation.
- In Kimmeria, the estimation of the maximum daily heating and cooling demand of one room within one-year period was carried out by the DUTH personnel using specialized numerical tools. The data of these calculations in combination with architectural plans and the occupation pattern are used to estimate the loads of all five rooms according to EN 12381 and ASHRAE CLTD / CFL / SCL methodologies.
- In the case of Santiago, the heating load is calculated following the methodology set out at the EN 12831:2017 Standard. Input data for this calculation were taken from the building plans, information obtained from the demo site manager as well as typical values for the thermal transmittance of the building elements for buildings of that region and year of construction included in one of the Spanish official tools for building energy rating assessment in existing buildings called CE3X.

The desired indoor temperature in heating mode operation is 20°C in all cases. In cooling mode operation, it is 24°C in Sopron and Thessaloniki, 26°C in Kimmeria. In conclusion, these load calculations although based on several assumptions, can be considered fairly accurate to be used as input in the simulations of the MiniStor system operation.

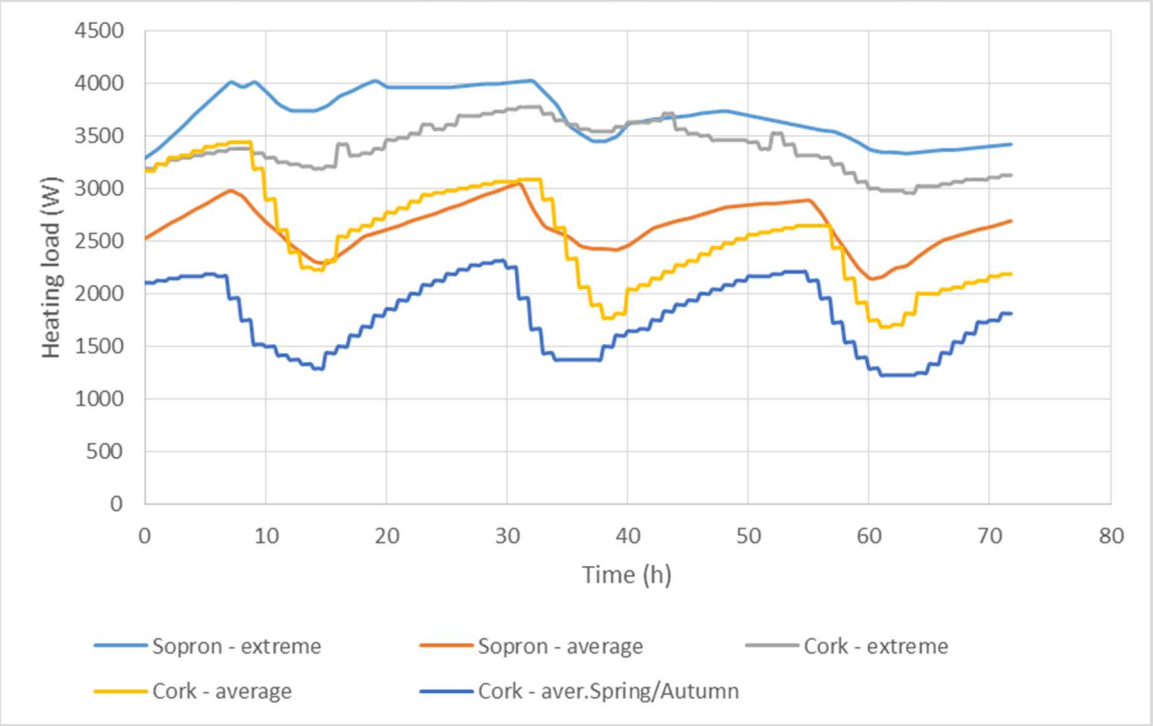

Figure 40: Extreme and average heating load in Sopron and Cork

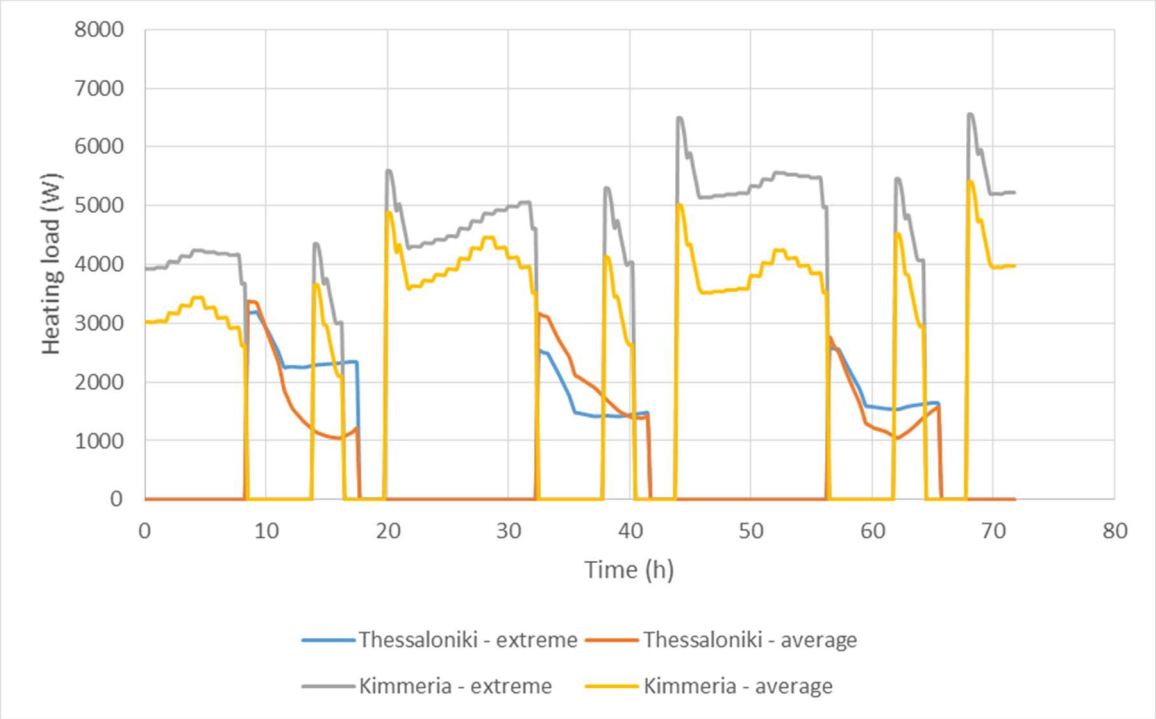

Figure 41: Extreme and average heating load in Thessaloniki and Kimmeria

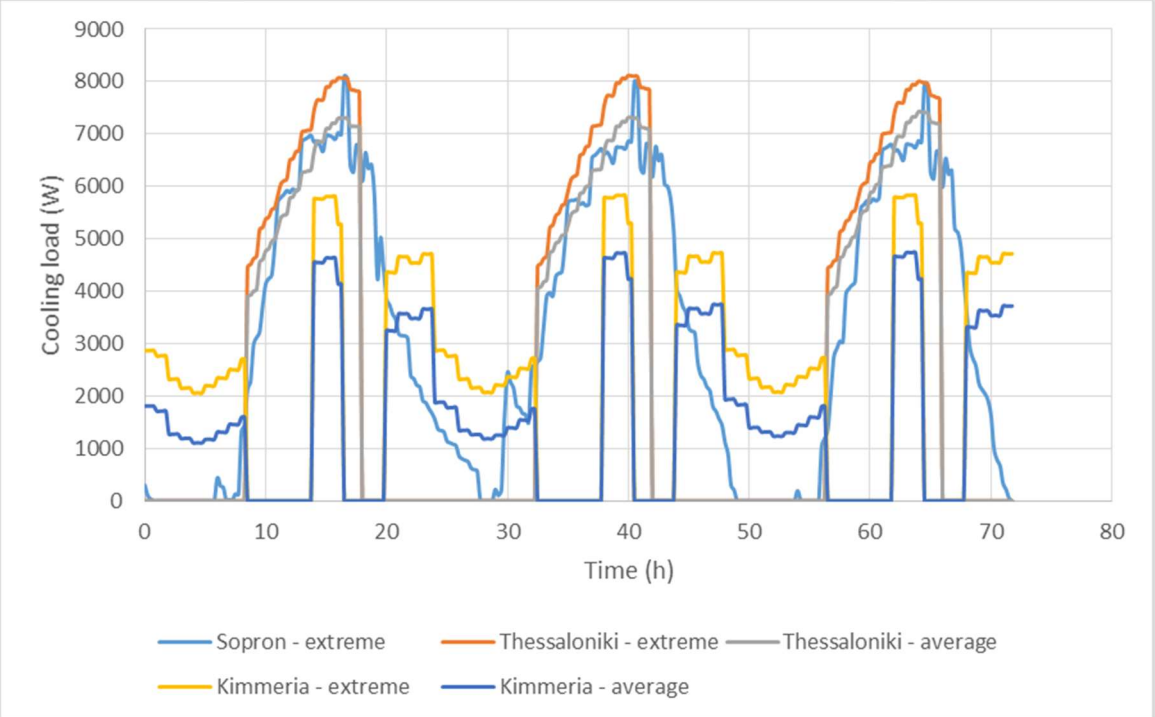

Figure 42: Extreme and average cooling load in Sopron, Thessaloniki and Kimmeria

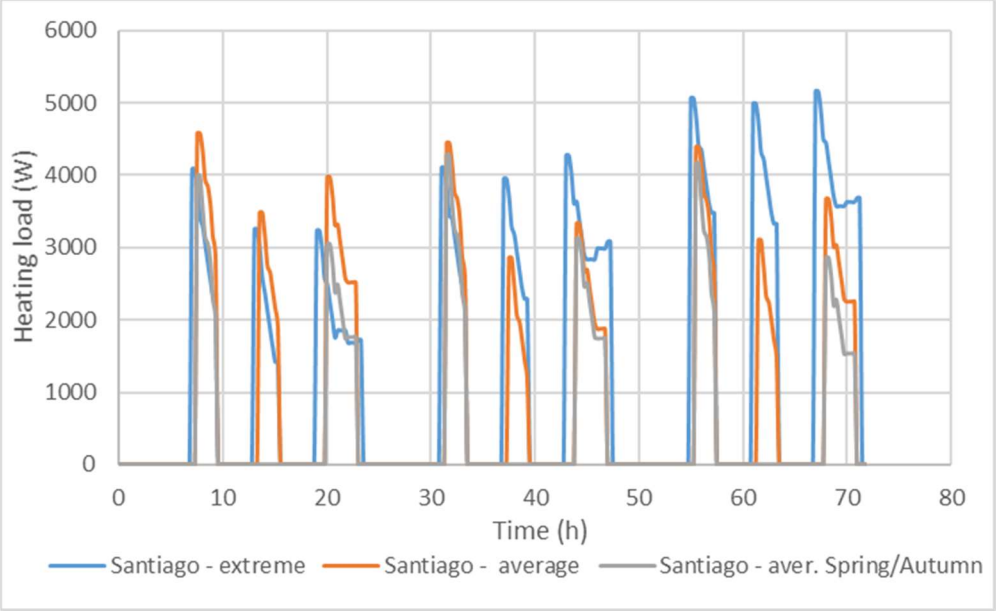

Figure 43: Extreme and average winter and average Spring/Autumn heating load in Santiago

4.2. Thermal system design parameters

As observed in Table 22 (in which all the main thermal design parameters of the integrated system for each demo site are presented), all demo sites have the same size TCM reactor as well as PCM storage tank. Furthermore, the buffer tank size is also the same in all of them except for Kimmeria, where the existing facility for the production of hot water with renewable energy sources provides the necessary heat input to the system. The operating pressure of the TCM decomposition reaction is 2 bar for the winter cases and 3 bar for the summer ones due to the compressor's minimum operating pressure ratio. The initial temperatures of the buffer tank layers and collectors' cells for sites with a PVT – Solar Collectors layout, during the average and extreme winter cases are: 40°C, 35°C, 10°C and for the average and extreme summer are 60°C, 55°C, 20°C, respectively.

Minimum temperature set for the activation of the Buffer tank – TCM reactor circuit for winter cases is 44 °C in Sopron's average winter, Cork (both average and extreme winter) and Thessaloniki's extreme winter, 50 °C in Sopron's extreme and Thessaloniki's average winter, 60 °C in Kimmeria (both extreme and average) and 65 °C in Santiago (both extreme and average). If solar energy is not sufficient enough, the backup electric heater is activated to complete the decomposition reaction, with a maximum output of 2kW. For the Kimmeria demo site, both in winter and summer cases has a set temperature of 53°C for the first reaction, and 65°C for the second reaction of the decomposition. In the Santiago demo case, it can be observed that the mass flows are increased in comparison to the other demo sites, due to the fact that the Hitachi HP is providing heat to the TCM reactor and in the simulations its nominal operating values were implemented.

Demo site	Sopron	Kimmeria	Cork	Thessaloniki	Santiago
PVT – Solar Collector Layout	9 PVTs (Glazed) 6 FPCs (ESCOSOL FMAX 2.4)	- -	4 PVTs (Glazed) 4 FPCs (ESCOSOL FMAX 2.0)	5 PVTs (Glazed) 5 PVTs (Glazed) 5 FPC (ESCOSOL FMAX 2.4)	20 PVT (Unglazed)

Mass flow of solar field to tank (kg/h)	554	-	400	500	1000
TCM size (kWh)	17.5				
PCM size (kWh)	Hot PCM – 3.6 kWh (SU58 material) Cold PCM – 6 kWh (SU11 material)				
Tank size (kg)	60				
Operating pressure of TCM decomposition reaction (bar)	2 (Winter –Spring/Autumn cases) 3 (Summer cases)				
Average and Extreme winter case scenarios					
Initial Temperature of buffer tank and cell (°C)	Thigh: 40 Tlow: 35 Tcell:10	-	Thigh: 40 Tlow: 35 Tcell:10	Thigh: 40 Tlow: 35 Tcell:10	Thigh: 40 Tlow: 35 Tcell:10
Mass flow from buffer tank to TCM reactor (kg/h)	360	468	360	360	1000
Operating pressure of TCM synthesis reaction (bar)	6	6	6	6	6.5
Activation temperature of decomposition reaction (°C)	Average 44 Extreme 50	Average 60 Extreme60	Average: 44 Extreme: 44	Average: 50 Extreme: 44	Average: 65 Extreme: 65
Average and Extreme summer case scenarios – for Cork and Santiago the average spring-autumn scenario is depicted					
Initial Temperature of buffer tank and cell (°C)	Thigh: 60 Tlow: 55 Tcell:20	-	Thigh:40 Tlow: 35 Tcell:10	Thigh: 60 Tlow: 55 Tcell:20	Thigh: 40 Tlow: 35 Tcell: 10
Mass flow from buffer tank to TCM reactor (kg/h)	360	468	360	500	1000
Operating pressure of TCM synthesis reaction (bar)	5	5	6	5	6.5
Activation temperature of decomposition reaction (°C)	Extreme: 70	Average: 70 Extreme: 70	Average: 44	Average: 70 Extreme: 70	Average: 65 Extreme: 65

Table 22: Thermal system design parameters

The temperature provided by the HP to the TCM reactor is steady at 65°C for both reactions of the decomposition and for all examined cases. Moreover, in USC demo site, same as Cork demo, the coverage of cooling demand will not be demonstrated, so an average Spring-Autumn scenario is investigated instead. Operating pressure differs depending on the thermal and cooling load of the dwelling. In all demo sites, it is set to 6 bar except for Santiago, where the pressure is 6.5 bar for the winter cases. As a result, the heat transfer fluid exiting the TCM reactor has a temperature of

63°C which is sufficient for household heating and charging of the hot PCM heat storage tank. For the summer cases in all demo sites except Cork, the operating pressure for synthesis is 5 bar. The evaporation of the ammonia will take place at 5°C, and the cold PCM storage tank can charge. In the demo sites of Cork and Santiago regarding the spring-autumn scenario, the pressure has been set at 6/6.5 bar respectively, due to the fact that there is no need for cooling.

4.3. Required electrical model inputs

For correct operation of the electrical model in TRNSYS, different inputs were mainly required: (1) weather data in the demo site locations, (2) electrical load profiles to be potentially covered by the MiniStor electrical system (i.e. PVT and batteries), and (3) an electricity-price signal to be considered in the decision-making process that prioritizes either the use of electricity from the grid or the use of electricity stored in the MiniStor system. Technical specifications of the equipment that will be installed in the system are also required and follow data of section 2.1.5, as well as control inputs of sub-systems directly or indirectly connected to the electrical system (e.g. solar thermal loop, TCM reactor). These controls have been preliminarily defined during the modelling process and will be detailed in full during the scope of WP5.

4.3.1. Weather data for PVT models

Weather data is one of the most important dynamic inputs to carry out the simulations in TRNSYS. For the electrical PVT model, Meteonorm files in TMY2 format were used as a highly accurate data source since they are based on standardized meteorological stations (PVSYST, 2020). More details can be found in D.2.2[5].

The following variables in the TMY files, obtained for every hour of the year, are of interest for the PVT models:

- Temperatures: dry bulb, dew point, wet bulb, effective sky or mains water temperatures; monthly or yearly average, minimum, or maximum temperatures.
- Humidity: relative humidity or humidity ratio.
- Wind: velocity, radiation.
- Solar radiation on the horizontal: total, global, direct, beam, sky diffuse, ground diffuse.
- Solar radiation for specified surface(s): total diffuse, sky diffuse, ground reflected diffuse.
- Other: latitude, longitude, precipitable water, horizontal visibility, ground reflectance, sky cover.

As an example, monthly values for global horizontal irradiation and global in-plane irradiation in Sopron can be observed in Figure 44:

[5] *D2.2: Definition of system context and limits for use*

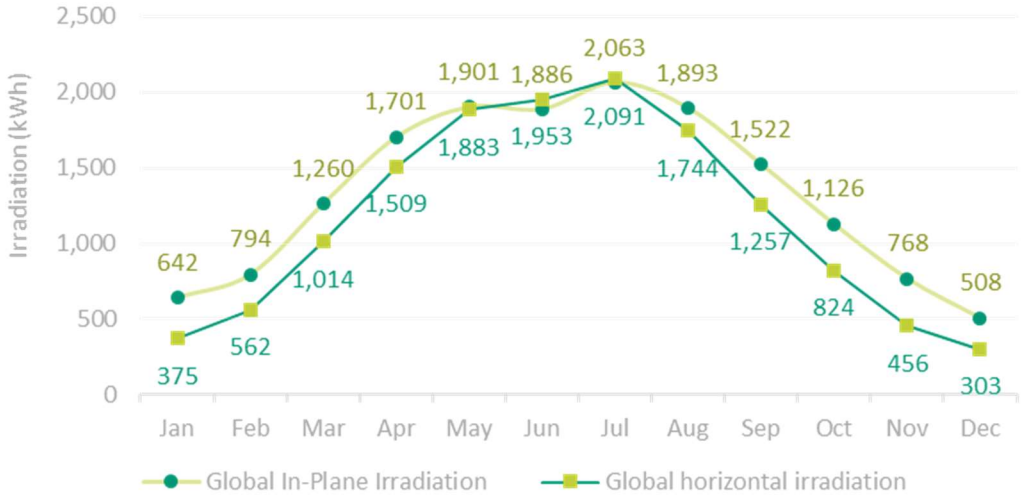

Figure 44: Monthly values for global in-plane and global horizontal irradiation in Sopron

4.3.2. Electrical demand profiles

For this deliverable, the electrical demand profiles are presented for two demonstration sites: Sopron and Thessaloniki. The other demo sites are in the process of calculation of their electrical demand profile and will be presented as an update as more data becomes available through on site monitoring.

a) Electrical demand profiles for Sopron

The electrical demand in the demo site in Sopron has been estimated based on average consumption in Hungary and foreseen consumptions based on planned uses, since the site is still under construction and there are no past-use registers. These estimations have been elaborated together with WOODSPRING, which is the partner responsible for this demo site.

According to the information provided by WOODSPRING, the electrical demand in Sopron will be mainly constituted by three separate uses: (1) an office, (2), an apartment (flat) and (3) and an electric vehicle. All of them present a very different daily consumption profile, and also a different occurrence profile along the week. Thus, apartment demand has a daily occurrence; office demand is present during weekdays (Monday to Friday) and electric vehicle is charged three times a week (Monday, Wednesday and Friday nights) (Figure 45 and Figure 46). The sum of these three contributions results in a peak demand of 3.78 kW with and average demand of 0.97 kW.

Figure 45: Weekly Sopron's household electrical demand

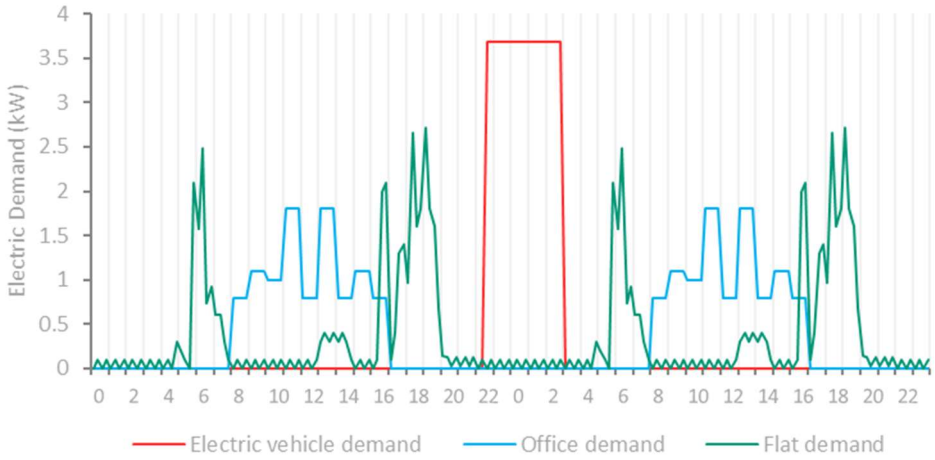

Figure 46: Two days of Sopron's household electrical demand

As observed in Figure 45 and Figure 46, all different demands mainly occur distributed in time and have different profiles:

- Most of the consumption in the flat takes place in the early morning and at night. The rest of the day, the consumption is negligible, except for the lunch period, when electrical demand slightly increases.
- The demand in the office exists only during working hours (08-17h), when there is occupancy.
- The electric vehicle consumes a constant power during night hours, when the flat and the office demands are minimal.

Figure 47 presents the weekly distribution of frequencies of occurrence for the electrical demand of the demo site, i.e. only considering apartment, office and car charge demand.

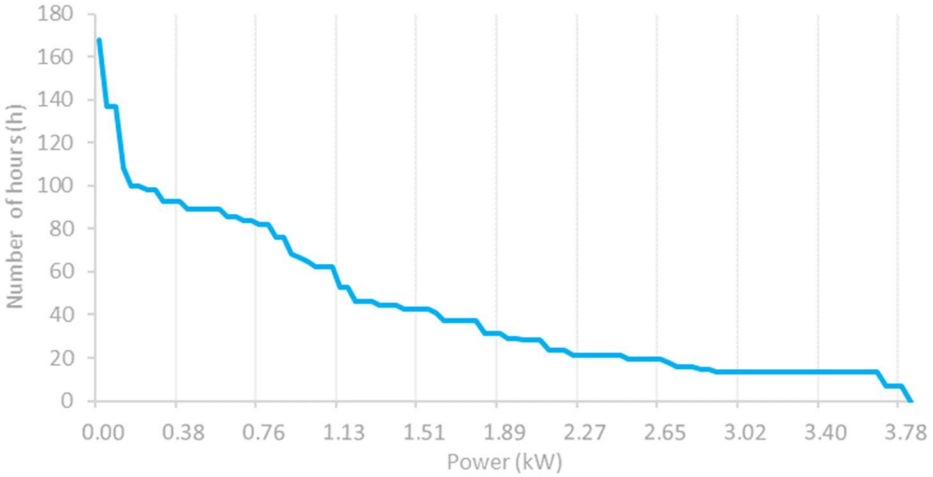

Figure 47: Weekly frequency of occurrence for Sopron's household electric power demand

Additionally, an estimated electrical demand for the MiniStor system has been considered based on the thermal models. Nevertheless, computational issues have limited the production of results, hence only one-cycle results for average and extreme conditions in winter and extreme conditions in summer have been obtained (Figure 48).

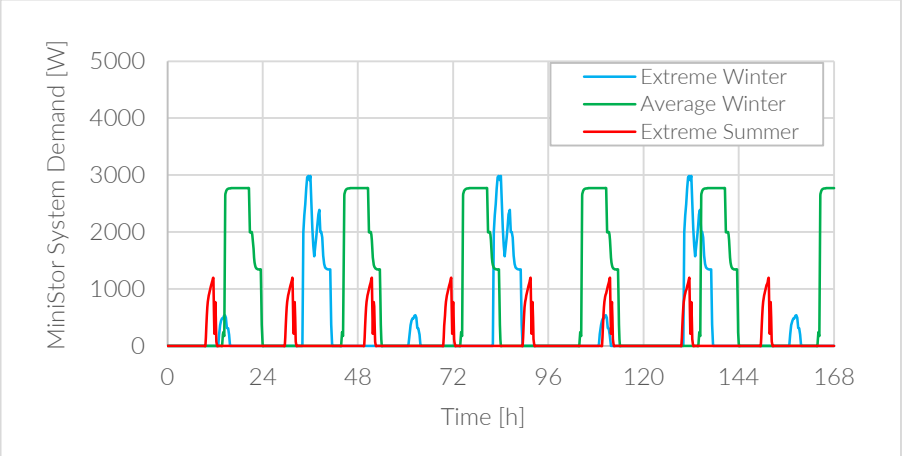

Figure 48: MiniStor system electrical demand. Sopron demo site

As consequence, different sets of MiniStor demands have been assigned to each month of the year to define the demand for the whole year. Following this approach and using the TMY2 file, extreme winter conditions have been assigned to January, February, November and December; winter average conditions to March; and extreme summer conditions to July and August. For the rest of months no heating or cooling demands have been assumed, so MiniStor electrical demand during these months has been assumed as null.

From the perspective of the MiniStor electrical sub-system (i.e. PVT system, batteries), the electrical demand of the whole MiniStor system is addressed as an additional load to be covered: either by the photovoltaic system when possible or by the electricity grid. Consequently, the total electrical demand resulting from the sum of the household estimated load and MiniStor electrical demand reaches a maximum electrical power of 5,2 kW and an average demand of 1,3 kW.

On a yearly basis, the total electric load covered by the system in the Sopron demo site is presented in Figure 49. Two main different scenarios in terms of total load can be identified from a preliminary analysis: one corresponding to summer months (i.e. June, July and August), and another referred to the rest of the months. In the first case, the total load averages 1,047 kWh, while in the second case it decreases down to 730 kWh.

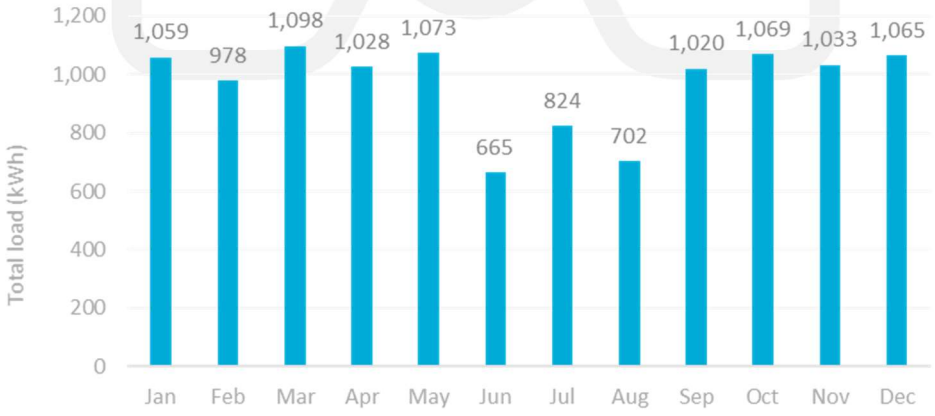

Figure 49: Total base electrical load. Sopron demo site

The main reason for these two different scenarios has been presented before and can be also found by looking at Figure 50, where the load breakdown is displayed. While the load corresponding to the building (office, flat and electric vehicle) is constant throughout the year and only presents slight differences due to the duration of each month, the load referred to the electrical consumption of MiniStor does change between months, varying from extreme winter periods, average winter periods, mild periods (no heating or cooling needed), and extreme summer periods.

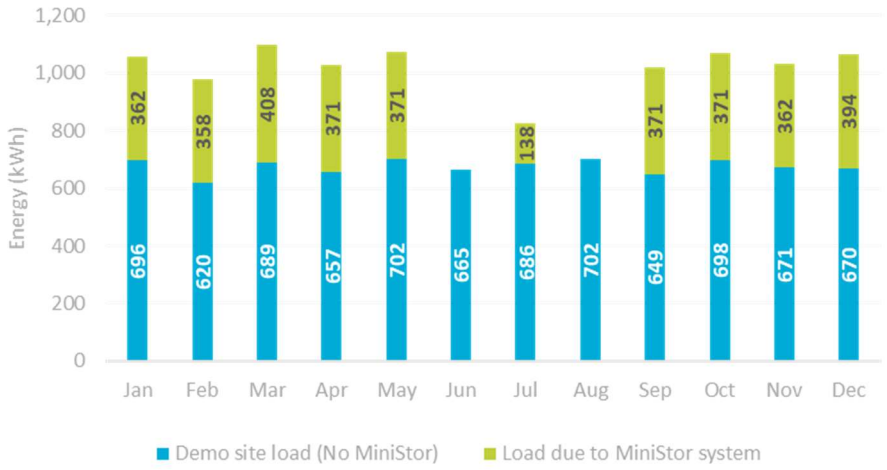

Figure 50: Electric load breakdown with contribution from MiniStor electrical system. Sopron demo site

b) Electrical demand profiles for Thessaloniki (pre-demo site)

The CERTH-ITI Smart Home, where the Thessaloniki demo will be implemented, is a testbed that resembles a home and has a high load due to the amount of sensors and monitoring equipment installed for research purposes. Therefore, it has a very high installed electrical power in comparison to a typical home. When not in use as a testbed, the Smart Home serves as an office building.

Among the existing electrical equipment, there are VRV type HVAC units, with a nominal electrical power of 14.61 kW. The building also has a PV installation and an on-grid inverter with a nominal power of 10 kW. They are equipped with 3 additional single-phase inverters for the connection of low voltage lithium-ion electrical batteries. The complexity of the existing electrical installation at this demo site, therefore, does not make feasible to carry out possible modifications in the context of the MiniStor project, due to the high cost involved and the scope of the intervention would not contribute to the power needs of the site.

Because of this, the PVT electrical system in this demo-site will be independent from the existing installation, *focused to meet mainly the electrical demand of the MiniStor system itself*. The system will have 10 PVT panels with a total nominal installed power of 2.6 kWp, with a hybrid 3-phase inverter with a nominal power of 3 kW.

The electrical demand included in the PVT electrical system simulation for this demo site corresponds only to the MiniStor system itself. The main electricity consumption is produced by compressors linked to the TCM reactor, an internal heat pump, and the electrical backup heater. Figure 51 (a) and Figure 51 (b) present the base electrical demand profiles of this system, which were estimated by CERTH within Task 3.1 through detailed thermodynamic simulations of the MiniStor System.

During the winter period, two typical electrical load profiles were defined (Figure 51), one corresponding to the “extreme winter ” and the other corresponding to the “average winter ”. In general, during wintertime, the MiniStor System performs the synthesis and decomposition processes during two days, so the typical electrical demand profile runs for 72 hours, with two main demand peaks: the first of 1.09 kW and the second of 2.75 kW. The “extreme winter day” profile was assigned to the winter months with less solar radiation and temperature (January and December), while the “average winter day” profile was assigned to the months of better environmental conditions (February, March and November).

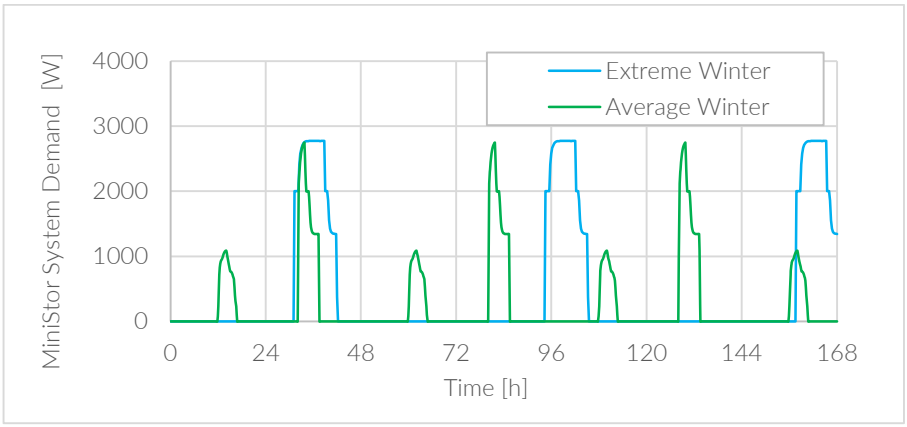

(a) Electrical winter profiles

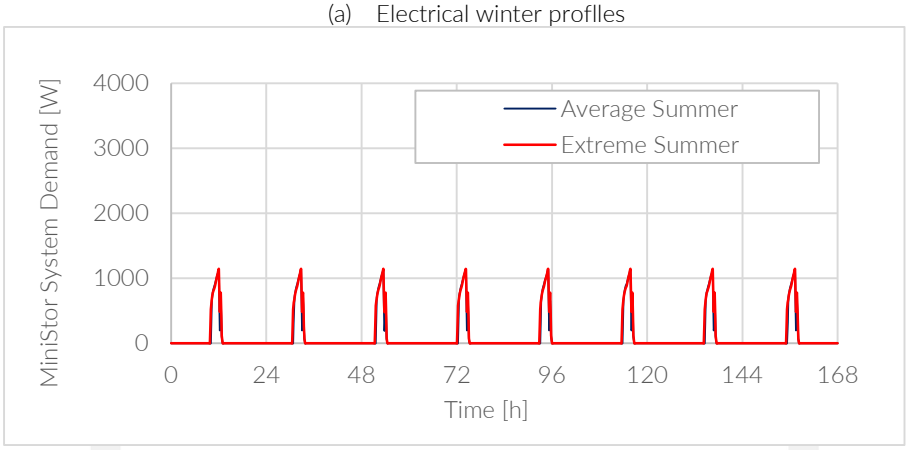

(b) Electrical summer profiles

Figure 51: MiniStor system electrical demand - Thessaloniki demo site

On the other hand, during the summer period, the synthesis and decomposition processes in the TCM reactor take place every 20.75 h, making the electricity demand of the MiniStor system have a cyclical behaviour every day (Figure 51-b). Likewise, during the summer period, two standard day-profiles were defined, one for "extreme summer day" and another for "average summer day", with power peaks of 1.09 and 1.08 kW respectively. As "extreme summer" profile were considered the days of July and August months; while, as an "average summer "profile were regarded the days of May, June and September months.

Figure 52 shows the evolution of the monthly electricity consumption of the MiniStor system in the Thessaloniki Demo. The annual electricity consumption of the system is 2460 kWh, of which 78% correspond to the winter months and only 22% correspond to the summer months.

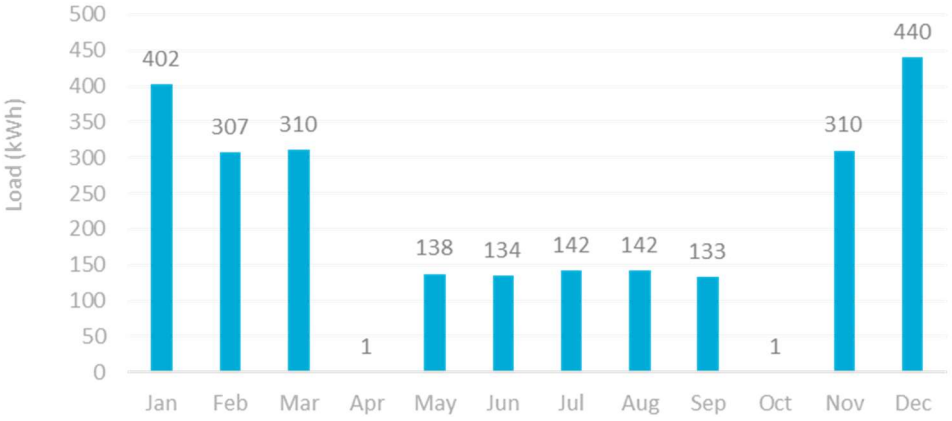

Figure 52: Total base electric load. Thessaloniki demo site (system self-consumption only)

4.3.3. Grid-price signal

The MiniStor system has been projected to be dynamically connected to the main grid in order to enhance, and ultimately optimize, the energy flows from a techno-economic perspective. As a first step, a price signal has been modelled referred to the changing price of electricity from the grid. In the scope of this task, the limit price has been set to the yearly average price to determine the moments for which covering the load with electricity from the grid was more cost-effective than doing so with electricity from MiniStor system (generated by the PVT or stored in batteries). This decision-making process will be examined in detail in Task 3.5, where it is envisioned to potentially charge the batteries with electricity from the grid during low-price periods and either using it or sending it back to the grid during high-price periods, hence allowing the price to reach a minimum value.

In this case, a system has been defined to prioritize consumption from batteries only when grid-electricity prices exceed a certain limit price. This method allows MiniStor to self-consume electricity when the market price is high and to store photovoltaic energy when the price is low enough. Nevertheless, an optimized selection of the limit price has been not studied in the scope of this task, but will be studied in detail in Task 3.5.

In any case, the price signal is needed for the model to determine on every moment which is the most convenient way of covering the load. For modelling purposes, an hourly price signal throughout the whole year has been considered. For Sopron and Thessaloniki demo sites, due to the lack of information about the exact prices that would be applied in each case according to local regulations, prices from the spot market in 2019 were used [61]. A more realistic approach will be proposed in Task 3.5 that will also examine current electricity market regulation and price signals for all demo sites.

The average price signal applied in the Sopron demo site for an average day, an average week and month is shown in Figure 53. The variability of the price during each period can be appreciated in this figure and also in Table 23.

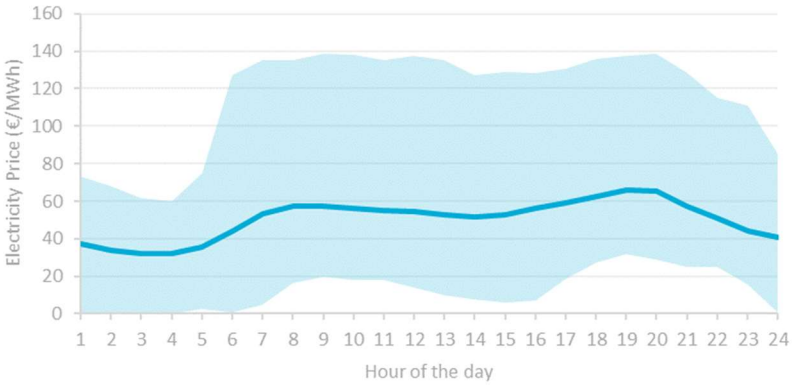

(a) Spot Market Prices during a day in 2019

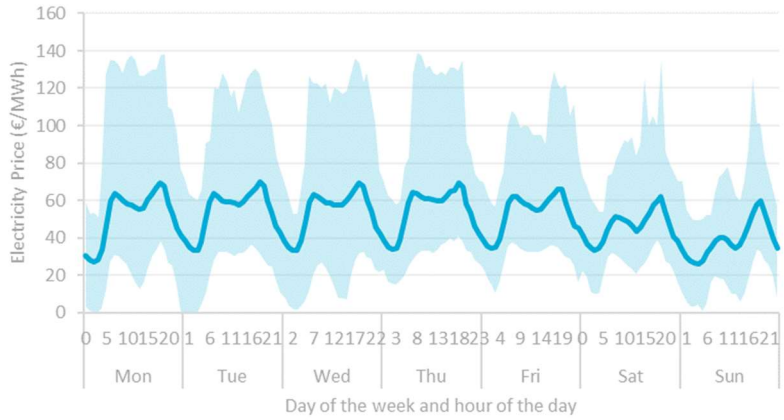

(b) Spot Market Prices during a week in 2019

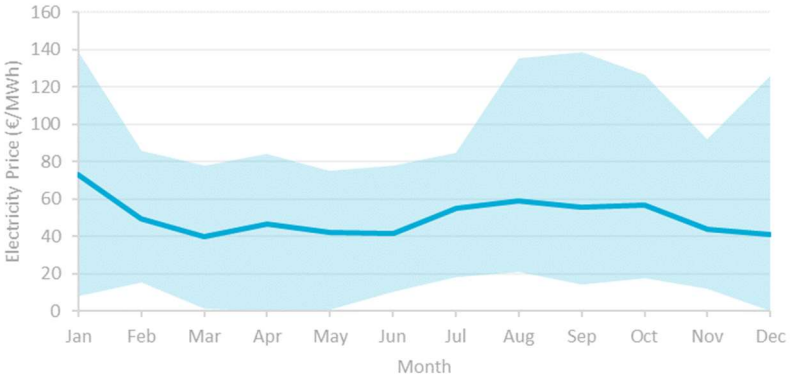

(c) Spot Market Prices during 2019

Figure 53: Hourly Average, Maximum and Minimum Spot Market Prices in Hungary - Source: [61]

Maximum Price (€/MWh)	138.82
Day at Max. Price	17/01/2019 8:00
Minimum. Price (€/MWh)	0.00
Day at Min. Price	24/12/2019 2:00
Average Price (€/MWh)	50.36

Table 23: Parameters of Hungarian electricity market prices

This implementation can be done in a similar way for the rest of demo sites in cases where more precise information about tariffs for residential consumers is not available at the moment of submitting the current report. Equivalent information is shown in Figure 54 for Greece, showing on average a lower price variability along the day, the week and the year compared to Hungarian electricity prices.

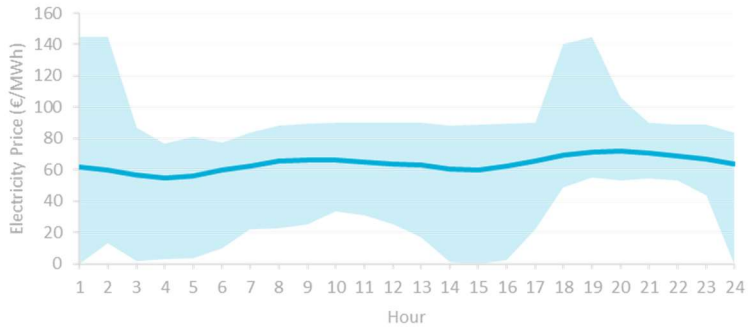

(a) Spot Market Prices during a day in 2019

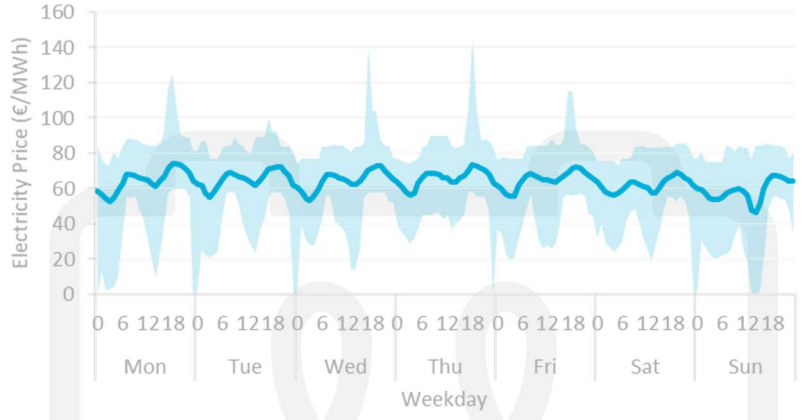

(b) Spot Market Prices during a week in 2019

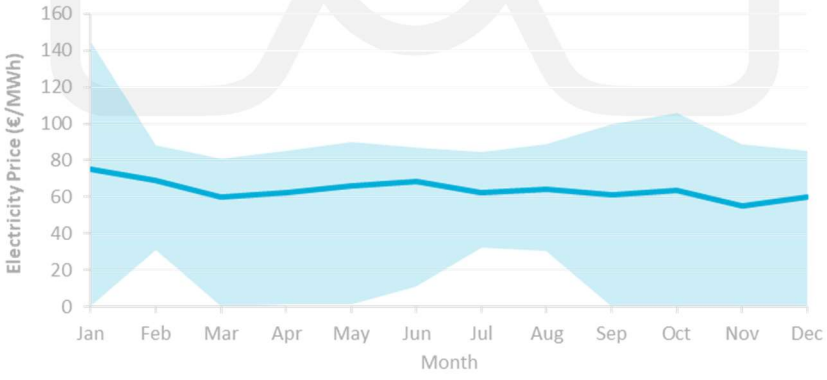

(c) Spot Market Prices during 2019

Figure 54: Hourly Average, Maximum and Minimum Spot Market Prices in Greece - Source: [61]

5. Integrated Thermal System Calculation Results

5.1. Parametric Investigation

For the parametric analysis of the integrated thermal system the Sopron demo site was selected, and specifically the average winter case study as well as the extreme summer case study. The aim of this parametric analysis is to identify the values of the critical variables that have an impact on the thermal systems behaviour in order to achieve optimal operation, charging and consumption strategy for each case scenario with minimum electrical consumption.

The solar heat input in Sopron for the selected parametric study is provided by one row of PVTs and two rows of four solar collectors each, with a mass flow from the solar field of 480 kg/h. The size of the TCM reactor is 17.5 kWh and the operating pressure of the decomposition is 2 bar. The time step of the simulations in 0.25 Hours. Input data for Sopron's average winter case are data of the 5th of March (Meteonorm Typical Meteorological Year). Due to low solar radiation in this case scenario the use of the electrical heater for the decomposition reaction is mandatory. The variables to be investigated are the following:

- Size of the buffer Tank: 50 L, 100 L, 200 L
- Mass from of the heat transfer fluid from the tank to the TCM reactor during the decomposition mode:1 kg/s, 0.6 kg/s, 0.4 kg/s, 0.1 kg/s
- Set temperature of tank/El. Heater outlet for the decomposition mode in winter: 60°C, 55°C
- Operating pressure of the TCM reactor during synthesis mode in winter: 5.5 bar, 6 bar, 6.5 bar
- Operating pressure of the TCM reactor during decomposition in summer case: 2 bar, 3 bar
- Activating temperature of TCM reactor for the decomposition in summer case: 60°C, 65°C, 70°C

5.1.1. Effect of buffer tank size

For this case, 3 simulations were chosen to be conducted in which the only changing variable is the buffer tank size. The decomposition mode in all cases has the same duration of 4.25 hours, same water inlet temperature of 60°C in the TCM reactor as well as same mass flow of 1 kg/s. The reaction begins when the buffer tank reaches its maximum temperature for each case scenario. As seen in the following diagram, the consumption of electrical heater at the beginning of the reaction presents different values in each case, which after approximately 30 min are eliminated. This is due to the different maximum temperature that each tank size can reach. The highest temperature that can be achieved with the above PVT-Solar Collectors layout is 53.9°C for a tank-size of 50 litres. In the 200 litres container case, the maximum temperature is 49.2°C, which implies for a temperature difference of 4.7°C. This results in an increase of the average power of the electrical heater by 16.7% for the 200 litres container compared to the 50 litres buffer tank.

In conclusion, in order to maximize the thermal load received by solar radiation, and to reduce as much as possible the electrical consumption of the backup heater, the smallest container of 50 litres is selected.

50 litres Buffer Tank	100 litres Buffer Tank	200 litres Buffer Tank
Maximum temperature reached from Solar Radiation (°C)		
53.9	52.1	49.2
Average Power of electrical heater (Watt)		
6471	6993	7549
Percentage of difference		
-	8%	16.7%

Table 24: Table of data obtained from the parametric case of different tank sizes

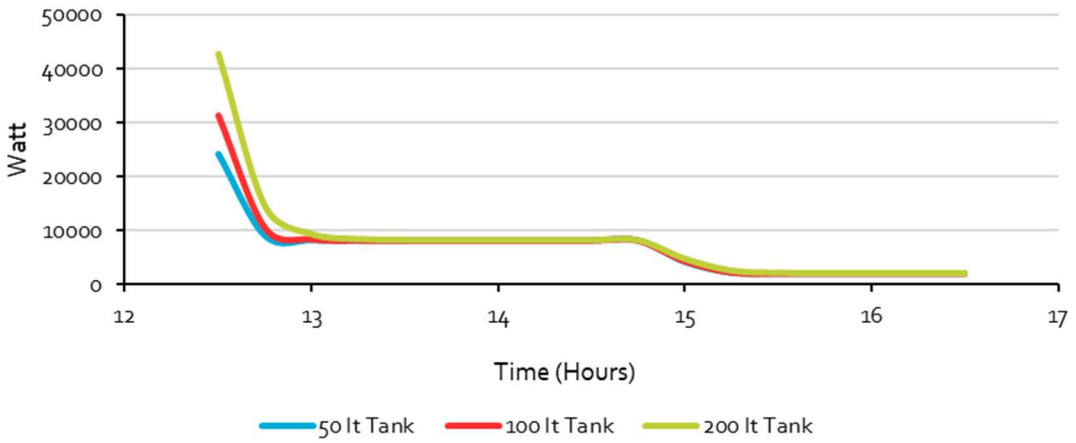

Figure 55: Consumption of the Electrical Heater for different tank sizes

5.1.2. Effect of heat transfer medium flow rate

The second parametric case concerns the mass flow from the buffer tank to the TCM reactor. For this case it was chosen to examine four scenarios, in which the only changing variable is the mass flow. The same buffer tank size and the same water inlet temperature of 60°C in the TCM reactor were considered in all scenarios. The figure below shows the evolution of four different heat duties (in Watts) of the HP condenser as well as the thermal load of the building for comparison reasons. It is also noticed that the heat output of the system at some point presents a large reduction in all cases. This is because the first reaction (8-4) of the decomposition is over and the second one (4-2) starts which has a much lower rate. During the first reaction, the thermal output of the system is noticeably greater than the thermal demand of the house. For the fluid mass flow of 1 kg/s, the excess heat is around 4800 Watt for 2.5 hours. By reducing the mass flow, it can be observed that the excess heat of the system is reduced as well. For the mass flow of 0.1 kg/s, the excess heat is around 1295 Watt for 5 hours. In addition, in this scenario the thermal demands of the building are met to a greater degree, since the total duration of the reaction is 9 hours. Finally, for the case of 0.1 kg/s the lowest electrical consumption of the backup heater, namely 2767 Watt, is observed.

1 kg/s	0.6 kg/s	0.4 kg/s	0.1 kg/s
Total time of reaction (Hours)			
4.5	4.75	5.25	9
Average power of the electrical heater (Watt)			
6471	5703	5066	2767
Excess Heat during the first reaction (Watt)			
~4800 (2.5 hours)	~4017 (2.75 hours)	~4006 (3 hours)	~1294 (5 hours)

Table 25: Table of data obtained from the parametric case of different medium fluid mass flows

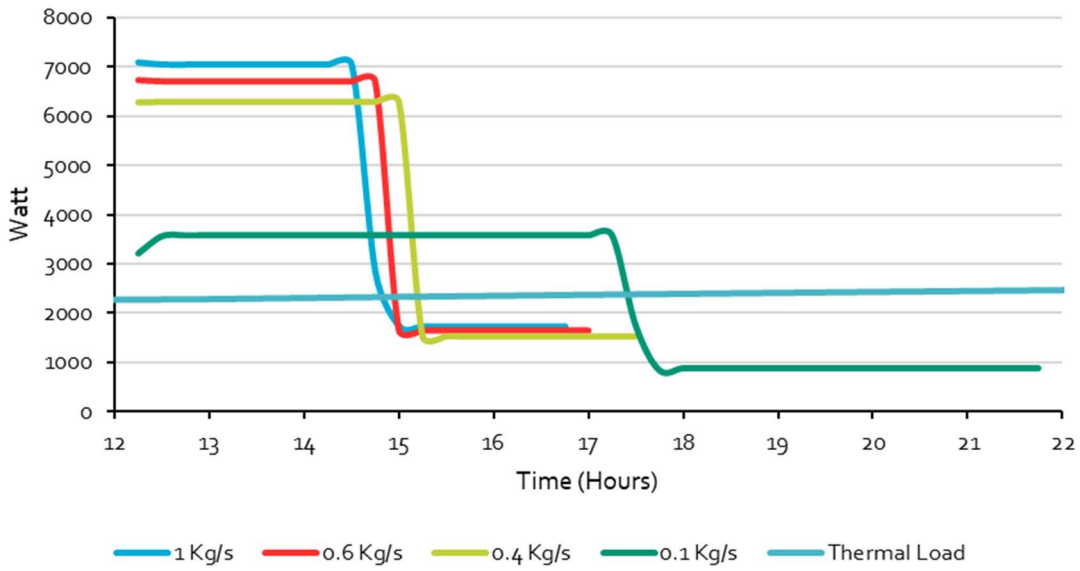

Figure 56: Distribution of generated thermal energy during decomposition for different medium fluid mass flows in comparison with building's thermal demand

5.1.3. Effect of heat transfer medium temperature

The third parametric case study concerns the inlet fluid temperature of the TCM reactor during the decomposition reaction. For this investigation it was chosen to study 2 cases in which the only changing variable is the inlet temperature, either fixed at 60°C or the range 55-60°C (to allow a wider range of inlet temperatures for the PVTs to operate). The buffer tank is 50 litres and the mass flow rate to the TCM is 0.1 kg/s. The synthesis reaction in both case scenarios has the same total duration of 7.9 hours and an operating pressure of 6 bar. The following Figure 57 displays the 2 different heat duties (in Watt) generated from the system as well as the thermal load of the building for comparison. It can be observed that in the case study with the fluid temperature fixed at 60°C, the duration of the decomposition is 9.5 hours which is 2.25 hours less than the 55-60°C case study. Furthermore, the excess heat generated during the 1st reaction for the 60°C case study is by 1176 Watt higher than the corresponding 55-60°C case.

60°C	55°C 1st Reaction - 60°C 2nd Reaction
Total time of decomposition reaction (hours)	
9.50	11.75
Excess heat and duration generated during the 1st reaction (Watt)	
~1294 (5 hours)	~ 118 (7.5 hours)
Total time of Decomposition and Synthesis reactions (hours)	
19.25	21.50

Table 26: Table of data obtained from the parametric case of different operating temperature for the decomposition reaction

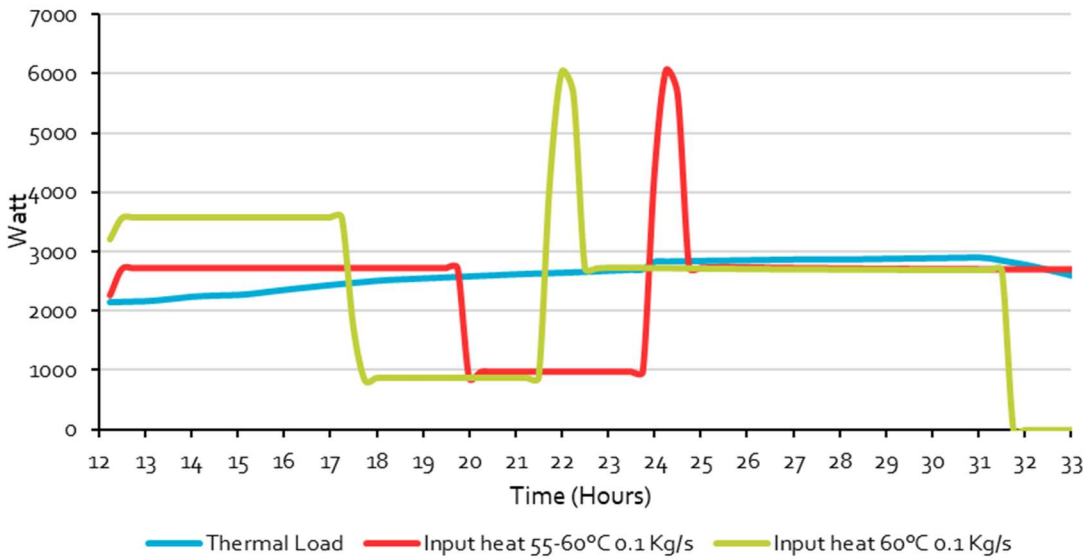

Figure 57: Distribution of generated thermal energy during charging and discharging for different operating temperature (charging mode) in comparison with building's thermal demand

5.1.4. Effect of TCM synthesis reaction pressure

The fourth parametric case study concerns the operating pressure of the TCM reactor during the synthesis reaction. For this case it was chosen to examine 3 cases in which the only changing variable is operating pressure. The synthesis reaction in all scenarios has the same set point for the output temperature of the cooling medium of the TCM reactor equal to 63°C. The figure includes the 3 different heat duties (in Watt) of the TCM reactor as well as the thermal load of the building for comparison. It can be observed that the total reaction time depends to a large extent on the operating pressure. At 5.5 bar the total reaction time is 19.5 hour, for 6 bar it is 10.5 hours and for 6.5 bar it is 7.9 hours. In this parametric study the goal is the thermal load that is produced to be as close as possible to the thermal demand of the building as well as to cover it as much as possible, thus reducing the store of the excess heat in the hot PCM. For the first two cases of 5.5 bar and 6.5 bar it is noticed that either there is not full coverage of the necessary demands or in the other hand, there is full coverage but too much excess heat is generated. The most suitable scenario for the synthesis reaction is the one with the 6 bar operating pressure where the thermal load produced is marginally tangent to the thermal demand for 7.9 hours.

5.5 bar	6 bar	6.5 bar
Total time of reaction (hours)		
19.5	10.5	7.9
Average heat generated from the thermal system (Watt)		
1576	2821	3717

Table 27: Table of data obtained from the parametric case of different operating pressures

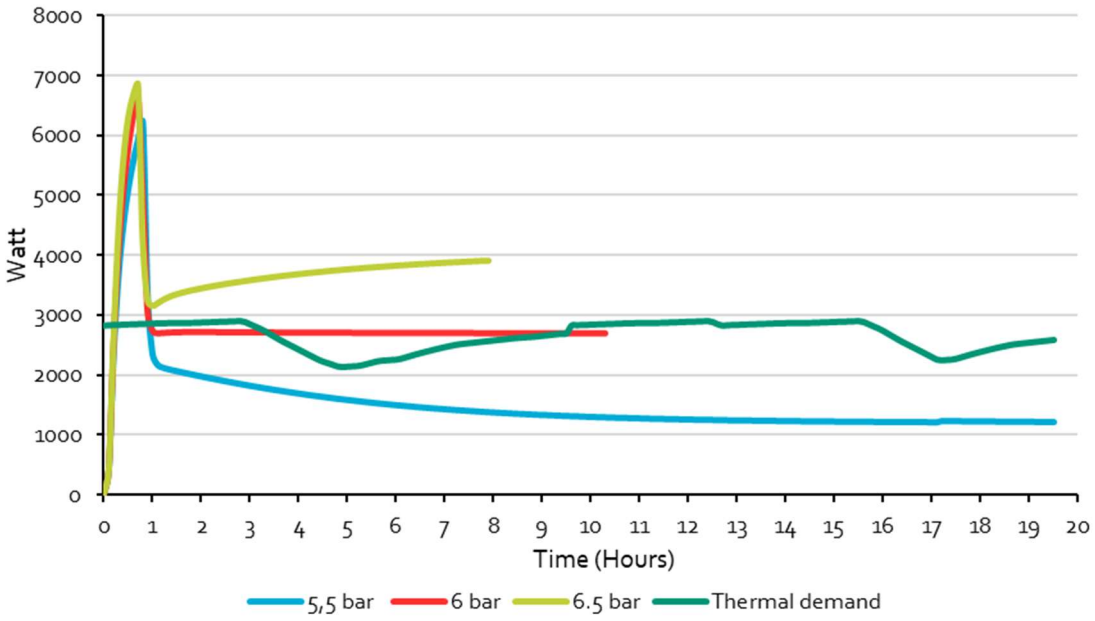

Figure 58: Distribution of generated thermal energy during synthesis for different operating pressures in comparison with building's thermal demand

5.1.5. Effect of TCM decomposition reaction pressure and activating temperature during the summer months

The fifth and final parametric case study concerns the operating pressure and activating temperature of the TCM reactor during the decomposition reaction in summer. The purpose of this parametric analysis is to observe the impact that different operating conditions for the decomposition will have on the system, both in terms of operating time and electrical consumption. For this reason, it was chosen to examine 3 cases in which two different operating pressures are investigated (2 and 3 bar) and for the 3 bar case, two different activating temperatures of 65°C and 70°C. The mass flow of heat transfer fluid from the buffer tank to the TCM reactor is 2 kg/s. The synthesis reaction in all scenarios has the same set point for the outlet temperature of the cooling medium of the TCM reactor equal to 57°C and an operating pressure of 5 bar.

Different types of heat exchangers can be used to dissipate the heat from the ammonia condensation. In the current investigation air and water-cooled heat exchangers are considered. For the NH3-water heat exchanger, the cold water supply can be provided by an external source, e.g. the central water supply system of the house, in which the temperatures even in the summer months are in the range of 21-25°C. In this case the condensation of ammonia can take place at 28°C, so the operating pressure during the decomposition of the TCM reactor as well as the compression pressure of gaseous ammonia will remain the same as in the average winter scenario, at 2 bar and 16 bar respectively. If an NH3-air heat exchanger (fan coil) is implemented, the condensation temperature of ammonia must be at least 5°C above the ambient temperature. For this reason, the TCM reactor needs to operate at 3 bar so that the gaseous ammonia can be compressed to 16 bar (minimum compressor pressure ratio of 5.5), and condensed at 40°C.

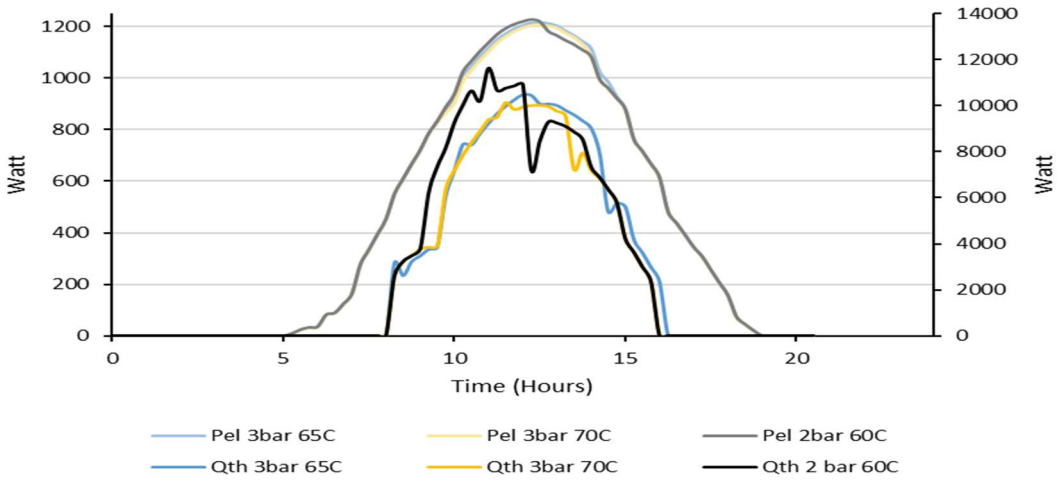

Figure 59: Distribution of generated thermal (right axis) and electrical energy (left axis) of the PVT-Solar collectors array for different operating pressures and activating temperatures of the decomposition reaction

Figure 59 displays the thermal and electrical energy generation from the PVT-Solar collectors array during the first day of the extreme summer scenario for all three examined cases. It can be observed that the electrical output of the PVTs shows very small differences between the different cases. Its highest value is 1226 W, registered at 12:25 pm. On the other hand, the generated thermal energy is very marked between the cases and reveals a strong relation to reactor pressure. The scenario with the highest thermal output of the collectors is the first one (2 bar, 60 °C), which is characterised by a reaction duration of 3.25 hours. The end of the reaction at 12:15 pm, coincides with a sharp decrease of the generated thermal energy (Black line). The two cases with the 3 bar operating pressure present a smoother distribution of the supplied solar energy, but even in these cases the sharp drop of the produced energy is observed at the time of the decomposition finalization.

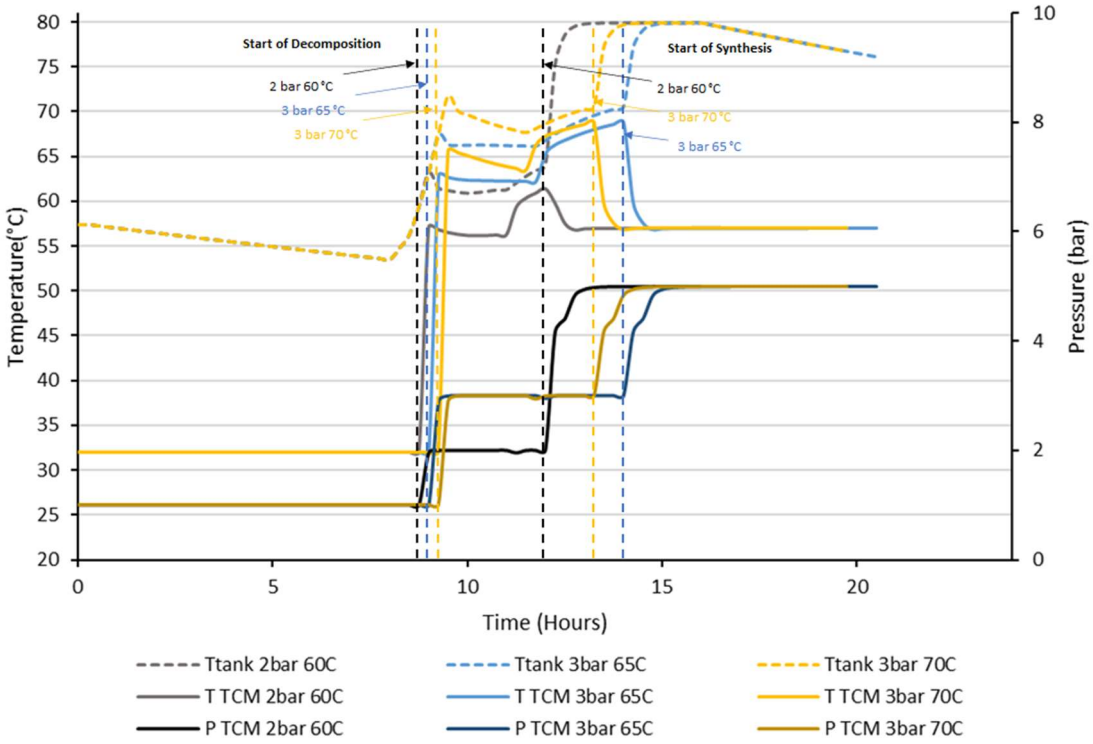

Figure 60: Distribution of temperature and pressure (right axis) of the TCM reactor and the buffer tank for different operating pressures and activating temperatures of the decomposition reaction during extreme summer case

In Figure 60, the temperature and pressure of the TCM reactor and the temperature of the buffer tank for the different scenarios are displayed. The first thing to note is the dependence of the decomposition starting time on the activating temperature. In the table below, it can be seen that the reaction starts earlier, at 9 am, in the case of reactor conditions of 2 bar / 60 °C (first scenario). The difference between each case is 15 min, therefore in the third scenario (3 bar, 70 °C) the reaction begins at 9:30 am. However, in this case the duration of the decomposition reaction is much shorter compared to the second case (3 bar, 65 °C), as it is finalized one hour earlier at 13:30. This is a result of the increased reaction rates due to the higher operating temperature of the TCM reactor.

	1st scenario	2nd scenario	3rd scenario
Reactor pressure & temperature	2 bar – 60 °C	3 bar – 65 °C	3 bar – 70 °C
Total time of decomposition reaction (hours)	3.25	5	4
Start time of decomposition	9:00 AM	9:15 AM	9:30 AM
End time of decomposition	12:15 PM	14:15 PM	13:30 PM

Table 28: Reactor conditions and decomposition reaction start, end and duration for the three examined scenarios

The scope of the fifth and last parametric scenario was to select the appropriate variables' values in order to reduce as much as possible the duration of decomposition phase during summer. The outcome indicates that the conditions of the first investigated case (2 bar, 60 °C) lead to the shortest reaction duration, but they involve the utilization of a water-NH_3 heat exchanger. If an air-NH_3 heat exchanger is selected, then the conditions of the third scenario (3 bar, 70 °C) combined with ammonia discharge pressure of 16 bar and condensing temperature of 40 °C, are the most suitable resulting in a total reaction duration of 4 hours. In all the following calculations the conditions of the first scenario are adopted, but this will have to be a subject of change if an air-NH_3 heat exchanger is actually selected for real system implementation.

5.1.6. Consolidated results from the thermal system sensitivity analysis

In the updated simulations, some of the proposed configurations of the parametric analysis have been altered. In particular, the operating pressure of the TCM reactor has been increased to 3 bar for the summer cases in order to overcome the ambient temperature during the ammonia condensation. This results in an increased activation temperature of the TCM reactor during decomposition, at 70°C for the summer cases. The final updated parameters of the proposed configuration are:

- Tank size: 60 L
- Mass flow from buffer tank to TCM reactor: 0.1 kg/s
- Operating pressure of TCM reactor during decomposition reaction (Winter/ Autumn-Spring months): 2 bar
- Operating pressure of TCM reactor during **decomposition** reaction (Summer months): 3 bar
- Operating temperature of TCM reactor during decomposition (Winter/ Autumn-Spring months): 55°C (1st reaction) and 60°C (2nd reaction)
- Operating pressure of TCM reactor during synthesis reaction (Winter/ Autumn-Spring months): 6 bar
- Operating pressure of TCM reactor during synthesis reaction (Summer months): 5bar

These key specifications are applied to all the following case studies.

5.2. Sopron demo site results

5.2.1. Sopron demo site thermodynamic results

5.2.1.1. Average Winter Case Sopron

In Figure 61, the heat demand of Sopron's demo site in comparison with the output heat of the system during the course of 1.5 day is presented. In addition, the electrical consumption of the backup heater is displayed. The first day, as the radiation value reaches the value of 500 W/m^2, the heat transfer medium circuit starts heating the reactor and the decomposition reaction is taking place for 0.5 hours. Afterwards the electrical heater is activated and the decomposition lasts for 9 hours. In order to cover the heat load, the electrical heater is activated at around 9.25 hours' time. At the start of the second day, the electrical heater stops operating as the synthesis reaction begins. During that time, the output heat from the system does not exceed the thermal demands of the building, the hot PCM is not charging.

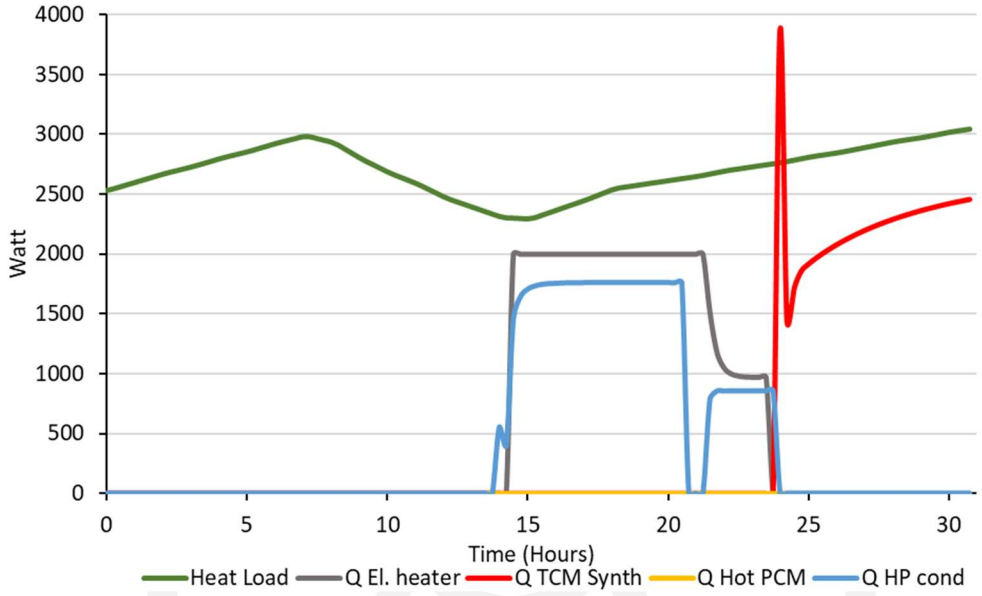

Figure 61: Heat demand in comparison with the input heat by the system and the consumption of the electrical heater for Sopron average winter case

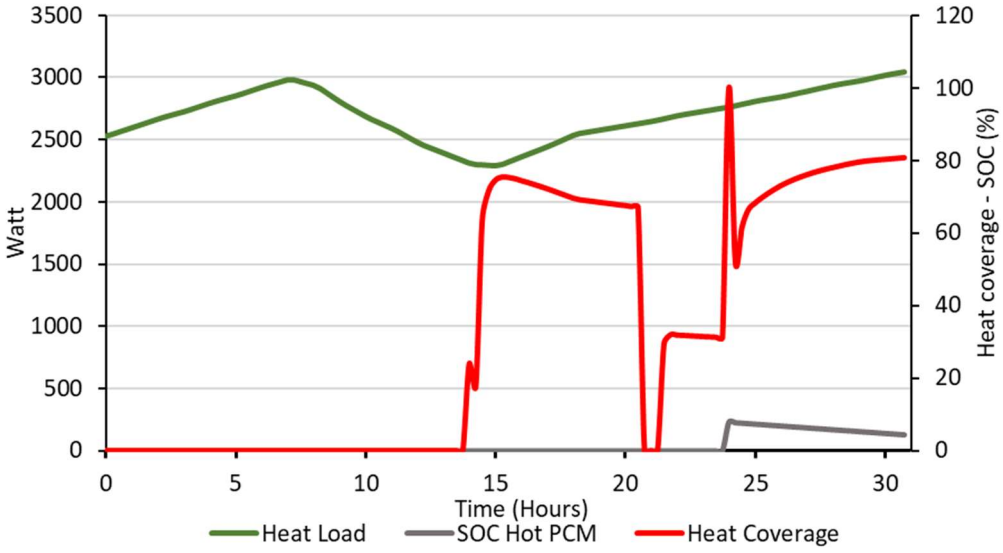

Figure 62: State of charge of the Hot PCM for Sopron average winter case

Error! Reference source not found. presents the total heat coverage provided by the system in comparison with the heat demand for Sopron average winter case. During the first 14 hours, when the system is based only on the heat input provided by solar radiation, the heat coverage of the system is zero. Immediately after that, when the electrical heater is activated, the system manages to cover 70-80% of the heating demands of the building for 7 hours during the first reaction (8-4) of the decomposition and for almost 6 hours during the synthesis with a average coverage of 77%. During the second reaction (4-2) of the decomposition (hour 65-70) the heat coverage of the system is at 35 %.

5.2.1.2. Extreme Winter case Sopron

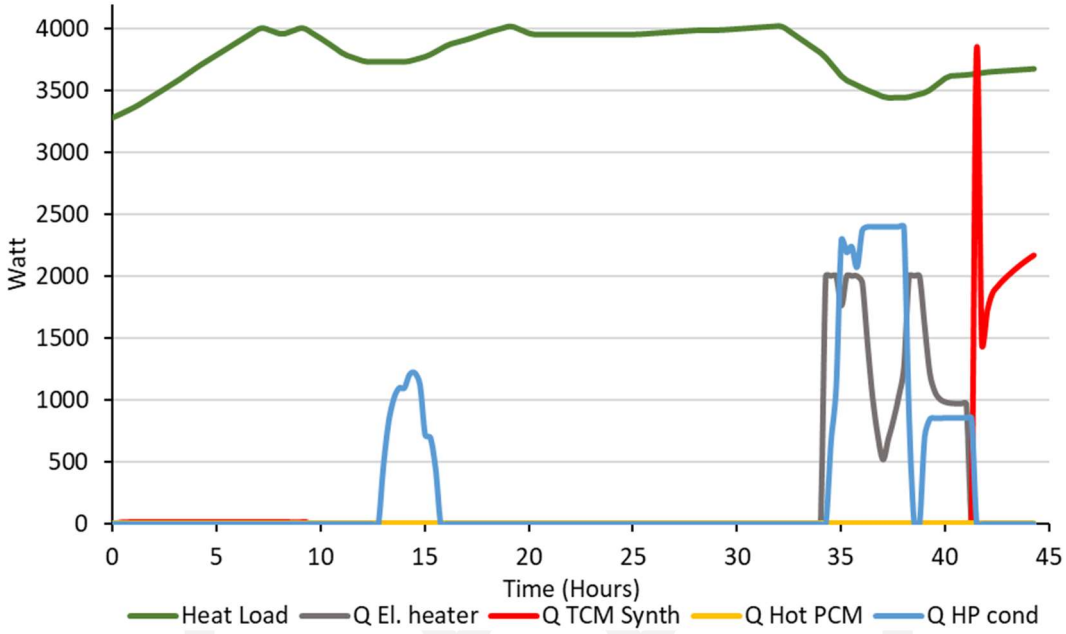

Figure 63: Heat demand in comparison with the input heat by the system and the consumption of the electrical heater for Sopron extreme winter case

In Figure 63, it can be seen the heat demand of Sopron's demo site in comparison with the heat input from the system during the course of the two days cycle. In addition, the electrical consumption of the backup heater is displayed. On the first day due to the significant radiation values that reach 600 W/m^2 for 5 hours, the heat transfer medium circuit starts heating the reactor and the decomposition reaction is taking place for 2.5 hours. The electrical heater was activated on the second day, in order to finish the decomposition reaction. In that day, the radiation is the highest of the two. Unfortunately, in the extreme winter scenario the average thermal demand of the build is quite high, above 3500 Watt and the decomposition reaction cannot fully cover the demand. That means that the hot PCM is not being charged at any point, since the thermal demands are not exceeded by the system. During the 2nd synthesis reaction (4-8), the heat duty of the reactor is closer to the thermal load than that of the decomposition reaction but again the generated heat is not enough for the coverage of the building's needs.

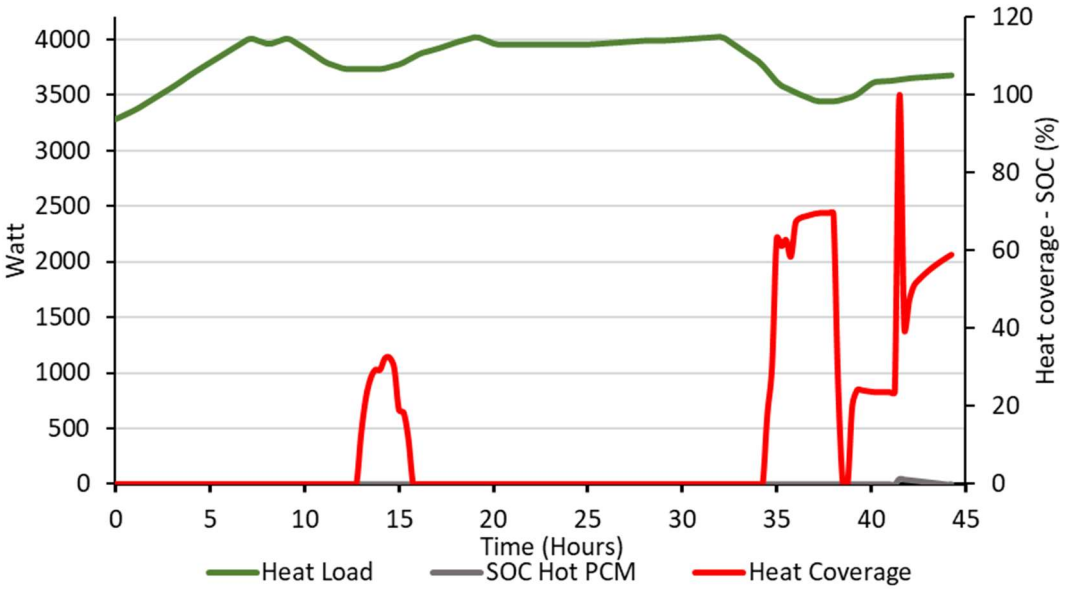

Figure 64: State of charge of the Hot PCM for Sopron extreme winter case

In Figure 64, the total heat coverage of the system in comparison with the heat demand for the Sopron extreme winter case is depicted. It can be observed that during the first day, when the reactor operation was only solar radiation driven, the heat coverage of the building is around 24% for 2.75 hours. On the second day, when the electrical heater is activated, the system managed to cover almost 70% of heating demands of the building for 5 hours during the first reaction of the decomposition (8-4). During the second reaction of the decomposition (4-2) the heat coverage of the system drops to 25% for 4 hours. During the synthesis reaction, the system manages to obtain 100% heat coverage very briefly and afterwards it stabilizes at around 60%.

5.2.1.3. Extreme Summer scenario Sopron

In Figure 65, the cooling demand of Sopron's demo site in comparison with the cooling input from the system during the course of the first day can be seen. The cooling demands of Sopron's demo site are high, with a peak value of 8 kW. In this case, decomposition is completed only utilizing the solar energy. The strategy for the decomposition is to minimize its duration so the synthesis reaction can start at the midday when the highest cooling demands are observed. In that way although the system achieves a small percentage of coverage (around 17%) of the buildings cooling load, the systems operating cycle is one day. Peak value of the cooling coverage is being obtained during the first reaction of the synthesis, but this high value of 43% is achieved only for a brief time.

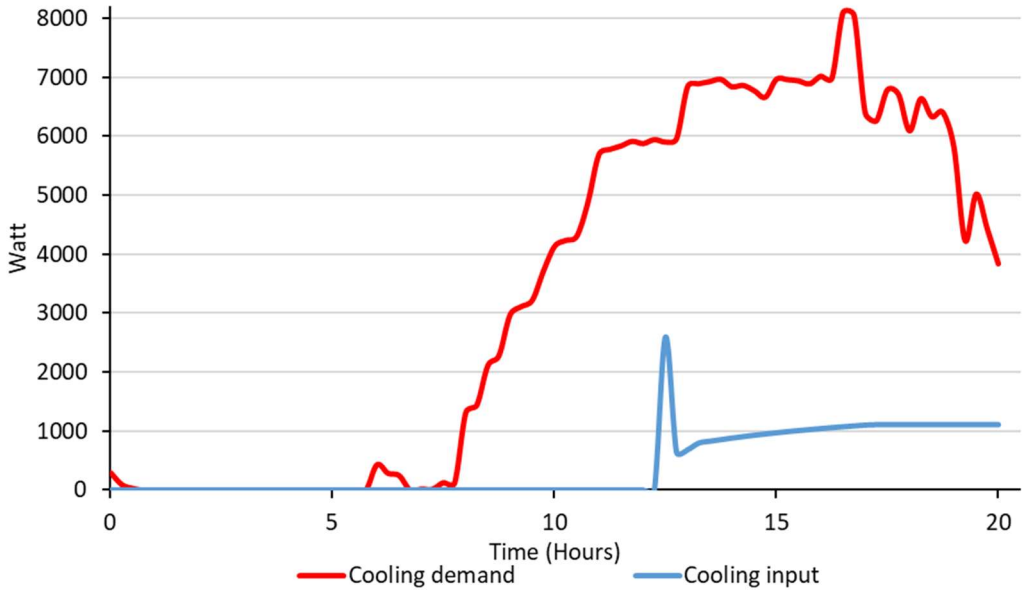

Figure 65: Cooling demand in comparison with the output cooling of the system for Sopron extreme summer case

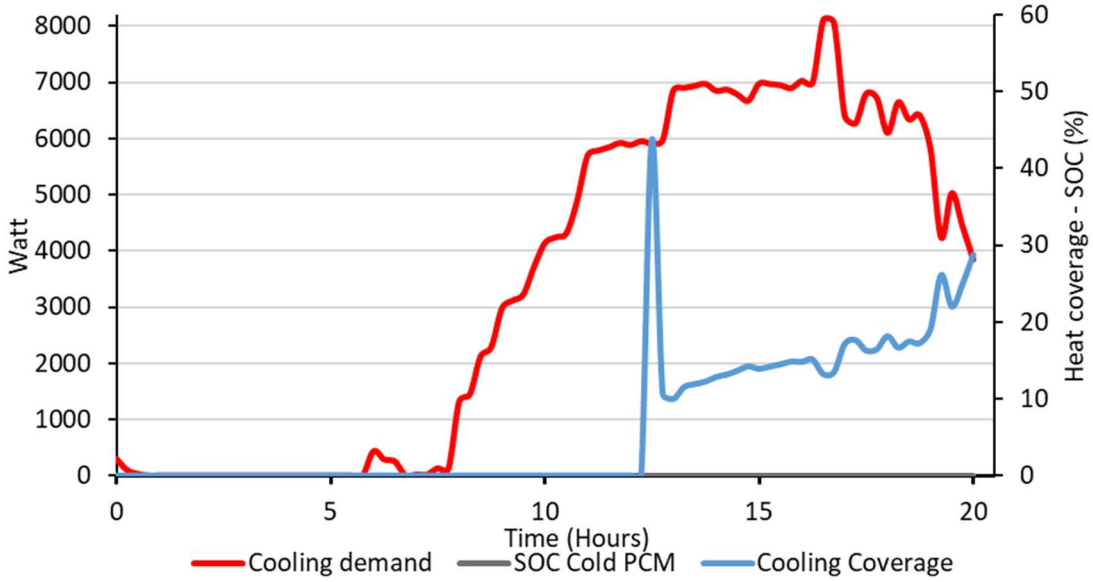

Figure 6667: Total cooling coverage percentage (right axis) of the system in comparison with the cooling demand for Sopron extreme summer case

5.2.2. Proposed design specifications for Sopron

In Table 29, the average outputs of average winter case scenario for the initial dimensioning of the system are displayed. Due to the fact that in both average and extreme cases, the usage of the electrical heater was mandatory for the completion of the decomposition reaction. The total duration of the system reactions is 17 hours, if radiation is high enough or an external heating source can be used and the cycle of the system can be limited to one day for both the average and extreme winter Sopron cases. The average generated heat during the decomposition is 1.3 kW. The synthesis reaction generated an average heat of 2.24 kW.

	Decomposition	Max values of Decomposition	Synthesis	Max values of synthesis
Time (Hours)	10	-	7	-
Heat transfer fluid mass flow (kg/h)	360	360	260	309
NH_3 Average mass flow (kg/h)	2.15	2.85	3.77	9.74
NH_3 Compressor duty (kW)	0.27	0.33	-	-
NH_3 Condenser duty (kW)	0.95	1.17	-	-
Heat Pump compressor duty (kW)	0.34	0.44	-	-
Heat Pump condenser duty (kW)	0.36	0.45	-	-
NH_3 Evaporator duty (kW)	-	-	1.2	3.2
TCM synthesis heat duty (kW)	-		2.24	3.87
Electrical heater duty (kW)	1.77	2	-	-

Table 29: Average outputs of average winter case scenarios for Sopron demo site

In Table 30, the average outputs of the extreme summer scenario for the initial dimensioning of the system are displayed. Due to the fact that in the extreme summer scenario the solar energy is adequate for the completion of the decomposition, the electrical heater is not utilized. The total duration of the reactions is 10.5 hours so the cycle of the system operation is one day. Average cooling generated during the synthesis reaction is 2.17 kW. The mass flow of the gaseous ammonia is 6.76 kg/h which is more than three times higher than the average and extreme winter cases, where the corresponding value is 2.15 kg/h. This is happening because of the reduction of the total time of decomposition from 10 hours to 2.75 hours. Due to the increase of the ammonia mass flow the duties of the ammonia condenser as well as of the ammonia compressor are similarly higher, 2.7 kW and 0.95 kW respectively.

	Decomposition	Max values for decomposition	Synthesis	Max values of synthesis
Time (Hours)	2.75	-	7.75	-
Heat transfer fluid mass flow (kg/h)	360	360	416	500
NH_3 Average mass flow (kg/h)	6.76	10.7	3.27	8
NH_3 Compressor duty (kW)	0.75	1.2	-	-
NH_3 Condenser (kW)	2.7	4.3	-	-
NH_3 Evaporator duty (kW)	-	-	1.05	2.6

Table 30: Average outputs of extreme summer case scenario for Sopron demo site

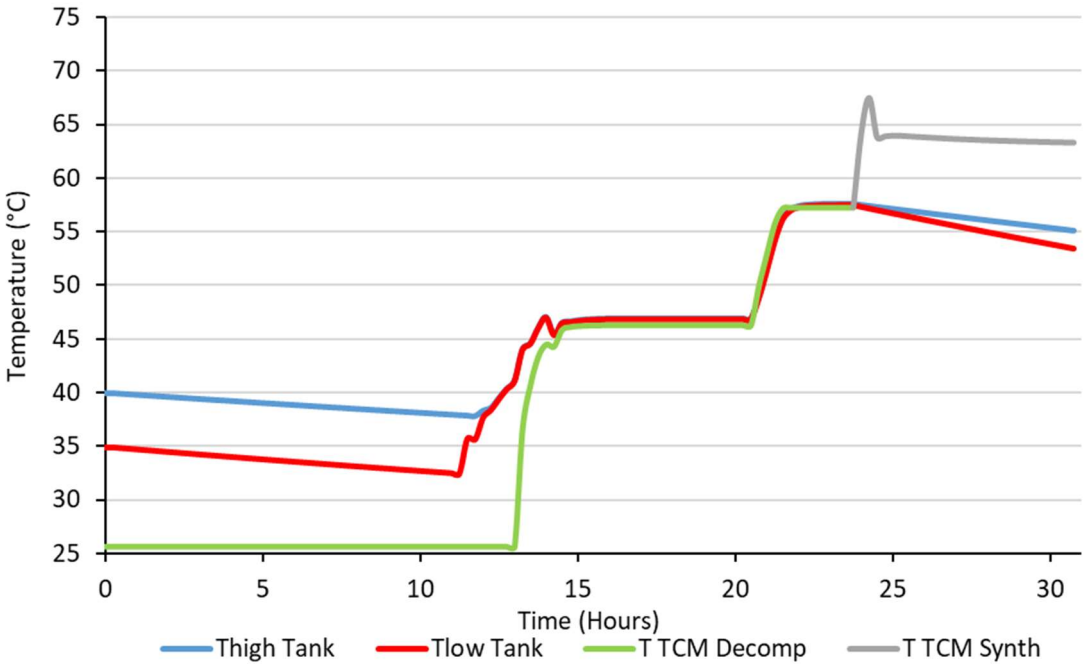

Figure 67: Temperature of the buffer tank and of the TCM reactor during decomposition and synthesis for Sopron's average winter case scenario

Due to the fact that the dimensioning of the system for Sopron demo site will be more probably based on the average winter case, more detailed figures of the main variables of the system have to be displayed. Figure 67 presents the temperatures of the buffer tank as well as the TCM reactor during the 1.5 days for the average winter case. During synthesis TCM reactor reached for a short time a peak temperature of 68°C.

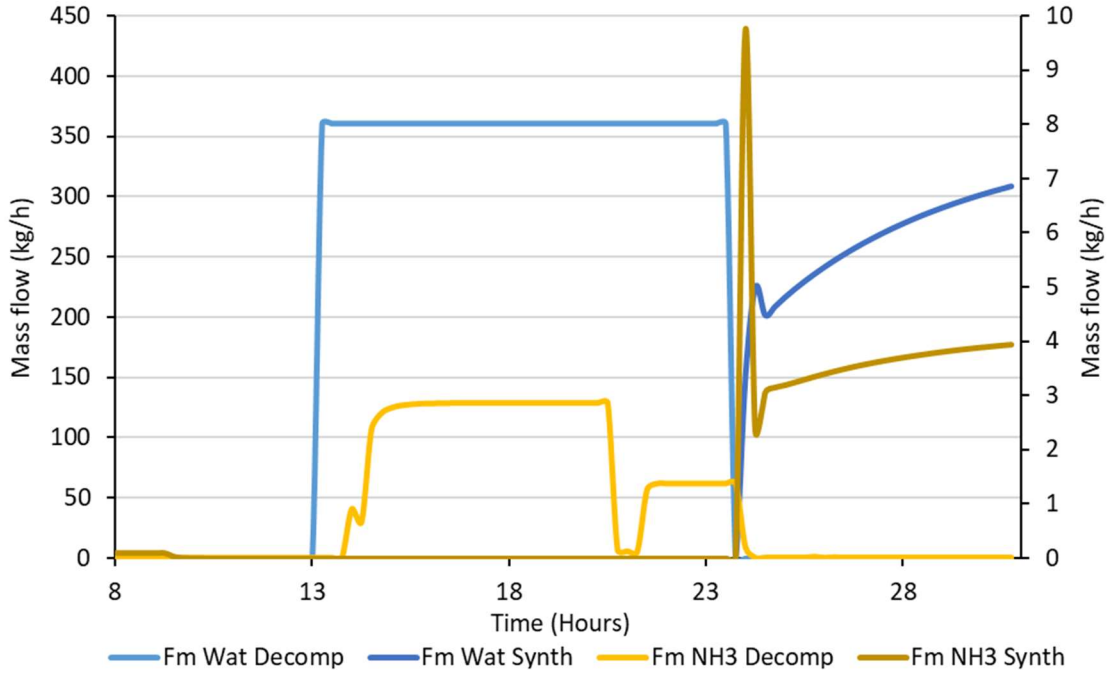

Figure 68: Mass flows of the heat transfer fluid and ammonia during decomposition and synthesis for Sopron's average winter case scenario

In Figure 68, the mass flows of the heating and cooling mediums as well as the mass flow of gaseous ammonia entering and exiting the TCM reactor are presented. Mass flow of gaseous ammonia exiting the TCM reactor has an average value of around 3 kg/h during the 1st reaction of

decomposition (8-4). In synthesis reaction ammonia mass flow entering the TCM reactor has a peak value of 9.74 kg/h for a short time but afterwards it stabilizes at 3.77 kg/h. The cooling medium of the TCM reactor during synthesis reaction has a peak mass flow rate value of 308 kg/h and an average value of 260 kg/h.

5.2.3. Sopron demo site electrical modelling results

This section presents the main results of the electrical model for Sopron demo site. Mainly, results on a monthly basis are included. More detailed results will be included in the scope of T3.5.

One of the most relevant figures with regards to MiniStor's electric system is the electricity production from the PVT system in Sopron (Figure 69). As can be observed, despite the slope of the collectors is intended to maximize the production during winter seasons while balancing economic and technical costs, the electricity outputs are larger during summer months when the radiation is also greater. Figure 69 also includes monthly values of in-plan radiation at equal orientation (azimuth and slope) as that for the collectors, showing a very direct correlation between electricity production and global radiation.

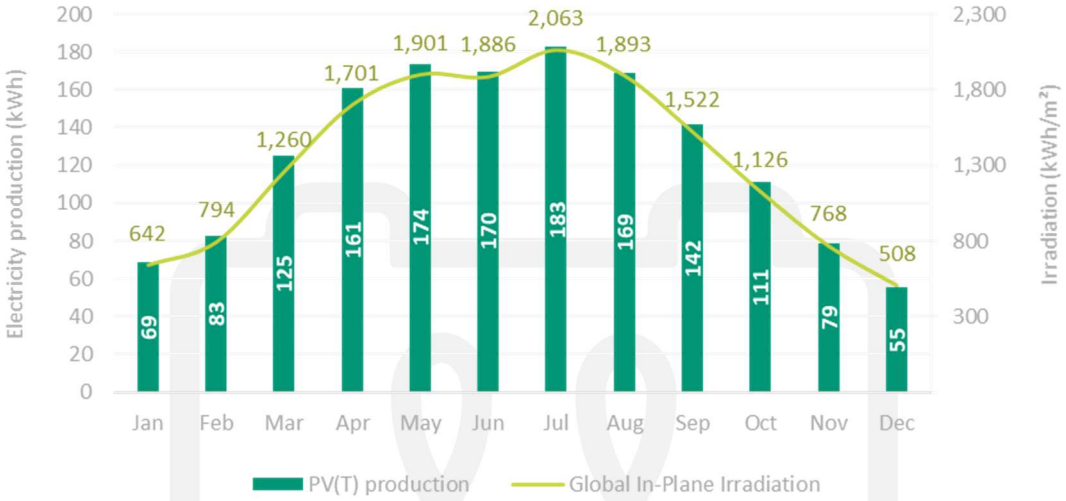

Figure 69: Monthly PV(T) electricity production and global in-plane irradiation. Sopron demo site

PVT electricity production is used to cover part of the load included in the demo site, which, as explained before, combines the electrical consumption that is needed to operate MiniStor system (e.g. ammonia compressor, dry cooler to dissipate excess heat, heat pump), and the electrical load demand of the demo site, which consists of an office, an apartment and an electric vehicle.

Nevertheless, electricity production is limited due to the restricted space to locate PVT collectors, leading to relatively low contributions of solar electricity production. Moreover, between the production in the PVT collectors and the consumption of electricity, there are losses of different nature such as conversion or charging losses, which eventually reduce the amount of energy available. This also explains the difference between production values from MiniStor electric system (Figure 69) and covered energy with this electricity (Figure 70).

Figure 70 presents the breakdown of the total load with regards to the system in charge of supplying the electricity: the main grid or MiniStor electric system (PV and batteries). As can be seen, the share of load that is supplied by solar electricity represents a small part of the total energy used to cover the total load, being lower in absolute and relative values during winter months due to combination of greater loads and lower production.

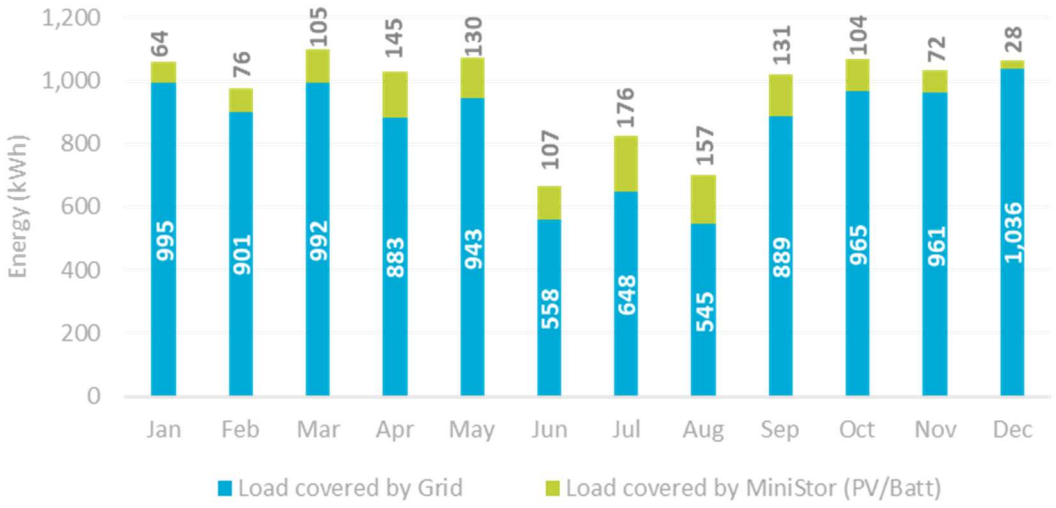

Figure 70: Load covered by grid or MiniStor electric system (PV/Batteries). Sopron demo site

Monthly values of the solar share are included in Figure 71, which highlights an average solar contribution of almost 14% of the total load, with peak rates of about 25% during summer (June, July and August) due to lower loads and higher irradiation, and minimum values of around 5-8% during winter (November, December, January and February). It is noticeable that despite the electricity production is maximum in July in absolute values, the solar share is lower because of a higher demand, which in turns corresponds to the existence of exceptional cooling needs.

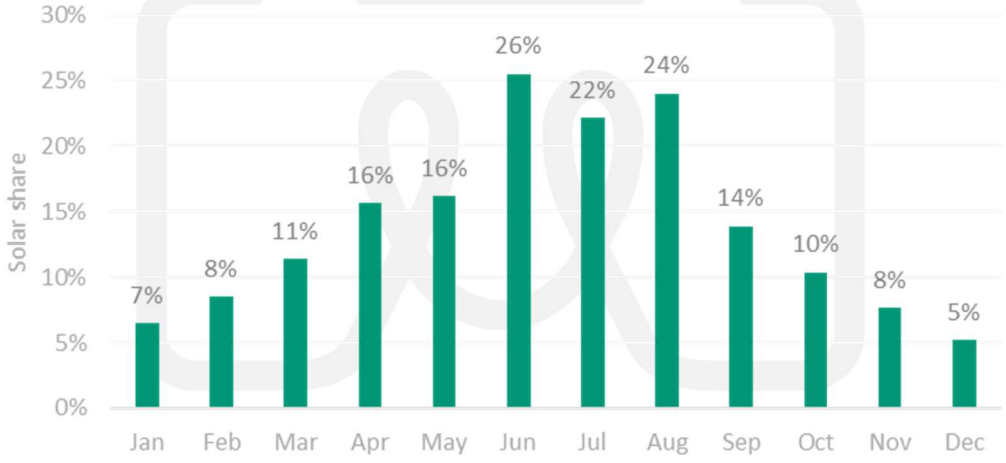

Figure 71: Monthly solar contribution; relation between solar production and total load by month. Sopron demo site

A more detailed breakdown of the electricity needed to cover total monthly loads is shown in Figure 72. Again, two main sources have been differentiated: the grid and MiniStor electrical system. However, in this case, these sources have been divided into two to consider the moment at which the electricity is provided.

MiniStor electrical system, basically constituted by the photovoltaics (PVT) modules and the batteries, can supply energy either directly from the PVT production (dark green in Figure 72), when both demand and production match, or from the batteries, when there is stored electricity and the main grid is not the best option (light green).

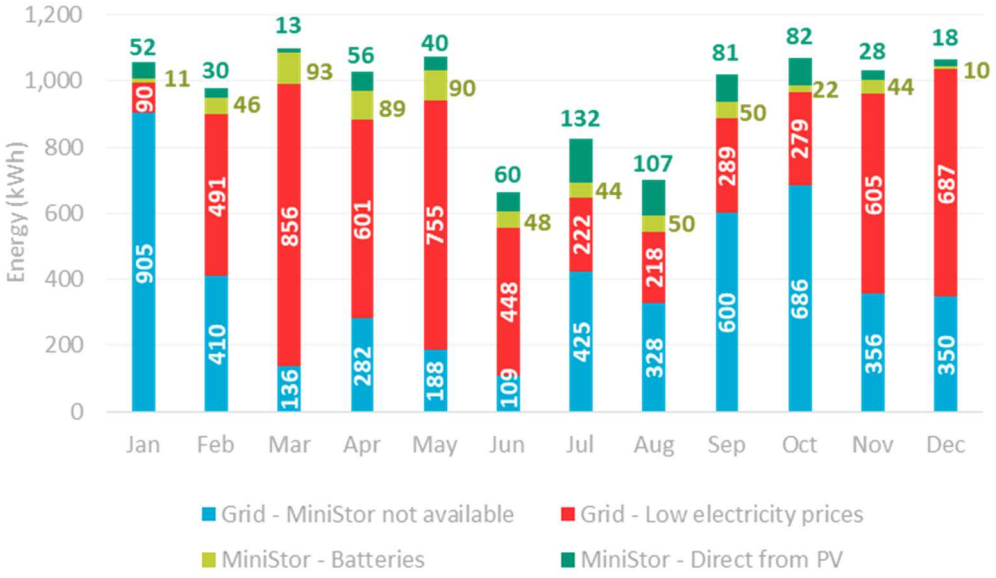

Figure 72: Load covered by each system. Sopron demo site

Regarding the electricity from the main grid, there are also two main options. First, electricity can be supplied to the load totally or partially because MiniStor system is not available to provide any (i.e. no production, no stored electricity), which is the most likely situation because the production is much lower than the demand (blue in Figure 72). Second, the grid can cover the load whenever MiniStor is available, but the grid-electricity price is lower than the limit price, hence is considered the best option from an economic perspective (red in Figure 72). During these periods, electricity production from MiniStor system will be stored in the batteries.

Figure 73 specifically shows the load that is covered by the main grid during low-price periods, as well as the monthly average grid-electricity prices (displayed in inverse order in the figure). Despite a more profound analysis is required to draw sound conclusions from the correlation between the implied variables, a clear trend between low prices and larger amounts of *cheap electricity* from the grid can be observed. Thus, for those months when the electricity prices are higher (e.g. January), the load covered by the grid due to low prices is smaller independently of the total load.

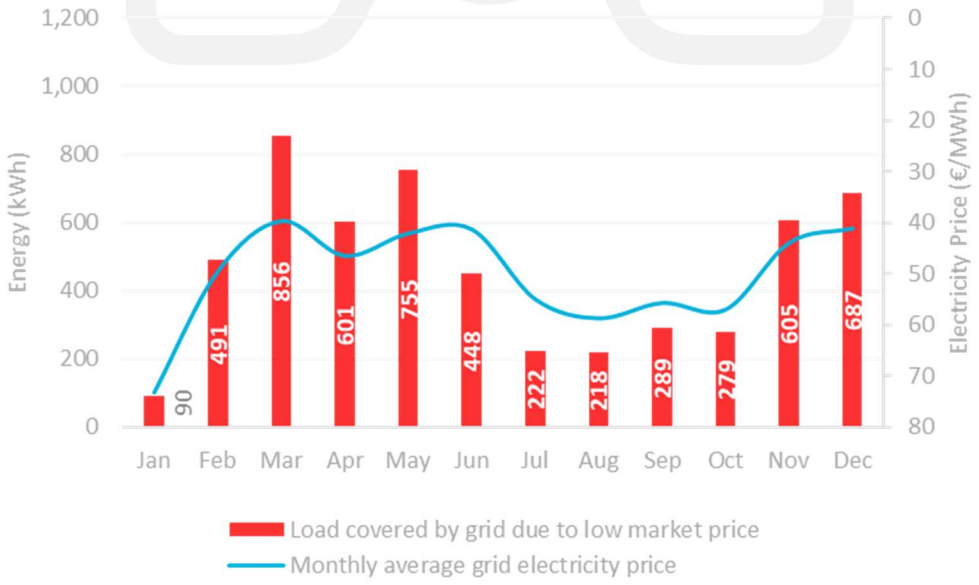

Figure 73: Load covered by grid due to the low market price. Sopron demo site

A similar trend can be identified in consequence when displaying the monthly average SOC of batteries and the electricity prices (Figure 74), even though, in this case, there is also a strong dependence on the radiation and PVT production. For instance, in January the prices are very high, but the average SOC is relatively low because the PVT production is also small. On average, the SOC throughout the year for the baseline conditions is of 26.6%.

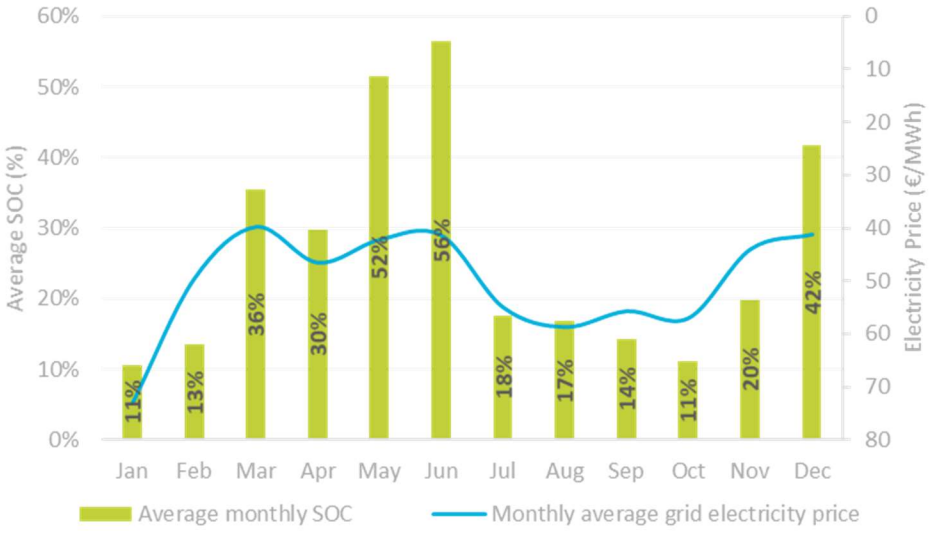

Figure 74: Monthly average State-Of-Charge of batteries (SOC). Sopron demo site

Nevertheless, as can be observed in Figure 75, over seven months of the year the SOC levels are of only 10%, which corresponds to the minimum level at which batteries are operated. More complex interaction analysis between the grid and the batteries will be performed in task 3.5, which may result in different figures in terms of average SOC and economic costs.

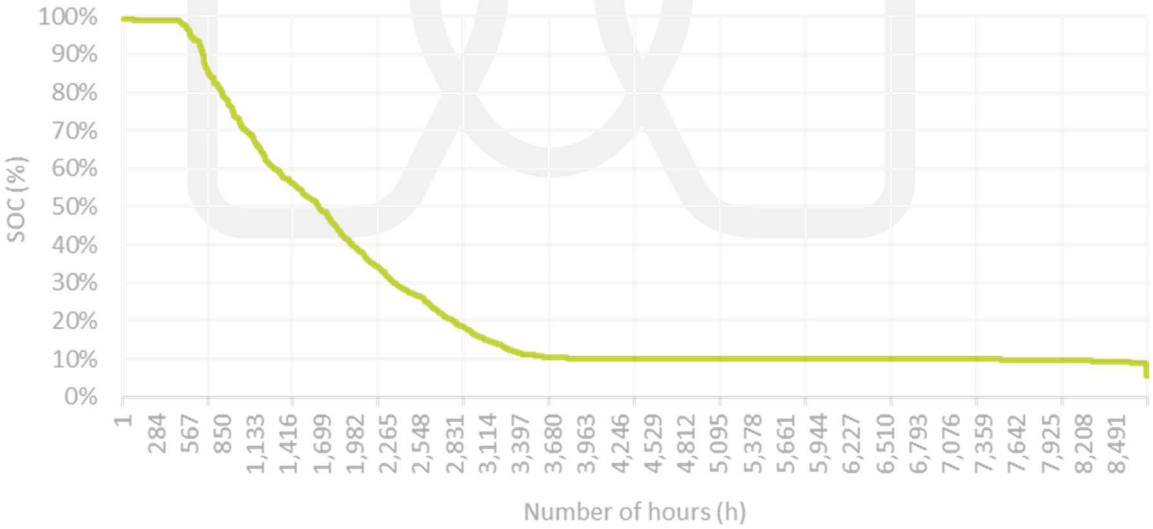

Figure 75: Hourly SOC rates during a year in decreasing order

Finally, the next figure provides a summarized comparison between the baseline scenario that has been an object of study during this task and the alternative scenario that has been proposed in Sopron. The main difference from an electric perspective is an increase of PVT collectors from six to nine, and a more detailed study of this alternative scenario will be included in task 3.5. As a first conclusion, the alternative scenario shows larger PVT production due to the higher amount of PVT collectors, which, as expected closely corresponds in number with the increase rate: 50% in both

cases. This greater production will significantly impact all previous results, including the solar contribution, and SOC of batteries[6].

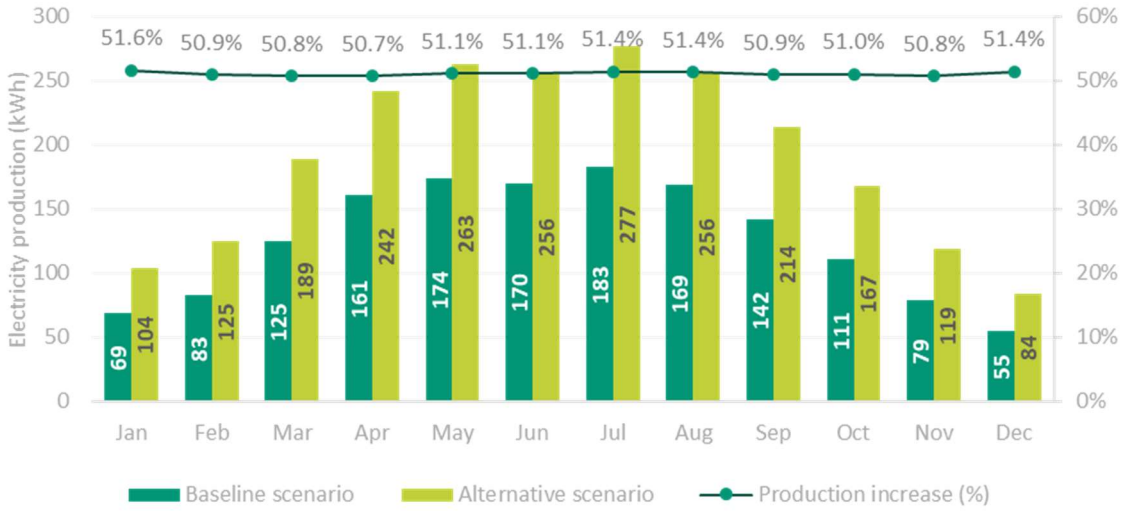

Figure 76: Comparison of baseline and alternative scenarios in terms of electricity (PV) production, and percentage increase of alternative over baseline productions. Sopron demo site

5.3. Kimmeria demo site results

5.3.1. Kimmeria demo site thermodynamic results

5.3.1.1. Average winter case scenario Kimmeria

In Figure 77 and Figure 79, the heat demand of the Kimmeria demo site in comparison with the output heat of the system during the course of one day is depicted. In Figure 78 and Figure 80, the total heat coverage provided by the system and the SOC of the hot PCM are presented in comparison with the heat demand of the building.

For the average winter case, the system manages to fully cover the heating needs for 4 hours and during the whole operation of the system presents an average heating coverage of 37%. For the extreme winter case, the system can cover the heating demand of the building for only 2.5 hours, during the 1st reaction of decomposition. In Kimmeria's case the auxiliary electrical heater is not activated. The system has an average heating coverage of 29%. Due to the fact that the synthesis reaction produces no excess heat in regard to the thermal demand, the hot PCM is not charged at the end of the operating cycle of the system in the extreme case scenario.

[6] *The simplified thermal results obtained from the electrical model indicates that the alternative scenario has no relevant impact in the thermal production in comparison to the base scenario. These results should be confirmed by a detailed thermodynamic simulation.*

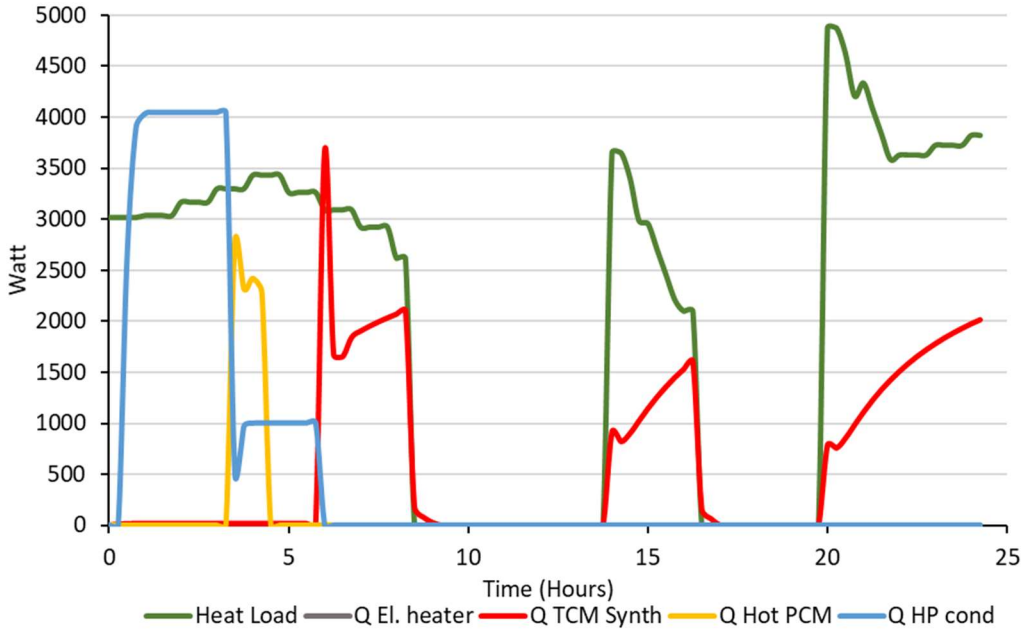

Figure 77: Heat demand in comparison with the input heat by the system and the consumption of the electrical heater for Kimmeria average winter case

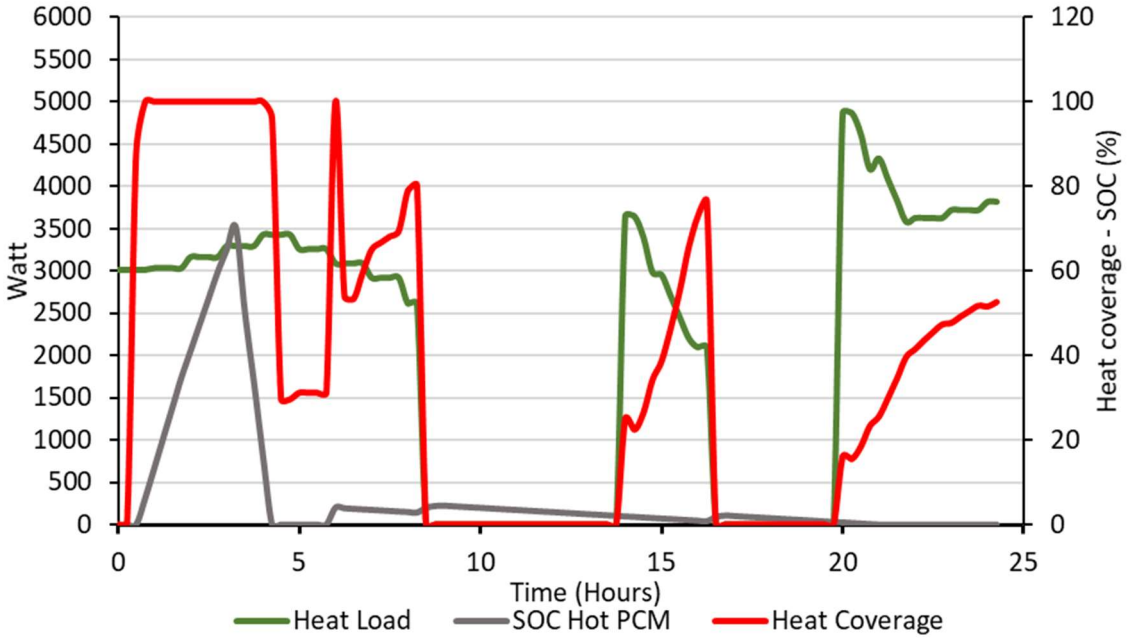

Figure 78: Total heat coverage and SOC of PCM percentage (right axis) of the system in comparison with the heat demand for Kimmeria average winter case

5.3.1.2. Extreme winter case scenario Kimmeria

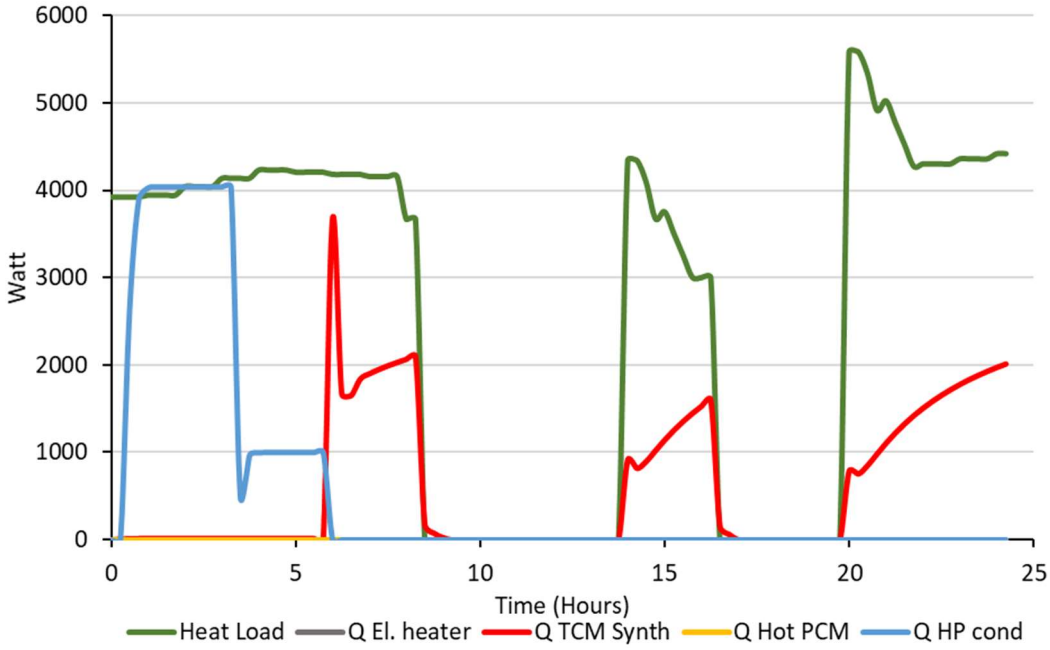

Figure 79: Heat demand in comparison with the input heat by the system for Kimmeria extreme winter case

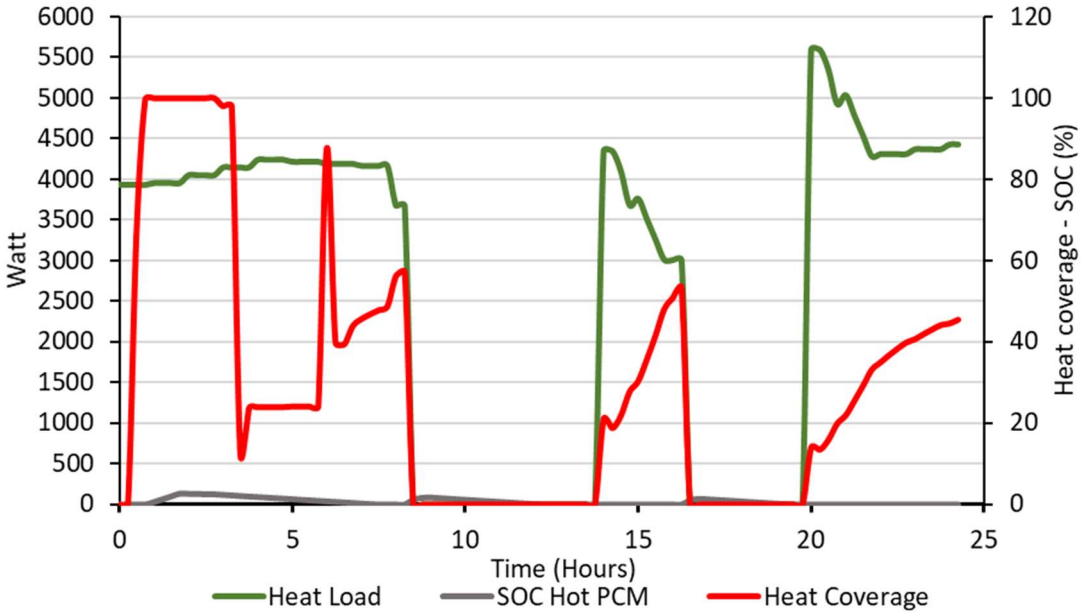

Figure 80: Total heat coverage and SOC of PCM percentage (right axis) of the system in comparison with the heat demand for Kimmeria extreme winter case

The heat demand of Kimmeria's demo site in comparison with the heat input from the system during the course of the one day cycle can be seen. The decomposition reaction is taking place for 5.5 hours. The hot PCM is only being charged for a little while but its SOC remains low during that time (below 5%), since the thermal demands are not exceeded by the system. During the 2nd synthesis reaction (4-8), the heat duty of the reactor is farther to the thermal load than that of the decomposition reaction and the generated heat is not enough for the coverage of the building's needs.

In Error! Reference source not found., the total heat coverage of the system in comparison with the heat demand for the Kimmeria extreme winter case is depicted. The heat coverage of the

building reaches 100% for 2.5 hours, at the time when the decomposition reaction takes place. The average heat coverage during the whole operating cycle is 48%. During the synthesis reaction, the system manages to obtain 55% heat coverage very briefly and an average of around 33%.

5.3.1.3. Average summer case scenario Kimmeria

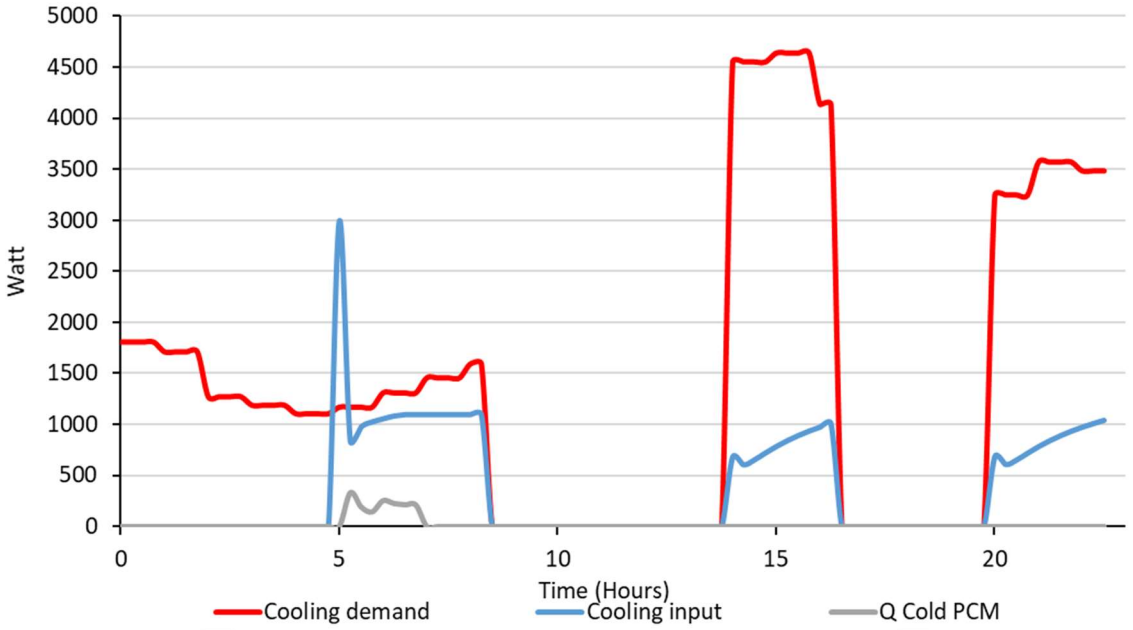

Figure 81: Cooling demand in comparison with the cooling input by the system for Kimmeria average summer case

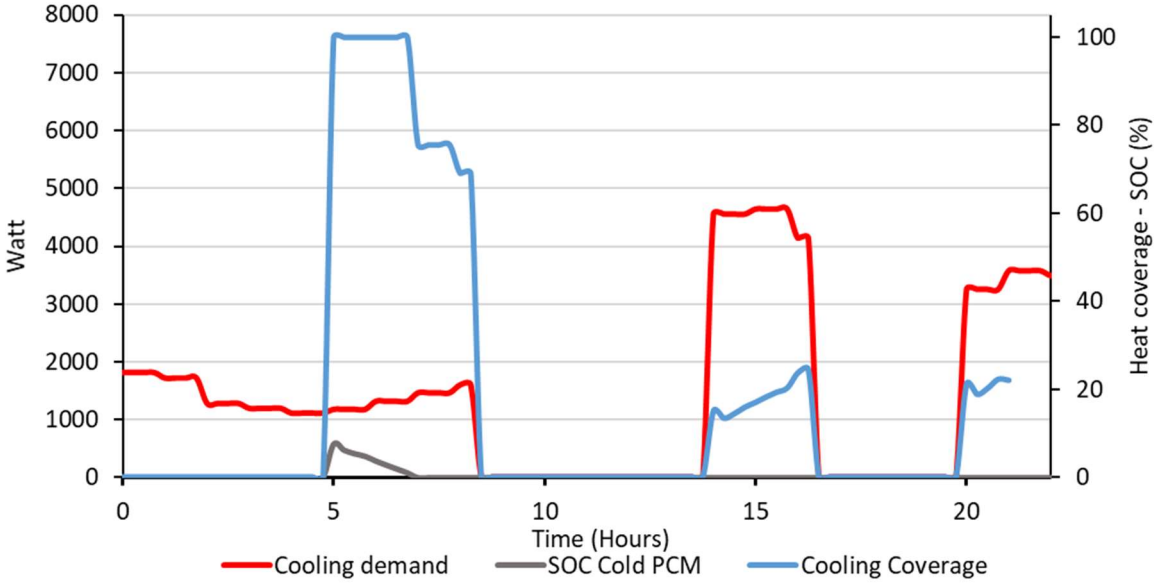

Figure 82: Total cooling coverage and SOC of cold PCM percentage (right axis) of the system in comparison with the cooling demand for Kimmeria average summer case

5.3.1.4. Extreme summer case scenario Kimmeria

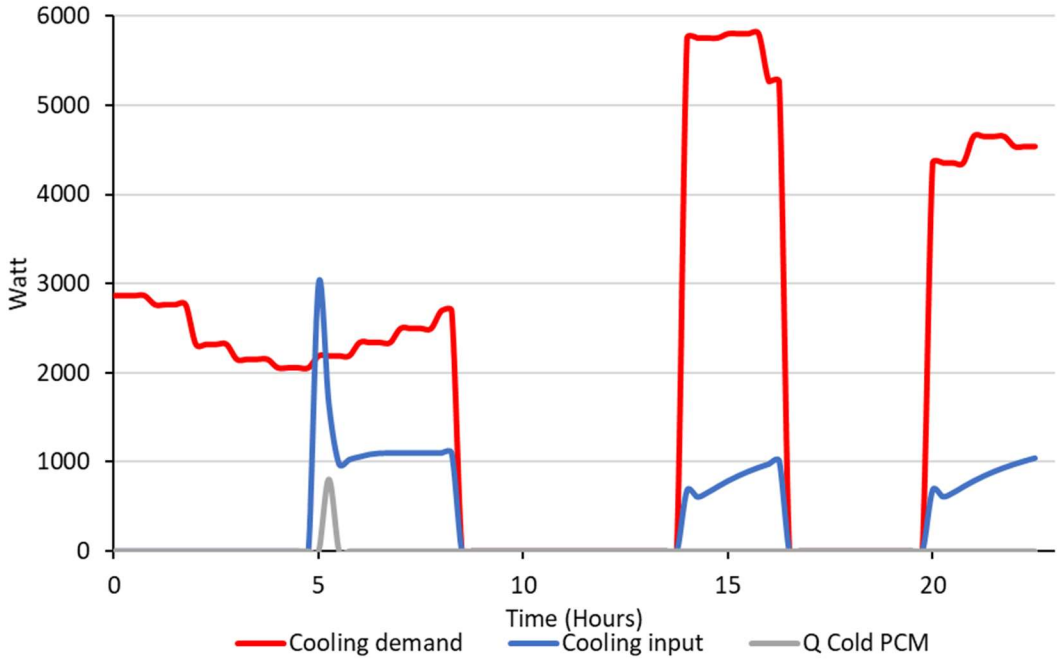

Figure 83: Cooling demand in comparison with the cooling input by the system for Kimmeria extreme summer case

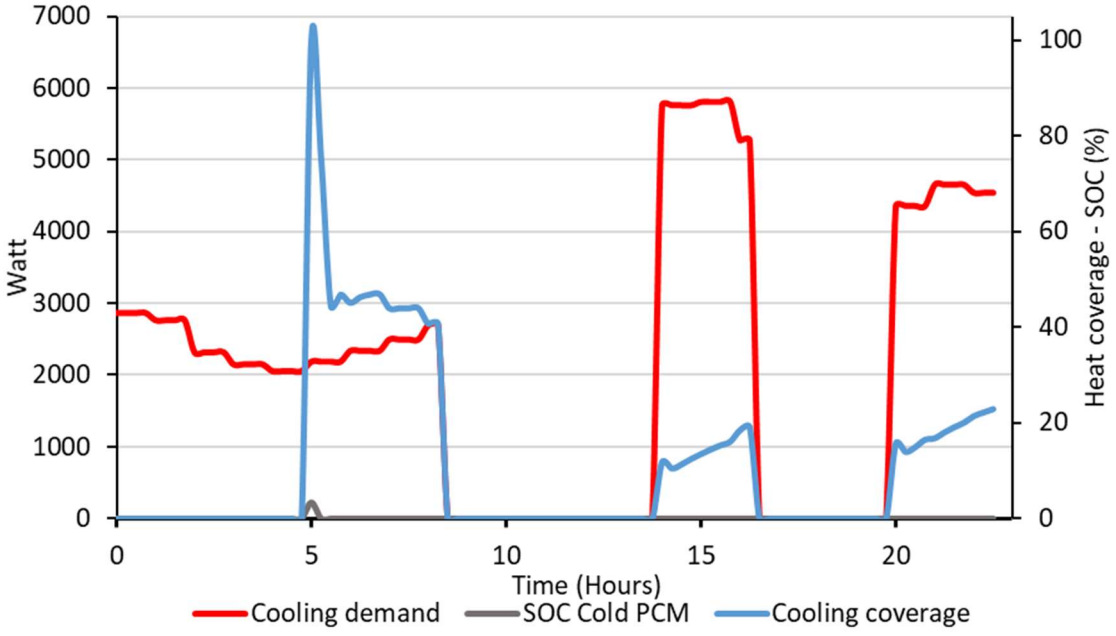

Figure 84: Total cooling coverage and SOC of cold PCM percentage (right axis) of the system in comparison with the cooling demand for Kimmeria extreme summer case

In Figure 81 and 83, the cooling demand of the Kimmeria demo site in comparison with the cooling input from the system for the two summer cases is presented while in Figure 82 and 84, the cooling demand in comparison with the cooling coverage. The cooling needs of the space under examination do not vary significantly, with a peak value of 4.6 kW and 4.8 kW for the average and extreme case scenario respectively. The average cooling duty generated by the ammonia evaporator is 0.97 kW. This is translated into an average cooling coverage of 48.2% and 30% of the space cooling needs for the average and extreme cases respectively. Peak values of the cooling coverage are being

obtained during the beginning of synthesis, when the corresponding first reaction (2-4) is taking place. The cold PCM is not charged at the end of the operating cycle of the system for both cases.

5.3.2. Proposed design specifications Kimmeria

Table 31 displays, the average outputs of average winter and summer scenarios for the initial dimensioning of the system. For the case of Kimmeria, in all examined scenarios the operational conditions for the decomposition reaction are the same. This is due to the absence of PVT and Solar Collectors in this demo site, since Kimmeria has its own facility for the production of hot water with renewable energy sources. For the synthesis reaction, the operating pressure changes in the summer cases and obtains a value of 5 bar. The total duration of the system reactions is 15 hours for the average winter case and 13.25 for the average summer case. The cycle of the system is one day for all the cases. Average generated heat during the reaction of the decomposition is 2.33 kW. The synthesis reaction generated an average heat of 1.56 kW for the winter case and a cooling duty from the ammonia evaporator of 0.97 kW in summer scenario.

	Decomposition	Max values for decomposition	Synthesis (Winter)	Max values for synthesis (Winter)	Synthesis (Summer)	Max values for synthesis (Summer)
Time (Hours)	5.5	-	9.5		6.5	-
Medium fluid mass flow (kg/h)	468	468	160	246	360	500
NH_3 Average mass flow (kg/h)	4.12	6.51	2.85	10	3	9.35
NH_3 Compressor duty (kW)	0.48	0.75	-	-	-	-
NH_3 Condenser duty (kW)	1.69	2.7	-	-	-	-
Heat Pump compressor duty (kW)	0.65	1	-	-	-	-
Heat Pump condenser (kW)	2.33	3.7	-	-	-	-
NH_3 Evaporator duty (kW)	-	-	0.92	3.2	0.97	3
TCM synthesis heat duty (kW)	-	-	1.56	3.67	1.76	3.93

Table 31: Average outputs of average winter and summer case scenarios for Kimmeria demo site

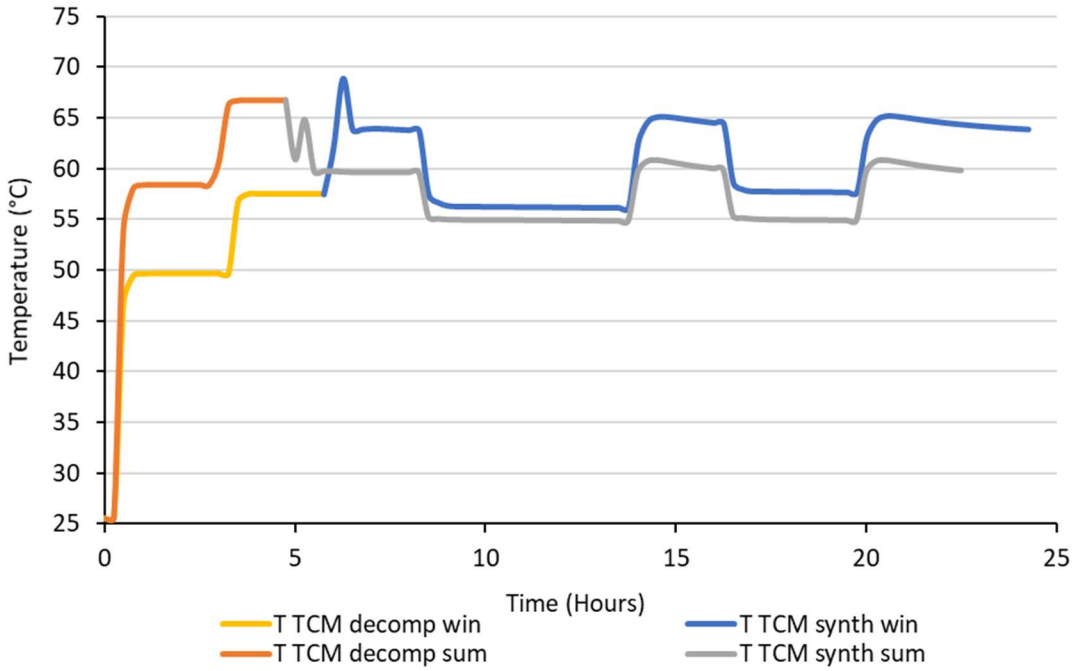

Figure 85: Temperature of the TCM reactor during decomposition and synthesis for Kimmeria average winter and summer case scenario

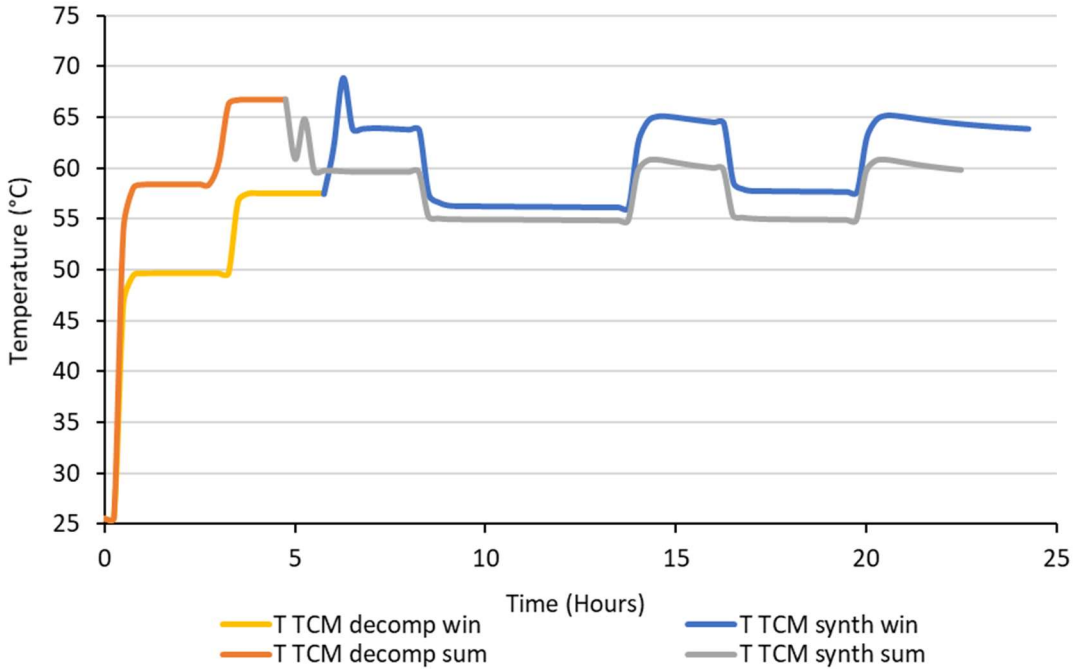

Figure 85 presents the temperatures of the TCM reactor during the simulation for the average winter case as well as for the synthesis mode in average summer case. During average winter case, in synthesis TCM reactor reached for a short time a peak temperature of 69°C. In the average summer case, the maximum temperature of the TCM reactor is 68°C, with an average of 57°C due to the fact that the heat generated has to be rejected into the environment.

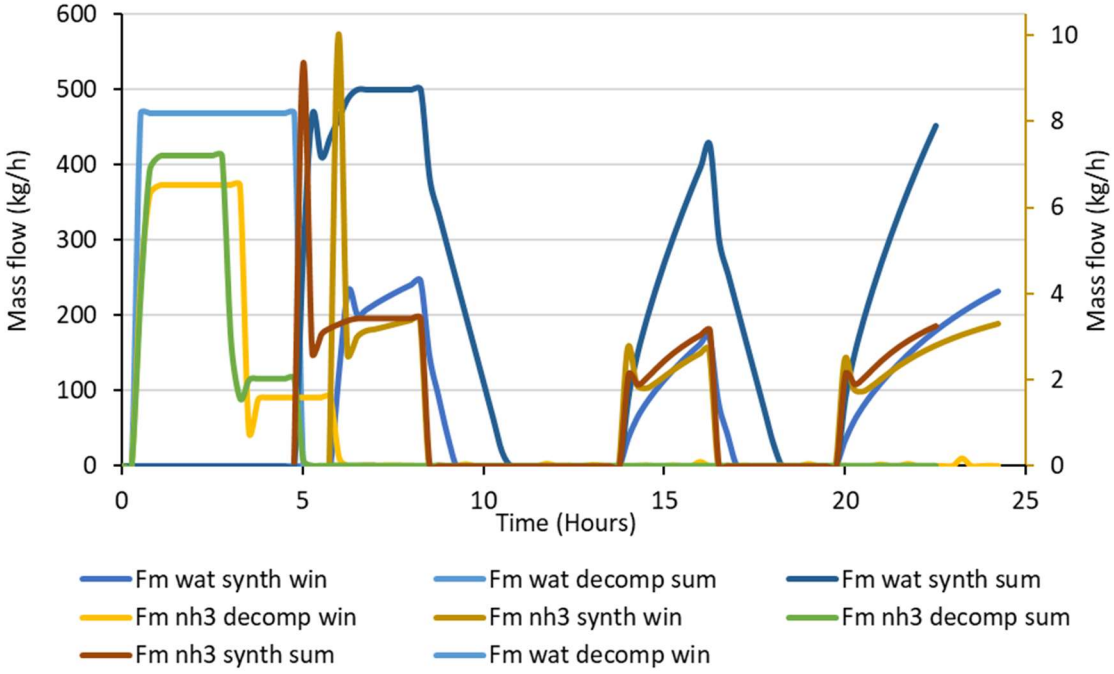

Figure 86: Mass flows of the heat transfer fluid (left axis) and ammonia (right axis) during decomposition and synthesis for Kimmeria average winter and summer case scenario

Figure 86 presents the mass flows of the heat transfer medium in heating and cooling mode as well as the mass flow of gaseous ammonia entering and exiting the TCM reactor. Mass flow of gaseous ammonia exiting the TCM reactor is stable at 6.5 kg/h during the decomposition reaction. In winter synthesis reaction ammonia mass flow entering the TCM reactor has a peak value of 10 kg/h for a short time but afterwards it stabilizes at 2.85 kg/h. In summer synthesis reaction ammonia mass flow entering the TCM reactor has a peak value of 9.35 kg/h for a short time but afterwards it stabilizes at 3 kg/h. The heat transfer fluid of the TCM reactor during winter synthesis reaction has a peak mass flow value of 240 kg/h and an average value of 160 kg/h and in summer synthesis reaction has a peak value of 500 kg/h and an average value of 360 kg/h.

5.4. Cork demo site results

5.4.1. Cork demo site thermodynamic results

5.4.1.1. Average winter case Cork

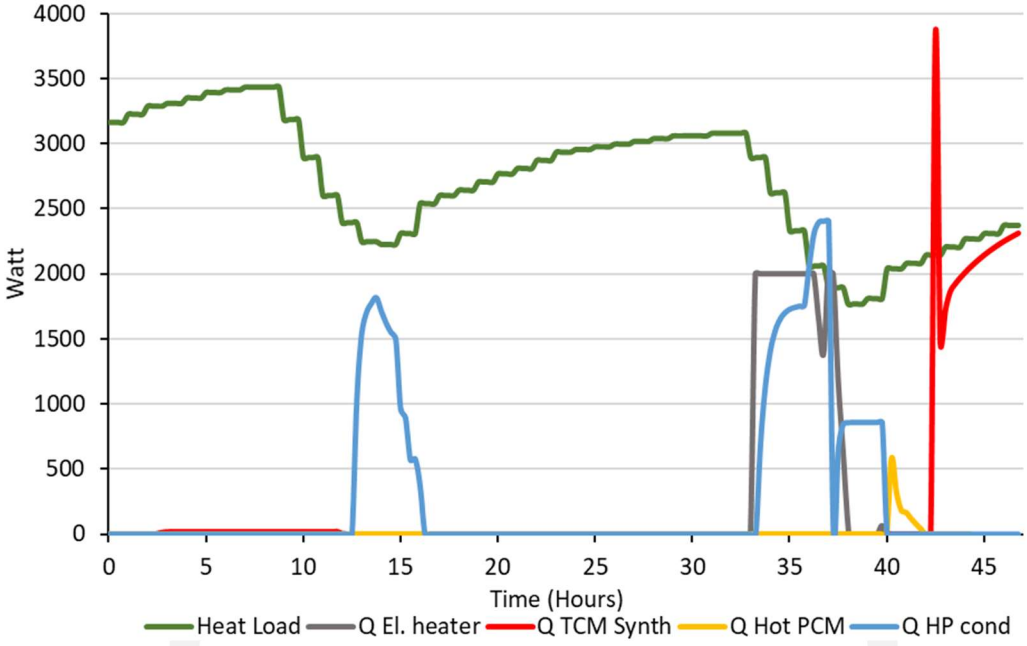

Figure 87: Heat demand in comparison with the input heat by the system and the consumption of the electrical heater for Cork average winter case

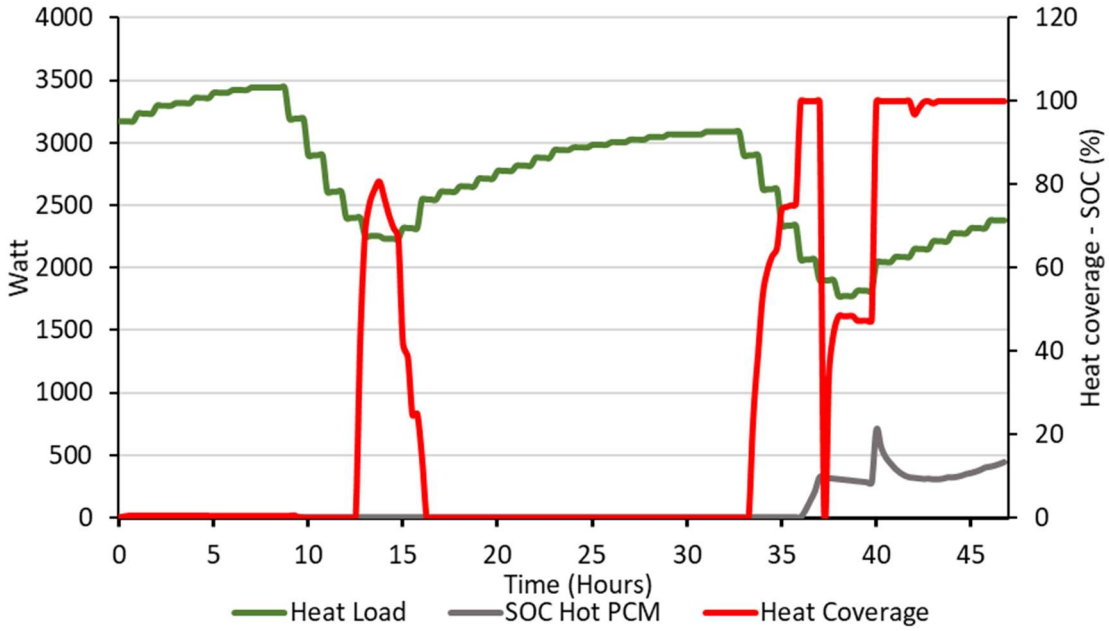

Figure 88: Total heat coverage and SOC of PCM percentage (right axis) of the system in comparison with the heat demand for Cork average winter case

5.4.1.2. Extreme winter case Cork

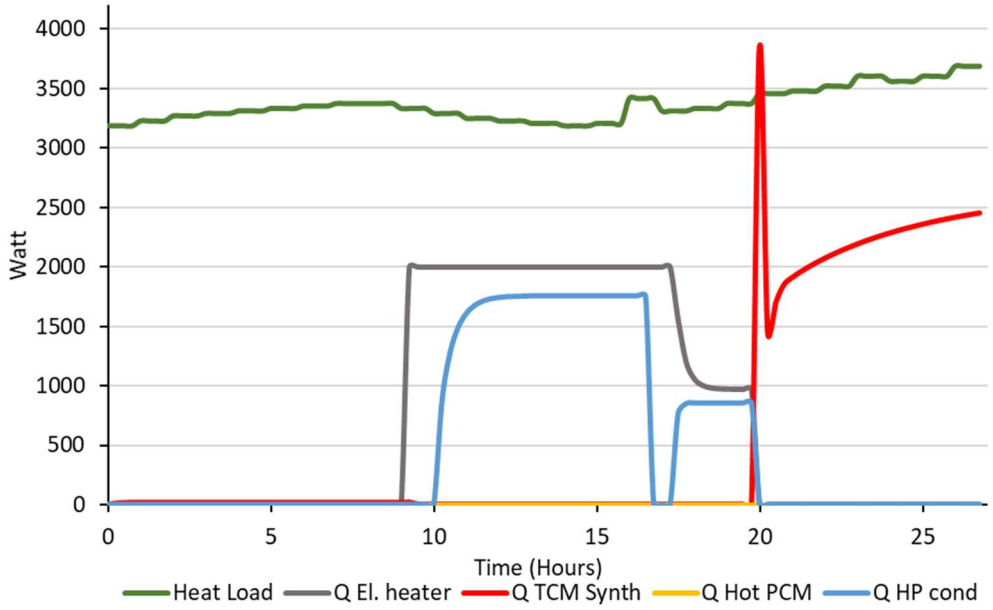

Figure 89: Heat demand in comparison with the input heat by the system and the consumption of the electrical heater for Cork average winter case

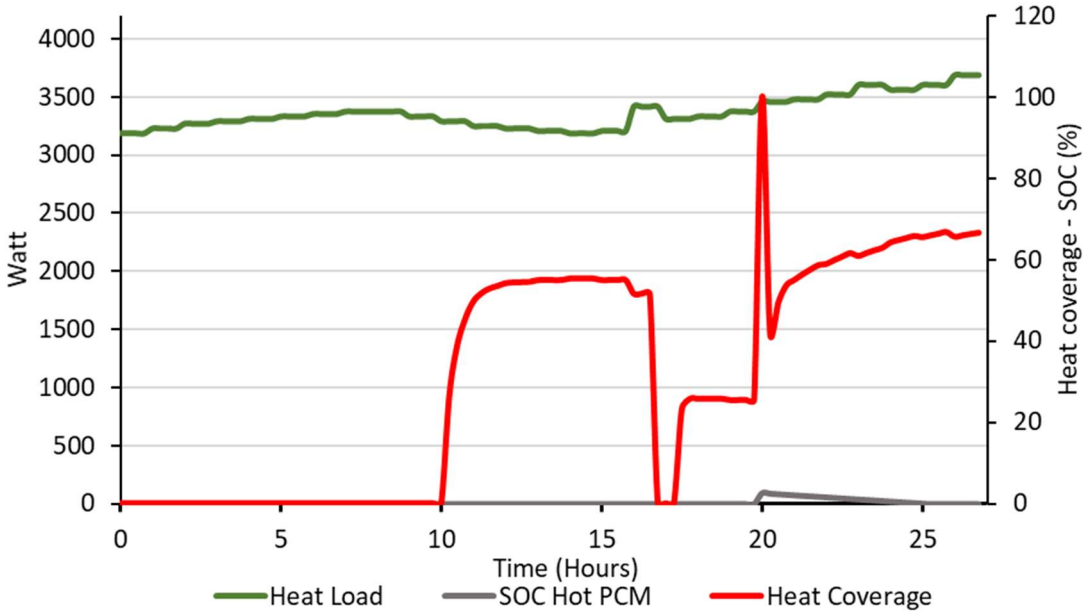

Figure 90: Total heat coverage and SOC of PCM percentage (right axis) of the system in comparison with the heat demand for Cork extreme winter case

In Figure 87 and Figure 9789, the heat demand of Cork demo site in comparison with the output heat of the system during the course of one day is depicted. In Error! Reference source not found.88 and Error! Reference source not found.90, the total heat coverage provided by the system and the SOC of the hot PCM are presented in comparison with the heat demand of the building.

For the average winter case, the system manages to fully cover the heating needs for 7 hours and in total presents an average heating coverage of 76%. For the extreme winter case, the system covers the heating demand of the building only very briefly, at around 20 hours time. The electrical heater is activated for 10.75 hours, hence the system reaches an average heating coverage of 52.4%. Due to the fact that the synthesis reaction does not produce excess heat in regard to the

thermal demand, the hot PCM is not being charged at the extreme case and reaches 20% SOC at the average case but only for a brief time.

5.4.1.3. Average Spring-Autumn case scenario Cork

In Cork's case, due to the climate conditions, there is no demand for cooling even during summer. In Figure 9591, the heat demand of Cork demo site in comparison with the output heat of the system during the course 30 hours is depicted, for the average spring-autumn case. In Figure 92, the total heat coverage provided by the system and the SOC of the hot PCM are presented in comparison with the heat demand of the building.

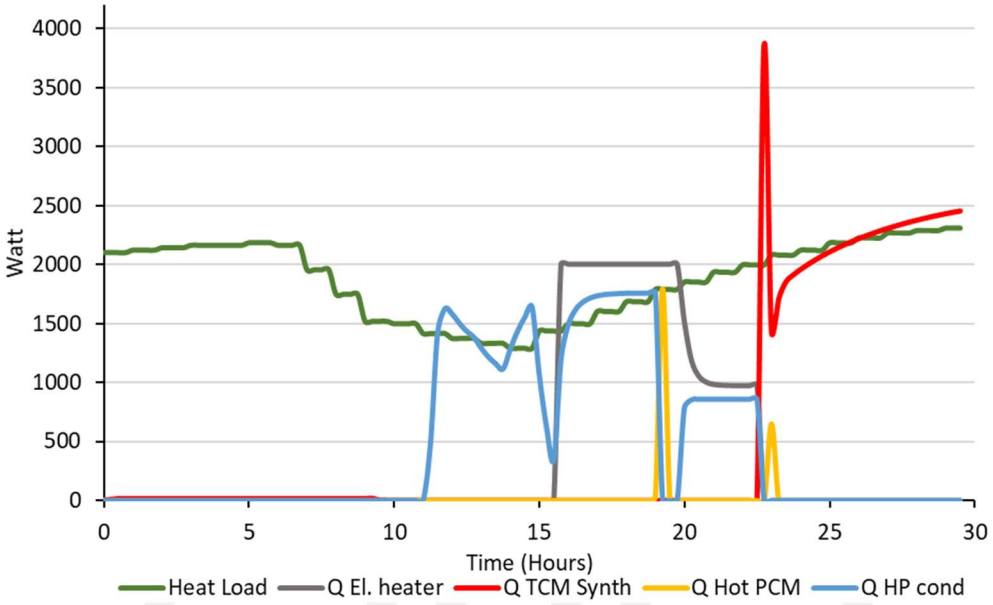

Figure 91: Heat demand in comparison with input heat by the system and the consumption of the electrical heater for Cork average spring-autumn case

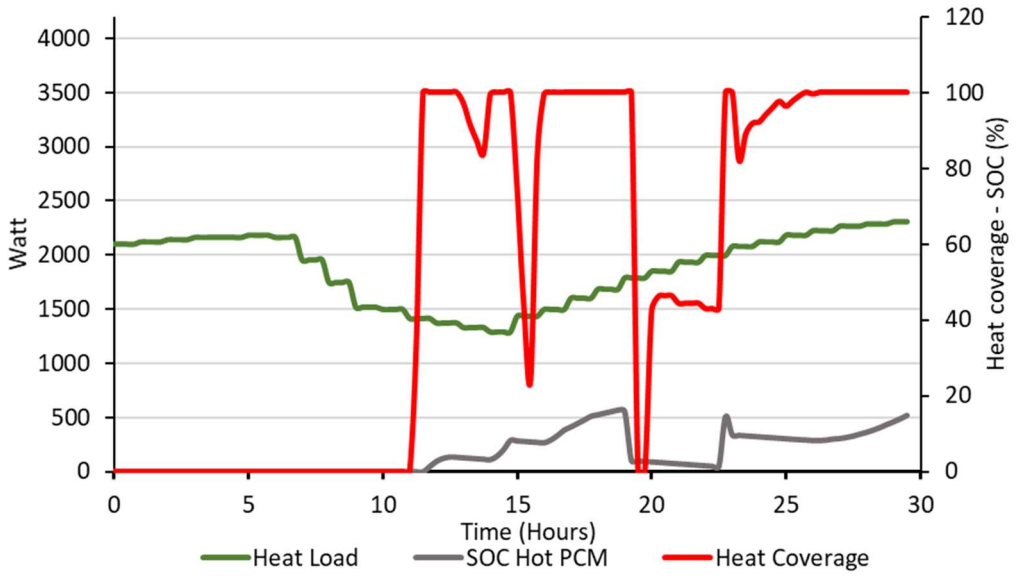

Figure 92: Total heat coverage and SOC of PCM percentage (right axis) of the system in comparison with the heat demand for Cork average spring-autumn case

The system manages to fully cover the heating needs for 9.75 hours and in total presents an average heating coverage of 86.7%. The electrical heater is activated for 7 hours. Due to the fact that the synthesis reaction does not produce too much excess heat in the majority of the cycle, the hot PCM is slowly being charged and its state of charge reaches at 15% as we approach 30 hours of operation.

5.4.2. Proposed design specifications Cork

In Table 32, the average outputs of average winter scenarios for the initial dimensioning of the system are displayed. Due to the fact that in all cases, the usage of the electrical heater was mandatory for the completion of the decomposition reaction, both decomposition and synthesis took place under the same operating conditions. The only thing that changes between the three cases is that in the case of average winter and average spring -autumn, the system on the first day executes partially the first reaction. The total duration of the system reactions is 46.75 hours for the average winter case, if radiation is high enough or an external heating source can be used and the cycle of the system is one day for the average and extreme winter Cork cases. Average generated heat during the first reaction of the decomposition is 1.4 kW and during the second reaction is 0.75 kW. The synthesis reaction generated an average heat of 2.24 kW.

	Decomposition	Max values for decomposition	Synthesis	Max values for synthesis
Time (Hours)	10	-	7	-
Medium fluid mass flow (kg/h)	360	360	261	309
NH_3 Average mass flow (kg/h)	2	3.9	3.8	9.8
NH_3 Compressor duty (kW)	0.24	0.45	-	-
NH_3 Condenser duty (kW)	0.85	1.59	-	-
Heat Pump compressor duty (kW)	0.32	0.6	-	-
Heat Pump condenser (kW)	1.17	2.2	-	-
NH_3 Evaporator duty (kW)	-	-	1.22	3.19
TCM synthesis heat duty (kW)	-	-	2.24	3.85
Electrical heater duty (kW)	1.22	2	-	-

Table 32: Average outputs of average winter case scenario for Cork demo site

Due to the fact that the dimensioning of the system for the Cork demo site will be most probably implemented for the average winter case, more detailed figures of the main variables of the system have to be displayed. Figure 93 presents the temperatures of the buffer tank as well as of the TCM reactor during the two days for the average winter case. During the synthesis phase, the TCM reactor reached for a short time a peak temperature of 67.4°C. Figure 94 shows the mass flows of the heat transfer medium as well as the mass flow of gaseous ammonia entering and exiting the TCM reactor. Mass flow of gaseous ammonia exiting the TCM reactor is stable at 2 kg/h, reaching its peak value of 3.9 kg/h during the 1st decomposition reaction (8-4). In synthesis reaction ammonia mass flow entering the TCM reactor has a peak value of 9.8 kg/h for a short time but afterwards it stabilizes at 3.8 kg/h. The heat transfer fluid of the TCM reactor during synthesis reaction has a peak mass flow value of 309 kg/h and an average value of 261 kg/h.

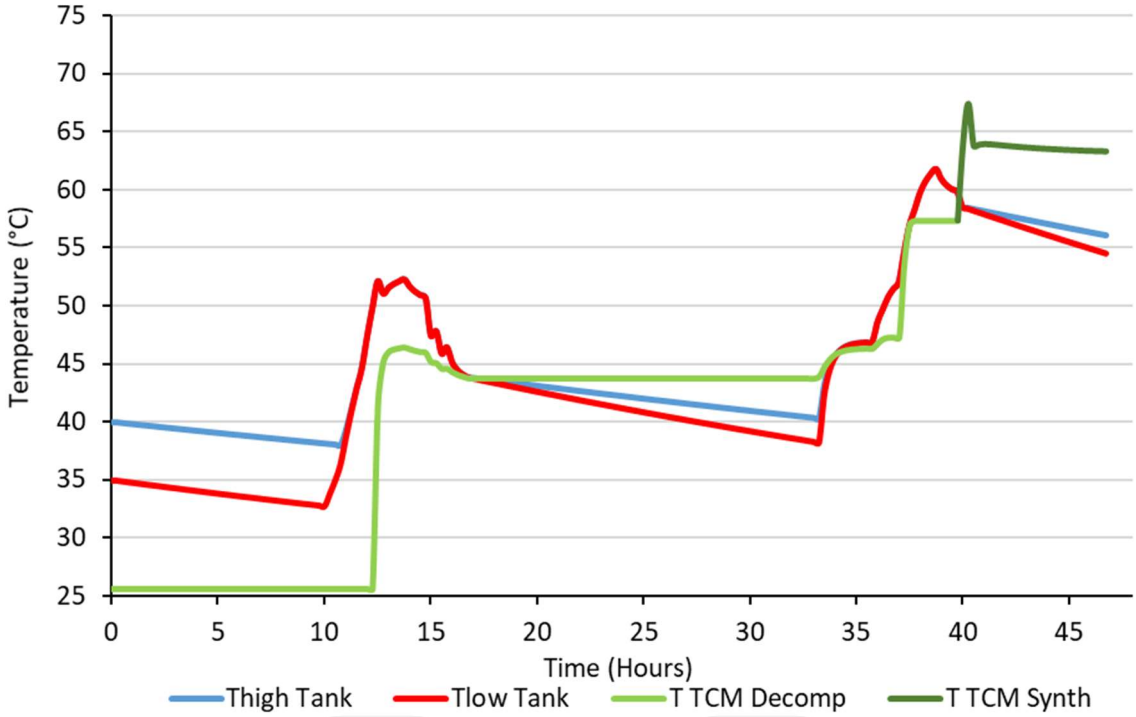

Figure 93: Temperature of the buffer tank and of the TCM reactor during decomposition and synthesis for Cork's average winter case scenario

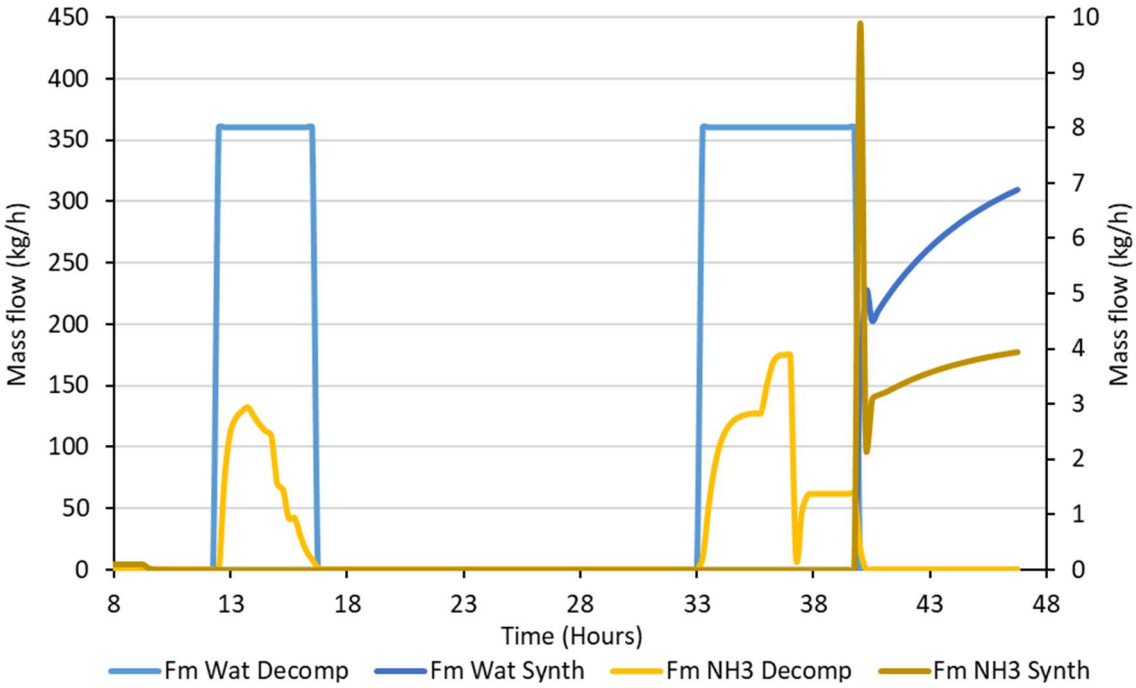

Figure 94: Mass flows of the heat transfer fluid and ammonia during decomposition and synthesis for Cork's average winter case scenario

5.5. Thessaloniki pre-pilot results

5.5.1. Thessaloniki thermodynamic results

5.5.1.1. Thessaloniki pre-pilot thermodynamic results

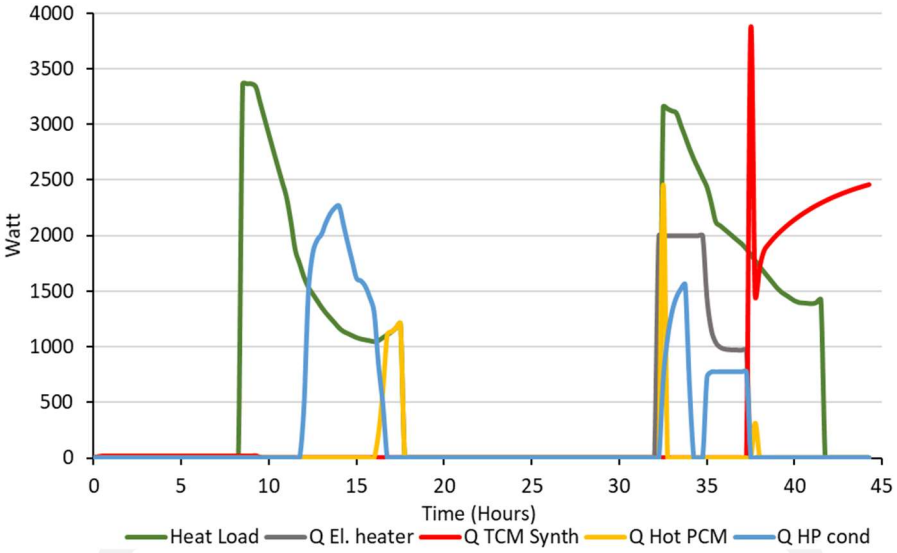

Figure 95: Heat demand in comparison with the input heat by the system and the consumption of the electrical heater for Thessaloniki average winter case

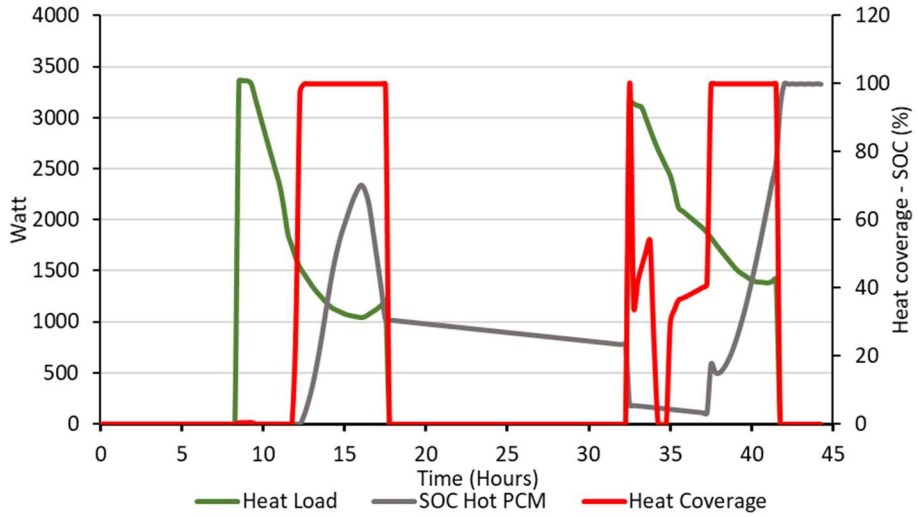

Figure 96: Total heat coverage and SOC of PCM percentage (right axis) of the system in comparison with the heat demand for Thessaloniki average winter case

5.5.1.2. Extreme Winter Thessaloniki

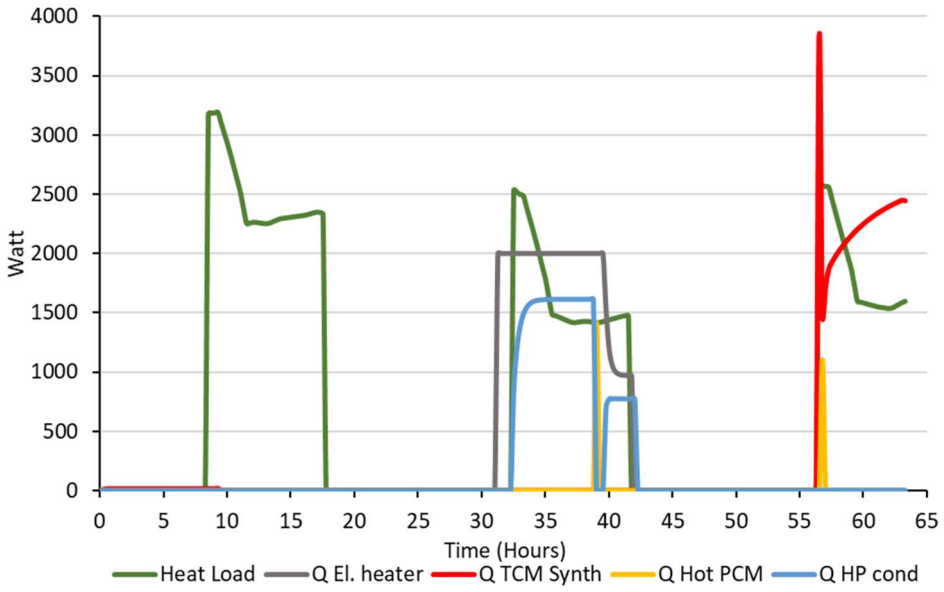

Figure 97: Heat demand in comparison with the input heat by the system and the consumption of the electrical heater for Thessaloniki extreme winter case

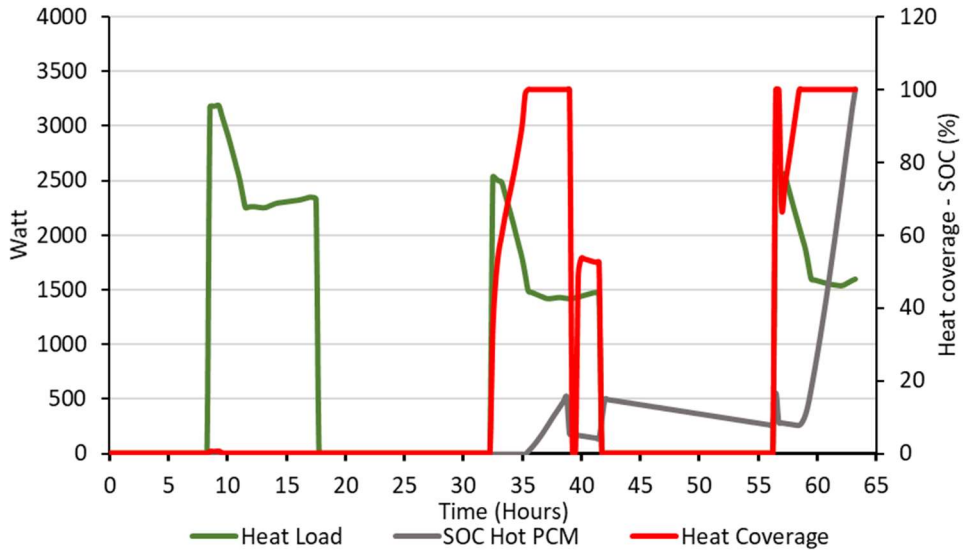

Figure 98: Total heat coverage and SOC of PCM percentage (right axis) of the system in comparison with the heat demand for Thessaloniki extreme winter case

In Figure 9596 and Figure 97, the heat demand of Thessaloniki demo site in comparison with the output heat of the system during the course of two and three days respectively is depicted. In **Error! Reference source not found.** and **Error! Reference source not found.**, the total heat coverage provided by the system and the SOC of the hot PCM are presented in comparison with the heat demand of the building. On the first day of the average case when the radiation value peaks at 770 W/m^2, the decomposition lasts for 2.5 hours, which is 0.5 hours more than the corresponding initial calculation, due to the reduced thermal inertia of the 17.5 kWh TCM reactor.

For the average winter case, the system manages to fully cover the heating needs for 9.75 hours during the two days period and in total presents an average heating coverage of 82%. Additionally, on the first day, the decomposition reaction is able to take place utilizing only solar radiation and covers the demand of the building by 97% for 5.75 hours, while also charging the PCM up to a SOC

value of 31%. The PCM supports the system to maintain the coverage of the demand 2.25 hours in total and at the end of the simulation it has a SOC value of 100%. For the extreme winter case, the system cannot cover the heating demand of the building on the first day, as the decomposition is not activated. From the second day onwards, when the auxiliary electrical heater is activated, the system has an average heating coverage of 73%. In total MiniStor system presents an average thermal coverage of 84% and 100% for 9.5 hours. Due to the fact that the synthesis reaction produces excess heat in regard to the thermal demand, the hot PCM is fully charged at the end of the operating cycle of the system in the extreme case scenario.

5.5.1.3. Average Summer Thessaloniki

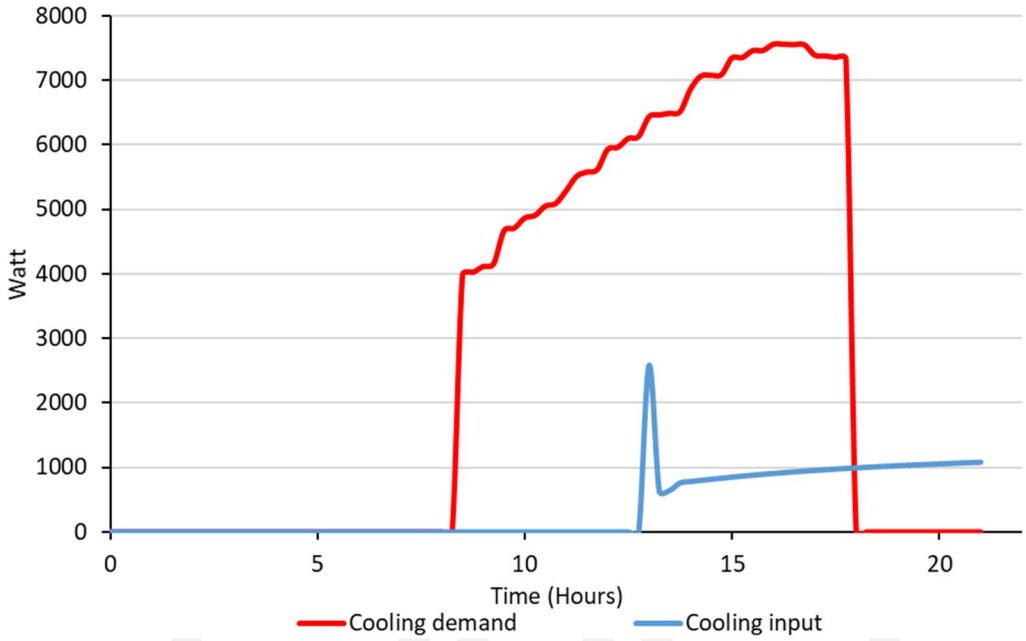

Figure 99: Cooling demand in comparison with the cooling input from the system for Thessaloniki average summer case

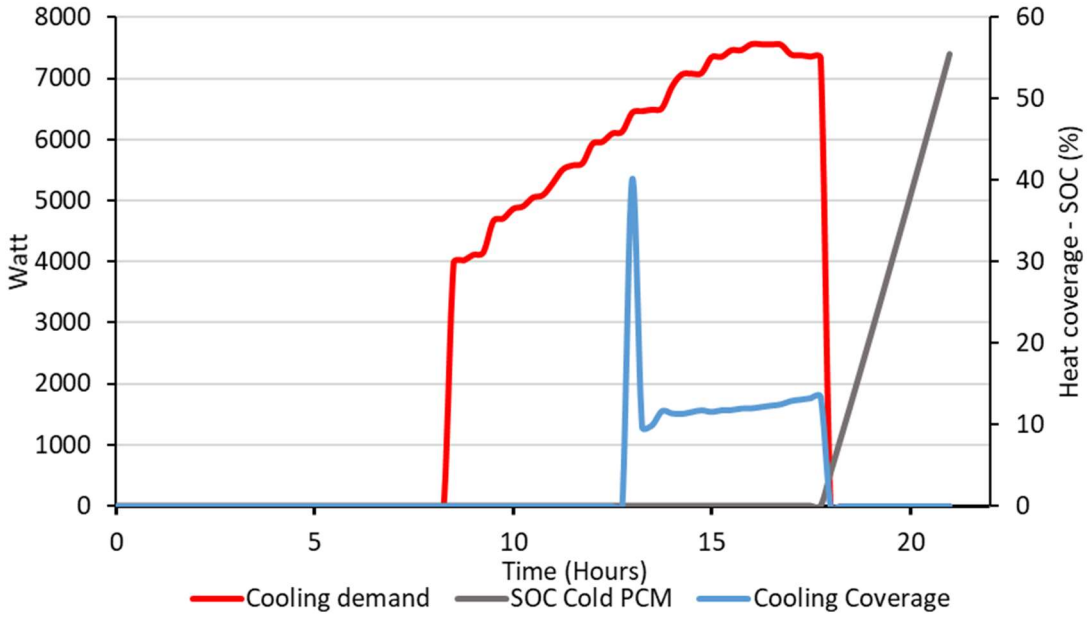

Figure 100: Total cooling coverage and SOC of cold PCM percentage (right axis) of the system in comparison with the cooling demand for Thessaloniki average summer case

5.5.1.4. Extreme Summer Thessaloniki

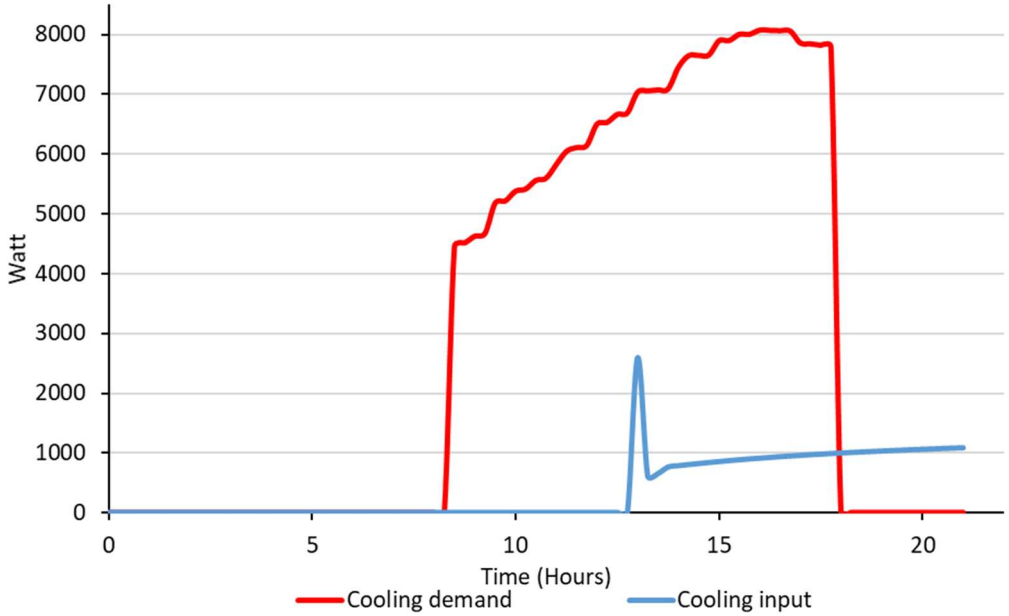

Figure 101: Cooling demand in comparison with the input cooling from the system for Thessaloniki extreme summer case

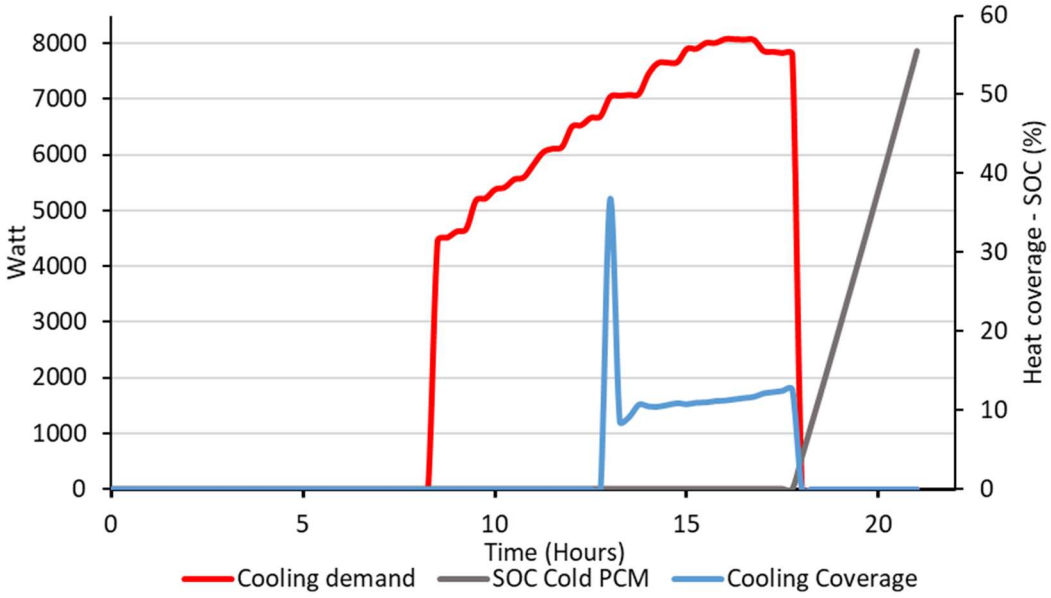

Figure 102: Total cooling coverage and SOC of cold PCM percentage (right axis) of the system in comparison with the cooling demand for Thessaloniki extreme summer case

In Figure 99 and 101**,** the cooling demand of the Thessaloniki pre-demo site in comparison with the cooling input from the system for the two summer cases is presented while in Figure 100 and 102 the cooling demand of the Thessaloniki pre-pilot in comparison with the cooling coverage. The cooling needs of the space under examination are high, with a peak value of 7.3 kW and 8kW for the average and extreme case scenario respectively. The decomposition reaction takes place on the first day so that immediately after the synthesis reaction can start and cover as much as possible the building's cooling needs. In the previous simulations, two subcases of the summer scenarios of Thessaloniki pre-demo site were identified and concerned one- and two-days operating cycle. In the updated simulation, the operating cycle of the system is 1 day, dedicated for the decomposition and for the synthesis reactions, since the different imposed operating conditions (mass flow of heat

transfer fluid, TCM thermal inertia, operating TCM pressure etc.) as well as the reduced TCM capacity reduced the cycle duration of the system. As a result, the average cooling duty generated by the ammonia evaporator is 1 kW. This is translated into an average cooling coverage of 13.3% and 12.4% of the space cooling needs for the average and extreme cases respectively. Peak values of the cooling coverage are being obtained during the beginning of synthesis, when the corresponding first reaction (2-4) is taking place. Since the synthesis reaction continues even when there is no cooling demand, the cold PCM is charged at the end of the operating cycle of the system for both case scenarios up to a value of 55%.

5.5.2. Proposed design specifications Thessaloniki

In Table 33, the average outputs of the average winter case scenario for the initial dimensioning of the system are displayed. In both winter average and extreme cases, the usage of the electrical heater was mandatory for the completion of the decomposition reaction. The total duration of the systems decomposition reaction **on the average winter case** is around 9.75 hours. If radiation is high enough or an external heating source can be used, the cycle of the system is two days for the average winter Thessaloniki cases. Average generated heat during the first reaction of the decomposition is 1.51 kW and during the second reaction is 0.7 kW. The synthesis reaction generated an average heat of 2.2 kW.

	Decomposition	Max values for decomposition	Synthesis	Max values for synthesis
Time (Hours)	9.75	-	7	-
Medium fluid mass flow (kg/h)	360	360	261	309
NH_3 Average mass flow (kg/h)	2.3	4	3.78	9.86
NH_3 Compressor duty (kW)	0.27	0.46	-	-
NH_3 Condenser duty (kW)	0.9	1.64	-	-
Heat Pump compressor duty (kW)	0.35	0.63	-	-
Heat Pump condenser (kW)	1.28	2.27	-	-
NH_3 Evaporator duty (kW)	-	-	1.2	3.2
TCM synthesis heat duty (kW)	-	-	2.24	3.86
Electrical heater duty (kW)	1.55	2	-	-

Table 33: Average outputs of average winter case for Thessaloniki pre-pilot site

In Table 33, the average outputs of the average summer case for the initial dimensioning of the system are displayed. Because in the average and extreme summer scenarios the solar energy is adequate for the completion of the decomposition, the electrical heater is not utilized. Only the average summer is analysed in this table, although the two cases have similar operational conditions. The total duration of the system reactions is 11 hours so the operation cycle is one day for the average summer Thessaloniki case. Average cooling generated during the synthesis reaction is 0.98 kW. The mass flow of the gaseous ammonia is 7.42 kg/h which is more than three times higher than the average winter case (2.3 kg/h). This is happening because of the reduction of the total time of decomposition from 9.75 hours to 2.75 hours. Due to the increase of the ammonia mass flow the

duties of the ammonia condenser as well as the ammonia compressor are higher and equal to 2.9 kW and 0.83 kW respectively.

	Decomposition	Max values for decomposition	Synthesis	Max values for synthesis
Time (Hours)	2.75	-	8.25	-
Medium fluid mass flow (kg/h)	500	500	358	472
NH_3 Average mass flow (kg/h)	7.43	10	3	8
NH_3 Compressor duty (kW)	0.83	1.1	-	-
NH_3 Condenser (kW)	2.9	4	-	-
NH_3 Evaporator duty (kW)	-	-	0.98	2.59

Table 34: Average outputs of average summer case for Thessaloniki pre-pilot site

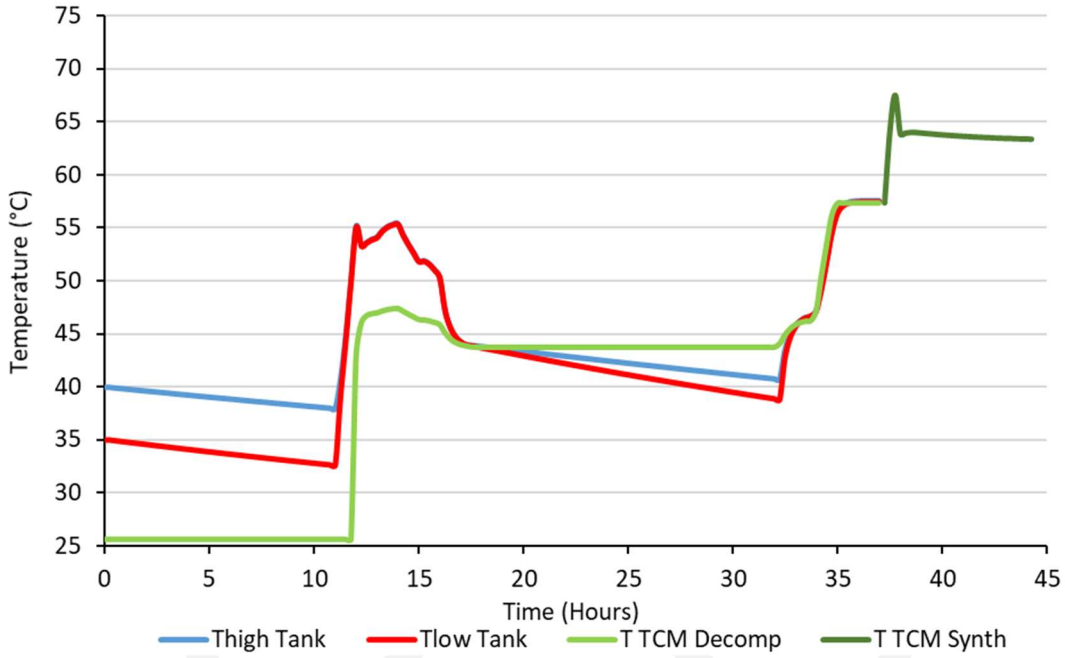

Figure 103: Temperature of the buffer tank and of the TCM reactor during decomposition and synthesis for Thessaloniki's average winter case

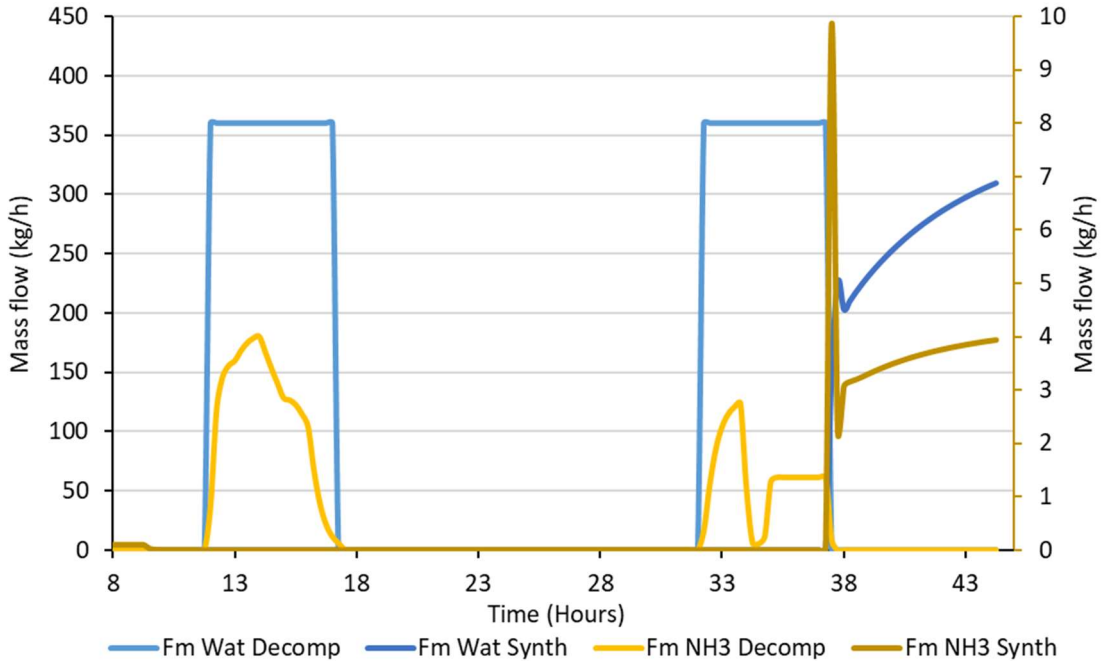

Figure 104: Mass flows of the heat transfer fluid and ammonia (right axis) during decomposition and synthesis for Thessaloniki's average winter case

The dimensioning of the system for the Thessaloniki pre-pilot site will have to take into account that the operating parameters of the system vary considerably between winter and summer. In addition, due to the fact that the demand profile is similar between the days and the cases, about 9-10 hours, the proposed system cycle is 1 day for the summer cases. Therefore, more detailed figures of the main variables of the system are provided. Figure 103103 presents the temperatures of the buffer tank as well as the TCM reactor during the two days for the average winter case. During the synthesis phase, the TCM reactor reached, for a short time, a peak temperature of 67°C. The mass flows of the heat transfer medium as well as the mass flow of gaseous ammonia entering and exiting the TCM reactor are presented in Figure 104. Mass flow of gaseous ammonia exiting the TCM reactor is averaged at 2.3 kg/h, reaching its peak value of 4 kg/h during the 1st reaction of decomposition (8-4). In the synthesis reaction, ammonia mass flow entering the TCM reactor has a peak value of 9.86 kg/h for a short time but afterwards it stabilizes around 3.6 kg/h. The fluid flow rate towards the TCM reactor during the synthesis reaction has a peak value of 309 kg/h and an average value of 261 kg/h.

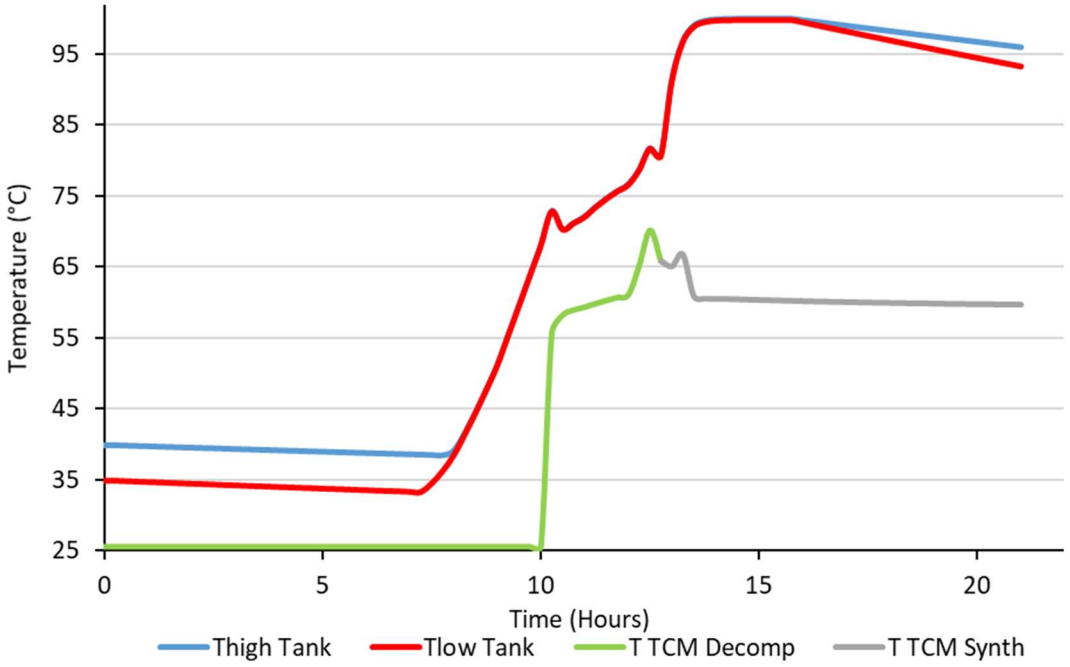

Figure 105: Temperature of the buffer tank and of the TCM reactor during decomposition and synthesis for Thessaloniki's average summer case

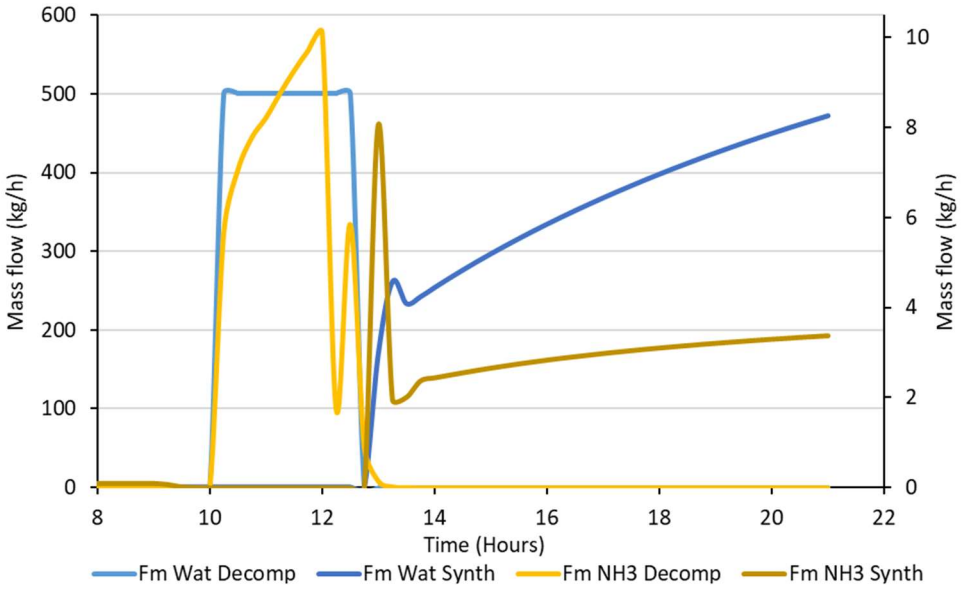

Figure 106: Mass flows of the heat transfer fluid and ammonia (right axis) during decomposition and synthesis for Thessaloniki's average summer case scenario

Figure 105, presents the temperatures of the buffer tank as well as of the TCM reactor during the one-day cycle for the average summer case. During decomposition, the TCM reactor reached for a short time a peak temperature of 70°C. In Figure 106 the mass flow of the heat transfer medium and of the gaseous ammonia entering and exiting the TCM reactor are shown. The mass flow of gaseous ammonia exiting the TCM reactor has an average value of 7.42 kg/h, reaching its peak value of 10 kg/h during the start of the second decomposition reaction (4-2). In the synthesis reaction, the ammonia mass flow entering the TCM reactor has a peak value of 8 kg/h for a short period but afterwards it stabilizes at around 2.9 kg/h. The mass flow of the heat transfer fluid of the

TCM reactor during synthesis reaction has a peak value of 472 kg/h and an average value of 358 kg/h.

5.5.3. Thessaloniki pre-pilot electrical modelling results

Similar to the previous case, this section presents the main results concerning electrical simulation for Thessaloniki Demo. The analysis was focused on monthly basis results. More detailed results will be included in the scope of T3.5.

The PVT electrical system will have 10 PVT panels with a total nominal installed power of 2.6 kWp, and a hybrid 3-phase inverter with a nominal power of 3 kW. The initial battery size has a storage capacity of 5.6 kWh. The simulations carried out considered base and alternative scenarios for the hydraulic connexion for the solar field, described in section 3.6.2. Both scenarios include in total 10 PVT panels and 5 Flat plate collectors (FPC). Regarding the final electrical results there are no relevant differences, and therefore, in this section are presented only the results for the base scenario[7].

The hybrid solar field has two important outputs: electrical production and thermal production. Electricity production is a key input for the MiniStor System since it is necessary to meet the electrical demand of the internal elements of the system, such as the internal heat pumps, the electrical backup, and the air cooler in the solar thermal circuit. Figure 107 shows the evolution of the electrical production of the PVT field throughout the year, which, as usual, follows the curve of incident solar radiation.

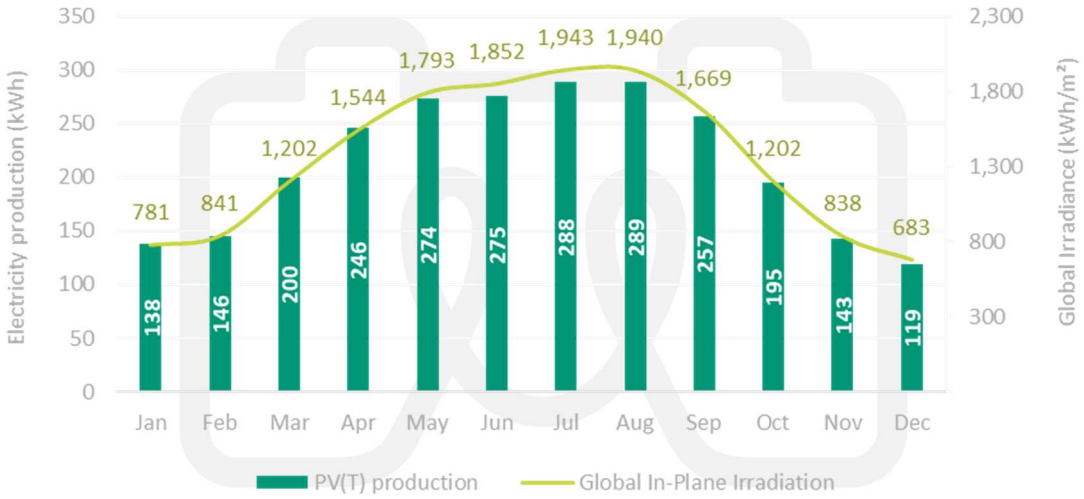

Figure 107: Monthly PV(T) electricity production and global in-plane irradiation. Thessaloniki demo site

In this demo, a total of 10 covered PVT panels were considered, with a total gross area of 16.1 m^2. The total production throughout the year is 2570 kWh, while the incident solar irradiance is 16288 kWh, which represents an average efficiency of 15.8% for the operating conditions considered in the simulation. This efficiency value, high throughout the year, is achieved, thanks to the optimal orientation of the PVT panels in this demo, with zero azimuth and an inclination close to latitude.

This electrical production is dedicated to meet the electrical demand of the Thessaloniki Demo, which, as section 4.3 presents, corresponds exclusively to the MiniStor system. At an annual level, both production and demand are similar, with values of 2570 kWh and 2427 kWh respectively. However, in winter there are deficits between 35% and 73%, so electricity from the grid must be used. On the contrary, in the summer months, there are surpluses between 93% and 122%. In this regard, Figure 108 shows the breakdown of the total load with regards to the system in charge of supplying the electricity: the main grid or MiniStor electric system (PV and batteries). Indeed,

[7] *The simplified thermal results obtained from the electrical model indicate that the alternative scenario has a slight improvement in thermal production in comparison to the base scenario. These results should be confirmed by a detailed thermodynamic simulation.*

throughout the year 900 kWh (37.1%) of electricity demand is covered by the PVT / batteries system, while the remaining 1,527 kWh (62.9%) are covered from the electricity grid.

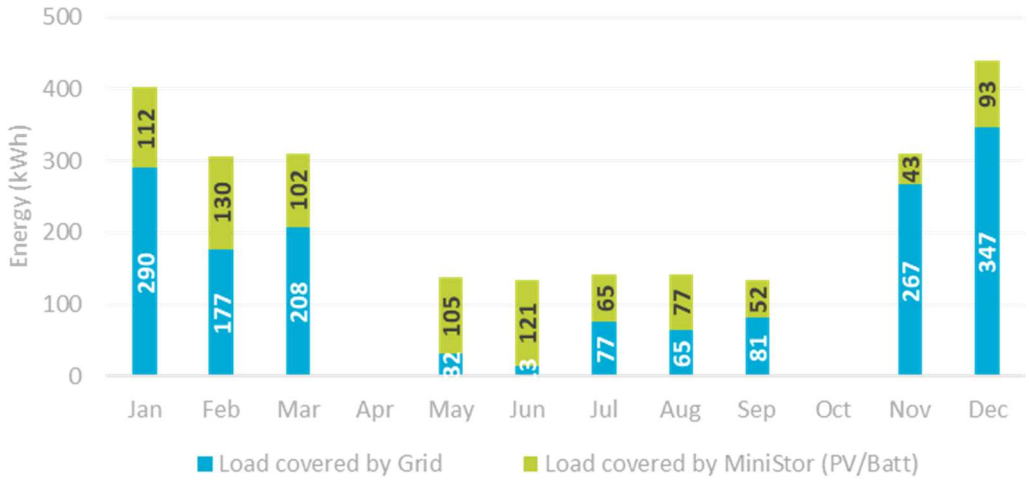

Figure 108: Load covered by grid or MiniStor electric system (PV/Batteries). Thessaloniki demo site

Figure 109 shows in detail the monthly electrical solar coverage factors obtained for Thessaloniki. Following the trend of incident solar radiation and electricity production, the lowest coverage factors occur in winter, with a minimum of 34% in January, while the highest coverage factors occur in summer with a maximum value of 204% in July. This indicates clearly that there is a surplus of electrical production in summer, which could serve other electrical receivers in the home or the MiniStor system. In the framework of Task 3.5, this topic will be analysed.

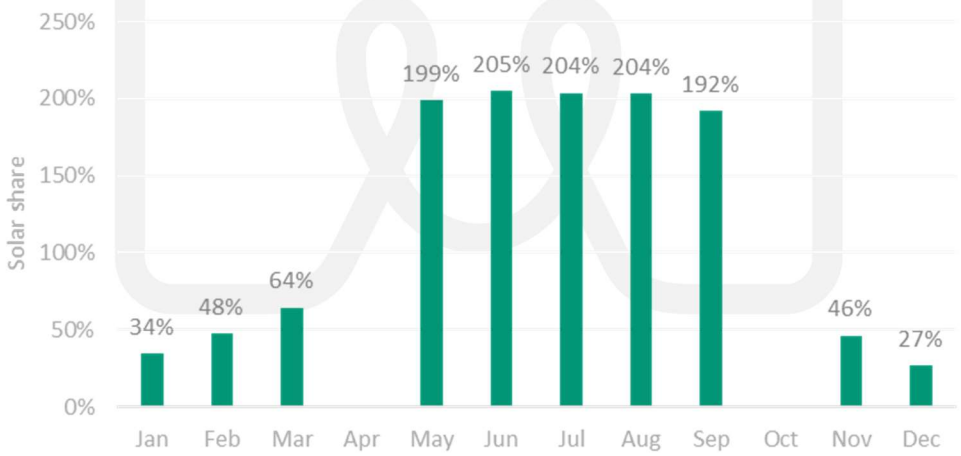

Figure 109: Monthly solar contribution; relation between solar production and total load by month. Thessaloniki demo site

In the same line exposed for the Sopron Demo, Figure 110 shows a more detailed breakdown of the electrical demand for the Thessaloniki Demo. In this case, the electrical demand is divided into four parts: (1) the electrical demand-supplied by the grid, when there is not PVT production (blue bars); (2) the electrical demand-supplied also by the grid, due to the low electricity prices (red bars); (3) the electrical demand-supplied directly by PVT panels without using electrical batteries (dark green bars), and (4) the electrical demand-supplied by PVT system, using the electricity stored in the ion-lithium batteries (light green bars).

In this graph, it is possible to see that during wintertime, the electricity supplied by the PVT system is sent to the electrical load from the PVT panels directly or through the electrical batteries, with similar proportions. During the summertime, a greater proportion of the electrical load is met directly from the PVT panels without using the electricity stored in the batteries. Despite the fact that there

is a surplus in electricity production during the summertime, the electrical demand cannot be completed covered by the PVT system. This behaviour suggests that the operation of the system and the battery size could be optimized in order to increase the use of electrical production by the MiniStor system. This analysis should be carried out in the framework of Task 3.5.

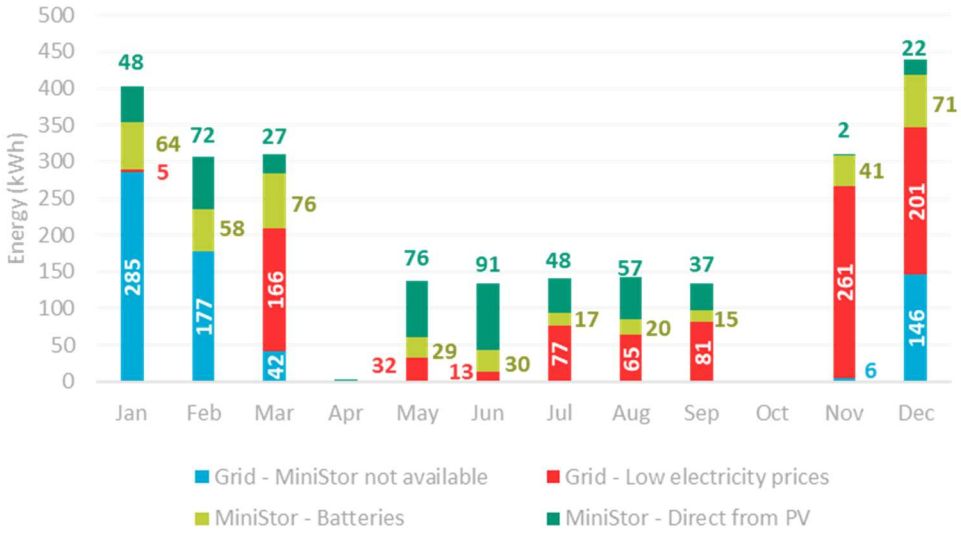

Figure 110: Load covered by each system. Thessaloniki demo site

Another point to underline concerning the electrical system is the option of using the PVT electrical production, taking into account the electricity price signal. This concept was already presented in section 4.3 and the previous demo results (Sopron Case). In summary, the PVT electrical system prioritizes the consumption of electricity from the grid, when the electricity price is low enough. In this case, the photovoltaic production is directly stored in the electrical li-ion batteries for later consumption, when the price is more expensive. About that operation mode, Figure 111 illustrates the evolution of the electricity consumption from the grid, when there are low electricity prices, as well, the evolution of the electrical price throughout the year. The curves show how during the months with lower electricity prices, such as March, November and December, electricity consumption from the grid increases.

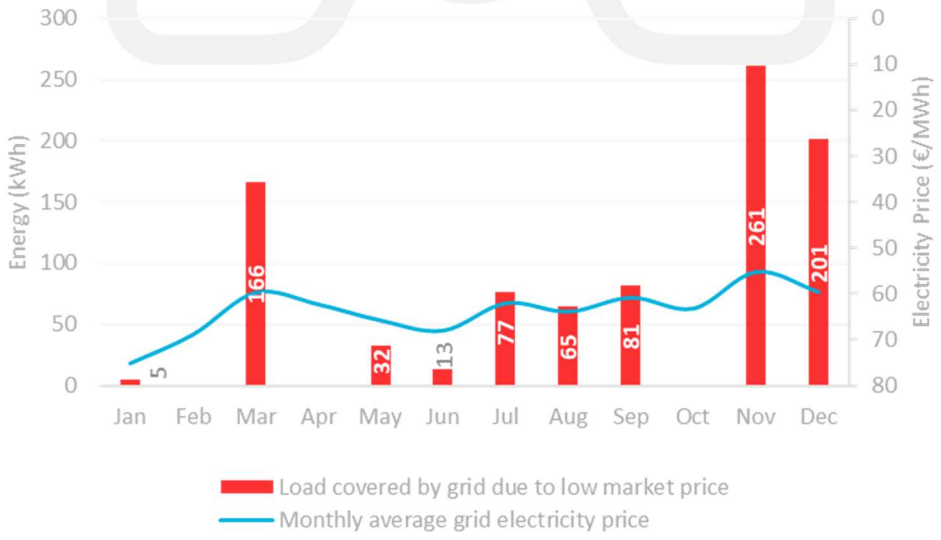

Figure 111: Load covered by grid due to low market price. Sopron demo site

Finally, as part of the analysis of the initial electrical system of Thessaloniki, the evolution of the state of charge of the electric batteries (SOC) was reviewed. Figure 112 shows the evolution of the

average monthly value of this indicator throughout the year. As expected, during the winter months, the SOC value is lower, due to the higher electricity demand, and the lower incident solar radiation; On the contrary, during the summer months, the SOC is always close to 100%, since the electricity demand is lower and at the same time the solar radiation and electricity production are higher.

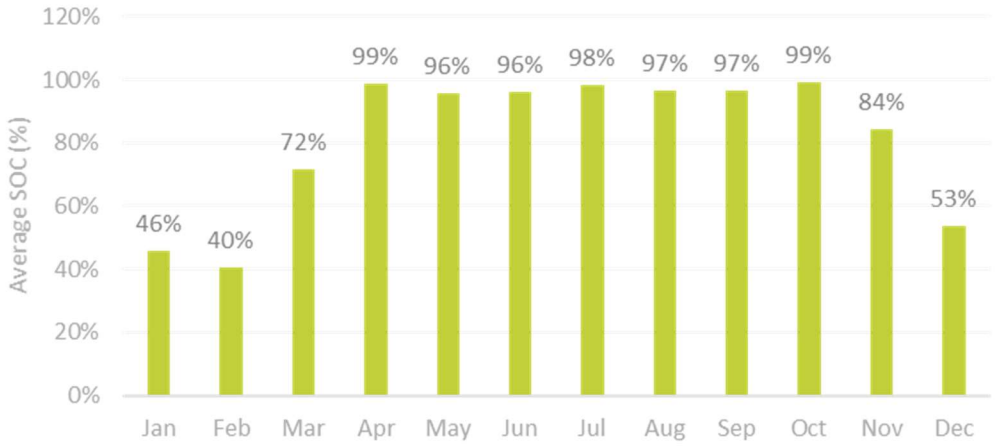

Figure 112: Monthly average State-Of-Charge of batteries (SOC). Thessaloniki demo site

In general, the model implemented in TRNSYS to simulate the electrical system, allows to properly analyse the electrical PVT production and the energy flows between the hybrid solar inverter and the different elements (PVT production, electrical grid, demand and batteries). Within the framework of Task 3.5, complementary simulations and analysis will be carried out, in order to optimize the use of the electrical energy produced, as well as the energy storage in the lithium-ion battery system, for the different MiniStor demo-sites.

5.6. Santiago pilot results

5.6.1.1. Santiago pilot thermodynamic results Average Winter

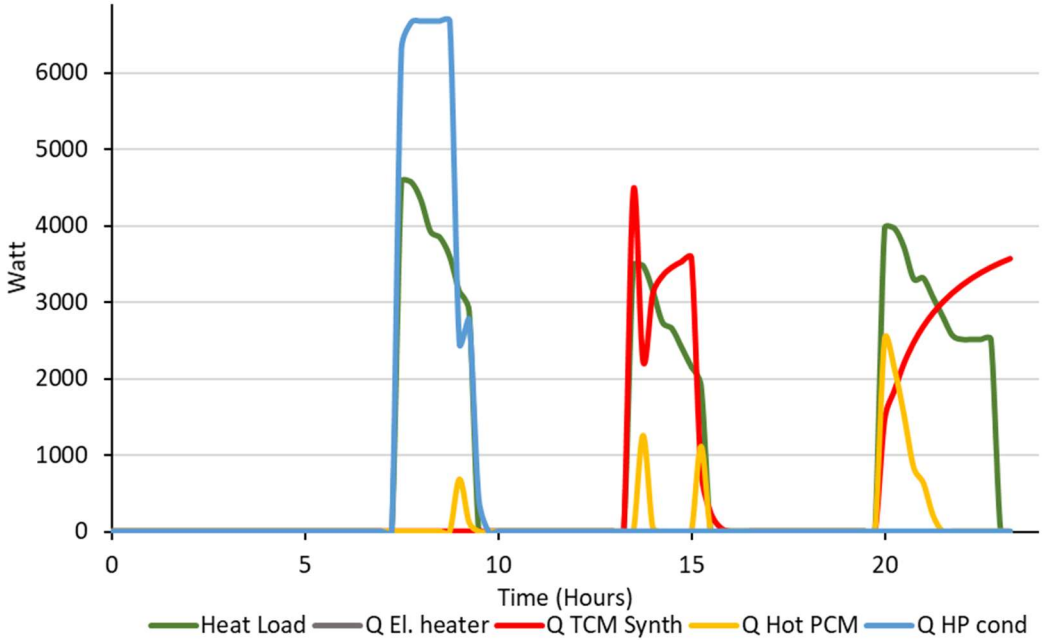

Figure 113: Heat demand in comparison with the input heat by the system and the consumption of the

electrical heater for Santiago average winter case

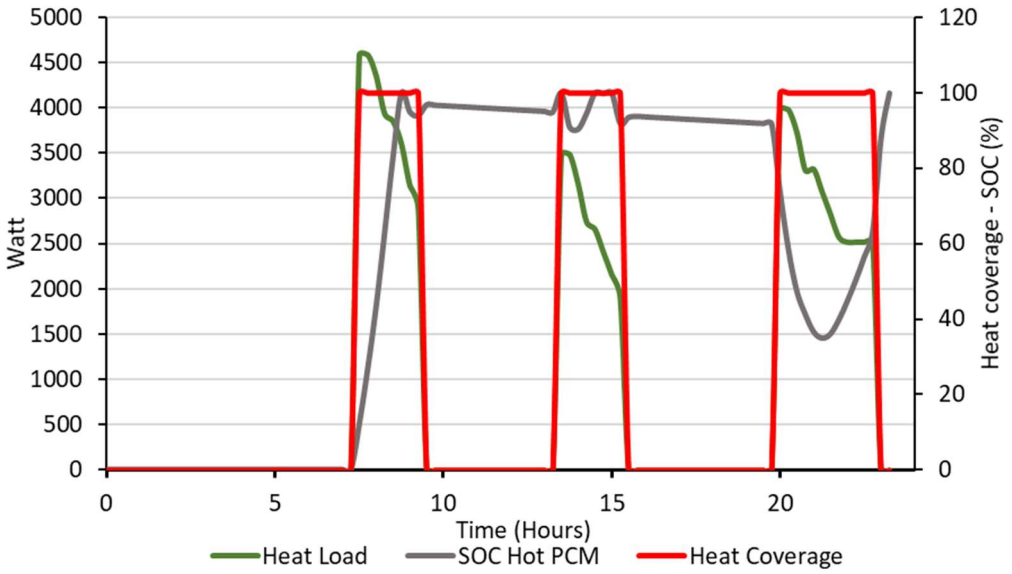

Figure 114: Total heat coverage and SOC of PCM percentage (right axis) of the system in comparison with the heat demand for Santiago average winter case

5.6.1.2. Extreme Winter Santiago

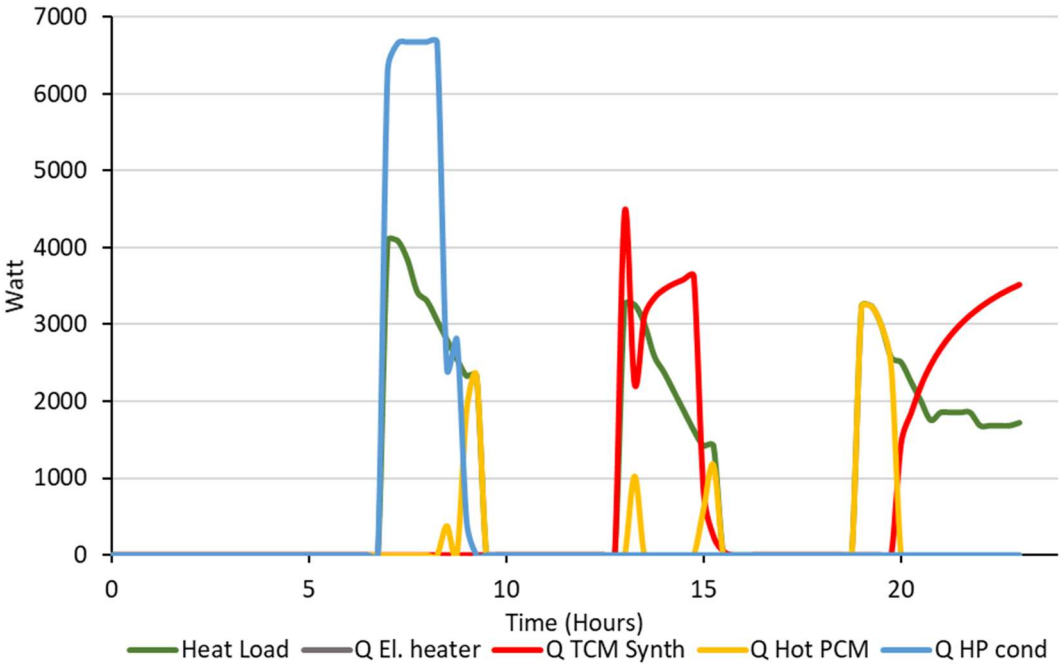

Figure 115: Heat demand in comparison with the input heat by the system and the consumption of the electrical heater for Santiago extreme winter case

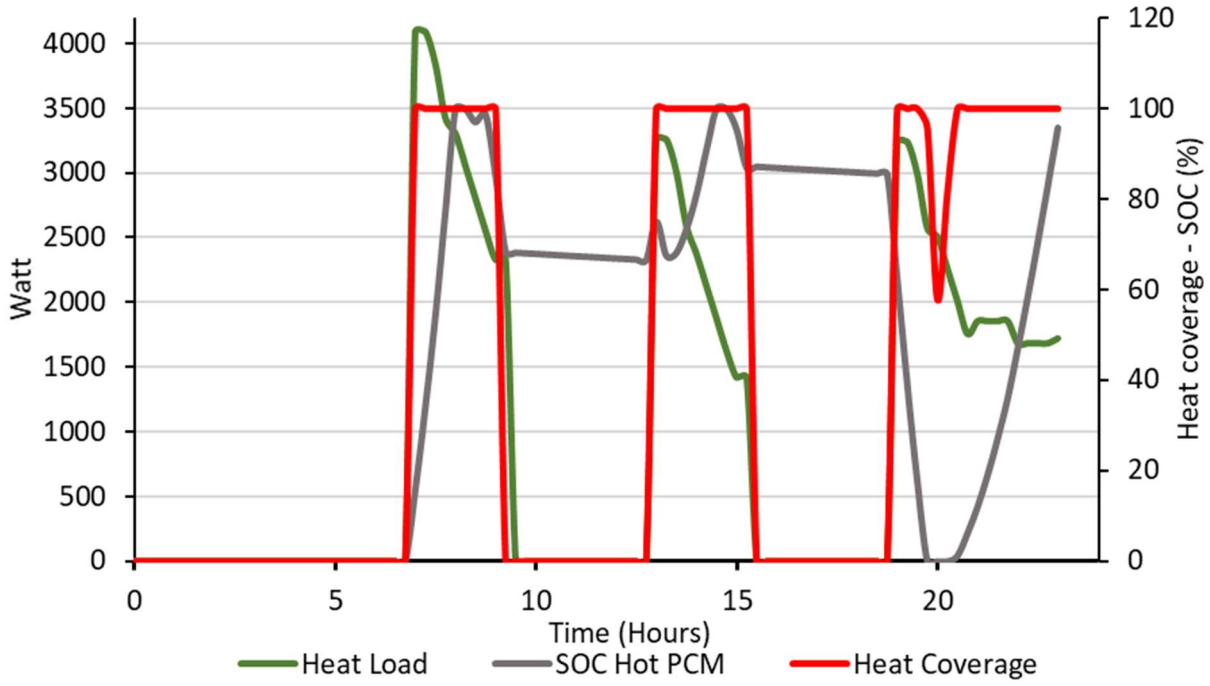

Figure 116: Total heat coverage and SOC of PCM percentage (right axis) of the system in comparison with the heat demand for Santiago extreme winter case

In Figure 95113 and 115, the heat demand of Santiago demo site in comparison with the output heat of the system during the course one day is depicted. In Figure 114 and 116 the total heat coverage provided by the system and the SOC of the hot PCM are presented in comparison with the heat demand of the building. On the first day of the average case, the decomposition lasts for 2.25 hours, due to the low thermal inertia of the 17.5 kWh TCM reactor.

For the average winter case, the system manages to fully cover the heating needs for 7 hours and in total presents an average heating coverage of 100%. At the end of the cycle, the PCM is also fully charged, reaching a SOC value of 100%. Thanks to the sufficient heat input provided by the additional heat pump (located between the PVT array and the buffer tank), the heating demand of the building has been met while at the same time the PCM is being charged. Also, the electrical heater is not activated at any point during the cycle. For the extreme winter case, the system can only cover the heating demand of the building for 8.25 hours. The system has an average heating coverage of 98%, again thanks to the heat input provided by the Hitachi heat pump. As in the average winter case, the electrical heater is not activated. Due to the fact that the synthesis reaction produces excess heat in regard to the thermal demand, the hot PCM is almost fully charged at the end of the operating cycle of the system in the extreme case scenario, with a SOC of 96%.

5.6.1.3. Average Spring-Autumn Santiago

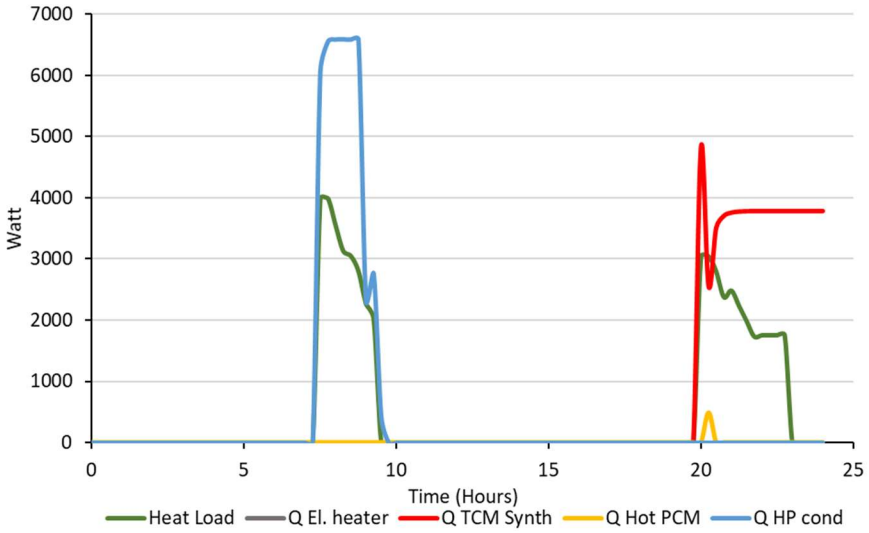

Figure 117: Heating demand in comparison with the heating input from the system for Santiago average spring-autumn case

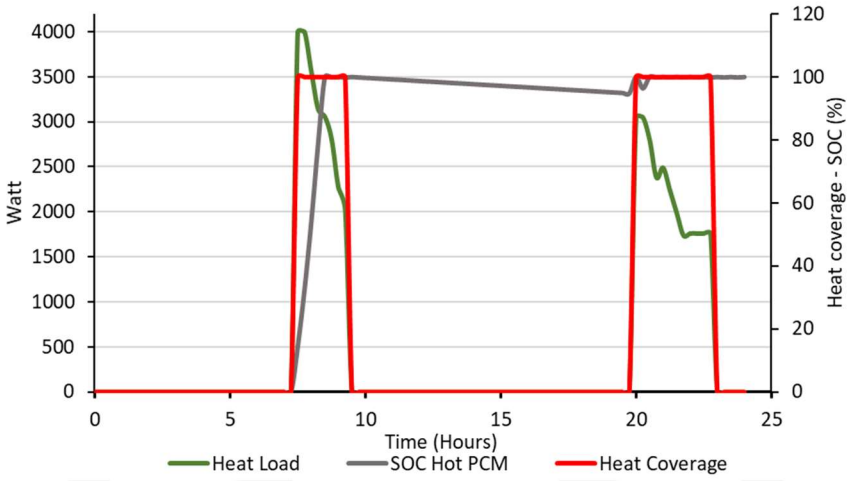

Figure 118: Total heating coverage and SOC of cold PCM percentage (right axis) of the system in comparison with the heating demand for Santiago average spring-autumn case

In Figure 117, the heating demand of the Santiago demo site in comparison with the heating input from the system for the average spring-autumn case is presented while in Figure , the heating demand of the Santiago pilot in comparison with the heating coverage. The heating needs of the space under examination reach a peak value of 3 kW, which is not drastically different from the winter scenarios. The decomposition reaction takes place within the first 10 hours, while the synthesis begins at around 20 hours' time. This is translated into a fully heating coverage of 100% of the space heating needs for the average spring-autumn case. The system manages to fully cover the building's heating demand for 5 hours. Since the synthesis reaction continues even when the heating demands decreases significantly, the hot PCM is again fully charged at the end of the operating cycle of the system, meaning a SOC of 100%.

5.6.1. Proposed design specifications Santiago

In Table 35, the average outputs of the average winter case scenario for the initial dimensioning of the system are displayed. In both winter average and extreme cases, the usage of the electrical heater was not mandatory for the completion of the decomposition reaction, in contrast with the other demo sites. The reason behind this is the fact that the additional heat pump provides heating

input much more effectively than the solar thermal panels, located in other demos. The total duration of the systems decomposition reaction on the average winter case is around 2.25 hours. Average generated heat during the reaction of the decomposition is 5 kW. The synthesis reaction generated an average heat of 2.86 kW.

	Decomposition	Max values for decomposition	Synthesis	Max values for synthesis
Time (Hours)	2.25	-	5.25	-
Medium fluid mass flow (kg/h)	1000	1000	353	454
NH_3 Average mass flow (kg/h)	8.9	11.8	5	10
NH_3 Compressor duty (kW)	1	1.37	-	-
NH_3 Condenser duty (kW)	3.64	4.83	-	-
Heat Pump compressor duty (kW)	1.4	1.85	-	-
Heat Pump condenser (kW)	5	6.68	-	-
NH_3 Evaporator duty (kW)	-	-	1.64	3.23
TCM synthesis heat duty (kW)	-	-	3	4.46
Hitachi HP (kW)	5.9	5.9	-	-

Table 35: Average outputs of average winter case for Santiago demo

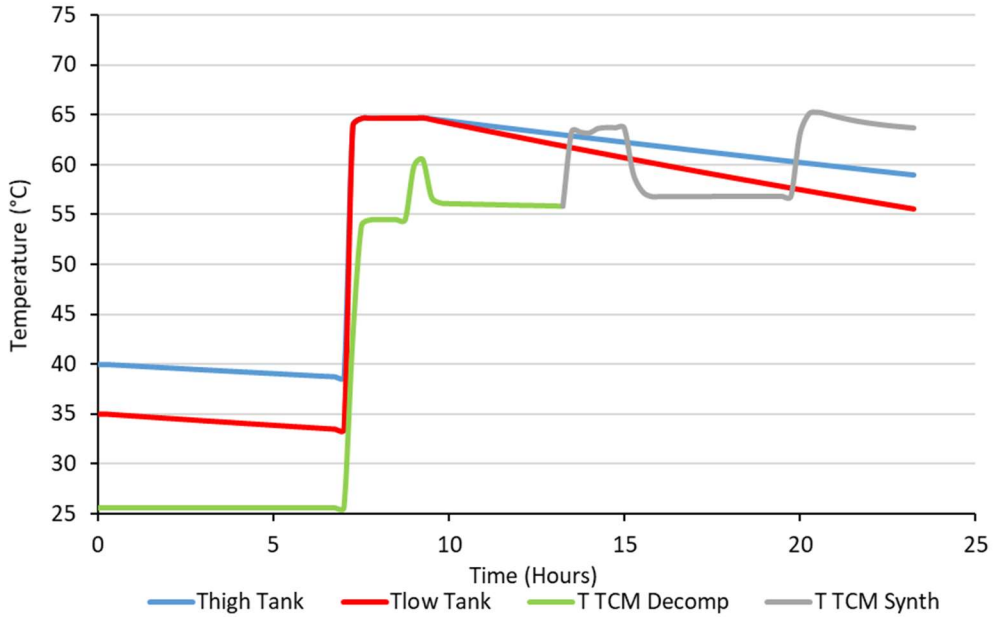

Figure 119: Temperature of the buffer tank and of the TCM reactor during decomposition and synthesis for Santiago's average winter case

The dimensioning of the system for the Santiago pre-pilot site will have to take into account that the operating parameters of the system in the average winter case. In addition, due to the fact that the demand profile is similar between the days and the cases, about 7-9 hours, the proposed system cycle is 1 day for the summer cases. Therefore, more detailed figures of the main variables of the system are provided. Figure 103119 presents the temperatures of the buffer tank as well as the TCM reactor during the first day for the average winter case. During the synthesis phase, the TCM reactor reached, for a short time, a peak temperature of 65°C. The mass flows of the heat transfer medium as well as the mass flow of gaseous ammonia entering and exiting the TCM reactor are presented in Figure 120. Mass flow of gaseous ammonia exiting the TCM reactor is averaged at 9.92 kg/h, reaching its peak value of 11.8 kg/h during the 1st reaction of decomposition (8-4). In the synthesis reaction, ammonia mass flow entering the TCM reactor has a peak value of 10 kg/h for a

short time but afterwards it stabilizes around 5.25 kg/h. The fluid flow rate towards the TCM reactor during the synthesis reaction has a peak value of 454 kg/h and an average value of 353 kg/h.

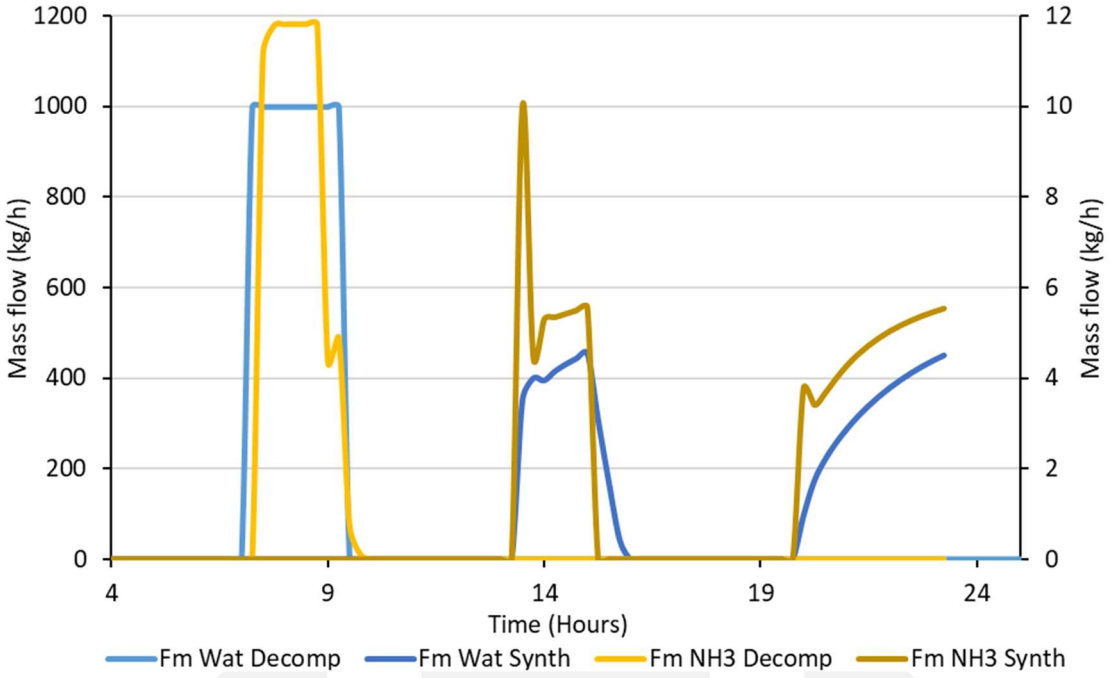

Figure 120: Mass flows of the heat transfer fluid and ammonia (right axis) during decomposition and synthesis for Santiago's average winter case scenario

6. Summary of MiniStor configuration results according to each demonstration site and future work

The results of Section 5 provide an initial assessment of the system in terms of its operational strategy and dimensioning. Several parameters and operational conditions of the MiniStor system have not been definitely decided during the implementation of the numerical simulations and compilation of this report. In those cases, assumptions are based on information provided by project partners. Therefore, the final configuration and dimensioning of the MiniStor system and related operating strategies may have differences from the outcomes of this assessment. These would be based on further data obtained from demo site monitoring (WP6), and the priorities that each demo site will have in terms of electricity or thermal energy production. For instance, the initial thermodynamic results summarised in Table 36 refer to the average winter case scenario in all demo sites, because the provision of heating storage capacity was considered as first priority. In case it is decided that the main priority of MiniStor in one of these demo sites is to provide cooling storage capacity, then system dimensioning will change.

Regarding the system's electrical model, a more detailed analysis of battery sizing for all demo sites will be implemented in the framework of Task 3.5. A more detailed approach concerning the electricity prices will also be taken into account. The complex interaction schemes between the batteries and the grid will be studied in more detail, leading to an optimised usage of electrical energy.

Table 36 provides a summary of the initial dimensioning of the MiniStor system for each of the four demonstration sites in terms of the maximum values for each of the main components.

Demonstration Site and System Feature									
Sopron		Kimmeria		Cork		Thessaloniki		Santiago	
PVT – Solar Collector Layout									
9 PVTs 6 FPCs		(none – existing sources to be used)		4 PVTs 4 FPCs		5 PVTs 5 PVTs 5 FPCs		20 PVT (Unglazed)	
Tank size (Kg)									
60		-		60		60		60	
Operating pressure of TCM decomposition reaction (bar)									
2		2		2				2	
Operating pressure of TCM synthesis reaction (bar)									
6		6		6		6		6.5	
Time for stage completion (Hours)									
Dec	Syn	Dec	Syn	Dec	Syn	Dec	Syn	Dec	Syn
10	7	5.5	6.5	10	7	9.75	7	2.25	5.25
Heat transfer fluid mass flow (kg/h)									
Dec	Syn	Dec	Syn	Dec	Syn	Dec	Syn	Dec	Syn
360	309	468	500	360	309	360	309	1000	454
NH_3 mass flow (kg/h)									
Dec	Syn	Dec	Syn	Dec	Syn	Dec	Syn	Dec	Syn
2.85	9.74	6.51	10	3.9	9.8	4	9.86	11.8	10
NH_3 Compressor duty (kW)									
Dec	Syn	Dec	Syn	Dec	Syn	Dec	Syn	Dec	Syn
0.44	-	0.75	-	0.45	-	0.46	-	1.37	-
NH_3 Condenser duty (kW)									
Dec	Syn	Dec	Syn	Dec	Syn	Dec	Syn	Dec	Syn
1.17	-	2.7	-	1.59	-	1.64	-	4.83	-
Heat Pump compressor duty (kW)									
Dec	Syn	Dec	Syn	Dec	Syn	Dec	Syn	Dec	Syn
0.44	-	1	-	0.6	-	0.63	-	1.85	-
Heat Pump condenser (kW)									
Dec	Syn	Dec	Syn	Dec	Syn	Dec	Syn	Dec	Syn
0.45	-	3.7	-	2.2	-	2.27	-	6.68	-
NH_3 Evaporator duty (kW)									
Dec	Syn	Dec	Syn	Dec	Syn	Dec	Syn	Dec	Syn
-	3.2	-	3.2	-	3.19	-	3.2	-	3.23
TCM synthesis heat duty (kW)									
Dec	Syn	Dec	Syn	Dec	Syn	Dec	Syn	Dec	Syn
	3.87	-	3.93	-	3.85	-	3.86	-	4.46
Electrical heater duty (kW)								HP Hitachi	
Dec	Syn	Dec	Syn	Dec	Syn	Dec	Syn	Dec	Syn
2	-	-	-	2	-	2	-	5.9	-

Table 36: Summary of the results (Max values) of the demo sites for the initial dimensioning of the MiniStor system

7. Conclusions

This deliverable has presented the development of a thermodynamic model for an integrated thermal system powered by a Photovoltaic thermal and solar thermal field, which is coupled to a thermochemical material reactor (TCM) and phase changing material units (PCM) for thermal energy storage. It also presents the initial calculations for an integrated electrical storage system (ESS) with li-ion batteries. The objective of developing this model is to perform the first preliminary simulations of system operation for all the demo sites involved in MiniStor, determining basic design and operational aspects of the system. Moreover, thermal and cooling loads were calculated to be used as model inputs in order to obtain credible initial suggestions for the dimensioning of the whole system. The electrical model of the system consisting of the PVTs, the electrical storage system, based on lithium-ion batteries and an inverter has been also developed in this deliverable and the system operation was examined on a yearly basis.

Simulations of the MiniStor electrical system reveal that in Sopron approximately 14% of the building annual electricity demand can be covered by the PVTs. Optimizing its use to respond to different pricing tariffs results in a clear correlation between lower prices paid by the end-user and larger amounts of electricity imported from the grid. The resulting average SoC of the battery in this site is about 27%. The demo site at Thessaloniki presents other needs since the main objective is to cover the electricity load of MiniStor components. On an annual basis, production and consumption are almost equal to each other, however a deficit is observed in winter and a generation surplus in summer. Consequently, the battery SoC is close to 100% for a period of seven months. The electrical model of the system will be further analyzed, and additional scenarios will be investigated in the framework of Task 3.5.

Photovoltaic thermal and solar collectors facilitate an efficient conversion of the solar energy into electricity and hot water for the TCM reactor. To boost this solar energy, the PVT- solar collector layout is equipped with a buffer tank for the smooth evolution of the outlet temperature from the solar field array. In addition, an electrical heater is added to raise the fluid temperature in adverse weather conditions. In that way, the targeted energy density of 213 kWh/m^3 is guaranteed for the needs of the decomposition phase in the TCM reactor. The PVT model developed in this deliverable was validated against simulation results from commercial software.

The thermochemical reactor is an essential component of the suggested process design, as it facilitates long term and efficient operation of the MiniStor system. The material in the TCM reactor is heated taking advantage of the solar energy, and the endothermic reaction combined with ammonia releases a gaseous ammonia stream. This stream is condensed, providing heat in usable form, and a Heat Pump is then used to elevate the energy of the released heat with a COP of 3.61. The ammonia is then ready to be circulated again and to repeat the endothermic reaction without corroding the tank or coalescing the TCM material. This allows for continuous and efficient production of thermal energy during the endothermic reaction of the TCM. Upon completion of the decomposition, the synthesis reaction is deployed. This exothermic reaction is enough to provide the building with thermal energy received by the system for completion of the endothermic reaction. When considering the entire system, both thermal energy from the Heat Pump Cycle as well as from the synthesis mode of the reactor result in an overall COP for heating equal to 1.8.

The PCM heat storage units facilitate the storage of excess heat generated during system operation, resulting in flexibility to use this excess when required. They also provide a smoother behavior of the overall system during the charging and discharging cycles, optimizing the charging and consumption strategy.

The simulations performed in this task considered different approaches regarding the system behavior, operating conditions and operation cycle duration. Ultimately, the system can be a self-powered one, providing thermal and cooling energy to the building. Simulation results show that for winter cases in the Sopron, Cork and Thessaloniki demo sites it is required to use a backup electrical heater to compensate when there is underproduction of heat from the solar field. The activation of the backup heater has a crucial impact by significantly reducing total system efficiency. On the other hand, in summer cases for Sopron and Thessaloniki demo sites the solar energy provided by the PVT- solar collector layout is adequate for completion of the decomposition phase of the TCM reactor.

Regarding overall energy coverage of the building, simulation results showed that in average winter cases, the system generated enough thermal energy to cover almost fully the thermal demands of the buildings during the 1st reaction of decomposition (8-4) and synthesis for all demo sites. For Sopron and Cork demo sites, the average winter case heat coverage is around 55%. In Kimmeria it is 100% for the decomposition reaction and 75% for the synthesis reaction. In the extreme winter cases, due to the higher thermal loads, heat coverage is expected to be significantly lower in Sopron and Cork, whereas in Thessaloniki it remains in the same values as in the average winter case. The size of the PCM heat storage unit compared to the magnitude of the thermal loads of the buildings, is directed mainly to provide a support to the dwelling's heating system operation. In case of independent operation, it manages to cover the thermal needs for about an hour. In Santiago the system manages to fully cover the heating needs and presents an average heating coverage of 100%. At the end of the cycle, the PCM is also fully charged, reaching a SOC value of 100%. Thanks to the sufficient heat input provided by the additional heat pump (located between the PVT array and the buffer tank), the heating demand of the building has been met while at the same time the PCM is being charged. In summer cases, the system cannot fully cover the cooling demands of the demo sites that require it. Specifically, the system provides a cooling coverage of 30% for the extreme summer case in Sopron. In Kimmeria, the system provides a cooling coverage of 48% and 30% for average and extreme summer cases respectively. For Thessaloniki, different day cycles (1-2) were investigated, with an average coverage of 13% for both average and extreme summer cases.

These thermodynamic simulation results provide an initial dimensioning of the overall system for each analyzed demo site. Due to the system being powered through solar energy, which varies between seasons of the year and geographic location, different system efficiencies are expected based on energy and mass balances. Further model optimization, specifically with regards to streamlined charging and consumption strategies, best TCM reactor sizes for each demo site as well as PVT-solar collector layouts, will be performed in order to lead to further enhancement of the key performance indicators and substantial reductions of the electrical usage of the MiniStor system. Verification of these calculations and assessment of actual system performance will be done in the context of T6.4 and T6.5, when physical prototypes of the MiniStor system will be installed in the demonstration sites and operation data will be collected according to key performance indicators defined in T6.1.

References

1. Report, J.S.f.P., *Energy Consumption and Energy Efficiency Trends in the EU-28 2000-2015*. 2018.
2. *Clean energy for all Europeans package*. Published: 20 October 2017 Last update: 12 March 2020 [cited 2019 9 December 2019]; Available from: https://ec.europa.eu/energy/topics/energy-strategy/clean-energy-all-europeans_en.
3. Bird, L., J. Cochran, and X. Wang, *Wind and solar energy curtailment: Experience and practices in the United States*. 2014, National Renewable Energy Lab.(NREL), Golden, CO (United States).
4. Dincer, I. and M. Rosen, *Thermal Energy Storage: Systems and Application;* , ed. J.W. Sons. 2011, Chichester, UK.
5. Sharma, A., et al., *Review on thermal energy storage with phase change materials and applications*. Renewable and Sustainable Energy Reviews, 2009. **13**(2): p. 318-345.
6. Hailu, G., *Seasonal Solar Thermal Energy Storage*, in *Thermal Energy Battery with Nano-enhanced PCM*. 2018, IntechOpen.
7. Kumar, A. and S.K. Shukla, *A Review on Thermal Energy Storage Unit for Solar Thermal Power Plant Application*. Energy Procedia, 2015. **74**: p. 462-469.
8. Waser, R., et al., *Fast and experimentally validated model of a latent thermal energy storage device for system level simulations*. Applied Energy, 2018. **231**: p. 116-126.
9. Cellat, K., et al., *2 years of monitoring results from passive solar energy storage in test cabins with phase change materials*. Solar Energy, 2019.
10. Malan, D.J., R.T. Dobson, and F. Dinter, *Solar Thermal Energy Storage in Power Generation Using Phase Change Material with Heat Pipes and Fins to Enhance Heat Transfer*. Energy Procedia, 2015. **69**: p. 925-936.
11. Grange, B., et al., *Impact of thermal energy storage integration on the performance of a hybrid solar gas-turbine power plant*. Applied Thermal Engineering, 2016. **105**: p. 266-275.
12. Belmonte, J.F., et al., *Air-based solar systems for building heating with PCM fluidized bed energy storage*. Energy and Buildings, 2016. **130**: p. 150-165.
13. Izquierdo-Barrientos, M.A., C. Sobrino, and J.A. Almendros-Ibáñez, *Energy storage with PCM in fluidized beds: Modeling and experiments*. Chemical Engineering Journal, 2015. **264**: p. 497-505.
14. Parsazadeh, M. and X. Duan, *Numerical and statistical study on melting of nanoparticle enhanced phase change material in a shell-and-tube thermal energy storage system*. Applied Thermal Engineering, 2017. **111**: p. 950-960.
15. Kant, K., A. Shukla, and A. Sharma, *Performance evaluation of fatty acids as phase change material for thermal energy storage*. Journal of Energy Storage, 2016. **6**: p. 153-162.
16. Baylin, F. and S.E.R. Institute, *Low Temperature Thermal Energy Storage: A State-of-the-art Survey*. 1979: Department of Energy, [Office of Energy Technology], Solar Energy Research Institute.
17. Godefroy, A., et al., *Hybrid thermochemical cycles for low-grade heat storage and conversion into cold and/or power*. Energy Conversion and Management, 2020. **225**: p. 113347.
18. Cot-Gores, J., A. Castell, and L.F. Cabeza, *Thermochemical energy storage and conversion: A-state-of-the-art review of the experimental research under practical conditions*. Renewable and Sustainable Energy Reviews, 2012. **16**(7): p. 5207-5224.
19. Zhang, Y. and R. Wang, *Sorption thermal energy storage: Concept, process, applications and perspectives*. Energy Storage Materials, 2020. **27**: p. 352-369.
20. Sharma, R. and E. Anil Kumar, *Study of ammoniated salts based thermochemical energy storage system with heat up-gradation: A thermodynamic approach*. Energy, 2017. **141**: p. 1705-1716.
21. Stitou, D., N. Mazet, and S. Mauran, *Experimental investigation of a solid/gas thermochemical storage process for solar air-conditioning*. Energy, 2012. **41**(1): p. 261-270.

22. Fitó, J., et al., *Hybrid system combining mechanical compression and thermochemical storage of ammonia vapor for cold production*. Energy Conversion and Management, 2019. **180**: p. 709-723.
23. Fitó, J., et al., *Definition and performance simulations of a novel solar-driven hybrid absorption-thermochemical refrigeration system*. Energy Conversion and Management, 2018. **175**: p. 298-312.
24. van der Pal, M. and R.E. Critoph, *Performance of $CaCl_2$-reactor for application in ammonia-salt based thermal transformers*. Applied Thermal Engineering, 2017. **126**: p. 518-524.
25. Oliveira, R.G., R.Z. Wang, and C. Wang, *Evaluation of the cooling performance of a consolidated expanded graphite–calcium chloride reactive bed for chemisorption icemaker*. International Journal of Refrigeration, 2007. **30**(1): p. 103-112.
26. Wang, L.W., et al., *Compound adsorbent for adsorption ice maker on fishing boats*. International Journal of Refrigeration, 2004. **27**(4): p. 401-408.
27. Sakamoto, Y. and H. Yamamoto, *Performance of Thermal Energy Storage Unit Using Solid Ammoniated Salt ($CaCl_2$-NH_3 System)*. Natural Resources, 2014. **5**(8): p. 337-342.
28. Bergene, T. and O.M. Løvvik, *Model calculations on a flat-plate solar heat collector with integrated solar cells*. Solar Energy, 1995. **55**(6): p. 453-462.
29. Zondag, H.A., et al., *The thermal and electrical yield of a PV-thermal collector*. Solar Energy, 2002. **72**(2): p. 113-128.
30. EndeF. *Hybrid solar installation Luxury Hotel Ibiza*. 25/09/2020]; Available from: https://endef.com/en/portfolio-items/hybrid-solar-installation-luxury-hotel-ibiza/.
31. Tyagi, V.V., S.C. Kaushik, and S.K. Tyagi, *Advancement in solar photovoltaic/thermal (PV/T) hybrid collector technology*. Renewable and Sustainable Energy Reviews, 2012. **16**(3): p. 1383-1398.
32. Duffie, J.A. and W.A. Beckman, *Solar Engineering of Thermal Processes*. Fourth ed. 2013, Hoboken, New Jersey, United States of America: John Wiley & Sons, Inc.
33. Mette, B., H. Kerskes, and H. Drück, *Concepts of long-term thermochemical energy storage for solar thermal applications – Selected examples*. Energy Procedia, 2012. **30**: p. 321–330.
34. Michel, B., P. Neveu, and N. Mazet, *Comparison of closed and open thermochemical processes, for long-term thermal energy storage applications*. Energy, 2014. **72**: p. 702-716.
35. Mauran, S., H. Lahmidi, and V. Goetz, *Solar heating and cooling by a thermochemical process. First experiments of a prototype storing 60kWh by a solid/gas reaction*. Solar Energy, 2008. **82**(7): p. 623-636.
36. Anyanwu, E.E., *Review of solid adsorption solar refrigeration II:: An overview of the principles and theory*. Energy Conversion and Management, 2004. **45**(7): p. 1279-1295.
37. *Worldwide Rechargeable Battery Market 2017-2030*. 2018, Paris (France): Avicenne.
38. Kalogirou, S.A. and Y. Tripanagnostopoulos, *Hybrid PV/T solar systems for domestic hot water and electricity production*. Energy Conversion and Management, 2006. **47**(18): p. 3368-3382.
39. del Amo, A., et al., *An innovative urban energy system constituted by a photovoltaic/thermal hybrid solar installation: Design, simulation and monitoring*. Applied Energy, 2017. **186**: p. 140-151.
40. Liang, R., J. Zhang, and C. Zhou, *Dynamic Simulation of a Novel Solar Heating System Based on Hybrid Photovoltaic/Thermal Collectors (PVT)*. Procedia Engineering, 2015. **121**: p. 675-683.
41. Buonomano, A., F. Calise, and M. Vicidomini, *Design, Simulation and Experimental Investigation of a Solar System Based on PV Panels and PVT Collectors*. Energies, 2016. **9**(497).
42. Magalhães, P.M.L.P., J.F.A. Martins, and A.L.M. Joyce, *Comparative Analysis of Overheating Prevention and Stagnation Handling Measures for Photovoltaic-thermal (PV-T) Systems*. Energy Procedia, 2016. **91**: p. 346-355.
43. Jonas, D., et al., *Performance modeling of PVT collectors: Implementation, validation and parameter identification approach using TRNSYS*. Solar Energy, 2019. **193**: p. 51-64.
44. Touafek, K., A. Khelifa, and M. Adouane, *Theoretical and experimental study of sheet and tubes hybrid PVT collector*. Energy Conversion and Management, 2014. **80**: p. 71-77.
45. Guo, C., et al., *Numerical simulation and experimental validation of tri-functional photovoltaic/thermal solar collector*. Energy, 2015. **87**: p. 470-480.

46. Ji, J., et al., *Distributed dynamic modeling and experimental study of PV evaporator in a PV/T solar-assisted heat pump*. International Journal of Heat and Mass Transfer, 2009. **52**(5): p. 1365-1373.
47. Xu, G., et al., *Simulation of a photovoltaic/thermal heat pump system having a modified collector/evaporator*. Solar Energy, 2009. **83**(11): p. 1967-1976.
48. Zhao, X., et al., *Theoretical study of the performance of a novel PV/e roof module for heat pump operation*. Energy Conversion and Management, 2011. **52**(1): p. 603-614.
49. Tsai, H.-L., *Design and Evaluation of a Photovoltaic/Thermal-Assisted Heat Pump Water Heating System*. Energies, 2014. **7**: p. 3319-3338.
50. Walker, G., *Evaluating MPPT converter topologies using a Matlab PV Model*. Journal of Electrical and Electronics Engineering, Australia, 2001. **21**.
51. Renon, H. and J.M. Prausnitz, *Local compositions in thermodynamic excess functions for liquid mixtures*. AIChE Journal, 1968. **14**(1): p. 135-144.
52. Redlich, O. and J.N.S. Kwong, *On the Thermodynamics of Solutions. V. An Equation of State. Fugacities of Gaseous Solutions*. Chemical Reviews, 1949. **44**(1): p. 233-244.
53. *https://www.nist.gov/srd/refprop*
54. *Trasient system simulation programa. Trnsys 18*. 2017.
55. Mourshed, M., *Relationship between annual mean temperature and degree-days*. Energy and Buildings, 2012. **54**: p. 418-425.
56. Skarbit, N., et al., *Employing an urban meteorological network to monitor air temperature conditions in the 'local climate zones' of Szeged, Hungary*. International Journal of Climatology, 2017. **37**(S1): p. 582-596.
57. Papakostas, K., T. Mavromatis, and N. Kyriakis, *Impact of the ambient temperature rise on the energy consumption for heating and cooling in residential buildings of Greece*. Renewable Energy, 2010. **35**(7): p. 1376-1379.
58. Azevedo, J.A., L. Chapman, and C.L. Muller, *Critique and suggested modifications of the degree days methodology to enable long-term electricity consumption assessments: a case study in Birmingham, UK*. Meteorological Applications, 2015. **22**(4): p. 789-796.
59. *European Standard EN 12831:2017. Energy performance of buildings - Method for calculation of the design heat load*. 2017, Brussels: Europen Committee for Standardization.
60. ASHRAE, *Handbook of Fundamentals*. 2009, Atlanta, GA, USA: American Society of Heating, Refrigeration, and Air-Conditioning Engineers.
61. *Day-ahead Prices*, in *European Network of Transmission System Operators for Electricity*. 2020.